SULFIDE OXIDATION AND (NANO)PARTICLE FORMATION ALONG REDOX GRADIENTS IN THE MARINE ENVIRONMENT

by

Alyssa J.L. Findlay

A dissertation submitted to the Faculty of the University of Delaware in partial fulfillment of the requirements for the degree of Doctor of Philosophy in Oceanography

Spring 2015

ProQuest LLC.
789 East Eisenhower Parkway
P.O. Box 1346
Ann Arbor, MI 48106 - 1346

SULFIDE OXIDATION AND (NANO)PARTICLE FORMATION ALONG REDOX GRADIENTS IN THE MARINE ENVIRONMENT

by

Alyssa J.L. Findlay

Approved: ____
Mark A. Moline, Ph.D.
Director of the School of Marine Science and Policy

Approved: ____
Nancy M. Targett, Ph.D.
Dean of the College of Earth, Ocean, and Environment

Approved: ____
James G. Richards, Ph.D.
Vice Provost for Graduate and Professional Education

I certify that I have read this dissertation and that in my opinion it meets the academic and professional standard required by the University as a dissertation for the degree of Doctor of Philosophy.

Signed:

George W. Luther III, Ph.D.
Professor in charge of dissertation

I certify that I have read this dissertation and that in my opinion it meets the academic and professional standard required by the University as a dissertation for the degree of Doctor of Philosophy.

Signed:

Thomas E. Hanson, Ph.D.
Member of dissertation committee

I certify that I have read this dissertation and that in my opinion it meets the academic and professional standard required by the University as a dissertation for the degree of Doctor of Philosophy.

Signed:

Dominic M. Di Toro, Ph.D.
Member of dissertation committee

I certify that I have read this dissertation and that in my opinion it meets the academic and professional standard required by the University as a dissertation for the degree of Doctor of Philosophy.

Signed:

Timothy J. Shaw, Ph.D.
Member of dissertation committee

ACKNOWLEDGMENTS

First, I would like extend a sincere thank you to my adviser, Dr. George Luther for his invaluable guidance, knowledge, and enthusiasm; and for his dedication to my growth as a scientist. I am so grateful for all that I have learned throughout my graduate studies in your group.

I would like to thank my committee members, Dr. Thomas Hanson, Dr. Dominic Di Toro, and Dr. Timothy Shaw. It has been a pleasure to work with each of you on the various aspects of this project, and I greatly value the time and expertise you have provided.

Thank you also to Dr. Gregory Druschel for mentoring me as an undergraduate, and for your continued support.

I was fortunate to have the opportunity to meet and collaborate with many people during the course of this work. Thank you to Dr. Clara Chan for her expertise in microscopy and helpful discussions, and to Drs. Brad Tebo and Matt Jones for sharing cruises on the Chesapeake. I would like to thank Drs. Maria dos Santos Afonso and Roberto Candal at the Universidad de Buenos Aires for being such welcoming hosts. Thank you also to Debbie Powell and Shannon Modla at the Delaware Biotechnology Institute for Scanning Electron Microscope assistance and training, and to the captains and crews of the R/V *Hugh R. Sharp* and R/V *Knorr* for successful cruises.

Thank you to Connie Edwards, Peggy Colon, Bethany Gibson, Janis Lopez, and Marcia Pettay for their help and patience with administrative details; and to Debbie Booth and Ellen Erbe for help with reference materials.

Thank you to my fellow lab members, past and present: Andrew Madison, Amy Gartman, Trish Hredzak- Showalter, David Chu, Mike McGinley, Shannon Owings, Véronique Oldham, Matt Siebecker, and Dan MacDonald for sharing adventures both in the field and in the lab. Thank you as well to my other CEOE friends, and to my community here in Delaware and beyond.

This work was supported by grants from NSF Marine Geology and Geophysics (OCE 1131109) and NSF Molecular and Cellular Biology (MCB-0919682) as well as a University of Delaware Dissertation Fellowship.

TABLE OF CONTENTS

Appendices

LIST OF TABLES

LIST OF FIGURES

ABSTRACT

Recent thermodynamic calculations and experimental work have demonstrated that the oxidation of sulfide to elemental sulfur by oxygen is slow. Moreover, additional studies have shown that nanoparticles are a widespread component of many environments. Here, the oxidation of sulfide to form elemental sulfur and the presence of metal sulfide and elemental sulfur nanoparticles were investigated along redox gradients in the water column of the Chesapeake Bay and in buoyant hydrothermal vent plumes (< 1.5 meters from the orifice) along the Mid-Atlantic Ridge.

The partitioning of trace metals into sulfide phases was found to differ between the bouyant plumes of three vent sites along the Mid-Atlantic Ridge due to differences in the metal to sulfide ratio of the vent fluid. Significant concentrations of HNO_3-extractable metals were found in the < 0.2 µm fraction at all three vent sites, indicating that these metals were incorporated into nanoparticulate pyrite.

Elemental sulfur nanoparticles (< 0.2 µm) were found to be a significant percentage of total S^0 in both the Chesapeake Bay water column and hydrothermal vent plumes. In the Chesapeake Bay, elemental sulfur is formed by both abiotic and biotic sulfide oxidation. Manganese oxides are the dominant available chemical oxidant for sulfide, and a strain of phototrophic sulfide oxidizing bacteria (PSOB), CB11, that was enriched from the Chesapeake Bay was shown to produce elemental

sulfur as a product of sulfide oxidation. In buoyant vent plumes, sulfide oxidation is abiotic, and the oxidation of sulfide through an iron catalytic cycle accounts for all elemental sulfur formed. These results indicate that nanoparticulate elemental sulfur should be a common component of a variety of different types of environments in which sulfur is cycled along an oxic/anoxic interface.

The oxidation of sulfide in the Chesapeake Bay was further investigated through incubation experiments that monitored sulfide loss in natural water samples and in cultures of CB11. Small increases in light intensity as low as 0.1 μEi were found to significantly affect sulfide loss in both sets of experiments, indicating the activity of PSOB in the Chesapeake Bay water column. PSOB need only comprise about 5 % of the total microbial community in order to account for all observed light-dependent sulfide loss. In order to explore the impact of variability in the water column redox structure on sulfide oxidation by PSOB, a one-dimensional diffusion-reaction model of the Chesapeake Bay water column was developed using kinetic parameters determined from the incubation experiments. The model simulations demonstrate that the contribution of PSOB to sulfide oxidation is highly variable and dependent upon the location of the oxic/anoxic interface in the water column.

Chapter 1

AN INTRODUCTION TO SULFUR SPECIATION AND REDOX CYCLING

1.1 Introduction

Sulfur chemistry has widespread biogeochemical significance in the environment. Sulfur readily binds with carbon, oxygen, and trace metals; and is an essential component in biological molecules such as amino acids (e.g. cysteine, methionine) and enzymes (e.g. ferrodoxins, coenzymeA). The reactivity of sulfur is governed by its oxidation state. In oxygenated environments, sulfur is primarily fully oxidized as sulfate (SO_4^{2-}), with an oxidation state of +6; and in anoxic environments, sulfur is present as hydrogen sulfide (Σ $HS^- + H_2S$), with an oxidation state of -2. Along redox gradients, sulfur is cycled between these two end-member species.

In most environments, sulfur cycling begins with the microbial reduction of sulfate to sulfide during organic matter decomposition (Jørgensen, 1982). The eight-electron oxidation of hydrogen sulfide back to sulfate then occurs stepwise via a suite of biological and chemical pathways including oxidation by oxygen or metal oxides (Millero 1987; Luther, 1991; Herszage and dos Santos Afonso, 2003; Pyzik and Sommer, 1981; Poulton, 2003) and by chemotrophic and phototrophic bacteria (Frigaard and Dahl, 2008 and references therin). This results in the formation of a wide variety of sulfur compounds with intermediate oxidation states such as polysulfides, elemental sulfur, thiosulfate, sulfite, and tetrathionate, which also participate in biological and geochemical reactions (Thamdrup et al., 1993; Finster et al., 1998). For example, sulfide, polysulfide, and elemental sulfur are precursors to the formation of pyrite via equations 1 and 2 (Rickard and Luther, 1997; Berner, 1970) and therefore play an important role in sediment geochemistry.

(1) $H_2S + FeS \rightarrow FeS_2 + H_2$
(2) $FeS + S^0 \rightarrow FeS_2$

Thus, understanding the processes of the sulfur cycle and their interactions with other elemental cycles along redox gradients is important in a variety of environmental settings. A summary of the complex web of abiotic and biotic pathways for sulfur transformations is depicted in Figure 1.1, and a more detailed summary of some of these processes follows.

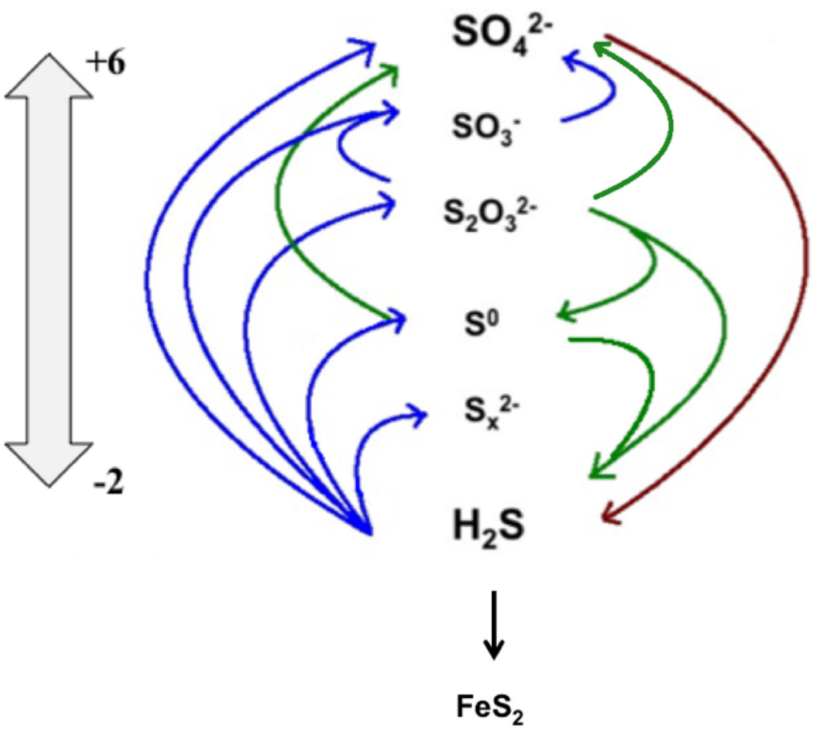

Figure 1.1 Overview of microbially-mediated sulfur cycling. Blue lines represent oxidation (biotic and abiotic), the red line represents microbial sulfate reduction, and green lines indicate microbial disproportionation of elemental sulfur (S^0) and thiosulfate ($S_2O_3^{2-}$). Sulfur is buried as pyrite, which may form from the reaction between iron and sulfide, polysulfides, or elemental sulfur.

1.2 Processes of the Sulfur Cycle

1.2.1 Sulfate Reduction

Organic matter decomposition occurs via a series of electron acceptors with decreasing free energy yields in the order $O_2 > MnO_2 > NO_3^- > FeOOH > SO_4^{2-}$ (Froelich, 1979). Sulfate is the second most prevalent soluble electron acceptor after oxygen (Zopfi et al., 2004), and microbially mediated sulfate reduction is widespread in sediments, soils, and anoxic water columns (equation 3; Jørgensen et al., 1979).

(3) $\frac{1}{2} SO_4^{2-} + CH_2O + H^+ \rightarrow \frac{1}{2} H_2S + CO_2 + H_2O$

Dissimilatory sulfate reduction as a microbial metabolism began 2.8 – 3.1 billion years ago (Schidlowski, 1988), and is currently carried out by a diverse group of anaerobic microorganisms. In order to be reduced, sulfate must first be activated by conversion to adenosine 5'-phosphosulfate (APS) by ATP sulfurylase. Then, APS reductase conducts the two-electron reduction of APS to sulfite, which is reduced to sulfide by sulfite reductase (Thauer et al., 1977). The result of this activity is the accumulation of sulfide in sediment pore-waters, which can play a role in maintaining suboxic or anoxic conditions in the overlying water column (Roden and Tuttle, 1992).

1.2.2 Sulfide Oxidation

Only 10 – 20% of sulfide produced globally by sulfate reduction is buried in the sediments via equations 1 and 2 (Jørgensen 1982). The majority is re-oxidized by a variety of possible chemical and biological processes. The following section will provide a brief description of the oxidation of sulfide to elemental sulfur by (1) oxygen, (2) manganese and iron oxides, and (3) phototrophic bacteria.

Sulfide oxidation by oxygen

In most aquatic environments, O_2 is the most prevalent oxidant; however, the direct oxidation of sulfide by oxygen is inhibited both thermodynamically and kinetically. A one-electron transfer via equation 4 is thermodynamically inhibited due to the formation of bisulfide radical and superoxide (Luther, 2010).

(4) $O_2 + H_2S \rightarrow HS\cdot + O_2^- + H^+$

The two-electron oxidation of sulfide to form elemental sulfur (equation 5) is thermodynamically favourable, but encounters a kinetic barrier because the electrons from sulfide must be unpaired in order to be transferred to the singly occupied lowest unoccupied molecular orbital (LUMO) of oxygen (Luther et al., 2011).

(5) $O_2 + H_2S \rightarrow S^0 + H_2O_2$

Under trace metal clean conditions, experimental observations of the sulfide oxidation rate yield a rate expression (equation 6)

(6) $-d[H_2S]/dt = k[H_2S][O_2]$

and a half-life for sulfide of 55 days (Luther et al., 2011). The addition of trace quantities of transition metals (specifically iron and manganese), which facilitate this reaction as bridging catalysts (Vasquez et al., 1989), shortens the half-life of sulfide in in oxic waters to 1-2 days (Millero et al., 1987).

Sulfide oxidation by manganese and iron oxides

In addition to catalyzing sulfide oxidation with oxygen, manganese and iron oxides may also react directly with sulfide. The one electron oxidation of sulfide by either oxidized iron or manganese faces the same thermodynamic barrier as equation 4 due to the formation of bisulfide radical, and so this reaction should proceed via a two-electron transfer that forms S^0. Although a single Mn^{4+} (MnO_2) may accept two electrons directly, Fe^{3+} cannot, and so bands of orbitals in iron or manganese oxide (nano)particles are important (Luther, 2010). Oxidized manganese is a better oxidant for sulfide than iron because the LUMO of Mn^{4+} is unoccupied, whereas the LUMO of Fe^{3+} is partially occupied, posing the same kinetic barrier as the oxidation of sulfide by oxygen due to the requirement for the electrons from sulfide to be unpaired (Luther, 2010).

The reaction between manganese and sulfide proceeds via equation 7

(7) $MnO_2 + H_2S + 2\ H^+ \rightarrow Mn^{2+} + S^0 + 2\ H_2O$

and follows the second order kinetics described by equation 8.

(8) $- d[H_2S]/dt = k[H_2S][MnO_2]$

The reaction rate is pH dependent, increasing from pH 2-5, and then decreasing at higher pH (Yao and Millero, 1993).

Sulfide is oxidized by iron via equation 9,

(9) $2\ FeOOH + H_2S + 4\ H^+ \rightarrow 2\ Fe^{2+} + S^0 +4\ H_2O$

which follows the second order expression in equation 10

(10) $–d[H_2S]/dt = k[H_2S][Fe(OH)_3]$

The reaction rate increases to pH 6.5 then decreases with increasing pH (Yao and Millero, 1996).

Phototrophic sulfide oxidation

Microorganisms are able to oxidize sulfide rapidly due to enzyme systems that overcome the barriers described above. Anoxygenic phototrophic sulfide oxidizing bacteria (PSOB) are found in a variety of environments in which both light and sulfide gradients overlap, including sediments (Preisler et al., 2007), microbial mats (Wahlund et al, 1991), and the stratified water columns of both freshwater and marine basins (Parkin and Brock, 1981; Guerrero et al., 1985; Overmann, 1992; Tonolla et al., 2003; Rimmer et al., 2008). In these environments PSOB occupy narrow niches where they must balance the flux of sulfide from below with the flux of light from above. They oxidize sulfide to sulfate and fix CO_2 photosynthetically as per the overall reaction (equation 11).

(11) $2\ CO_2 + H_2S + 2\ H_2O + \text{light} \rightarrow 2\ CH_2O + SO_4^{2-} + 2\ H^+$

In reality; however, this process proceeds in steps, beginning with a two-electron oxidation of sulfide that forms zero-valent sulfur (S^0 or S_x^{2-}), as an obligate intermediate (equation 12; Chan et al., 2008).

(12) $CO_2 + 2\ H_2S + 2\ H^+ + \text{light} \rightarrow CH_2O + 2\ S^0 + H_2O$

PSOB fall into two main categories: the purple sulfur bacteria (PSB), which consist of *Chromatiaceae and Ectothiorhodospiraceae*; and green sulfur bacteria (GSB), which consist of *Chlorobiaceae*. PSB are adapted to higher light intensity (8 – 10.5 μEi/ mol CO_2; Brune, 1989) and lower sulfide concentrations. Their main photosynthetic pigment is BChl a, which is contained in phototrophic antennae at concentrations of 20 -2000 molecules BChl a per reaction center (Zuber and Cogdell, 1995). They form globules of elemental sulfur that are stored intracellularly as a product of sulfide oxidation. GSB are generally adapted for lower light intensities (3.5–4.5 μEi /mol CO_2) than PSB (Frigaard and Dahl, 2008). Their main photosynthetic pigments are BChl c, d, and e (depending upon the particular strain) that are contained in chlorosomes and can be concentrated up to 5000 – 8000 BChl molecules per reaction center (Frigaard et al., 2003), thus making GSB well adapted to conduct photosynthesis at low light intensities. GSB oxidize sulfide to polysulfides (Brune, 1989), which are deposited extracellularly as elemental sulfur (van Gemerden, 1986). Many GSB can also oxidize intermediate sulfur compounds such as thiosulfate and elemental sulfur if sulfide is not present.

During photosynthetic sulfide oxidation, light is used to transport electrons from sulfide to the electron carrier NAD^+ via reverse electron transport (Griesbeck et al., 2000). There are two enzymes that may be used for sulfide oxidation: sulfide:quinone oxioreductase (SQR) and flavocytochrome c (FCC). SQR is found in a variety of microorganisms, including PSOB, cyanobacteria, and archaea; and catalyzes sulfide oxidation with an isoprenoid quinone. In PSOB, SQR is essential for sulfide oxidation (Chan et al., 2009). Polysulfide is the first product of sulfide oxidation, which then forms elemental sulfur after being released from the enzyme (Griesbeck et al., 2002). The second of these enzymes, FCC, transfers electrons from sulfide to c-type cytochromes that then transfer the electrons to the photosynthetic reaction center (Frigaard and Dahl, 2008). This enzyme has been demonstrated to be non-essential for sulfide oxidation; however, it may be important as a high-affinity system utilized under low sulfide concentrations, as there is a large redox potential difference between FCC and the photosynthetic reaction center (Brune, 1995).

Oxidation of external elemental sulfur is less well understood (Frigaard and Dahl, 2008), but is expected to begin with some form of activation of or attachment to the sulfur particle (Chan et al., 2008). Experiments with the purple sulfur bacterium *Allochromatium vinosum* have shown that chains of elemental sulfur are more bioavailable than cyclic elemental sulfur or S_8 (Franz et al., 2007); however it is not known if this is also true for other types of PSOB.

1.3 Size Fractionation of Metal Sulfide and Elemental Sulfur Particles in the Environment

Recent research has demonstrated that previous classification of the fractions < 0.2 µm or < 0.45 µm as "dissolved" does not represent the actual complexity of this operationally defined category, which may contain nanoparticles as well as truly dissolved species (Hochella, 2001; Gilbert and Banfield, 2005; Wigginton et al., 2007; Yücel et al., 2011; Gartman et al., 2014). The formation of nanoparticles during mineral precipitation and dissolution reactions or biological activity has environmental significance for several reasons. First, nanoparticles may react differently than bulk minerals due to their higher surface area to volume ratio (Hochella et al, 2008). Second, nanoparticles have implications for the transport of elements in the environment, as they do not settle rapidly from the water column because of their small size (Yücel et al., 2011). Furthermore, nanoparticles are known to play an important role in microbial processes, including the metabolism of iron (Chan et al., 2009) and manganese (Webb et al., 2005).

Under reducing conditions, sulfur speciation is closely linked with that of trace metals; and metal sulfide clusters and nanoparticles have been demonstrated to be important in a variety of environments (Luther and Rickard, 2005) by changing the bioavailability of sulfide (Luther et al., 2008) and eliminating the toxicity of certain metals (Bianichi et al. 2002). Metal sulfide nanoparticles do not oxidize rapidly (Rozan et al., 2000; Gartman and Luther, 2014), and thus represent a mechanism for transport of both reduced sulfur and trace metals from anoxic to oxic environments. For example, the stabilization of iron in nanoparticulate pyrite represents an important transport mechanism for iron emitted from hydrothermal vents (Yücel et al., 2011; Gartman et al., 2014), which could impact the oceanic iron budget (Tagliabue et al., 2010). Other metal sulfide nanoparticles such as CdS, ZnS, PbS, and CuS formed as a result of sulfate reduction in the presence of reduced trace metals have been found in freshwater environments polluted by acid mine waste (Banfield and Zhang, 2001), but few studies have characterised this fraction in marine settings.

Elemental sulfur forms as a stable intermediate of sulfide oxidation via the reactions outlined in section 1.1.2 above. Despite the prevalence of elemental sulfur along redox gradients in a variety of different environments (Jørgensen, 1979; Hastings and Emerson, 1988; Luther et al., 1991; Ciglenecki et al., 1996; Ramsing et al., 1996 Zopfi et al., 2001 Ma et al., 2006; Li et al., 2008; Zerkle et al., 2010; Kamyshny et al., 2011), little is known about its speciation or reactivity. Orthorhombic S_8 is the thermodynamically stable form of elemental sulfur at ambient temperature and pressure; however, studies have shown that elemental sulfur produced by microbial activity may have different characteristics than bulk S_8 (Kleinjan et al., 2003). Moreover, elemental sulfur nanoparticles formed via either biological or chemical oxidation of sulfide would have important biogeochemical implications. Nanoparticulate sulfur could be more bioavailable than bulk S_8, or more reactive in chemical and diagenetic reactions (e.g. reaction 2).

1.4 The Importance of Sulfur in the Biogeochemical Evolution of the Oceans

Consideration of the processes described above is important both in the investigation of modern environments and for understanding the biogeochemical history of modern oceans, as sulfur cycling was instrumental in the evolution of current marine chemistry. The Archaean Ocean (> 2.5 billion years ago) was anoxic, iron rich, and depleted in sulfur (Canfield et al., 2000). The oxygenation of the atmosphere during the Great Oxygenation Event (approximately 2.5 billion years ago) led to a transition in ocean chemistry from this anoxic, ferruginious Archaean Ocean to the oxygenated modern oceans. This transition occurred in stages during which ocean chemistry varied greatly. During the Proterozoic aeon (0.5-2.5 billion years ago), ocean chemistry was affected by increased continental weathering due to the rise of oxygen in the atmosphere brought about by the onset of oxygenic photosynthesis. Increased continental weathering led to an increase in seawater sulfate concentrations, which in turn enhanced microbial sulfate reduction and the production and accumulation of sulfide. This marked the first transition of the ocean from ferruginous to sulfidic approximately 1800 million years ago (Poulton et al., 2004).

Between 1800 to 700 million years ago, as oxygenic photosynthesis became more prevalent and atmospheric oxygen concentrations increased, the upper layer of the water column became oxygenated, leading to a chemically stratified system with an oxic surface layer and a sulfidic deep layer (Canfield, 1998). At the resulting oxic/anoxic interface, sulfur was actively cycled between its reduced and oxidized forms. This dynamic chemical transition impacted the microbiology, as the sulfur cycle was an important source of energy for microbes in both the Archaean and Proterozoic Oceans (Sleep and Bird 2008). As oxygen penetrated deeper into the water column, pushing the oxic/anoxic interface out of the photic zone, the habitat available for anaerobic phototrophic sulfide oxidizing bacteria would have become increasingly limited.

Modern oxic/anoxic interfaces represent analogues to the chemical transition of the oceans, and thus may provide deeper understanding of ancient biogeochemical processes. These interfaces still exist in a variety of different environments where anoxia is driven primarily by the decomposition of organic matter, such as sediments and the water column of stratified systems (e.g. the Black Sea, meromictic lakes); and are found also at hydrothermal vents, where anoxic vent fluid formed through hydrothermal circulation in the earth's crust (Tivey, 2007) mixes with oxic ocean bottom water.

1.5 Study Sites

1.5.1 The Chesapeake Bay

The Chesapeake Bay is the largest estuary in the United States, beginning at the mouth of the Susquehanna River and ending at the Atlantic Ocean (Hagy et al., 2004) with a watershed of 165800 km^2. It is a partially stratified estuary, where water transport follows a two-layer gravitational circulation pattern with saline water flowing up-estuary and fresh water flowing down-estuary (Pritchard, 1952). In the summer, salinity gradients coupled with an influx of nutrients and high biological activity lead to the development of suboxic to anoxic deep-water throughout much of the mesohaline region of the Bay. A suboxic zone between the oxic surface and anoxic deep layers in which neither oxygen nor sulfide are detectable may form during slack tide at the chemical interface created by the density stratification (Lewis et al., 2007). This interface is a place of dynamic chemical and biological activity and elemental cycling.

Anoxia in the Chesapeake Bay is highly variable. First, it is transient during the course of the year, setting up in the late spring, peaking in the summer, and eroding during the late summer and early fall. Second, the extent of summer anoxia varies interannually, depending upon the degree of the spring freshwater and nutrient inputs (Officer et al., 1984). Finally, in addition to annual and inter-annual variation in oxygen concentrations, tidal forcing and wind-induced mixing of the water column result in changes in the oxygen penetration depth and the depth of the chemical interface on shorter time scales (Lewis et al., 2007; Scully, 2010).

The primary cause of oxygen depletion in the Bay is the decomposition of phytoplankton (Jonas and Tuttle, 1990). Then, sedimentary sulfate reduction increases oxygen demand and helps to maintain anoxic conditions in the bottom waters (Roden and Tuttle, 1992). The precipitation of iron sulfides does not represent a major removal mechanism for sulfide from the water column, as typical porewater Fe^{2+} concentrations in the mesohaline region of the Chesapeake Bay are < 10% of sulfide concentrations, and only 4-8% of sulfide produced via sulfate reduction is buried as pyrite (Roden and Tuttle, 1992). Furthermore, sedimentary pyrite concentrations are particularly low in years when the bottom waters are anoxic (Roden and Tuttle, 1993), with a typical FeS_2/FeS ratio of 0.55-0.22 (Berner, 1979). The reason for low sulfur burial is the prevalence of manganese over iron in this system, as manganese oxides are a stronger oxidant for sulfide than iron oxides (Aller and Rude, 1988), which also react with sulfide or sulfur to precipitate as FeS or FeS_2. As a consequence of the low burial rate for sulfur, sulfur cycling is highly active, and most of the sulfide produced in the sediments will eventually be reoxidized.

Although phototrophic sulfide oxidizing bacteria have not previously been studied in the Chesapeake, the observation of rapid (half-life of 15 minutes) light dependent sulfide oxidation by Luther et al. (1988) that was inhibited by the addition of formaldehyde (Figure 1.2) suggested an unknown biological component to sulfide oxidation in the Bay. This observation, coupled with more recent reports of phototrophic sulfur bacteria in similar low-light environments such as the water column of the Black Sea (Overmann, 1992; Manske et al., 2005; Marschall et al., 2010) indicates a potential role for these bacteria in the sulfur cycle of the Bay. The Chesapeake Bay is an interesting system in which to study PSOB, as it represents an analogue to the ancient ocean during later periods of the anoxic/oxic transition, when oxic conditions dominated and stratification was transient (Hanson et al., 2013). Understanding the niches occupied by PSOB in such environments could help to interpret microfossils and cast light on the redox structure of ancient oceans (Overman, 2008).

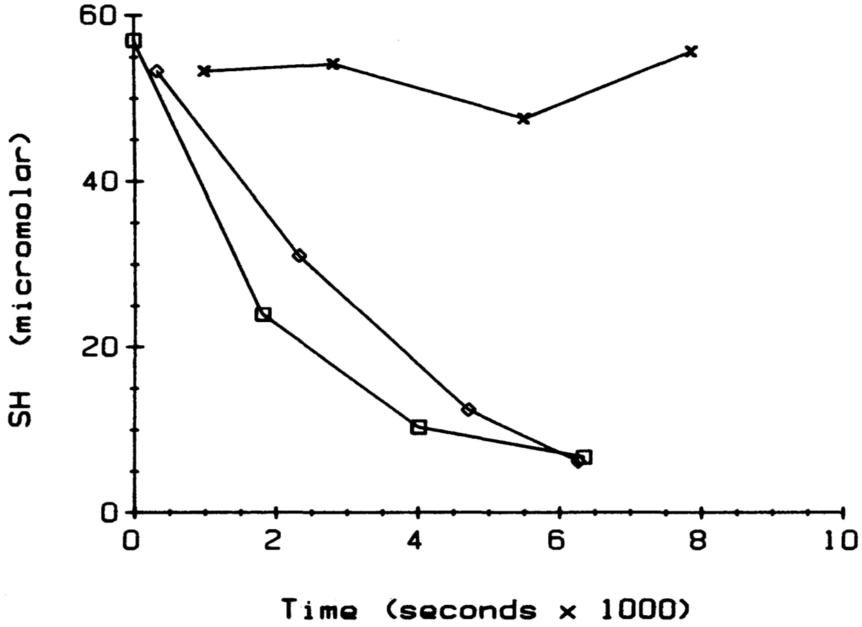

Figure 1.2 Results of experiment conducted in Chesapeake Bay water. X markers signify water samples fixed with formaldehyde, and the other symbols signify incubations in the light. Figure taken from Luther et al. (1988).

The specific location at which this study took place (Figure 1.3) has been characterized previously (Lewis et al., 2007). It is a shallow hole (25 m deep, 4 km long and 0.8 km wide) bordered in the west by the main channel (approximately 18 m deep) and in the east by Kent Island.

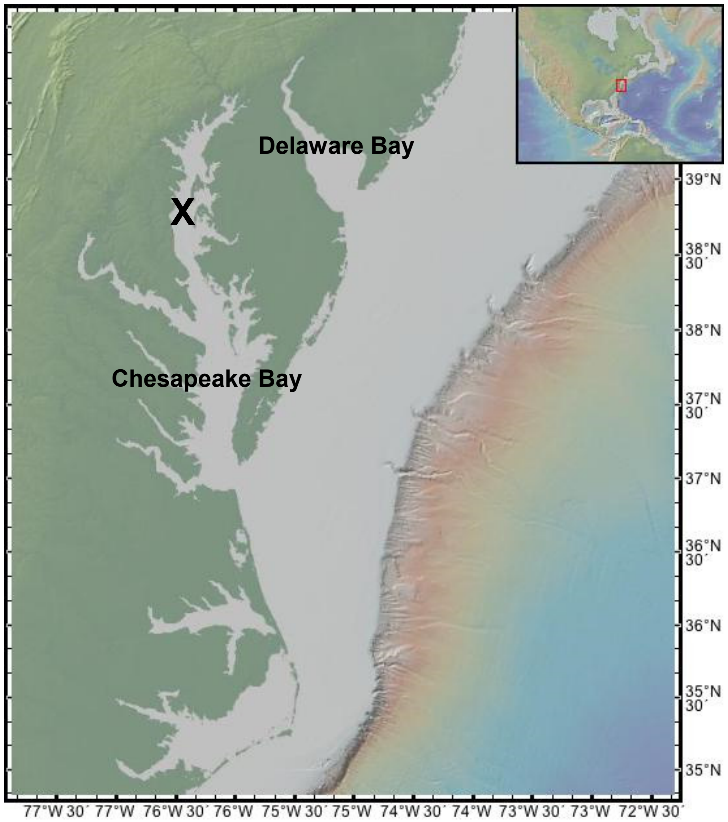

Figure 1.3 Location of study site depicted by the black **X** (38º58.8' N; 76º22' E). Map created using GeoMapApp (http://www.geomapapp.org).

1.5.2 Hydrothermal Vents along the Mid-Atlantic Ridge

Deep-sea vents represent a very different sort of system in which an oxic/anoxic interface is present; one detached from the photic zone and in which biogeochemical cycling is driven by the alteration of fluids entrained in the earth's crust, and the large temperature, pH, and chemical differences between those fluids and seawater. At the vent orifice, hot, reduced, metal-rich vent fluid mixes with cold, partially oxygenated ocean bottom water, leading to the precipitation of metal sulfide particles (Sarradin et al., 2008). The hydrothermal vent system is composed of three distinct sections: (1) the end-member vent fluid, (2) the buoyant plume that rises vertically and forms as the vent fluid mixes with ocean water and cools; and (3) a neutrally buoyant plume that forms and spreads horizontally once the density of the buoyant plume is equal to that of the ambient seawater (approximately 200-500 m above the vent orifice).

Although vent fluid strongly impacts the area immediately surrounding the vents, its impact on the global oceans has previously been disregarded due to the precipitation of large quantities of metal sulfides and oxides from the rising plume (Mottl et al., 1990). Recent studies; however, have indicated that metals are stabilized either as complexes with organic molecules (Bennett et al., 2008) or as nanoparticulate metal sulfides such as pyrite (Yücel et al, 2011; Gartman et al., 2014) within the buoyant and neutrally buoyant plume that could persist long enough to be transported from the vent site (Yücel et al., 2011; Gartman and Luther, 2014).

During this study, three vent fields (Rainbow, TAG, and Snakepit) along the

Mid-Atlantic Ridge were sampled. The **Rainbow** vent field is hosted in ultramafic rock, and due to the uniform chemistry of its vent fluid is thought to have a single source (Charlou et al., 2002). Iron is an order of magnitude in excess of sulfide at Rainbow. Concentrations of nanoparticulate pyrite up to 1 mM have been found in the rising plume at Rainbow; however, this represents only a small fraction of total iron (< 5 %) (Gartman et al., 2014). The **Trans-Atlantic Geotraverse** (TAG) vent site is basalt-hosted, and consists of black smoker vents clustered on a large sulfide mound. Iron concentrations at TAG are only in two-fold excess of sulfide. The **Snakepit** vent field is located in the rift valley close to the top of a volcanic ridge (Thompson et al., 1988), and like TAG is basalt-hosted. Iron and sulfide concentrations at Snakepit are approximately equivalent. The iron to sulfide ratio has implications for particle formation and oxidation in the buoyant and non-buoyant plumes, and the variation in this ratio between Rainbow, TAG, and Snakepit allows the study of potential differences in metal sulfide particle formation at each vent.

1.6 Dissertation Structure

Sulfur chemistry is closely linked to that of trace metals due to both the formation of metal sulfide particles and the oxidation of sulfide to elemental sulfur; and is also strongly influenced by microbial activity. Two areas of recent research have demonstrated (1) that nanoparticles are an important component of a variety of environments and may indicate biological activity, and (2) that trace metals and microorganisms are vital for sulfide oxidation due to thermodynamic and kinetic barriers to sulfide oxidation by oxygen. The research presented in this dissertation aims to build on this work by exploring the role of nanoparticles, trace metals, and microorganisms in sulfur cycling in the environment. Specifically, this dissertation will investigate processes responsible for abiotic and biotic sulfide oxidation, the distribution and size fractionation of elemental sulfur, and the partitioning of trace metals in two different marine systems: the Chesapeake Bay and hydrothermal vents along the Mid-Atlantic Ridge. Throughout this work, several size fractions will be considered and discussed.

(1) The < 0.2 μm fraction (nanoparticulate + dissolved species)

(2) The > 0.2 μm fraction (particulate)

(3) The unfiltered fraction ($\Sigma < 0.2$ μm + > 0.2 μm fractions)

The dissertation is structured as follows. In Chapter 2, the partitioning of trace metals (Cu, Cd, Zn, Pb, Cd, Co) into sulfides and other particles in buoyant vent plumes along the Mid-Atlantic Ridge will be presented. This work complements the work of Gartman et al. (2014) that measured nanoparticulate pyrite in these samples.

In Chapter 3, the concentration, distribution, and size fractionation of elemental sulfur will be documented in both the Chesapeake Bay and in buoyant hydrothermal vent plumes, and a strain of PSOB enriched from the Chesapeake Bay will be shown to produce nanoparticulate elemental sulfur as a product of sulfide oxidation. These results will be compared with previous studies of elemental sulfur in similar environments. This work was published in *Geochimica et Cosmochimica Acta* in 2014.

Chapter 4 will investigate light dependent sulfide oxidation in the Chesapeake Bay. The sulfide oxidation kinetics of PSOB enrichment cultures from the Bay will be quantified, and results from field and laboratory experiments that constrain the effect of varying light intensity and sulfide concentration on the rate of sulfide oxidation by these PSOB will be presented.

In Chapter 5, a one-dimensional diffusion-reaction redox model of the Chesapeake Bay water column will be developed and applied to four years of physical and chemical data from the Bay that illustrate variable redox conditions. The kinetic data determined in Chapter 4 will be used to quantify the impact that photosynthetic sulfide oxidizing bacteria have on sulfide oxidation in the water column and to investigate how they are affected by variation in light and water column redox conditions.

Chapter 6 summarizes the major findings of this study, and poses questions for further study. Two appendices follow: Appendix A gives the results from laboratory sulfide oxidation experiments with RSC1, a low-light adapted brown colored GSB isolated from Bahamian sink holes, and Appendix B gives the computer code for the model presented in Chapter 5.

REFERENCES

Aller R. C. and Rude P. D. (1988) Complete oxidation of solid phase sulfides by manganese and bacteria in anoxic marine sediments. *Geochim Cosmochim Acta* **52**, 751-765.

Bennett, S. A., Achterberg, E.P., Connelly, D.P., Statham, P.J., Fones, G.R., German, C.R., 2008. The distribution and stabilization of dissolved Fe in deep-seahydrothermal plumes. Earth Planet. Sci. Lett. 270, 157–167.

Berner R.A. (1970) Sedimentary pyrite formation. *Am. J. Sci.* **268,** 1-23.

Berner R. A., Baldwin T., and Holdren Jr. G. R. (1979) Authigenic iron sulfides as paleosalinity indicators. *Jour. Econ. Paleo. Mineral.* **49**, 1345-1350.

Bianchini A., Bowles K.C., Brauner C.J., Gorsuch J.W., Kramer J.R. and Wood C.M. (2002) Evaluation of the effect of reactive sulfide on the acute toxicity of silver(I) to Daphnia magna, Part 2. Toxicity results. *Environ. Toxciol. Chem*. **21**, 1294–1300.

Brune, D. C. (1989) Sulfur oxidation by phototrophic bacteria. *Biochim Biophys Acta* **975**,189-221.

Canfield D.E., Thamdrup B., Fleischer S. (1998) Isotope fractionation and sulfur metabolism by pure and enrichment cultures of elemental sulfur disproportionating bacteria. *Limnol Oceanogr*. **43**, 253-264

Canfield D. E., Habicht K. S., Thamdrup B. (2000) The Archean sulfur cycle and the early history of atmospheric oxygen. *Science*, **288**, 658–661

Chan L.K., Morgan-Kiss R., Hanson T.E. (2008). Sulfur oxidation in *Chlorobium tepidum*: genetic and proteomic analyses. In Microbial sulfur metabolism ed Christiane Dahl, Cornelius Friedrich Springer press Heidelberg, Germany.

Chan, L.K., Morgan-Kiss, R.M., and Hanson, T.E. (2009) Functional analysis of three sulfide:quinone oxidoreductase homologs in Chlorobaculum tepidum. *J Bacteriol* **191**, 1026–1034.

Chan C.S., Fakra S.C., Edwards D.C., Emerson D., Banfield J. F. (2009). Iron oxyhydroxide mineralization on microbial extracellular polysaccharides. *Geochim Cosmochim Acta* **7**, 3807-3818.

Charlou J.L., Donval J.P., Fouquet Y., Jean-Baptiste P., Holm N. (2002) Geochemistry of high H_2 and CH_4 vent fluids issuing from ultramafic rocks at the Rainbow hydrothermal field (36° 14' N, MAR). *Chem Geol*. **191**, 345–359.

Chen K.Y. and Morris J.C. (1972) Kinetics of oxidation of aqueous sulfide by oxygen. *Environ Sci Technol.* **6**, 529-537.

Ciglenečki I., Kodba B., and Ćosović B. (1996) Sulfur species in Rogoznica Lake. *Mar. Chem.* **53,** 101-110.

Finster, K., Liesack W. and Thamdrup B. (1998) Elemental Sulfur and Thiosulfate Disproportionation by Desulfocapsa sulfoexigens sp. nov., a New Anaerobic Bacterium Isolated from Marine Surface Sediment. *Appl. Environ. Microb.* **64**, 119-125.

Franz B., H. Lichtenberg, Hormes J., Modrow H., Dahl C. and Prange A. (2007) Utilization of solid 'elemental' sulfur by the phototrophic purple sulfur bacterium Allochromatium vinosum: a sulfur K-edge X-ray absorption spectroscopy study. *Microbiology* **153**, 1268-1274.

Frigaard N.U. and Dahl C. (2008). Sulfur Metabolism in Phototrophic Sulfur Bacteria. *Adv. Microb. Physiol.* **54**,103-200.

Frigaard N.U., Gomez Maqueo Chew A., Li H., Maresca J.A., Bryant D.A. (2003). *Chlorobium tepidum:* Insights into the structure, physiology, and metabolism of a green sulfur bacterium derived from the complete genome sequence. *Photosynth. Res.* **78**, 93-117.

Froelich, P., Klinkhammer, G., and Bender, M. (1979) Early oxidation of organic matter in pelagic sediments of the eastern equatorial Atlantic: suboxic diagenesis. *Geochim Cosmochim Acta* **43**, 1075-1090.

Gartman A, Findlay A.J., Luther III G.W. (2014) Nanoparticulate pyrite and other nanoparticles are a widespread component of hydrothermal vent black smoker emissions. *Chem. Geol.* **366**, 32-4.

Gartman, A and Luther III G.W. (2014) Oxidation of synthesized sub-micron pyrite (FeS_2) in seawater. *Geochim Cosmochim Acta* **144**, 96-108.

Gilbert, B. and Banfield J. F. (2005). Molecular-Scale Processes Involving Nanoparticulate Minerals in Biogeochemical Systems. *Rev Mineral Geochem.* **59**, 109-155.

Griesbeck C., Hauska G., and Schütz M. (2000) Biological sulfide oxidation: Sulfide:Quinone Reductase (SQR), the primary reaction. In: Pandalai, S.G. (ed): Recent Research Developments in Microbiology, Vol. 4, 179-203. Research Signpost, Trivadrum India.

Griesbeck, C., Schütz, M., Schödl, T., Bathe, S., Nausch, L., Mederer, N.,Vielreicher, M. and Hauska, G. (2002) Mechanism of sulfide-quinone oxidoreductase investigated using site-directed mutagenesis and sulfur analysis. *Biochemistry* **41**, 11552–11565.

Guerrero, R., E. Montesinos, C. Pedros-Alio, I. Esteve, J. Mas, H. van Gemerden, P.A. G. Hofman and J. F. Bakker (1985) Phototrophic Sulfur Bacteria in Two Spanish Lakes: Vertical Distribution and Limiting Factors. *Limnol Oceanogr.* **30**, 919-931.

Hagy J.D., Boynton W.R., Keefe C.W., Wood K.V. (2004) Hypoxia in Chesapeake Bay, 1950-2001: Long-Term Change in Relation to Nutrient Loading and River Flow. *Estuaries* **27**, 634-658.

Hanson T.E., Luther III G.W., Findlay A.J., MacDonald D. J., and Hess D. (2013) Phototrophic sulfide oxidation: environmental insights and methods for kinetic analysis. *Front. Microbiol.* **4.**

Hastings D. and Emerson S. (1988) Sulfate reduction in the presence of low oxygen levels in the water column of the Cariaco Trench. *Limnol. Oceanogr.* **33**, 391-396.

Herszage J. and dos Santos Afonso M. (2003) Mechanism of Hydrogen Sulfide Oxidation by Manganese(IV) Oxide in Aqueous Solutions. *Langmuir* **19**, 9684-9692.

Hochella M.F. (2001) There's plenty of room at the bottom: Nanoscience in geochemistry. *Geochim Cosmochim Acta* **66**, 735 – 743.

Hochella, M. F., S. K. Lower, Maurice P. A., Lee Penn R., Sahai N, Sparks D. L., Twining B.S. (2008). Nanominerals, Mineral Nanoparticles, and Earth Systems. *Science* **319**(5870): 1631-1635.

Jonas R.B. and Tuttle J.H. (1990) Bacterioplankton and Organic Carbon Dynamics in the Lower Mesohaline Chesapeake Bay. *Appl Environ Microbiol.* **56**, 747-757.

Jørgensen B.B., Gijs Kuenen J., Cohen Y. (1979). Microbial transformations of sulfur compounds in a stratified lake (Solar Lake, Sinai). *Limnol Oceanogr*. **24**, 799-822.

Jørgensen, B. B. (1982) Ecology of the bacteria of the sulphur cycle with special reference to anoxic-oxic interface environments. *Arch Microbiol*. **298**, 543-561.

Kamyshny A., Zerkle A.L., Mansaray Z.F., Ciglenečki I., Bura-Nakić E., Farquhar J. and Ferdelman T.G. (2011) Biogeochemical sulfur cycling in the water column of a shallow stratified sea-water lake: Speciation and quadruple sulfur isotope composition. *Mar. Chem.* **127**, 144-154.

Kleinjan W.E., Keizer A. and Janssen A.J.H. (2003) Biologically Produced Sulfur. *Top. Curr. Chem.* **230**, 167-188.

Lewis B.L., Glazer B.T., Montbriand P.J., Luther III G.W., Nuzzio D.B., Deering T., Ma S., Theberge S. (2007) Short-term and interannual variability of redox-sensitive chemical parameters in hypoxic/anoxic bottom waters of the Chesapeake Bay. *Mar Chem* **105**, 296-308.

Li X., Taylor G. T., Astor Y. and Scranton M. I. (2008) Relationship of sulfur speciation to hydrographic conditions and chemoautotrophic production in the Cariaco Basin. *Mar. Chem.* **112**, 53-64.

Luther III, G.W., Ferdelman T., and Tsamakis E. (1988) Evidence suggesting anaerobic oxidation of the bisulfide ion in Chesapeake Bay. *Estuaries* **11**, 281-285.

Luther III, G.W., Ma, S., Trouwborst, R., Glazer, B., Blickley, M., Scarborough, R.W., Mensinger, M.G. (2004) The roles of anoxia, H2S and storm events in fish kills of dead end canals of Delaware Inland Bays. Estuaries **27**, 551-560.

Luther III G.W., Glazer B.T., Ma S., Trouwborst R.E., Moore T.S., Metzger E., Kraiya C., Waite T.J., Druschel G., Sundby B., Taillefert M., Nuzzio D.B., Shank T.M., Lewis B.L., and Brendel P.J. (2008) Use of voltammetric solid-state (micro)electrodes for studying biogeochemical processes: Laboratory measurements to real time measurements with an in situ electrochemical analyzer (ISEA). *Mar Chem* **108**: 221-235.

Luther III G.W., Church T.M., Powell D. (1991) Sulfur speciation and sulfide oxidation in the water column of the Black Sea. *Deep-Sea Res.* **38**, 1121-1137.

Luther G. W., Findlay A. J., MacDonald D. J., Owings S. M., Hanson T. E., Beinart R. A. and Girguis P. R. (2011) Thermodynamics and Kinetics of sulfide oxidation by oxygen: a look at inorganically controlled reactions and biologically mediated processes in the environment. *Front. Microbiol.* **2**.

Luther III G.W. (1991) Pyrite synthesis via polysulfide compounds. *Geochim. Cosmochim. Acta* **55**, 2839- 2849.

Luther, G., III (2010) The Role of One- and Two-Electron Transfer Reactions in Forming Thermodynamically Unstable Intermediates as Barriers in Multi-Electron Redox Reactions. *Aquat Geochem*. **16**, 395-420.

Ma S., Noble A., Butcher D., Trouwborst R. E. and Luther III G.W. (2006) Removal of H_2S via an iron catalytic cycle and iron sulfide precipitation in the water column of dead end tributaries. *Estuar Coast Shelf Sci.* **70**, 461-472.

Manske, A.K., Glaeser, J., Kuypers, M.M. and Overmann, J. (2005) Physiology and phylogeny of green sulfur bacteria forming a monospecific phototrophic assemblage at a depth of 100 meters in the Black Sea. *Appl Environ Microbiol*, **71**, 8049-8060.

Marschall, E., Jogler M., Hessge U., and Overmann J. (2010) Large-scale distribution and activity patterns of an extremely low-light-adapted population of green sulfur bacteria in the Black Sea. *Environ Microbiol*. **12**, 1348-1362.

Millero F.J, Sotolongo S. and Izaguirre M. (1987) The oxidation kinetics of Fe(II) in seawater. *Geochim. Cosmochim. Acta* **51**,793-801.

Möckel H.J. (1984) Retention of sulphur and sulphur organics in reversed-phase liquid chromatography. *J Chromatography* **317**, 589-614.

Mottl M.J. and McConachy T.F. (1990) Chemical processes in buoyant hydro-thermal plumes on the East Pacific Rise near 21 N. *Geochim Cosmochim Acta* **54**, 1911-1927.

Officer, C.G., Biggs R.B., Taft J.L., Cronin L.E., Tyler M.A., Boynton W.R. (1984) Chesapeake Bay anoxia: Origin, development, and significance. *Science* **23**: 22-27.

Overmann J., Cypionka H., and Pfennig N. (1992) An extremely low-light-adapted green sulfur bacterium from the Black Sea. *Limnol Oceanogr.* **37,** 150-155

Parkin T.B. and Brock T.D. (1981) The role of phototrophic bacteria in thesulfur cycle of a meromictic lake. *Limnol. Oceanogr.*, **26**, 880-490

Poulton, S.W., Fralick, P.W., and Canfield, D.E. (2004) The transition to a sulphidic ocean approximately 1.84 billion years ago. *Nature*, **431**, 173-177.

Poulton S.W. (2003) Sulfide oxidation and iron dissolution kinetics during the reaction of dissolved sulfide with ferrihydrite. *Chem Geol.* **202**, 79-94.

Preisler A., de Beer D., Lichtschlag A., Lavik G., Boetius A., and Jørgensen B.B. (2007) Biological and chemical sulfide oxidation in a Beggiatoa inhabited marine sediment. *ISME Jour.* **1**, 341-353.

Pritchard D.W. (1952) Salinity distribution and circulation in the Chesapeake estuarine system. *J Mar Res*. **11**, 106-123.

Pyzik A.J. and Sommer S.E. (1981) Sedimentary iron monosulfides: kinetics and mechanism of formation. *Geochim. Cosmochim. Acta* **45**, 687–698.

Ramsing N.B., Fossing H., Ferdelman T.G., Andersen F., and Thamdrup B. (1996) Distribution of bacterial populations in a stratified fjord (Mariager Fjord, Denmark) quantified by in situ hybridization and related to chemical gradients in the water column. *App. Environ. Microbiol.* **63**, 1391-1404.

Rickard D. and Luther III G.W. (1997) Kinetics of pyrite formation by the H_2S oxidation of iron (II) monosulfide in aqueous solutions between 25 and 125ºC: The mechanism. *Geochim. Cosmochim. Acta* **61,**135-147.

Rimmer, A., Ostrovsky I., Yacobi Y.Z. (2008) Light availability for *Chlorobium phaebacteroides* development in Lake Kinneret. *J Plank Res.* **30**, 765-776.

Roden E.E. and Tuttle J.H. (1992) Sulfide release from estuarine sediments underlying anoxic bottom water. *Limnol. Oceanogr.* **34**, 725-738.

Roden E.E. and Tuttle J.H. (1993) Inorganic sulfur cycling in mid and lower Chesapeake Bay sediments. *Mar Ecol Prog Ser.* **93**, 101-118.

Rozan T.F., Theberge S.M., and Luther III G.W. (2000) Quantifying elemental sulfur (S^0), bisulfide (HS^-) and polysulfides (Sx^{2-}) using a voltammetric method. *Geochim. Cosmochim. Acta* **415**, 175-184.

Sarradin, P.M., Lannuzel D., Waeles M., Crassous P., Le Bris N., Caprais J.C., Fouquet Y., Fabri M.C., and Riso R. (2008) Dissolved and particulate metals (Fe, Zn, Cu, Cd, Pb) in two habitats from an active hydrothermal field on the EPR at 13°N. *Sci Total Environ.* **392**, 119-129.

Schidlowski M. (1988) A 3800-million-year isotopic record of life from carbon in sedimentary rocks. *Nature* **333**, 313–318.

Scully M.E. (2010) Wind Modulation of Dissolved Oxygen in Chesapeake Bay. *Estuaries Coasts* **33**, 1164–1175.

Sleep N.H. and Bird D.K. (2008) Evolutionary ecology during the rise of dioxygen in the earth's atmosphere. *Phil. Trans. R. Soc. B* **363**, 2651-2664.

Stookey L.L. (1970) Ferrozine---a new spectrophotometric reagent for iron. *Anal Chem.* **42**, 779-781.

Tagliabue A., Bopp L., Dutay J.C., Bowie A.R., Chever F., Jean-Baptiste P., Bucciarelli E., Lannuzel D., Remenyi T., Sarthou G., Aument O., Gehlen M., Jeandel C. (2010) Hydrothermal contribution to the oceanic dissolved iron inventory. *Nature Geosci* **3**, 252-256.

Thamdrup B., Finster K., Hansen J.W. and Bak F. (1993) Bacterial Disproportionation of Elemental Sulfur Coupled to Chemical Reduction of Iron or Manganese. *Appl. Environ. Microbiol.* **59**, 101-108.

Thauer R.K., Jungermann K., Decker K. (1977) Energy conservation in chemotrophic anaerobic bacteria. *Bacterol Rev.* **41**,100-180.

Thompson G., Humphris S.E., Schroeder B., Sulanowska M. (1988) Active vents and massive sulfides at 26°N (TAG) and 23°N (Snakepit) on the Mid-Atlantic Ridge. *Can Mineral.* **26**, 697–711.

Tivey M.K (2007) Generation of Seafloor Hydrothermal Vent Fluids and Associated Mineral Deposits. *Oceanography*. **20**, 50-65.

Tonolla M., Peduzzi S., Hahn D., and Peduzzi R. (2003) Spatio-temporal distribution of phototrophic sulfur bacteria in the chemocline of meromictic Lake Cadagno (Switzerland). *Microb Ecol.* **43**, 89-98.

Van Gemerden H. (1986) Production of elemental sulfur by green and purple sulfur bacteria. *Arch Microbiol.* **146**, 52-56.

Wahlund, T. M., C. R. Woese, R. W. Castenholz, and M. T. Madigan. 1991. A thermophilic green sulfur bacterium from New Zealand hot springs, Chlorobium tepidum sp.-nov. *Arch Microbiol.* **156**, 81-90.

Webb S.M., Tebo B.M., Barger J.R. (2005) Structural Influences of Sodium and Calcium Ions on the Biogenic Manganese Oxides Produced by the Marine Bacillus Sp., Strain SG-1. Geomicrobiol l **22**, 3-4.

Wigginton N.S., Haus K. L., and Hochella M.F. (2007) Aquatic environmental nanoparticles. *J Environ Monitor*, **9**, 1306-1316.

Yao W, Millero F.J. (1993) The rate of sulfide oxidation by δMnO_2 in seawater. *Geochim Cosmochim Acta* **57**, 3359–3365.

Yao W. and Millero F.J. (1996) Oxidation of hydrogen sulfide by hydrous Fe(III) oxides in seawater. *Mar Chem* **52**, 1-16.

Yücel M., Gartman A., Chan C.S., Luther III G.W. (2011) Hydrothermal vents as a kinetically stable source of iron-sulphide-bearing nanoparticles to the ocean. *Nature Geosci* **4**, 367-371.

Zerkle A. L., Kamyshny A., Kump L. R., Farquhar J., Oduro H. and Arthur M. A. (2010) Sulfur cycling in a stratified euxinic lake with moderately high sulfate: Constraints from quadruple S isotopes. *Geochim. Cosmochim. Acta* **74**, 4953-4970.

Zopfi J., Ferdelman T. G., Jørgensen B. B., Teske A. and Thamdrup B. (2001) Influence of water column dynamics on sulfide oxidation and other major biogeochemical processes in the chemocline of Mariager Fjord (Denmark). *Mar. Chem.* **74**, 29-51.

Zopfi J, Ferdelman T.G., and Fossing H. (2004) Distribution and fate of sulfur intermediates—sulfite, tetrathionate, thiosulfate, and elemental sulfur—in marine sediments in Amend, J.P., Edwards, K.J., and Lyons, T.W., eds., Sulfur biogeochemistry—Past and present: Boulder, Colorado, Geological Society of America Special Paper 379, p. 97–116.

Zuber, H. and Cogdell, R.J. (1995) Structure and organization of purple bacterial antenna complexes. In: Anoxygenic Photosynthetic Bacteria (R.E. Blankenship, M.T. Madigan and C.E. Bauer, eds), Advances in Photosynthesis, Vol. 2, pp. 315–348. Kluwer Academic Publishers, Dordrecht.

Chapter 2

TRACE METAL CONCENTRATION AND PARTITIONING IN THE FIRST 1.5 METERS OF HYDROTHERMAL VENT PLUMES ALONG THE MID-ATLANTIC RIDGE: TAG, SNAKEPIT, AND RAINBOW

Abstract

In order to determine the significance of metal fluxes from hydrothermal vents, understanding the speciation, reactivity, and possible transformations of metals and metal sulfides within the hydrothermal plume is critical. In this study, we measure the concentration and partitioning of trace metals (Fe, Mn, Cu, Cd, Co, Pb, Ni) as well as sulfide phases and silicon within the first 1.5 meters of the rising plume at three vent fields (TAG, Snakepit, and Rainbow) along the Mid-Atlantic Ridge. A combination HCl/HNO_3 leaching method was used to differentiate metals present in metal mono-sulfides from those in pyrite and chalcopyrite. At all three vent sites, Mn, Si, and Fe are primarily in the < 0.2 μm (filtered) portion, while Cu, Co, Cd, and Pb are mainly in the unfiltered fraction. At TAG and Snakepit copper is correlated with cobalt, and zinc is correlated with cadmium and lead. At Rainbow, zinc, cadmium and lead are correlated, but copper and cobalt are not correlated. These data are consistent with a lower sulfide to metal ratio found at Rainbow. Significant concentrations of HNO_3-extractable metals were found in the < 0.2 μm fraction at all three vent sites.

2.1 Introduction

Hydrothermal activity, widespread along plate boundaries, results in large fluxes of metals emitted from vents into the surrounding seawater. These metals have potential impact on both the local and global scales and could influence the trace metal budget of the oceans (Butterfield et al., 2003; Tagliabue et al., 2010). The trace metal content of end-member vent fluid varies between vents, dependent on the composition of the rock in which the hydrothermal circulation occurred, as well as the temperature, redox condition, pH, and concentration of inorganic ligands such as sulfide and chloride (Metz and Trefry, 2000).

Minerals form when this metal-rich, hot, and highly reduced vent water mixes with cold, partially oxygenated ocean bottom water (Haymon, 1983). Previous research has demonstrated that there are two main phases of metal precipitation within the hydrothermal plume. Initially, metal sulfides form, and later, as the plume becomes more oxic, iron oxides precipitate, scavenging metals and oxyanions on to their surfaces. Within the rising plume, decreasing temperature and increased mixing of seawater with vent fluid are instrumental in controlling the distribution of metal sulfides and trace metals. The temperature change affects the solubility of many minerals (Seyfried and Ding, 1995), and mixing alters the pH of the solution. The higher pH induces the precipitation of metal sulfide minerals (Rickard, 1995).

Until recently, the predominant assumption has been that most metals emitted from vents thus precipitate either as sulfide or oxide minerals, settling out in a radius of a few kilometers surrounding the hydrothermal vent site (Feely et al., 1987; Mottl et al., 1990), which lead to the conclusion that vents do not contribute significant quantities of transition metals to the oceans. More recent research; however, suggests that metals, specifically iron, may be stabilized either as complexes with organic molecules (Bennett et al., 2008; Sander and Koscinsky, 2011) or as nanoparticulate metal sulfides such as pyrite, which may incorporate other metals into its structure (Yücel et al, 2011) and is a common component of hydrothermal emissions (Gartman et al., 2014). Nano-scale particles would settle from the water column at rates of only a meter or two per year, giving them the opportunity to escape the area immediately surrounding the vent field (Yücel et al, 2011). Additionally, nanoparticulate metal sulfides do not oxidize rapidly under standard conditions (Rozan et al., 2000, Luther and Rickard, 2005), and at typical ocean bottom water temperatures of 2-4 ºC oxidative processes would be approximately four times slower. Pyrite in particular oxidizes very slowly due to the stable low spin electronic configuration of ferrous iron when bound to the S_2^{2-} ligand (Luther, 1990; Gartman and Luther, 2014).

In order to understand the potential impact of hydrothermal venting as a source of trace metals to the greater oceans, the size distribution and mineral speciation of trace metals in the rising plume must be considered. Previous studies at the Mid-Atlantic Ridge (MAR) have characterized trace metal distribution and mineralogy in end-member fluid (Charlou et al., 2002; Douville et al., 2002), in the rising plume 10-150 meters from the top of the TAG mound (Rudnicki and Elderfield, 1993) and into the neutrally buoyant plume (> 300 m above the vent site) (Trefry et al 1985; German 1991; Ludford et al., 1996; Edmonds et al., 2004). These studies are fundamental to determining the chemical composition of the vent fluid, and the types of particles that are dispersed from the immediate vicinity of venting. However, there is a paucity of information about an integral component: processes that occur in the initial stages of seawater mixing in the rising plume, within the first few hundred centimeters from the vent orifice.

The initial stage of the buoyant plume, characterized by very steep physical and chemical gradients between vent and seawater, is of particular importance because the formation of most minerals will occur near the vent source, with 50-60 % seawater mixed with the vent fluid (Klevenz et al., 2011). In Gartman et al. (2014) the geochemistry of the < 0.2 µm fraction of iron in hydrothermal fluid and within the first meter of the orifice was investigated. Nanoparticulate pyrite was found to be a significant component of < 0.2 µm iron at the Rainbow, TAG, and Snakepit vent sites (up to 5 % of < 0.2 µm iron). In the study presented here, we present measurements of trace metal and sulfide concentration and speciation in < 0.2 µm and unfiltered samples taken from the vent fluid and within the first 1.5 meters of the rising plume at those same three vent sites along the Mid-Atlantic Ridge. We consider the separation of metals into four different fractions: unfiltered and < 0.2 µm HCl and HNO_3 extractable metals, and consider differences in metal partitioning between the three sites.

2.1.1 Study Sites

The Trans-Atlantic Geotraverse (TAG), Snakepit, and Rainbow vent sites (Figure 2.1) were sampled along the Mid-Atlantic Ridge, a slow spreading plate boundary moving at rates less than 3 cm/year (Schmidt et al., 2007). The vent fluid at these three sites has the highest trace metal content of vent fields along the MAR (Douville et al., 2002).

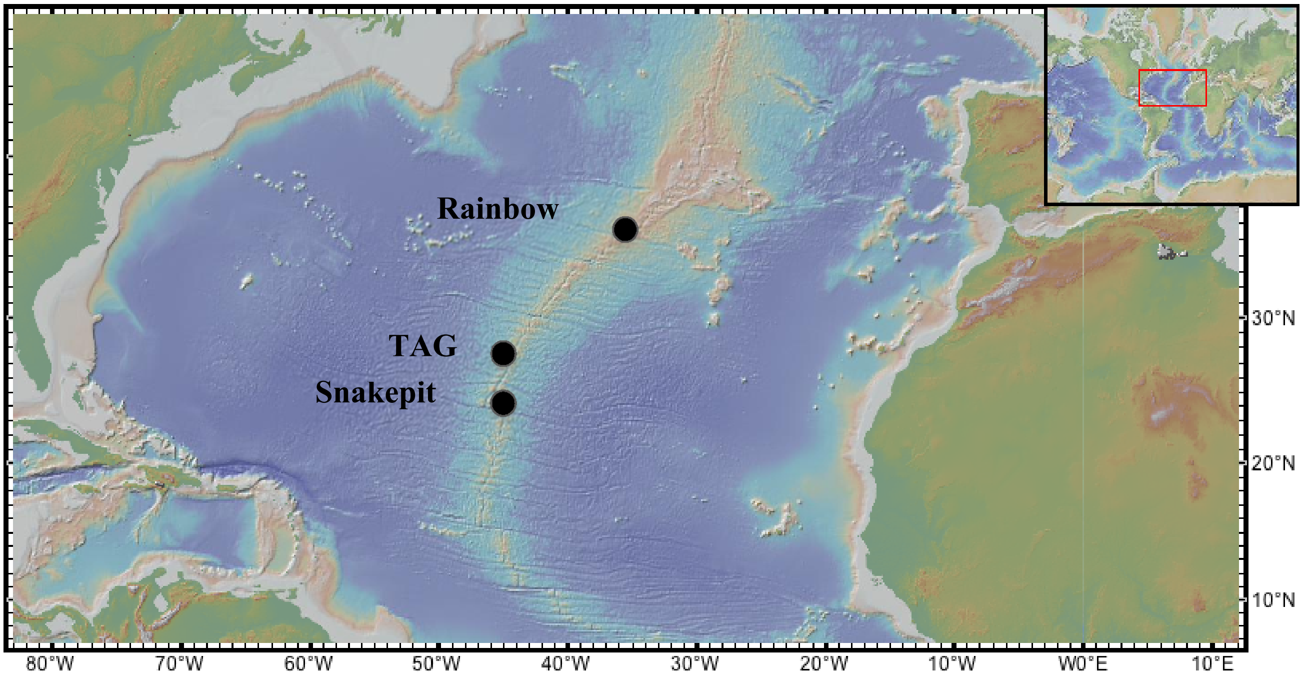

Figure 2.1 Map showing the location of the vent sites visited along the MAR. Map courtesy of http://www.geomapapp.org.

The TAG vent field (26˚ 8’ N, 44˚ 50’ W) lies at a depth of 3620 m on a mound 200 meters wide by 50 m high, and contains high temperature (360-364 ºC) black smokers (Hannington et al., 1995) that are clustered together. The lower temperature (265-300 ºC) white smokers observed previously have since become extinct (Gartman et al., 2014). The heat source at TAG is approximately 1000 m deeper than that of other MAR vent fields (Crawford et al., in Rona, 2010). At TAG, movement of the neutrally buoyant plume is primarily influenced by the tides (Edmonds et al., 2003).

The Snakepit vent field (23˚ 22’ N, 44˚ 57’ W), at 3460 m depth, is a massive sulfide deposit comprised of black smokers (Crawford et al., 2010). TAG and Snakepit represent basalt hosted vent fields of deeper water depths and higher pressures where phase separation does not occur. The black smokers at Snakepit have been named previously (Lalou et al., 1993), and samples were taken from the Moose (23 22.14 N, 44 57.07 W) and Beehive (23 22.12 N, 44 57.13 W) vents.

The Rainbow vent field (36˚ 14’ N, 33˚ 54’ W), located 2310 m deep, is comprised of serpentinised peridotite and contains high temperature vents (up to 365 ºC) that are characterized by low shipboard pH (2.8), low sulfide, and Fe concentrations and order of magnitude higher than those at TAG and Snakepit (Douville et al., 2002; Gartman et al., 2014; this work). Vent fluid from Rainbow has a uniform composition, indicating that it comes from a single source (Charlou et al., 2002). Chloride concentrations are elevated as a result of phase separation, which concentrates the fluid to brine and increases metal solubility (Desbruyeres et al., 2001). The vent fluid at Rainbow is high in organics, which is significant because capping by organics is a potential stabilization mechanism for nanoparticles (Lau and

Kim, 2008; Wang et al., 2009; Mullaugh and Luther, 2010). Bulk pyrite deposits at Rainbow show high degrees of trace metal substitution for iron, and contain large quantities of copper, zinc, and cobalt (Marques et al., 2007). Dispersion of the neutrally buoyant plume, and further transport of hydrothermally emitted species at Rainbow is primarily driven by bottom water currents (Edmonds et al., 2003).

2.2 Methods

2.2.1 Sample Collection

Field studies along the Mid-Atlantic Ridge were conducted aboard the R/V *Knorr* from 16 October until 9 November 2012. All end-member vent and rising plume samples at the Mid-Atlantic Ridge were taken by the Remotely Operated Vehicle (ROV) Jason II using Titanium Major Samplers. In order to obtain samples, the pilots of the ROV Jason II placed the nozzle of the sampler into the vent orifice. Depending upon where in the plume the sample was collected, once either shimmering fluid or black smoke was observed emitting from the sampler, the sample was taken. For samples within the chimney orifice, sample collection was conducted directly after taking the temperature of the vent fluid within the orifice using the high temperature probe supplied by Jason. For rising plume samples, the Jason pilot held the Major in one manipulator and the temperature probe in the other. Onboard ship, samples taken higher in the plume were observed to be darker with particles than those taken nearer to the orifice.

Upon recovery of the samples on board the ship, the pH of the fluid was measured, and subsamples were taken from the Major Sampler to preserve for analysis of metals and sulfur species in both unfiltered and filtered (through a 0.2 µm filter) fractions. Throughout this paper, the unfiltered fraction contains particles and dissolved species, and the < 0.2 µm filtered fraction contains (nano)particles < 0.2 µm and dissolved species.

2.2.2 Metals Analysis

Leaching procedure

Metals in soluble metal sulfides were differentiated from metals associated with pyrite using the HCl/HNO_3 acid leach method of Huerta-Diaz and Morse (1992) as detailed in Yücel et al. (2011) and Gartman et al. (2014). Both filtered (0.2 µm) and unfiltered sub-samples were taken from the Major Samples and each sample was split into two and put in clean falcon tubes. One portion was fixed with concentrated trace metal clean HCl and the other HNO_3. Both fractions were allowed to sit for at least eight hours prior to analysis. Fe-measurements were conducted shipboard at this time, and the remaining sample was frozen for analysis of other trace metals upon return to shore. Nitric acid is used as an oxidizing acid capable of dissolving minerals with a pyrite structure (pyrite or chalcopyrite), which are not soluble in HCl.

Fe measurements

Iron measurements of both unfiltered and filtered HCl and HNO_3 treated samples were taken shipboard using a UV-VIS absorbance at 562 nm and the ferrozine method of Stookey (1979). Samples were buffered in 2.5 M ammonium acetate prior to addition of the ferrozine reagent. After the initial analysis, the samples were treated with hydroxylamine hydrochloride as a reducing agent in order to measure total iron. Fe^{3+} was determined by the difference between these numbers; however, no Fe^{3+} was detectable in any of our samples.

Trace metals

Magnesium (Mg), manganese (Mn), copper (Cu), cobalt (Co), zinc (Zn), cadmium (Cd), lead (Pb), and nickel (Ni) were measured in samples using a Thermo Electron Corporation Finnigan Element XR Inductively Coupled Plasma Mass Spectrometer (ICP-MS) at low resolution. Prior to analysis, samples that had been acidified, leached and frozen shipboard were allowed to sit for a minimum of 8 hours to separate refractory phases (particles not dissolved by acid leaches) prior to subsampling for analysis. Subsamples were diluted 100 times in a solution of 5.2 nM iridium in 2 % Ultrex® nitric acid and 18 megaohm water (Barnstead). Preparation of the dilutions and analysis with the mass spectrophotometer were conducted under trace metal clean conditions. Samples were calibrated using an internal standard based on instrument response for replicate mixed standards. The response was normalized using the ratio between the counts for each metal and those for the internal standard of iridium in which the samples were diluted.

2.2.3 Silicon Measurements

Silicon was analyzed on a Thermo Intrepid II XSP Inductively Coupled Plasma Atomic Emission Spectrometer (ICP-AES) at 212 nm. The detection limit was 1.67 µM silicon. A standard curve was prepared with NIST traceable commercial stock in a 2 % HNO_3 matrix (same as the diluted samples). Ytrium (0.51 mM) was used as an internal standard. Samples were allowed to defrost for 3 days in order to eliminate polymerization (Kobayashi, 1967) before making dilutions in 18 megaohm water (MilliQ).

2.2.4 Sulfide Measurements

Acid volatile sulfide (AVS) and chromium reducible sulfide (CRS) were measured using the method of Fossing and Jøregensen (1989) after shipboard fixation and storage. To prepare the samples, 2 mL of 0.5 M NaOH and 5 mL of 0.1 M zinc acetate were added to 5 mL of sample to fix free sulfide and FeS sulfide as ZnS. Both unfiltered and 0.2 µm filtered samples were fixed, and the samples were immediately frozen and stored at -20 ºC. Prior to analysis onshore, samples were thawed and added to deoxygenated glass reaction vessels. Then, five mL of 3 M HCl were added to liberate the fixed sulfide as H_2S gas. After 1.5 hours of purge and trap, sulfide gas from the AVS portion was trapped as HS^- in 10 mL of anoxic 0.1 M trace metal clean

NaOH (Wu and Boyle, 1998) in a glass test tube, and the NaOH solution was analyzed on a hanging mercury drop electrode (HMDE) controlled by an AIS DLK-100A potentiostat. Sulfide was monitored at a potential of -0.6 V versus a saturated calomel electrode. In order to extract the CRS fraction, fresh NaOH was added to new test tubes, purged, then 4 mL acidified Cr(II) were injected into the reaction vessels. Cr(II) was prepared by reducing a Cr(III) solution on an amalgamated zinc column. After the addition of Cr(II), the mixture was allowed to purge and trap H_2S for an hour, then the NaOH containing trapped sulfide was again analyzed on the HMDE.

2.2.5 SEM/EDS

Samples of preserved filters from both the hot vent fluid and the buoyant plume were imaged using a scanning electron microscope. Samples were prepared by filtering 30 mL of vent fluid through a 0.2 μm Nuclepore filter, rinsed with deionized water to remove seawater salt, and dried under a flow of argon gas. Once dried, the filters were then attached to aluminum stubs with carbon paint and stored in petri dishes. Prior to analysis on the SEM both the filters and stubs were carbon coated with a Bench top Turbo III Denton Vacuum with a cold sputter module.

Imaging and elemental analyses were conducted on a Hitachi S-4700 scanning electron microscope located in the Delaware Biotechnical Institute in Newark, DE using Inca analysis software. Micrographs were taken using the Ultra-High resolution mode at 3 kV and 25 μA. Analysis and elemental mapping with an Energy Dispersive x-ray Spectrometer (EDS) equipped with an Oxford Inca X-act detector were done under Analysis mode, at 15 kV and 25 µA.

2.3 Results

2.3.1 Composition of End-member Vent Fluid

The concentration of magnesium in the 0.2 µm filtered samples is used as a proxy to measure the extent of mixing between vent fluid and ambient seawater in the rising plume. End-member vent fluid has Mg concentrations of 0 mM (Edmond et al., 1982), and end-member seawater has a Mg concentration of 53 mM. Once the magnesium concentration for each sample is known, it is then possible to calculate the percentage of seawater that has been entrained in the vent fluid as the plume rises, and to correct concentrations for this dilution (von Damm et al., 1985). The calculated concentrations of metals for end-member solutions (Mg=0) are reported in Table 2.1. These values are calculated only for samples taken from within the vent orifice.

Table 2.1 Calculated trace metal, silicon, and sulfide concentrations for end-member vent fluid (Mg=0). Concentrations obtained from the unfiltered nitric acid portion of vent-fluid samples were used for the calculation. pH is the value measured on the ship. Sulfide is from the sum of unfiltered AVS and unfiltered CRS. *SP-1 through SP-5 are from the Beehive vent. SP-6 is from Moose.

Vent Field	Sample	Shipboard pH	[Sulfide] (μM)	[Si] (mM)	[Fe] (mM)	[Mn] (μM)	[Co] (μM)	[Ni] (μM)	[Cu] (μM)	[Zn] (μM)	[Cd] (nM)	[Pb] (nM)
Rainbow	RB-1	5.34	368	3.50	23.9	1026	10.5	27.5	117	204	872	2108
	RB-2	2.87	954	3.09	23.7	1299	12.3	3.90	29.2	86.2	428	1216
	RB-3	3.16	498	3.02	25.3	1529	18.1	2.23	5.24	18.6	56.5	111
	RB-4	3.28	1030	3.95	27.6	1646	17.4	5.04	22.0	67.5	282	880
	RB-5	4.65	1180	2.16	20.6	1220	18.7	3.29	0.196	1.04	5.73	42.3
TAG	TAG-1	3.01	3500	8.27	5.74	415	1.94	4.09	14.4	26.8	124	371
	TAG-2	3.2	462	8.09	5.71	376	1.62	2.27	8.07	18.4	90.6	286
	TAG-3	3.03	3640	8.12	5.77	466	2.09	2.67	10.1	27.5	121	332
	TAG-4	4.36	4380	17.9	11.0	1320	2.20	11.9	13.6	50.4	229	511
	TAG-5	4.8	2900	9.18	5.83	367	2.15	4.22	13.9	29.7	142	388
	TAG-6	2.98	3610	7.92	5.54	418	2.08	2.54	12.4	27.1	123	342
	TAG-7	4.15	6280	15.4	10.3	755	2.80	4.14	19.6	42.2	195	684
	TAG-8	5.11	6250	24.9	13.4	1350	2.56	15.8	11.3	37.4	171	619
	TAG-9	4.56	4020	4.88	5.52	525	1.86	2.87	13.1	27.6	125	442
	TAG-10	4.92	2300	9.89	5.07	1030	1.01	11.2	6.95	12.8	66.8	214
	TAG-11	3.38	6370	7.00	4.75	363	1.45	2.35	19.2	19.9	104	274
Snakepit	SP-1	5.17	2710	4.94	0.991	210	5.01x10^{-3}	2.55	0.116	1.55	15.1	51.0
	SP-2	4.42	5110	8.84	3.50	349	0.198	3.02	3.40	30.0	213	939
	SP-3	3.22	4720	7.91	3.14	330	7.12x10^{-2}	1.46	1.05	14.0	103	476
	SP-4	3.45	6170	8.26	4.05	285	5.16x10^{-2}	0.937	1.35	28.1	183	700
	SP-5	3.29	4400	8.03	3.70	356	0.199	1.14	1.80	24.1	152	584
	SP-6*	3.19	1540	8.79	4.02	377	0.370	1.21	4.88	25.2	181	804

The total metal concentrations that we report for vent fluid in Table 2.1 are within an order of magnitude or less of those previously reported for these vent sites (Desbruyeres et al., 2001; Douville et al., 2002; Charlou et al., 2002). Copper is a notable exception, with concentrations an order of magnitude lower than previously measured values, and will be discussed below in section 3.5.3. Metal to sulfide ratios (M:S) were calculated for each vent site as an average for all samples using the sum of the chalcophile elements (Fe, Co, Ni, Cu, Zn, Cd, Pb) to total AVS. Rainbow has a M:S of 31.2 ± 16, TAG has M:S 1.88 ± 1.1, and Snakepit has M:S 1.94 ± 2.7. Metal concentrations are higher and sulfide concentrations are lower at Rainbow than at TAG or Snakepit due to the ultramafic, rather than basaltic, rocks surrounding the vent site (Charlou et al., 1997). Nickel concentrations are similar at all three sites.

2.3.2 Effect of Seawater Mixing on Unfiltered Trace Metals

2.3.2.1 TAG

Figure 2.2a shows the relationship between< 0.2 μm and unfiltered trace metals and < 0.2 μm (filtered) magnesium at TAG for all nitric acid treated samples. All metals except for nickel decrease in concentration with increasing seawater dilution (r^2 values > 0.57). Iron and manganese are both present predominately in the < 0.2 μm fraction, whereas Cu and Co are mainly present in the unfiltered fraction. Zinc, cadmium, and lead are also mainly particulate; however with increased seawater mixing and increased distance from the orifice the percentage of the metal in the < 0.2

μm fraction increases. This increase may occur as larger particles settle more rapidly than smaller ones, and also indicates that there is very little particle growth in the buoyant plume. If particle growth were occurring, the fraction of particulate material would increase with distance from the orifice, particularly in the first meter where venting is still focused enough to keep larger particles suspended (Converse et al., 1983). The decreasing percentage of particulates observed in our data across all three vent sites indicates that nanoparticulate minerals and dissolved metals persist within the first 1.5 meters of the plume.

Figure 2.2 Metal correlations with filtered Mg at (a) TAG and (b) Snakepit from samples extracted samples. Iron data from Gartman et al. (2014). For clarity in the discussion (Section 4.1) an estimate of temperature is given on the upper x-axis based on an approximation between seawater mixing and temperature. Note that for Cu, Zn, Pb, and Cd the filtered concentration in presented on the right y axis.

(a) TAG

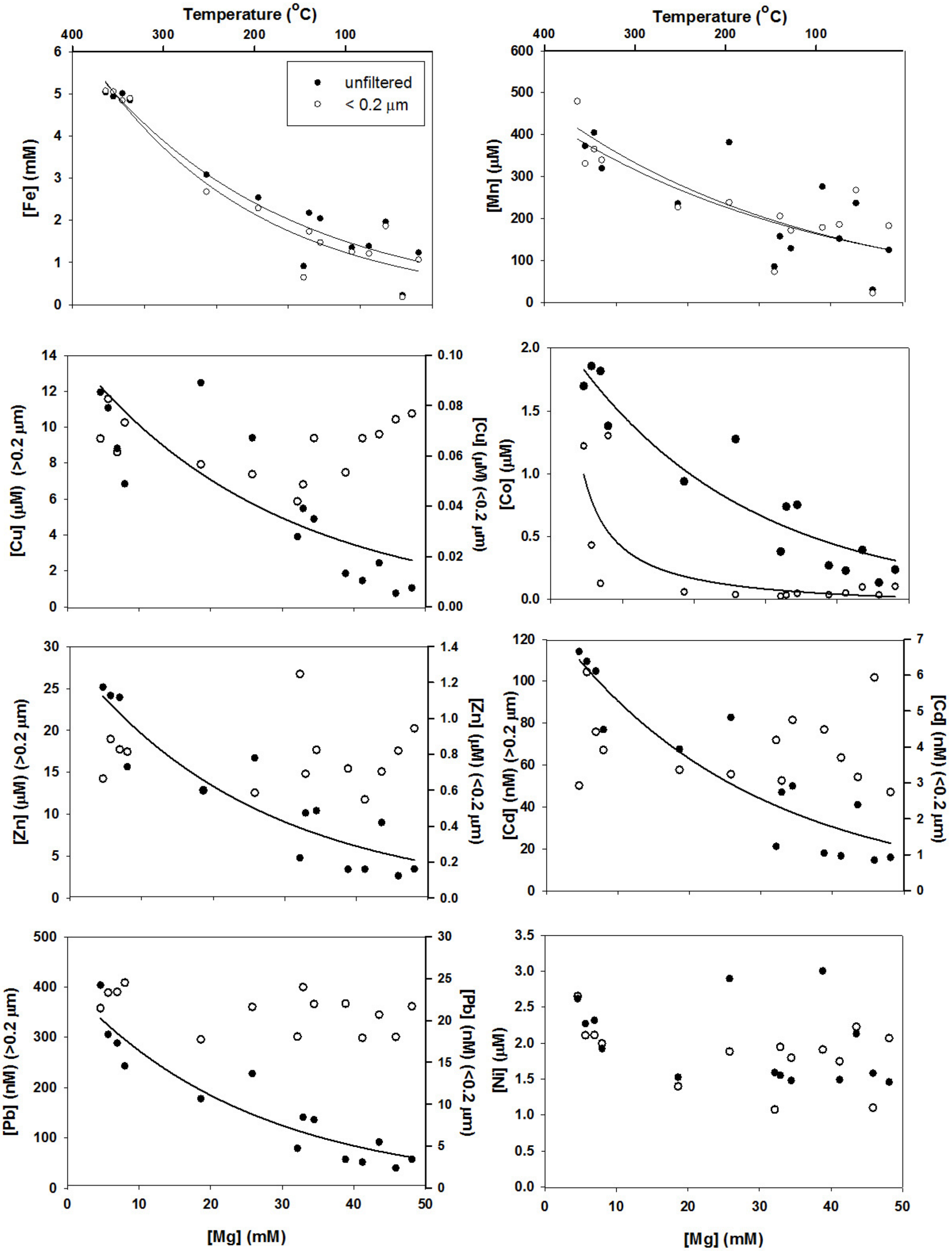

Temperature (°C)
400
300
200
100
[Fe] (mM)
unfiltered
< 0.2 µm
[Mn] (µM)
[Cu] (µM) (>0.2 µm)
[Cu] (µM) (<0.2 µm)
[Co] (µM)
[Zn] (µM) (>0.2 µm)
[Zn] (µM) (<0.2 µm)
[Cd] (nM) (>0.2 µm)
[Cd] (nM) (<0.2 µm)
[Pb] (nM) (>0.2 µm)
[Pb] (nM) (<0.2 µm)
[Ni] (µM)
[Mg] (mM)
[Mg] (mM)

(b) Snakepit

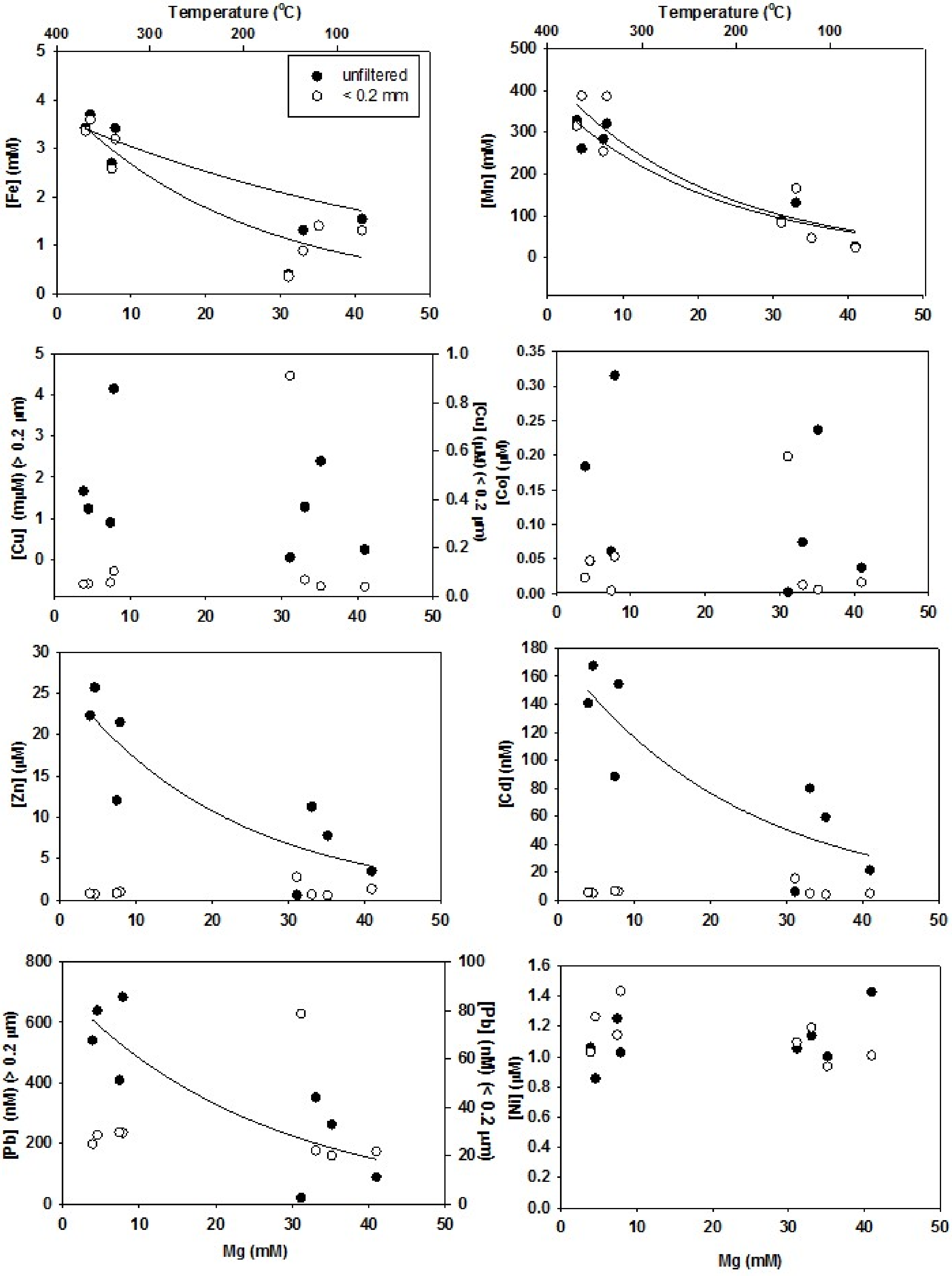

Temperature (°C)
400
300
200
100
[Fe] (mM)
unfiltered
< 0.2 mm
[Mn] (mM)
[Cu] (mμM) (> 0.2 μm)
[Cu] (μM) (< 0.2 μm)
[Co] (μM)
[Zn] (μM)
[Cd] (nM)
[Pb] (nM) (> 0.2 μm)
[Pb] (nM) (< 0.2 μm)
[Ni] (μM)
Mg (mM)
0
10
20
30
40
50

2.3.2.2 Snakepit

Figure 2.2b shows < 0.2 µm and unfiltered metal versus < 0.2 µm magnesium concentrations for all nitric acid-extracted samples from Snakepit. Iron, manganese, cadmium, zinc, and lead all decrease as magnesium concentrations increase and seawater is entrained in the vent fluid. Iron and manganese are predominantly present in the < 0.2 µm fraction while copper, cobalt, zinc, cadmium, and lead are in the particulate fraction.

Figure 2.3 shows the partitioning of < 0.2 µm and unfiltered manganese, copper, and zinc for samples taken in the Moose rising plume at Snakepit between the HCl and HNO_3 extractable fractions as well as the percentage of these metals that is present either in the unfiltered fraction or as nanoparticulate/dissolved (< 0.2 µm) entities. Manganese is present predominately in the < 0.2 µm fraction, and only 13 % is particulate in the most well mixed sample (93 % seawater). There is no significant difference between Mn extracted by the HCl and HNO_3 leaches.

Copper is mainly in the unfiltered fraction. Although the majority of copper remains in the unfiltered fraction, the < 0.2 µm fraction increases from 2.5-16 % with seawater mixing. Copper is extracted by nitric acid, and not HCl, consistent with its incorporation into pyrite or chalcopyrite.

The fraction of zinc that is particulate decreases from 95-61 % as the plume rises and mixes with seawater. Zinc is extracted in the HCl leach, which is expected because ZnS dissolves in HCl and ZnS_2 has not been observed in the environment.

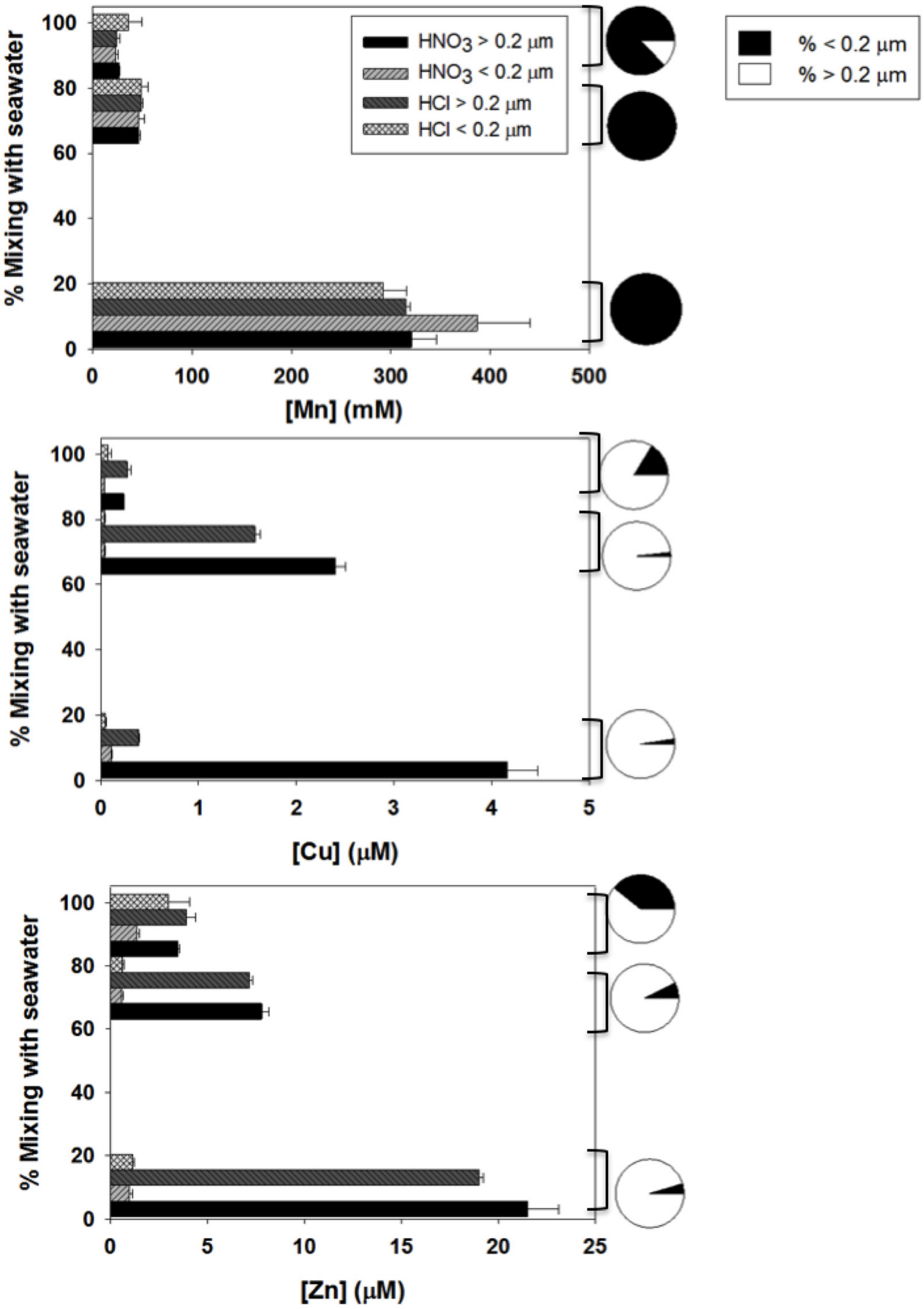

HNO3 > 0.2 µm
HNO3 < 0.2 µm
HCl > 0.2 µm
HCl < 0.2 µm
% < 0.2 µm
% > 0.2 µm
% Mixing with seawater
0
20
40
60
80
100
0
100
200
300
400
500
[Mn] (mM)
% Mixing with seawater
0
20
40
60
80
100
0
1
2
3
4
5
[Cu] (µM)
% Mixing with seawater
0
20
40
60
80
100
0
5
10
15
20
25
[Zn] (µM)

Figure 2.3 Partitioning of Mn, Cu, and Zn in the buoyant plume at Snakepit (11, 73, 93% SW) between HCl and HNO_3 extractable fractions, and the percentage of the metal in each size fraction as the vent fluid mixes with seawater. Mn is mainly in the < 0.2 μm fraction and is soluble in HCl. Copper is mostly particulate and has a significant component that is soluble only in HNO_3. The percentage of zinc that is particulate decreases with seawater mixing, and is soluble in HCl.

2.3.2.3 Rainbow

Table 2.2 gives the concentrations for metals from < 0.2 μm and unfiltered nitric acid treated samples. Iron, cobalt and manganese both decrease with increasing Mg. In the rising plume, iron and manganese remain predominantly in the < 0.2 μm fraction and Co, Cu, Zn, Cd, and Pb are mainly in the unfiltered fraction.

Table 2.2 Concentration of metals at Rainbow in all nitric acid samples.

Sample	Filter	[Mg] (mM)	[Fe] (mM)	[Mn] (μM)	±	[Co] (μM)	±	[Ni] (μM)	±	[Cu] (μM)	±	[Zn] (μM)	±	[Cd] (nM)	±	[Pb] (nM)	±
RB-2	filt	3.72	22.0	1240	110	8.36	0.71	3.63	0.25	0.11	8.0×10^{-3}	0.57	0.041	3.58	0.24	18.5	1.3
	unfilt		22.4	1210	84	11.4	0.83	3.81	0.41	27.1	2.26	80.2	6.6	398	38.4	1130	97
RB-3	filt	4.31	23.3	1130	23	3.43	0.08	2.05	0.25	0.0552	6.8×10^{-3}	12.8	1.6	22.7	2.8	33.4	4.1
	unfilt		21.8	1410	180	16.6	2.0	2.44	0.056	4.81	0.16	17.1	0.47	51.9	2.5	102	3.9
RB-6	filt	9.12	18.4	655	5.8	2.68	0.044	5.24	0.21	0.0779	2.9×10^{-3}	0.824	0.031	4.16	0.15	18.9	0.79
	unfilt		17.6	817	31	11.0	0.39	1.48	0.017	4.13	0.17	12.0	0.69	49.4	9.9	240	20
RB-4	filt	17.7	15.1	1240	50	3.51	0.14	3.35	0.20	0.097	5.0×10^{-3}	0.656	0.035	3.85	0.23	21.3	1.1
	unfilt		15.2	1100	57	11.6	0.60	4.78	0.36	14.6	0.64	44.9	2.3	188	100	586	60
RB-5	filt	28.0	9.27	483	61	0.883	0.12	2.84	0.25	0.0926	0.024	0.490	0.0565	2.70	1.6	20.0	1.4
	unfilt		9.70	575	35	8.83	0.56	1.55	0.13	0.126	0.008	1.10	0.0714	3.92	0.38	24.4	1.5
RB-7	filt	38.4	3.27	208	11	1.63	0.093	2.15	0.16	0.0645	4.8×10^{-3}	0.406	0.030	2.63	0.20	17.1	1.3
	unfilt		3.27	298	23	3.26	0.24	4.32	0.25	20.8	1.28	46.8	2.6	188	11	513	30
RB-1	filt	43.7	4.19	252	7.3	1.71	0.048	2.81	0.093	1.05	0.012	3.24	0.038	17.6	1.2	57.7	0.45
	unfilt		3.80	180	2.3	1.85	0.017	4.82	0.077	20.5	0.94	35.9	0.86	153	7.6	370	11

2.3.3 Sulfur Speciation in the Plume

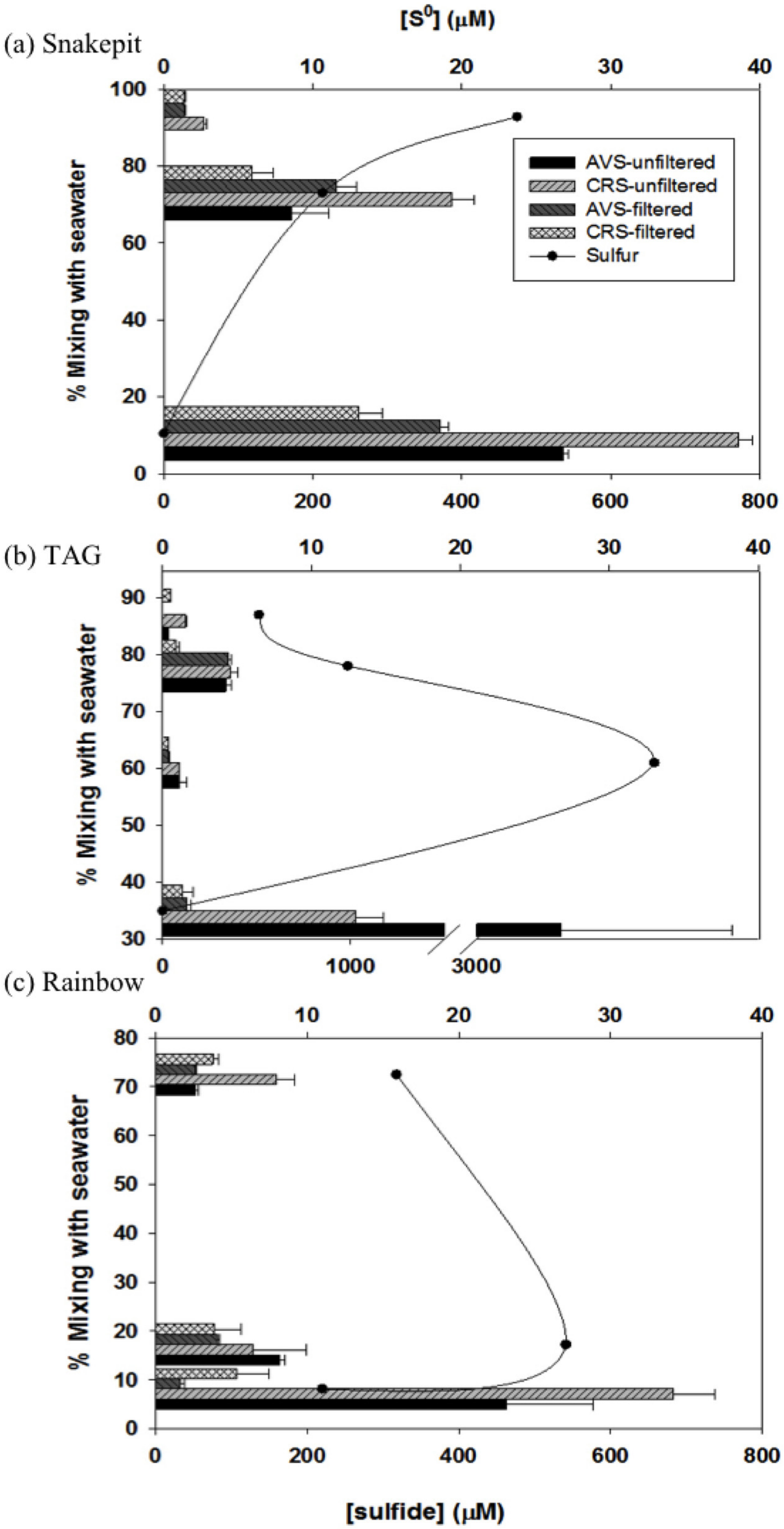

Figure 2.4 Concentrations of filtered and unfiltered AVS/CRS and total elemental sulfur in the rising plume at (a) Snakepit and (b) TAG. Sulfur concentrations from Chapter 3 and methods described therein.

Figure 2.4 shows the distribution of the AVS and CRS sulfide fractions and elemental sulfur in the rising plume at each of the three sites. AVS is composed of H_2S, HS^-, FeS, and other labile metal sulfides (ZnS, CdS, PbS) (Morse and Luther, 1999). CRS is composed of FeS_2 and $FeCuS_2$ (Fossing and Jørgensen, 1989). TAG has the highest measured total sulfide concentration (4130 μM) composed of unfiltered AVS (3110 μM) and CRS (1030 μM) in the hydrothermal fluid. Unfiltered CRS is the dominant sulfide fraction at Snakepit with concentrations up to 771 μM. Rainbow has the lowest total sulfide concentrations of any of the vent sites studied. In an end-member vent sample at Rainbow, (pH of 2.8) unfiltered CRS is the largest fraction at 683 μM, followed by unfiltered AVS (463 μM). With further mixing there is no significant difference between the fractions (Figure. 2.4c). Particulate and nanoparticulate elemental sulfur reported as S^0 were found at all three vent sites at concentrations up to 33 μM (Chapter 3). TAG had the highest concentrations of total elemental sulfur, while Rainbow had the highest concentration of elemental sulfur (12 μM) in the < 0.2 μm fraction. Elemental sulfur is expected to precipitate prior to or during iron sulfide formation (Chadwell et al., 2001), and in vent water dilutions greater than 95 % (Klevenz et al., 2011).

2.3.4 Silicon

Figure 2.5 shows < 0.2 µm and unfiltered silicon concentrations versus < 0.2 µm magnesium for TAG (Figure 2.5a) Snakepit (Figure 2.5b) and Rainbow (Figure 2.5c). Silicon concentrations were correlated with Mg ($r^2 > 0.78$), and were predominately in the < 0.2 µm fraction at all three vent sites. Average calculated endmember (to 0 mM Mg) silicon concentrations were 11.05 ± 5.9 at TAG, 7.8 ± 1.5 at Snakepit, and 3.1 ± 0.66 at Rainbow (see Table 2.1). These concentrations were approximately half those that have been previously reported (Douville et al., 2002); however, silicon concentrations are expected to be variable with time (Von Damm et al., 1995)

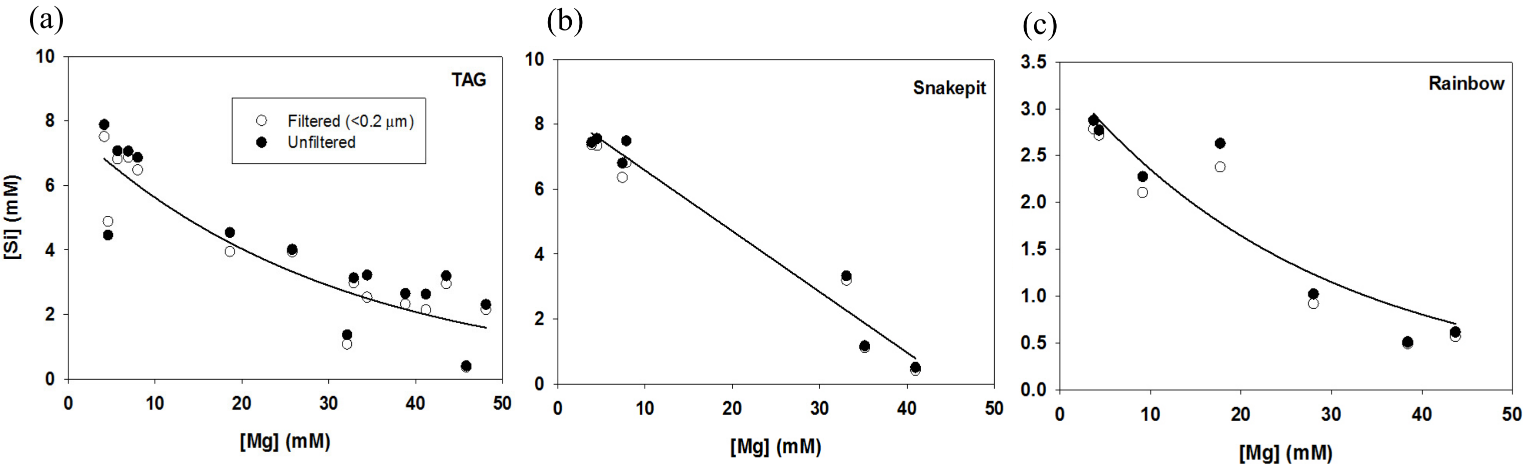

Figure 2.5 Unfiltered and filtered (< 0.2 µm) silicon concentrations from (a) TAG, (b) Snakepit, and (c) Rainbow.

2.3.5 Association of Trace Metals in the Buoyant Plume

Figure 2.6 (a,b,c) shows the correlation between unfiltered copper versus unfiltered cobalt, in the nitric acid treated samples, whereas Figure 2.6 (d,e,f) shows unfiltered zinc versus unfiltered lead, and cadmium at all three sites. At TAG (Figure 6a,d) and Snakepit (Figure 2.6b,e), copper is correlated with cobalt, and cadmium and lead are correlated with zinc, indicating that these metals are co-precipitating. This is significant as unfiltered copper is mainly extracted in the HNO_3 leach, but unfiltered zinc is extracted in HCl, consistent with different metal sulfide phases within the unfiltered fraction of these metals. At Rainbow (Figure 2.6 c,f) cadmium and lead correlate with zinc, but unlike the other two sites copper and cobalt are not correlated. The following section will describe the distribution of these metals in more detail.

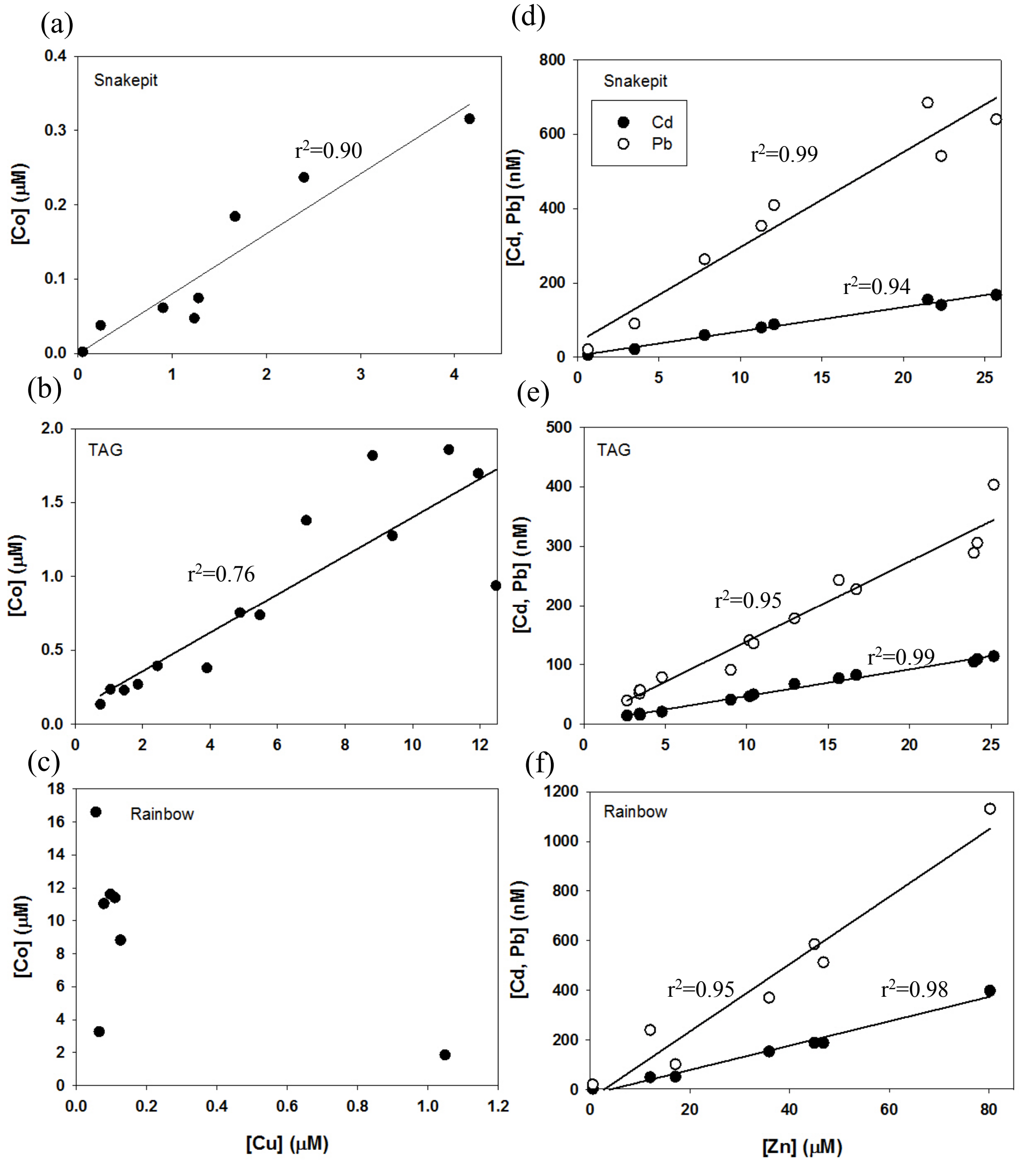

Figure 2.6 Correlation between concentrations of Co and Cu, Zn and Cd, and Zn and Pb at (a, d) Snakepit (b, e) TAG and (c, f) Rainbow (r^2= Co=0.41, Pb= 0.15). Copper and cobalt, and zinc and lead are not correlated at Rainbow. Metal concentrations are from unfiltered, nitric acid treated samples.

2.3.5.1 Iron

In the first 1.5 meters of the plume, iron is mainly present in the < 0.2 μm fraction. Previous study of the iron speciation in these samples demonstrated that the < 0.2 μm < 0.2 μm fraction at all three sites contains pyrite nanoparticles, which may incorporate other metals into their structure (Gartman et al., 2014). Thus, the < 0.2 μm fraction contains not only dissolved Fe^{2+}, but also iron sulfide (FeS, FeS_2) nanoparticles. At TAG, unfiltered copper, zinc, and lead are correlated with unfiltered Fe (Figure 2.7a,b). The correlation between zinc and iron at TAG could be due to simultaneous precipitation of ZnS and iron sulfide particles (Yücel et al., 2011) or incorporation of iron into sphalerite (Scott, 1983). At Snakepit (Figure 2.7c) only manganese and copper are correlated with Fe, and at Rainbow (Figure 2.7d) only manganese and cobalt are correlated with iron. Manganese is correlated with iron at all three sites because both are present mainly in the same fraction (< 0.2 μm). The correlation is not likely due to the precipitation of Fe-Mn phases or adsorption of Mn onto iron oxides as oxidized iron was not detected in any samples taken from the three vent sites. Unfiltered silicon is also correlated with unfiltered iron at all three sites and shown in Figure 2.7; however at Snakepit only the vent fluid samples correlate with iron. The two samples taken from the Moose plume (grey circles, Figure 2.7c) do not follow this relationship, perhaps due to Si precipitation with increasing pH in the rising plume at this site.

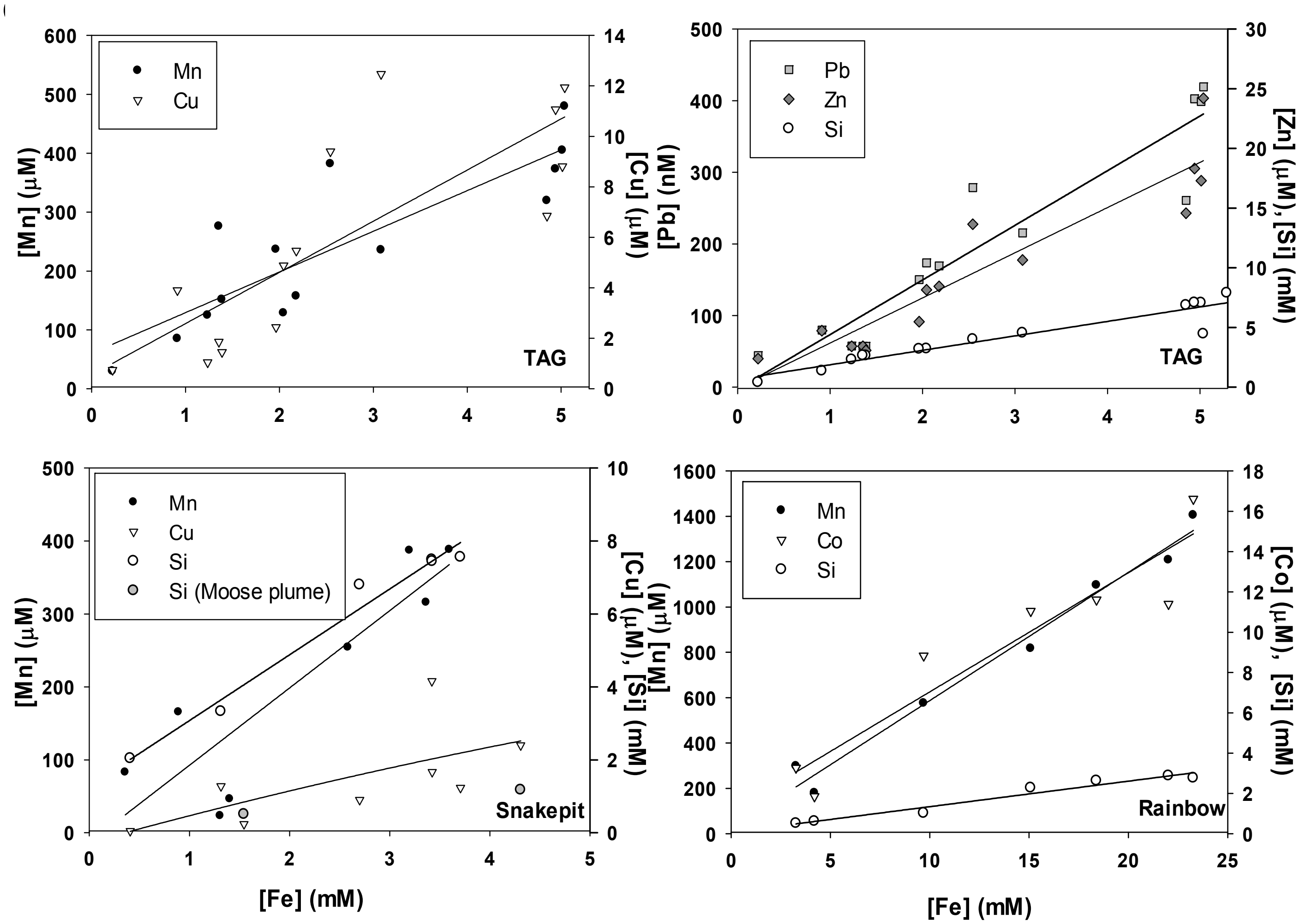

Figure 2.7 Trace metals (unfiltered, HNO_3 leach) and unfiltered silicon correlated to unfiltered iron at (a, b) TAG (r^2 Mn=0.98, Cu=0.88, Zn=0.65, Pb=0.74, Si=0.90) (c) Snakepit (r^2 Mn=0.88, Cu=0.87, Si=0.98) and (d) Rainbow (r^2 Mn=0.78, Cd=0.88, Si=0.96). Copper and cobalt, and zinc and lead are not correlated with unfiltered iron at Rainbow.

The precipitation of metal sulfides may provide a site for further nucleation of pyrite (Yücel et al., 2011, Gartman et al., 2014) because the nucleation of pyrite in acidic (pH < 7) waters below 300 °C is slow (Shoonen and Barnes, 1991; Wilkin and Barnes, 1997). We calculated the maximum rate of pyrite formation in the high temperature fluid at TAG to be 7.7 nmol $L^{-1}s^{-1}$, decreasing to 6.80 x 10^{-5} nmol L^{-1} s^{-1} at 37.6 °C (calculations based on kinetics from Rickard, (1997)). Thus, the nucleation of other metal sulfides may provide energetically favorable surfaces for continued precipitation of pyrite in the plume. Silicates may also form around metal sulfide centers, as was observed in nanoparticles from Lau Basin vent fluid (Gartman et al., 2014).

2.3.5.2 Manganese

Manganese is correlated with iron (Figure 2.7), as both of these elements are present in the < 0.2 μm fraction in the first meter of the plume at all three vent sites. Despite this initial similarity in their behavior, iron is much more reactive than manganese with respect to both oxidation and particle formation: the residence time of Fe in the neutrally buoyant plume is minutes to hours (Field and Sherrell, 2000), but the residence time of manganese is weeks to years (Mandernack and Tebo, 1993). In modeling element behavior and particle formation in the plume, Klevenz et al. (2011) predict low concentrations of Mn in particles, and no precipitation of manganese oxides should occur close to the vents due to slow oxidation kinetics of Mn^{2+} at pH < 9 (Morgan, 2005; Luther, 2010). At all three vent sites, manganese is mainly present in the < 0.2 μm fraction, a result consistent with prior studies (Klinkhammer 1985, Sands et al., 2012).

2.3.5.3 Copper and Cobalt

Unfiltered copper trends with unfiltered iron at TAG and Snakepit (Figure 2.7a,b,c) as it readily precipitates with iron in sulfide minerals such as chalcopyrite ($FeCuS_2$) and is incorporated as a trace constituent into pyrite (FeS_2). Cobalt typically precipitates with copper in chalcopyrite at temperatures greater than 350 °C (Metz and Trefry, 2000). Cobalt is correlated with copper at TAG and Snakepit, but not at Rainbow, and copper and iron are not correlated at Rainbow. The lower sulfide concentrations and higher metal:sulfide ratio at Rainbow means that fewer metals will precipitate as metal sulfide minerals (Klevenz et al., 2011). Unfiltered copper concentrations in our samples are an order of magnitude lower than expected based on the endmember values presented in Douville et al. (2002) and do not correlate to Mg. It is likely that much of the copper has already been precipitated as chalcopyrite at high temperatures within the vent chimney (Seyfried and Ding, 1995; Tivey, 1995) (see Section 2.4.2.1 for discussion). Chalcopyrite was detected via XRD in the TAG hydrothermal fluid (Gartman et al., 2014).

2.3.5.4 Zinc, Lead, and Cadmium

Unfiltered zinc is correlated with both unfiltered cadmium and lead at all three vent sites (Figure 6d, e, f). The unfiltered fraction of Cd and Pb also shows a correlation to < 0.2 μm Mg concentrations at TAG and Snakepit (Figure 2.2). Due to the lower temperature at which ZnS forms, these metals have not been considerably precipitated from the plume, in contrast to Cu, and demonstrate more conservative behavior within the dilution range of our samples. Zn, Cd, and Pb are not correlated with Mg at Rainbow.

2.3.5.5 Nickel

Nickel concentrations show no trend with unfiltered Fe, Mn or < 0.2 μm Mg at any of the vent sites. Trocine and Trefry (1988) reported similar findings in the TAG plume, where Ni did not correlate with Fe, Mn, or total suspended matter. Nickel is not leached in hydrothermal circulation, and is slow to react in mineral formation processes (Morse and Luther, 1999).

2.3.6 Differences in Particle Formation Between Vent Sites

Our data set is unique in that it allows the investigation of possible mineral formation processes and metal partitioning during the early stages of the rising plume, less than 1.5 meters from the vent orifice. Moreover, because similar samples were obtained for three different vent fields we are also able to make inter-site comparisons between the hydrothermal fluid, and processes occurring in the early stages of the plume < 1.5 meter from the vent orifice.

As demonstrated by Figures 2.6 and 2.7, the associations between metals are similar at both TAG and Snakepit, but differ at Rainbow, which suggests that different precipitates are forming in the plumes of each vent site. There are several possible reasons for this observed difference. First, the Rainbow vent fluid contains higher concentrations of chloride (750 mM) than TAG (650 mM) and Snakepit (550 mM) (Douville et al., 2002). Chloride increases the solubility of many metals, and so may keep greater quantities of these metals in solution rather than allowing them to form particles. More importantly, the total metal:sulfide ratio at Rainbow is the highest of the three vent sites. This ratio affects the type and quantity of metal sulfide minerals that will reach their saturation state and precipitate. German et al. (2010) calculated that only 4 % of total iron at Rainbow could precipitate as sulfide minerals, and present evidence for very little iron precipitation between end member fluid and the neutrally buoyant plume, despite iron oxide formation further on in the plume.

Additionally, although Rainbow has lower silicon than the other sites (Figure 2.5), silicon is likely to be important for particle formation and trace metal distribution at Rainbow due to its low sulfide and high iron concentrations. Figure 2.8 shows an SEM micrograph of iron silicate particles caught on a 0.2 µm filter from the rising plume at Rainbow. EDS mapping shows clearly overlapping areas of concentrated Fe (Figure 2.8b) and Si (Figure 2.8c) in the particles lying diagonally on the filter. The formation of significant quantities of iron silicate or oxide (nano)particles with respect to iron sulfides would result in changes in trace metal distribution, as trace metal partitioning in oxides and silicates is very different from that in sulfides (Walther, 2005).

2.3.7 Nanoparticulate Metals

2.3.7.1 Nitric Acid Soluble Metals in the < 0.2 µm Fraction

Thus far, the results presented have predominately focused on the unfiltered, nitric acid-extracted metal concentrations; however, it is important also to investigate the < 0.2 µm fraction, as particles present in this portion will be much slower to settle and could be transported to the wider ocean (Yucel et al., 2011, Gartman et al., 2014). The < 0.2 µm fraction can be characterized by comparing the metals extractable in the hydrochloric acid (consisting of dissolved metals and metal monosulfides) and nitric acid leaches (consisting of dissolved metals, metal monosulfides, and pyrite/chalcopyrite nanoparticles). The concentration of a metal that is only soluble in nitric acid (Δ-N) is obtained by subtracting the hydrochloric acid concentration from the nitric acid concentration (equation 1).

(1) $\Delta\text{-N} = [M]_{HNO3} - [M]_{HCl}$

A two-tailed t-test was conducted to determine significant differences between the two fractions, with p-values less than 0.1 used to establish significance.

The concentration of nitric acid soluble metal and the percentage of the total < 0.2 µm fraction are presented in Table 2.3. The results presented in Table 2.3 demonstrate the diversity of metal speciation within the < 0.2 µm fraction. At least some portion of < 0.2 µm Co, Cu, Zn, Cd, and Pb is present in the nitric acid soluble fraction at each vent site, with the exception of Cd and Pb at TAG. Metals with significant nitric acide-extractable concentrations follow the order [Cu]> [Co]≈

[Zn]>[Pb]>[Cd] that is consistent with the preferential partitioning of these metals as trace constituents in pyrite (Morse and Luther, 1999). Metals in the < 0.2 µm fraction are present either as constituents of pyrite nanoparticles in the nitric acid fraction, as discrete metal sulfides and dissolved entities soluble in HCl, or as silicate nanoparticles. These species will each have different reactivity with respect to oxidation and particle growth. In particular, pyrite nanoparticles oxidize slowly (Gartman and Luther, 2014) and so the presence of trace metals means that pyrite nanoparticles may serve not only as a source of iron to the larger oceans (Yücel et al., 2011), but as a source of other trace metals as well.

Table 2.3 Composition of the < 0.2 µm fraction for all samples. The percentage of < 0.2 µm metal concentration/unfiltered metal concentrations is presented for HNO3-extractable Fe, Mn, Co, Cu, Zn, Cd, and Pb in vent fluid and in the first 1.5 meters of the rising plume at each vent site. The concentration of < 0.2 µm, nitric acid soluble metal (Δ-N) is presented for Co, Cu, Zn, Cd, and Pb in samples where there is a significant difference between HNO3 and HCl leaches. Samples in bold are samples that also contained nanoparticulate pyrite (Gartman et al., 2014). Samples in italics are from the rising plume and are presented with mixing information. The plume samples at Snakepit are from the Moose vent. %Δ-N/total is the percentage of nitric acid-extractable metal/total < 0.2 µm metal concentration.

		Fe	Mn	Co			Cu			Zn			Cd			Pb		
VENT	Sample	% NP[a]	% NP[a]	% NP[a]	Δ-N (μM)	% Δ-N /total	% NP[a]	Δ-N (μM)	% Δ-N /total	% NP[a]	Δ-N (μM)	% Δ-N /total	% NP[a]	Δ-N (nM)	% Δ-N /total	% NP[a]	Δ-N (nM)	% Δ-N /total
RAINBOW	**RB-2**	**100**	**100**	**73**			**0.40**	**0.0393**	**35.9**	**0.71**			**0.90**			**1.6**		
	RB-4	95	100	30	1.47	42.0	0.66			1.5			2.0	0.780	20.3	3.6		
	RB-5	96	84	10			74			45			69			82		
	RB-1	91	71	93	0.589	34.4	5.1	1.01	96	9.0			11			16	28.2	49
	plume samples (% mixing with seawater)																	
	8.1	*94*	*81*	*21*	*0.614*	*17.9*	*1.1*			*75*	*12.0*	*94.2*	*44*	*17.9*	*78.8*	*33*	*11.2*	*34*
	17	*100*	*80*	*24*			*1.9*			*6.8*	*0.133*	*16.1*	*8.4*			*7.9*		
	72	*100*	*70*	*50*			*0.31*			*0.87*			*1.4*			*3.3*		
TAG	TAG-7	100	94	81			0.56			3.1			4.2			6.1		
	TAG-1	100	100	72	0.110	9.03	0.56	0.0104	16	2.6			2.6			5.3		
	TAG-6	**97**	**89**	**23**			**0.75**			**3.7**			**5.6**			**7.6**		
	TAG-3	100	90	7			0.70	$8.64\mathrm{x}10^{-3}$	14	3.5			4.2			8.1		
	TAG-2	**87**	**100**	**94**			**1.1**			**5.2**			**5.1**			**10**		
	TAG-11	**90**	**96**	**6**			**0.45**			**4.6**			**5.0**			**10**		
	TAG-15	**71**	**62**	**3**			**0.56**			**3.5**			**3.9**			**9.5**		
	TAG-9	80	100	5	$9.89\mathrm{x}10^{-3}$	29.3	0.89			6.8			6.5			17		
	TAG-5	72	100	6	$8.46\mathrm{x}10^{-3}$	18.0	1.4			7.9			9.5			16		
	TAG-10	**92**	**100**	**14**			**2.9**			**21**	**0.146**	**20.2**	**25**			**39**		
	TAG-4	95	100	25			2.8			7.8			7.7			23		
	TAG-8	**86**	**100**	**43**	**0.0438**	**42.7**	**7.4**	**0.0323**	**42**	**27**	**0.427**	**45.2**	**17**			**38**		
	plume samples (% mixing with seawater)																	
	61	*96*	*85*	*7*			*1.1*	*0.0182*	*43*	*26*			*20*			*23*		
	78	*87*	*100*	*22*			*4.6*	*0.0413*	*55*	*16*			*22*			*35*		
	86	*81*	*73*	*28*	*0.0122*	*33.1*	*10*			*31*			*41*			*45*		
SNAKEPIT	**SP-5**	**100**	**96**	**13**			**3.1**	**0.013**	**26**	**3.6**	**0.180**	**22.3**	**4.1**			**4.6**	**4.97**	**20**
	SP-4	100	100	100	0.0110	23.0	4.2	$9.57\mathrm{x}10^{-3}$	19	2.8	0.146	20.2	3.1			4.5	8.43	30
	SP-3	100	90	7.5			6.4	0.008	15	7.1			7.5			7.2		
	SP-1	76	95	1.0	0.186	93.5	5.2	0.854	94	23			40	8.86	57.0	27	49.7	63
	SP-2	**66**	**100**	**17**			**5.4**	**0.017**	**25**	**6.2**			**6.0**			**6.3**		
	plume samples (% mixing with seawater)																	
	15	*100*	*100*	*17*	*0.0206*	*38.5*	*2.5*	*0.055*	*52*	*4.7*			*4.1*			*4.3*		
	66	40	*100*	*2.4*			*1.8*			*7.5*			*7.0*			*7.6*		
	77	*81*	*87*	*43*			*16*			*39*			*23*			*24*		

[a] Percentage of < 0.2 μm metal concentration/total unfiltered metal for nitric acid extracable concentrations.

2.3.7.2 Effect of Seawater Mixing on < 0.2 µm Trace Metals

At these sites, most metals, with the exception of iron and manganese, are predominately particulate (Table 2.3). A greater portion of copper is removed from solution at Rainbow, with under 2 % of copper present in the < 0.2 µm fraction in the first meter except for vent fluid sample (RB-5) that had < 0.2 µm Cu as 74 % of the total Cu concentration. The composition of Rainbow vent fluid should be similar because it comes from a single source (Charlou et al., 2002), and so this difference may be due to variability in either precipitation in the chimney or sample heterogeneity. Rainbow also has the lowest percentage of Mn in the < 0.2 µm fraction (70 to 80 %) of the three vents sites. Since manganese oxides are not expected to form, the higher percentage of particulate Mn is likely due to the absorption of Mn^{2+} onto other particles, or incorporation into silicates. Although the neutrally buoyant plume at Rainbow is enriched in iron oxide particles (Edmonds and German, 2004), we find that within the first meter iron is reduced and remains > 94 % in the < 0.2 µm fraction. Prior HNO_3 extraction and analysis of these samples showed that a significant portion (up to 5.24 %) of < 0.2 µm iron at Rainbow is present as pyrite nanoparticles and SEM data suggest formation of silicate nanoparticles as well (Gartman et al., 2014 and Figure 2.8). Iron oxides are not present in the first 1.5 m of the rising plume, as we detected neither Fe^{3+} nor oxygen in the plume over the range sampled. An iron catalytic cycle with sulfide and oxygen likely occurs, consuming O_2 and maintaining reduced iron concentrations at this point in the plume (Chapter 3).

The results in Table 2.3, and in Figures 2.6 and 2.7, highlight the importance of studying the early portions of the buoyant plume in understanding the dynamics of a particular vent field. In a study of particles from the neutrally buoyant plume approximately 200-300 meters above the vents at Rainbow, Edmonds and German (2004) found partitioning behavior for chalcophile elements (Fe, Cu, Zn) to be similar to that observed in other neutrally buoyant plumes emanating from basalt-hosted vent sites. Our data demonstrate; however, that nearer to the vent orifice and before the hydrothermal fluid is extensively diluted with seawater, there exist clear differences in the behavior of these metals between vent sites with respect to particle formation and trace metal association. Differences between vents sites are evident in (1) the changing association of trace metals with iron between the three vent sites, (2) the correlations between Cu, Co, Zn, Pb, and Cd at TAG and Snakepit, but not at Rainbow, (3) the higher percentage of < 0.2 μm Cu and Co at TAG and Zn, Cd, and Pb at Snakepit, and (4) the higher percentage of Mn that is particulate at Rainbow than at the other two sites. These differences in fluid chemistry play an important role in early plume processes affecting these metals, and indicates that other processes occur as the plume ages, resulting in a more homogenous distribution pattern.

2.4 Discussion

2.4.1 Metal Sulfide Particle Formation

In general, a significant amount of chalcophile metals precipitate (10^6-10^7 kg/year) with sulfide in the rising plume (James and Elderfield, 1996) and are preferentially removed in the following order: Cu > Co > Zn > Cd (Douville et al., 2002). Consistent with our results, the thermodynamic modeling of Klevenz et al. (2011) demonstrated that initially both iron and manganese are present in the (operationally defined) dissolved fraction, and copper and zinc precipitate rapidly compared to iron at low seawater mixing. Zn typically forms its own discrete sulfide precipitate apart from pyrite, incorporating both Cd and Pb, because the water exchange rates of these metals (measured at 25 °C) are faster than those of iron and thus will form sulfide minerals independent of iron sulfides (Morse and Luther, 1999; Yücel et al., 2011). In contrast, cobalt has a slower water exchange rate, and is thus incorporated into pyrite or chalcopyrite. Copper has a faster water exchange rate than iron and so it acts as a seed particle around which iron sulfides form.

Seyfried and Ding (1995) provide a model and experimental data to demonstrate metal behavior as cooling hydrothermal fluid seeps through the seafloor into the vent chimney. As a result of the cooling of hydrothermal fluid from 400-350 °C, the solubility of both pyrite and chalcopyrite decreases several orders of magnitude. The solubility of copper decreases an additional order of magnitude between 350 and 300 °C, while that of iron decreases by only 6 %.

This leads into a general conceptual model of metal sulfide precipitation in the plume: copper sulfides precipitate first, followed by zinc sulfides, then iron sulfides, and later iron oxides (Klevenz et al., 2011). Trace metals selectively co-precipitate with these major mineral constituents; cobalt is typically associated with chalcopyrite ($FeCuS_2$) and cadmium and lead are found in sphalerite (ZnS).

Chalcopyrite precipitates at temperatures between 250 and 350 ºC via the reaction of aqueous reduced copper and pyrite (equation 2; Rickard and Cowper, 1994). The reaction is first order with respect to the dissolved Cu^+ concentration.

(2) $2\ Cu^+ + FeS_2 \rightarrow CuFeS_2 + Cu^{2+}$

The rate of chalcopyrite formation shows strong temperature dependence. At temperatures above 200 ºC the reaction proceeds rapidly and is expected to preclude other interactions between copper and the iron sulfide system (Rickard and Cowper, 1994). The rapid formation of chalcopyrite in the end-member fluid removes the majority of the copper from solution prior to other metal sulfide particle formation.

Following chalcopyrite formation, as temperatures fall further and the pH increases due to seawater entrainment, zinc sulfide minerals precipitate. Sphalerite is the dominant zinc-bearing mineral in hydrothermal deposits, and precipitates at temperatures less than 200 ºC (Metz and Trefry, 2000) and at pH less than 7 (Ding and Seyfried, 1995). Sphalerite precipitation is highly dependent upon both temperature and pH, and decreasing concentrations of sulfide in solution also induce precipitation of ZnS (Hayashi et al., 1990). At temperatures higher than 200 °C, the stability of zinc-chloride complexes increases (Tagirov and Seward, 2009) and they are expected to dominate zinc speciation (Hsu-Kim et al., 2008), increasing zinc solubility. Once the temperature drops, these chloride complexes become less stable and reaction and complexation with sulfide become more important for zinc speciation (Tagirov et al., 2007) with solubility decreasing.

Finally, iron sulfides, including greater quantities of pyrite, are expected to precipitate in waters with a seawater percentage of 50-60 % (Klevenz et al., 2011). The rate of pyrite formation is less dependent on temperature than that of chalcopyrite (Rickard and Cowper, 1994; Rickard and Luther, 1997; Rickard, 1997), and the kinetics follow a sigmoidal curve between 25–125 ˚C, with the peak in rate attributed to changes in the FeS reactant over this temperature range. At hydrothermal vents, pyrite formation likely occurs mainly through the H_2S pathway (equation 3) rather than the polysulfide pathway due to the faster kinetics, prevalence of reactants, and lower pH of the vent environment.

(3) $FeS + H_2S \rightarrow FeS_2 + H_2$

The reaction of H_2S with FeS is a second order reaction dependent upon both the concentration of FeS and H_2S.

A shift occurs in plume composition from metal sulfides to metal oxides as the plume entrains more seawater and becomes more oxidizing (Trocine and Trefry, 1988). At this stage metal sulfides can begin to oxidize and dissolve, and particle reactive elements such as Cu, Mg, and Pb can be scavenged by iron oxides. No oxidized iron was detected for either unfiltered or < 0.2 µm fractions in any of our samples, indicating that within the initial meter of these buoyant plumes, metal speciation is still dominated by metal sulfides.

2.4.2 Silicate Particle Formation: Reverse Weathering

Silicon may play an important role in particle formation in the rising plume, particularly at vents with low sulfide concentrations. In addition to the data shown in Figure 2.8 additional SEM analyses showed that aluminosilicates were present in samples taken from the TAG rising plume (at a pH of approx. 7) at the MAR (Gartman, 2013). Iron silicate nanoparticles were found in the vent fluid at Lau Basin (Gartman et al., 2014), iron sulfur particles containing silica, and iron silicate particles containing sulfur have been found higher in the rising plume of EPR (McConaghy and Mottle, 1990) and amorphous silica has been observed to coat vent chimneys, particularly at lower temperatures (Koski et al., 1994). Unlike sulfide, which will oxidize or precipitate with other metals, silicon is less reactive under the conditions of the early plume. Silica precipitates at near-neutral pH and high sweater mixing ratios (Conrad et al., 2007), which is consistent with our results showing that it remains primarily in the < 0.2 μm fraction early in the plume.

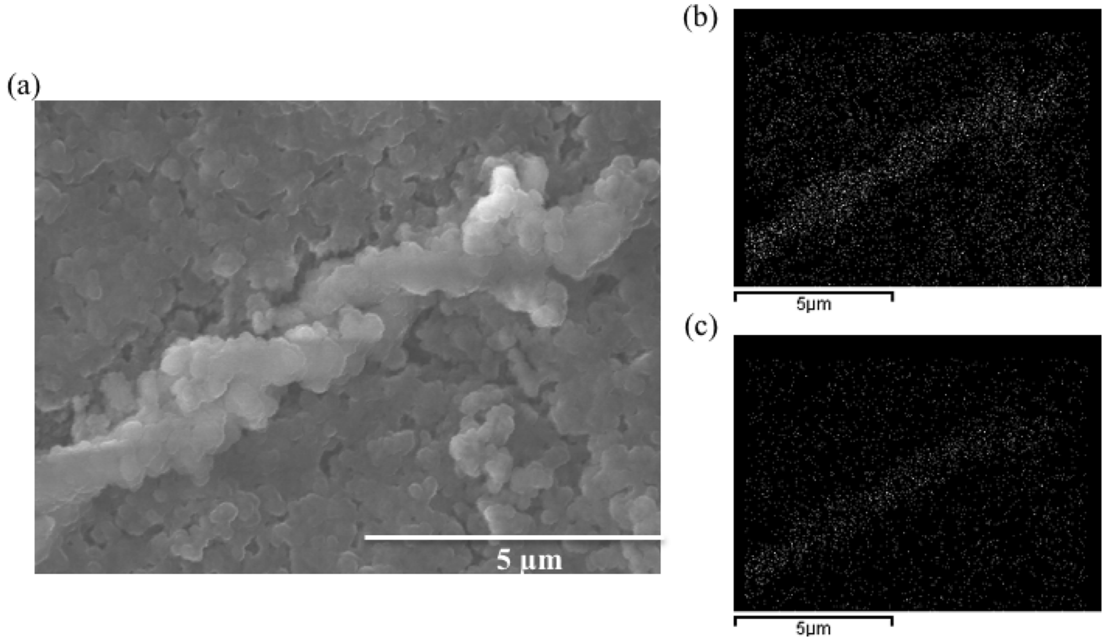

Figure 2.8 (a) SEM micrograph taken of particles caught on a 0.2 µm filter from the rising plume at Rainbow (8 % mixing, shipboard pH 7.7). EDS elemental mapping clearly showed overlap between areas of Fe (b) and Si (c)

The observation of iron silicates at Rainbow (Figure 2.8) is highly significant as it indicates that reverse weathering is occurring within the vent plume, and may account for the particulate manganese (Table 2.3). Reverse weathering occurs via the general reaction shown in equation 4 (Aller, 2013)

(4) $SiO_2 + Al(OH)_4^- + (Fe^{2,3+}, Mg^{2+}, Mn^{2+}) + F^- + HCO_3^- \rightarrow$ metal-rich aluminosilicates $+ CO_2 + H_2O$

Reverse weathering was initially postulated by Mackenzie and Garrels (1966) to be important for the mass balance of elements in the oceans, and it has been speculated that the high temperature formation of clays at hydrothermal crests could be partially responsible for maintaining the pH of the oceans (von Damm and Edmond, 1984). This process is not widespread in the oceans; however, it has been observed in estuaries and river deltas with high sedimentation rates (Michalopoulos and Aller, 1995). Due to the elevated metal and silica concentrations in vent fluid and high sedimentation rates in the rising plume, hydrothermal vent plumes represent another important potential location for reverse weathering.

2.5 Conclusions

An investigation of trace metal partitioning and size fractionation was conducted in the vent fluid and within the first 1.5 meters of three hydrothermal plumes along the MAR. At each vent site, iron and manganese remain in the < 0.2 μm fraction, whereas copper, cobalt, zinc, lead, and cadmium are predominately particulate. Manganese behaviour contrasts with the chalcophile elements with increased seawater mixing. Up to 30 % of Mn is particulate at high seawater:vent fluid ratios, specifically at Rainbow, potentially due to incorporation of Mn into silicate particles via reverse weathering, but for the other metals the percentage of particulates decreases.

At TAG and Snakepit, copper was correlated with cobalt, and zinc was correlated with cadmium and lead. At Rainbow, zinc correlates with cadmium and lead; but copper and cobalt are not correlated. The differences in metal associations between the vent sites indicate that different precipitates are forming in the Rainbow plume than at TAG or Snakepit due to the unique chemical composition of the Rainbow vent fluid. The results at TAG and Snakepit are consistent with the generally accepted conceptual model for metal sulfide mineral precipitation in the plume (Trocine and Trefry, 1988; Ding and Seyfried, 1995; Metz and Trefry, 2000; Klevenz et al., 2011). As vent fluid rises and mixes with seawater, first copper and cobalt precipitate in chalcopyrite, then zinc, lead, and cadmium precipitate in a discrete sulfide phase, followed by the formation of larger quantities of iron sulfides. Significant nitric acid extractable concentrations of all trace metals ([Cu]> [Co] ≈ [Zn]>[Pb]>[Cd]) were measured in the < 0.2 μm fraction at all three vent sites. At Rainbow, the formation of iron silicates may play an important role in affecting the distribution of chalcophile elements. SEM micrographs combined with elemental maps showing overlapping Fe and Si indicate that reverse weathering occurs in hydrothermal vent plumes.

Our dataset is unique in that it focuses on the very early stages of the buoyant plume (within 1.5 m from the orifice). That these particle formation processes are observed within the first meter of the plume highlights how rapidly particle nucleation and growth occur in this dynamic environment, and thus the importance of this initial mixing zone for controlling metal fluxes from the vents to the larger oceans.

REFERENCES

Abellea, M., Radford-Knoery J., Appriou P., Bougault H., Charlou J.L., Donval J.P., Etoubleau J., Fouquet Y., German C.R., Miranda M. (1998) Manganese distribution in the water column near the Azores Triple Junction along the Mid-Atlantic Ridge and in the Azores domain. *Deep Sea Res*. 45, 1319-1338.

Bennett S. A., Achterberg E.P., Connelly D.P., Statham P.J., Fones G.R., and GermanC.R. (2008) The distribution and stabilization of dissolved Fe in deep-seahydrothermal plumes. *Earth Planet Sci Lett.* **270**, 157–167.

Butterfield D.A., Seyfried,J.W.E., Lilley M.D. (2003) Composition and evolution of hydrothermal fluids. In: Halbach, P.E., Tunnicliffe, V.,Hein, J.R. (Eds.), Energy andMass Transfer in Marine Hydrothermal Systems. Dahlem University Press, Berlin, Germany, pp. 123–161.

Chadwell S.J., Rickard D., Luther III G.W. (2001) Electrochemical Evidence for Metal Polysulfide Complexes:Tetrasulfide ($S_4{}^{2-}$) Reactions with Mn^{2+}., Fe^{2+}, Co^{2+}, Ni^{2+}, Cu^{2+}, and Zn^{2+}. *Electroanalysis* **13**, 21-29.

Charlou J.L., Donval J.P., Douville E., Jean-Baptiste P., Radford-Knoery J., Fouquet Y., Dapoigny A., Stievenard M. (2000) Compared geochemical signatures and the evolution of MenezGwen (37 50VN) and Lucky Strike (37 17VN) hydrothermal fluids, south of the Azores Triple Junction on the Mid-Atlantic Ridge. *Chem Geol*. **171**, 49– 75

Charlou J.L., J.P. Donval, Y. Fouquet, P. Jean-Baptiste, N. Holm (2002). Geochemistry of high H_2 and CH_4 vent fluids issuing from ultramafic rocks at the Rainbow hydrothermal field (36° 14' N, MAR). *Chem Geol.* **191**, 345–359.

Conrad C.F., Icopini G.A., Yasuhara H., Bandstra J.Z., Brantley S.L., Heaney P.J.,(2007) Modeling the kinetics of silica nanocolloid formation and precipitation in geologically relevant aqueous solution. Geochim Cosmochim Acta **71**, 531-542.

Converse D.R., Holland H.D. and Edmond J.M. (1983) Flow rates in the axial hot spring of the East Pacific Rise (21 N): implications for the heat budget and the formation of massive sulfide deposits. *Earth Plant Sci Lett.* **69,** 159-175.

Desbruyeres D., Almeida A., Biscoito M., Comet T., Khripounoff A., Le Bris N.,Sarradin P.M., Segonzac M. (2000) A review of the distribution of hydrothermal vent communities along the northern Mid-Atlantic Ridge:dispersal vs. environmental controls. *Hydrobiologia*. **440**, 201-216.

Ding K., Seyfried Jr. W.E., Zhang Z., Tivey, M.K., Von Damm K.L., Bradley A.M. (2005) The in situ pH of hydrothermal fluids at mid-ocean ridges *Earth Plant Sci Lett* **237**, 167-174.

Douville E., Charlou J.L., Oelkers E.H., Bienvenu P., Jove Colon C.F., Donval J.P., Fouquet Y., Prieur D., Appriou P. (2002) The Rainbow vent fluids (36°14’N, MAR): the influence of ultramafic rocks and phase separation on trace metal content in Mid-Atlantic Ridge hydrothermal fluids. *Chem Geol.* **184**, 37-48.

Edmond J.M., Von Damm K.L., McDuff R.E., and Measures C.I. (1982) Chemistry of hot springs on the East Pacific Rise and their effluent dispersal. *Natur*e **297**, 187-9l.

Edmonds H.M. and C. R. German (2004) Particle geochemistry in the Rainbow hydrothermal plume, Mid-Atlantic Ridge. *Geochim Cosmochim Acta*, **68**,759-772.

Feely R.A, Lewison M, Massoth G.J., Robert-Baldo G., Lavelle J.W., Bryne R.H., VonDamm, K.L., and Curl Jr. H.C. (1987) Composition and dissolution of Black Smoker particulates fro active vents on the Juan de Fuca Ridge. *J Geophys Res*. **92,** 11347-11363.

Field M.P, Sherrell R.M. (2000) Dissolved and particulate Fe in a hydrothermal plume at 9°45′N, East Pacific Rise: Slow Fe (II) oxidation kinetics in Pacific plumes. *Geochim Cosmochim Acta* **64**, 619-628.

Findlay A.J, Gartman A, MacDonald D., Hanson T.E., Shaw T., Luther III G.W. (2014) Distribution and size fractionation of elemental sulfur in aqueous environments: The Chesapeake Bay and Mid-Atlantic Ridge. *Geochim Cosmochim Acta* **142**: 334-348.

Fossing H. and B. B. Jørgensen (1989) Measurement of bacterial sulfate reduction in sediments: Evaluation of a single-step chromium reduction method. *Biogeochemistry* **8**, 205-222.

Gartman A. (2013). *The formation, oxidation and distribution of pyrite nanoparticles emitted from hydrothermal vents: A laboratory and field based approach*. Ph.D. Dissertation, University of Delaware.

Gartman A and Luther III G.W. (2014) Oxidation of synthesized sub-micron pyrite (FeS_2) in seawater. *Geochim Cosmochim. Acta* **144***,* 96-108.

Gartman A, Findlay A.J, Luther G.W III (2014) Nanoparticulate pyrite and other nanoparticles are a widespread component of hydrothermal vent black smoker emissions. *Chem Geol.* **366**, *32-41*

German C.R., Thurnherr A.M., Knoery J., Charlou J.L., Jean-Baptiste P., and Edmonds H.N. (2010) Heat, volume, and chemical fluxes from submarine venting: A synthesis of results from the Rainbow hydrothermal field, 36°N MAR. *Deep Sea Res.* **57**, 518-527.

German C.R., Campbell A.C., Edmond J.M. (1991) Hydrothermal scavenging at the Mid‐Atlantic Ridge—Modification of trace‐element dissolved fluxes. *Earth Planet. Sci. Let.* **107**, 101-114.

German, C. R. and von Damm K.L. (2004) Hydrothermal processes. *Treatise Geochem.* **6**, 181-222.

Hannington M. T., Larocque A., Petersen S., Rona P. (1995). The occurrence of gold in sulfide deposits of the TAG hydrothermal field, MAR. *Canadian Mineral* **33**, 1285-1310.

Hayashi K, Sugaki A, Kitakaze A. (1990) Solubility of sphalerite in aqueous sulfide solutions at temperatures between 25-degrees and 240-degrees *Geochim Cosmochim Acta* **54**, 715-725.

Haymon R.M. (1983) The growth history of hydrothermal black smoker chimneys. *Nature* **301**, 695-698

Hochella, M. F., S. K. Lower, Maurice P. A., Lee Penn R., Sahai N, Sparks D. L., Twining B.S. (2008). Nanominerals, Mineral Nanoparticles, and Earth Systems. *Science* **319**(5870): 1631-1635.

Hsu- Kim H., Mullaugh K.M., Tsang J.J., Yücel M., Luther III.G.W. (2008) Formation of Zn- and Fe-sulfides near hydrothermal vents at the Eastern Lau Spreading Center: implications for sulfide bioavailabilty to chemoautotrophs. *Geochem. Trans*. **9**, 6.

Huerta- Diaz M.A. and Morse J.W. (1992) Pyritization of trace metals in anoxic marine sediments. *Geochim. Cosmochim. Acta* **56**, 2681-2702.

James R.H. and Elderfield H. (1996) Chemistry of ore-forming fluids and mineral formation rates in an active hydrothermal sulfide deposit on the Mid-Atlantic Ridge. *Geology* **24**, 1147 – 1150.

Klevenz V., Bach W., Schmidt K., Hentscher M., Koschinsky A., Petersen S. (2011) Geochemistry of vent fluid particles formed during initial hydrothermal fluid–seawater mixing along the Mid□Atlantic Ridge. *Geochem Geophys Geosys*. **12**

Klinkhammer G., Rona P., Greaves M., and Elderfield H. (1985) Hydrothermal manganese plumes in the Mid-Atlantic Ridge rift valley, *Nature* **314**, 727-731.

Kobayashi J. (1967) Chemical Environment in the aquatic habitat. Eds Golterman H.L. and Clymo R.S. Noord-Hollandsche Uitgevers Maatschappu, Amsterda. Pp. 41-55.

Lalou C., Reyss J., Brichet E., Arnold M., Thomson G., Fouquet Y., Rona P.A. (1993) New age data fro Mid-Atlantic Ridge hydrothermal sites: TAG and Snakepit chronology revisted. *Jour Geophys Res.* B, 9705-9713.

Lau B.L.T and Hsu-Kim, H (2008) Precipitation and Growth of Zinc Sulfide Nanoparticles in the Presence of Thiol-Containing Natural Organic Ligands. *Environ Sci Technol. 42*, 7236-7241.

Ludford E.M., Palmer M.R., German C.R., and Klinkhammer G.P. (1996) The geochemistry of Atlantic hydrothermal particles. *Geophys Res Lett.* **23**, 3503 – 3506.

Luther III G. W. (1990) The frontier-molecular-orbital theory approach in geochemical processes. In *Aquatic Chemical Kinetics* (ed. W. Stumm), pp. 173–198. Wiley, New York.

Luther III G.W., Rozan T.F., Taillefert M., Nuzzio D.B., Di Meo C., Shank T.M., Lutz R.A., Cary S.C. (2001) Chemical speciation drives hydrothermal vent ecology. *Nature* **410**, 813-816

Luther III G.W. (2010) The Role of One- and Two-Electron Transfer Reactions in Forming Thermodynamically Unstable Intermediates as Barriers in Multi-Electron Redox Reactions. *Aquat Geochem* **16**, 395-420.

Luther III G.W. and D.T. Rickard. (2005) Metal sulfide cluster complexes and their biogeochemical importance in the environment. *J Nanopart Res* **7**, 389- 407

Luther III G.W., S. M. Theberge, T.F. Rozan, (2002) Aqueous copper sulfide clusters as intermediates during copper sulfide formation. *Environ Sci Technol.* **36**, 394 –402.

Mandernack K.W. and B.M. Tebo (1993) Manganese scavenging and oxidation at hydrothermal vents and in vent plumes. *Geochim Cosmochim Acta* **57**, 3907-3923.

Marques A., Barriga F., Chavagnac V., and Fouquet Y. (2006) Mineralogy, geochemistry, and Nd isotope composition of the Rainbow hydrothermal field, Mid-Atlantic Ridge. *Mineralium Deposita* **41**, 52-67.

Metz S. and Trefry J.H. (1993) Field and laboratory studies of metal uptake and release by hydrothermal precipitates. *Jour Geophys Res.* **98,** 9661-9666.

Metz S. and Trefry J. H. (2000) Chemical and mineralogical influences on concentrations of trace metals in hydrothermal fluids. *Geochim Cosmochim Acta* **64**, 2267-2279.

Morel F.M.M., Hudson R.J.M., Price N.M. (1991) Limitation of productivity by trace metals in the sea. *Limnol Oceanogr.* **36**, 1742-1755.

Morgan J.J. (2005) Kinetics of reaction between O_2 and Mn(II) species in aqueous solutions. *Geochim Cosmochim Acta* **69**, 35–48.

Morse, J.W. and Luther III G.W. (1999) Chemical influences on trace metal-sulfide interactions in anoxic sediments. *Geochim Cosmochim Acta* **63**, 3373–3378.

Mottl M. J. and McConachy T.F. (1990) Chemical processes in buoyant hydro-thermal plumes on the East Pacific Rise near 21 N. *Geochim Cosmochim Acta* **54**, 1911-1927.

Mullaugh K. and Luther III G.W. (2011) Growth kinetics and long-term stability of CdS nanoparticles in aqueous solution under ambient conditions. *J Nanoparticle Res.* **13,** 393-404.

Tagirov B.R., Suleimenov O.M., Seward T.M. (2007) Zinc complexation in aqueous sulfide solutions: Determinationof the stoichiometry and stability of complexes via ZnS(cr)solubility measurements at 100 C and 150 bars. *Geochim Cosmochim Acta* **71**, 4942–4953.

Tagirov B.R. and Seward T.M. (2010) Hydrosulfide/sulfide complexes of zinc to 250 °C and the thermodynamic properties of sphalerite. *Chem Geol.* **269**, 301–311.

Tivey M.K. (1995). Modeling chimney growth and associated fluid flow at seafloor hydrothermal vent sites. In: HumphrisSE, ZierenbergRA, MullineauxLS, ThomsonRE, editors. *Seafloor hydrothermal systems: Physical, chemical, biological, and geological interactions*. Washington, DC: American Geophysical Union. pp 158–177.

Rickard D. (1997) Kinetics of pyrite formation by the H_2S oxidation of iron (II) monosulfide in aqueous solutions between 25 and 125°C: The rate equation. *Geochim Cosmochim Acta*, **61**, 115-134.

Rickard, D. and G. W. Luther III (1996) Kinetics of pyrite formation by the H2S oxidation of iron (II) monosulfide in aqueous solutions between 25 and 125°C: The mechanism. *Geochim Cosmochim Acta* **61**, 135-147.

Rickard, D. and Cowper M. (1994) Kinetics and mechanism of chalcopyrite formation from Fe(I1) disulphide in aqueous solution (>200 ^{o}C). *Geochim Cosmochim Acta* **58**, 3795-3802.

Rickard D. and Luther III G.W. (2005) Metal sulfide complexes and clusters. *Sulfide Mineralogy and Geochemistry.* **61**, 421-504.

Rickard D., Griffith A., Oldroyd A., Butler I.B., Lopez-Capel E., Mannin D.A.C., and Apperley D.C. (2006) The composition of nanoparticulate mackinawite, tetragonal iron(II) monosulfide. *Chem Geol.* **235**, 286-298.

Rona P D., Dyment J., Murton B. (2010) Diversity of Hydrothermal Vents on Slow Spreading Ridges. Washington, D.C., American Geophysical Union.

Rozan T.F., Lassman M.E., Ridge D.P., and Luther III G.W. (2000) Evidence for iron, copper and zinc complexation as multinuclear sulphide clusters in oxic rivers. *Nature* **406**, 879-882.

Rudnicki M.D. and Elderfield H. (1993) A chemical model of the bouyand and neutrally bouyan plume above the TAG vent field, 26 degrees N, Mid-Atlantic Ridge. *Geochim Cosmochim Acta* **57**, 2939 – 2957.

Sander S.G. and Koscinsky A. (2011) Metal flux from hydrothermal vents increased by organic complexation. *Nature Geosci.* **4**, 145-150.

Sands C.M., Connelly D.P., Statham P.J., and German C.R. (2012) Size fractionation of trace metals in the Edmond hydrothermal plume, Central Indian Ocean. *Earth Planet Sci Lett.* **319**, 15-22.

Sarradin, P.M., Lannuzel D., Waeles M., Crassous P., Le Bris N., Caprais J.C., Fouquet Y., Fabri M.C., and Riso R. (2008) Dissolved and particulate metals (Fe, Zn, Cu, Cd, Pb) in two habitats from an active hydrothermal field on the EPR at 13°N. *Science Total Environ.* **392**, 119-129.

Schmidt K., Koschinky A., Garbe-Schönberg D., de Carvalho L.M., and Seifert R. (2007) Geochemistry of hydrothermal fluids from the ultramafic□hosted Logatchev I hydrothermal field, 15°N on the Mid□Atlantic Ridge: Temporal and spatial investigation. *Chem Geol*. **242**, 1–21.

Scott S.D. (1983) Chemical behaviour of sphalerite and arsenopyrite in hydrothermal and metamorphic environments. *Mineralogy*. **47**, 427-435.

Seyfried W.E. and Ding K. (1995) Phase equilibria in subseafloor hydrothermal systems: a review of the role of redox, temperature, pH, and dissolved Cl on the chemistry of hot spring fluids and Mid-Ocean Ridges. Seafloor Hydrothermal Systems: Physical, Chemical, Biological, and Geological Interactions (ed Humphris S.E., Zierenber R.A., Mullineaux L.S., and Thomson R.E.) American Geophysical Union.

Shoonen M.A.A. and Barnes H.L. (1991) Reactions forming pyrite and marcasite from solution: I. Nucleation of FeS2 below 100°C. *Geochim Cosmochim Acta*, **55**, 1495-1504.

Stookey L.L. (1970) Ferrozine- A New Spectrophotometric Reagent for Iron. *Anal Chem.* **42**, 779-781.

Stumm W. and Morgan J.J. (1996) Aquatic Chemistry, Chemical Equilibria and Rates in Natural Waters. 3rd ed. John Wiley & Sons, Inc., New York, NY, USA.

Tagliabue A., Bopp L., Dutay J.C., Bowie A.R., Chever F., Jean-Baptiste P., Bucciarelli E., Lannuzel D., Remenyi T., Sarthou G., Aument O., and Gehlen M., Jeandel C. (2010) Hydrothermal contribution to the oceanic dissolved iron inventory. *Nature Geosci.* **3**, 252-256.

Trefry J.H., Trocine R.P., Klinkhammer G.P., and Rona P.A. (1985) Iron and copper enrichment of suspended particles in dispersed hydrothermal plumes along the Mid-Atlantic Ridge. *Geophys Res Lett.* **12**, 506 – 509.

Trocine R. P. and J.H. Trefry (1988) Distribution and chemistry of suspended particles from an active hydrothermal vent site on the Mid-Atlantic Ridge at 26 N. *Earth Planet Sci Lett*. **88**, 1-15.

Von Damm K.L., Edmond J.M., Grant B., Measures C.I., Walden B., and Weiss R.F., (1985) Chemistry of submarine hydrothermal solutions at 21 N, East Pacific Rise. *Geochim Cosmochim Acta* **49**, 2197– 2220.

Von Damm K.L., Oosting S.E., Kozlowski R., Buttermore L.G., Colodner D.C., Edmonds H.N., Edmond J.M., Grebmeir J.M. (1995) Evolution of East Pacific Rise hydrothermal vent fluids following a volcanic eruption. *Nature* **375**, 47 – 50.

Walther J.V. (2005) Essentials of Geochemistry. Jones and Bartlett Publishers

Wang D., Wang Q., and Wang T. (2009) Controlled growth of pyrite FeS_2 crystallites by a facile surfactant-assisted solvothermal method. *Cryst Eng Comm*. **12**, 755–761.

Wilkin, R.T. and Barnes H.L. (1997) Formation processes of framboidal pyrite. *Geochim Cosmochim Acta*. **61**, 323-339

Wu J. and Boyle E. A. (1998) Determination of iron in seawater by high resolution isotope dilution inductively coupled plasma mass spectrometry after $Mg(OH)_2$ coprecipitation. *Anal Chim Acta*. **367**, 183-191.

Yücel M., Gartman A., Chan C.S., Luther III G.W. (2011) Hydrothermal vents as a kinetically stable source of iron-sulphide-bearing nanoparticles to the ocean. *Nature Geosci* **4**, 367-371.

Chapter 3

DISTRIBUTION AND SIZE FRACTIONATION OF ELEMENTAL SULFUR AQUEOUS ENVIRONMENTS: THE CHESAPEAKE BAY AND MID-ATLANTIC RIDGE

Abstract

Elemental sulfur is an important intermediate of sulfide oxidation and may be produced via abiotic and biotic pathways. In this study the concentration and size fractionation of elemental sulfur were measured in two different sulfidic marine environments: the Chesapeake Bay and in buoyant hydrothermal vent plumes along the Mid-Atlantic Ridge. Nanoparticulate sulfur (< 0.2 µm) was found to comprise up to 90 % of the total elemental sulfur in anoxic deep waters of the Chesapeake Bay. These data were compared with previous studies of elemental sulfur, and represent one of the few reports of nanoparticulate elemental sulfur in the environment. Additionally, a strain of phototrophic sulfide oxidizing bacteria isolated from the Chesapeake Bay was shown to produce elemental sulfur as a product of sulfide oxidation. Elemental sulfur concentrations are also presented from buoyant hydrothermal vent plumes located along the Mid-Atlantic Ridge. In the Mid-Atlantic Ridge plume, S^0 concentrations up to 33 µM were measured in the first meter of rising plumes at three different vent sites, and nanoparticulate S^0 was up to 44 % of total elemental sulfur present.

3.1 Introduction

Zero-valent sulfur (ZVS) species, meaning compounds in which sulfur is in a neutral oxidation state, can form via a variety of biotic and abiotic pathways. As a (meta)stable intermediate of sulfide oxidation, elemental sulfur (S^0), and other ZVS species such as polysulfides (S_x^{2-}) may be important components of microbial (Schauder and Muller, 1993; Franz, 2007) and geochemical (Luther, 1990) processes in natural waters. .

The oxidation of sulfide to elemental sulfur by molecular oxygen requires a two electron oxidation of sulfide. The one electron transfer from sulfide to oxygen is thermodynamically unfavorable (Luther, 2010). The two electron transfer from sulfide to oxygen, although thermodynamically favorable, is kinetically inhibited. In order for a two electron transfer from sulfide to oxygen to occur, the electrons from sulfide must first be unpaired, (Luther, 1990) which poses a kinetic barrier to the oxidation (Luther et al., 2011). Oxidation of sulfide by oxygen can be facilitated with the aid of a bridging metal catalyst (Yao and Millero, 1996), which facilitates the transfer of electrons from sulfide to oxygen. Elemental sulfur has been observed as an oxidation product of sulfide oxidation by manganese oxides (Herszage and dos Santos Afonso, 2003) and iron (oxy)hydroxides (Pyzik and Sommer, 1981; Luther, 1991; Poulton, 2003).

Due to these thermodynamic and kinetic constraints on abiotic sulfide oxidation in the absence of metal catalysts, micro-organisms play an important role in mediating sulfide oxidation environmentally, forming elemental sulfur as the first stable oxidation product (Taylor and Wirsen, 1997; Frigaard and Dahl, 2008). Biotic sulfide oxidation kinetics are orders of magnitude more rapid than abiotic pathways (Luther et al., 2011). The exact composition of elemental sulfur produced by different types of bacteria is a matter of debate; however, in general, microbially produced elemental sulfur is hydrophilic and of lower density than inorganically produced sulfur (Kleinjan et al., 2003). Microbially produced sulfur can be intracellular, such as that produced by purple sulfur bacteria, or extracellular, as in green sulfur bacteria (van Gemerden et al., 1986; Frigaard and Dahl, 2008), and may have a protein coating. The actual globules are not the more crystalline orthorhombic sulfur, but rather a more hydrated form of S_8 rings or chains (Prange et al., 2002). In addition to bacteria that produce elemental sulfur as a product of sulfide metabolism, many bacteria, such as *Sulfurospirillum arcachonense*, *Desulfurella acetivorans*, and *Shewanella putrefaciens* utilize elemental sulfur and polysulfides as an energy source (Schauder and Muller, 1993; Franz et al., 2007; Sievert et al., 2007). Elemental sulfur is also an important source of energy for many archaea, and can be utilized as either an electron donor for aerobic archaea such as the *Acidianus* and *Sulfolobus* species, or an electron acceptor for anaerobic archaea (Kletzin et al., 2004).

Zerovalent sulfur species have been observed in a variety of natural environments, and nanoparticulate elemental sulfur has been synthesized and characterized in the laboratory (Ghosh and Dam, 2009; Deshpande et al., 2008; Guo et al., 2006; Steudel, 2003). Elemental sulfur has been found in the water columns of stratified lakes (Zerkle et al., 2010; Kamyshny et al., 2011), and in marine environments, including tidal pools (Kamyshny and Ferdelman, 2010), inland bays (Ma et al., 2006), the Black Sea (Luther et al., 1991; Jørgensen, 1991; Trowbourst et al., 2006), and the Cariaco Basin (Hastings and Emerson, 1988; Li et al., 2008). Sulfur has also been found in sediments (Yücel et al, 2010; Lichtschlag et al., 2012) and in sediment porewaters (Luther et al., 1986; Rozan et al., 2000; Wang and Tessier, 2009). The size of elemental sulfur affects its chemical reactivity (Steudel, 2003) and thus its availability to microorganisms as a substrate (Franz et al., 2007). Despite the influence of particle size on chemical and biological processes, the size distribution of elemental sulfur in the environment has not yet been widely studied. Elemental sulfur measured in sediments is reported as unfiltered extractions (Troelsen and Jørgensen, 1982; Wang and Tessier, 2009; Lichtslag et al., 2012). In the water column, reports of elemental sulfur have been presented as unfiltered totals (Zopfi et al., 2001), as the fraction caught on a 0.2 μm filter (Ma et al., 2006), and only a few studies have investigated the fraction passing through a filter. Kamyshny and Ferdelman (2010) measured S^0 in the filtrate passing a 5 μm filter, Kamyshny et al. (2011) passing a 1.2 μm filter, Zerkel et al. (2010) passing both a 0.45 and a 0.2 μm filter, and Li et al. (2008) in that passing a 0.2 μm filter.

In this study, we operationally define the portion of sulfur passing through a 0.2 μm filter as nanoparticulate and the fraction caught on the filter as particulate. Total elemental sulfur refers to the sum of these two fractions. We present data on the presence and distribution of particulate and nanoparticulate elemental sulfur in two distinct marine environments (the Chesapeake Bay and the Mid-Atlantic Ridge), as well as in cultures of anoxygenic phototrophic sulfide oxidizing bacteria. In particular we show that nanoparticulate elemental sulfur exists in both the Chesapeake Bay and the Mid-Atlantic Ridge, and we highlight the importance of nanoparticulate elemental sulfur as a component of biotic and abiotic cycling in these different systems.

3.1.1 Study Sites

The Chesapeake Bay is a partially mixed and seasonally anoxic estuary. An oxic upper layer and an anoxic deep layer develop in the spring and summer due to temperature and salinity gradients (Officer et al., 1984). The deep layer can become sulfidic, resulting in a suboxic zone in which neither oxygen nor sulfide is detected is typically present (Lewis et al., 2007). The study site on the Chesapeake Bay is a hole south of the Chesapeake Bay bridge (Station 858; 38°58.8′ N; 76°22′ E) that is 25 meters deep, measures 0.4 km in length, and 0.8 km in width (Lewis et al., 2007).

The Rainbow, Trans-Atlantic Geotravers, (TAG) and Snakepit vent sites were sampled along the Mid-Atlantic Ridge (MAR) a slow spreading plate boundary moving at rates less than 3 cm/year (Schmidt et al., 2007). The vent fluid at these three sites has the highest trace metal content of vent fields along the MAR (Douville et al., 2002) and iron and sulfide data from each site are given in Table 3.1. The Rainbow vent site (36˚ 14’ N, 33˚ 54’ W) at 2300 m depth is comprised of serpentinised peridotite and contains high temperature vents (up to 365 ºC) characterized by low shipboard pH (2.8), high iron concentrations, and high chlorinity (Marques et al., 2007). The vent fluid at Rainbow is enriched in metals and organics, and is relatively low in sulfide. TAG (26˚ 8' N, 44˚ 50' W) at 3600 m depth (T < 365 ˚C, pH > 3.14) and Snakepit (23˚ 22' N, 44˚ 57' W) at 3500 m depth (T < 358 ˚C, pH > 3.2) are basalt hosted massive sulfide deposits and contain high temperature black smokers at depths approximately 1000 m deeper than Rainbow (Desbruyères et al., 2001) with iron concentrations an order of magnitude lower and sulfide concentrations approximately five times higher than those of Rainbow (Douville et al., 2002; Gartman et al., 2014). The TAG vent field is located on a large sulfide deposit approximately 50 m high and is located 1500 meters from the rift valley, and Snakepit is located in the rift valley close to the top of a volcanic ridge (Thomson et al., 1988).

Table 3.1 Maximum iron and sulfide concentrations in vent fluid for each vent site

Vent Site	**[AVS] (μM) unfiltered**	**[CRS] (μM) unfiltered**	**[Fe^{2+}] (mM)**	**Pyrite (< 0.2 μm) (μM)[a]**
Rainbow	496	1130	22.4	1.15
Snakepit	3810	1030	3.60	0.0962
TAG	3870	1800	5.08	0.234

[a] From Gartman et al., 2014

3.2 Methodology

3.2.1 Sample Collection

Work was done in the Chesapeake Bay on two separate cruises aboard the R/V *Sharp* on 27-30 July 2011 and 17-19 August 2012. Samples were collected in cleaned Nalgene bottles from either Niskin bottles on the ship-board CTD or from Nalgene tubing attached to a plastic Rule Industries water pump, which was connected to a cage containing an *in situ* micro CAT CTD sensor as well as an Analytical Instrument Systems *in situ* electrochemical analyzer. Salinity and temperature data were collected from the ship's CTD sensor.

Field studies along the Mid-Atlantic Ridge were conducted aboard the R/V *Knorr* from 16 October until 10 November 2012. All rising plume samples at the Mid-Atlantic Ridge were taken by the ROV Jason II using Titanium Major Samplers. Neutrally buoyant plume samples were obtained using Niskin bottles on the ship's CTD rosette. The neutrally buoyant plume was identified using the deviation in percent beam transmittance from local ambient deep water, and values for this change were all greater than 0.3 %.

In measuring intermediate sulfur species in environmental samples, care must be taken to avoid oxidation of the sample, as these species are reactive. In the Chesapeake Bay, sample collection and processing was rapid (<10 minutes from when the sample was taken). In order to limit oxidation, subsamples taken from Niskin bottles were collected with no headspace. The time from subsampling the Niskin bottle until the completion of sample processing was typically less than 2 minutes. Voltammetric measurements of sulfide conducted *in situ* and onboard the ship on subsamples from the Niskin bottles demonstrated comparable sulfide concentrations in the water column and in samples from the Niskin bottles, indicating that little oxidation of sulfide occurred in the sampling time. The half-time of sulfide in the Chesapeake is approximately 30 minutes in the light (Luther et al., 1988), and sulfide oxidation in the dark in anoxic conditions has been shown to be negligible (Luther et al., 1988; Hanson et al., 2013).

The titanium samplers used at the MAR provide 700 mL of material, and it takes approximately 10 -15 seconds to fill the sampler. In this time, the current of the bottom waters frequently changes so that the water collected from the plume is temporally and spatially different and thus represents an average of fluid composition over the collection period. Due to the time constraints associated with deep-sea sampling, samples in the Titanium Major Samplers typically reached the surface 2-12 hours after collection, and the fluid had cooled to ambient bottom water temperatures (2 °C) by this time. Cooling to 2 °C would slow reaction kinetics by an order of magnitude or more, helping to preserve the chemical speciation in the sample. Once onboard ship, sample processing for S^0 analysis was rapid. Finally, our data indicated that further oxidation of sulfide in the Titanium Major Sampler did not occur (section 3.4).

3.2.2 Sulfide Measurements

*Chesapeake Bay***.**

For Chesapeake Bay samples, sulfide concentrations were determined at slack tides using *in situ* voltammetry controlled by a DLK sub II In Situ Electrochemical Analyzer (ISEA) designed by Analytical Instrument Systems (AIS). Gold amalgam working electrodes made after the method of Luther et al. (2008) were used on each cast along with a solid state Ag/AgCl reference electrode and a platinum counter electrode. Cyclic voltammetry was run from -0.1 V to -1.8 V, and back to -1.8 V at a scan rate of 2 volts per second after conditioning at -0.9 V for 5 seconds then at -0.1 V for 2 seconds. These electrodes are capable of measuring an array of redox active species including oxygen, sulfide, thiosulfate, elemental sulfur, iron, and manganese (Luther et al., 2008). The detection limit of this method is 0.2 μM for sulfide and polysulfides and 3 μM for oxygen.

For shipboard sulfide oxidation experiments, sulfide was measured using voltammetry and the experimental methods that have been described in Luther et al. (2011) and Hanson et al. (2013). Briefly, an electrochemical cell was set up containing a 100 μm gold amalgam working electrode, a Ag/AgCl reference electrode and a platinum counter electrode which were run using an AIS DLK-60 potentiostat. Cyclic voltammetric scans were run from -0.1 to -1.8 V using a method with the conditioning potentials of -0.9 and -0.1 V as outlined above. Fifty mL of anoxic sample water spiked with 50 μM 3-(3,4-dichlorophenyl)-1,1-dimethylurea (DCMU) were added to the electrochemical cell. DCMU was used to inhibit oxygenic photosynthesis. Anoxic conditions were maintained throughout the experiments using a glove bag purged with ultrahigh purity argon, and light intensity was monitored with a LI-COR Biosciences LI-1400 data logger light meter.

MAR

For Mid-Atlantic Ridge samples, unfiltered concentrations of acid volatile and chromium reducible sulfide (AVS/CRS) were measured using the method of Fossing and Jøregensen (1989) after shipboard fixation and storage. To prepare the samples, 2 mL of 0.5 M NaOH and 5 mL of 0.1 M zinc acetate were added to 5 mL of sample to fix free sulfide and FeS sulfide as ZnS. The samples were immediately frozen and stored at -20 ºC and thawed prior to analysis onshore. Thawed samples were added to deoxygenated glass reaction vessels. After the samples were added, five mL of 3 M HCl were added to liberate HS^- and FeS as H_2S gas. After purging with ultra-high purity argon for 1.5 hours, the sulfide gas liberated was trapped as HS^- in 10 mL of anoxic 0.1 M trace metal clean NaOH (Wu and Boyle, 1998) in a glass test tube. The NaOH solution was analyzed on a hanging mercury drop electrode (HMDE) controlled by an AIS DLK-100a potentiostat, with sulfide monitored at a potential of -0.6 V. Fresh NaOH was added to new test tubes, purged, then 4 mL acidified Cr(II) were injected into the reaction vessels. Cr(II) was prepared by reducing a Cr(III) solution on an amalgamated zinc column. After the addition of Cr(II) the mixture was allowed to purge and trap H_2S for an hour, then the NaOH containing trapped sulfide was again analyzed on the HMDE.

Although *in situ* voltammetry was also conducted in the rising plume at MAR vents, voltammetric measurements for sulfide were not conducted in the lower portions of the plume (< 1 m) as sulfide concentrations were too high to be measured with this method, and the temperature was above the thermal limit of the electrodes. Additionally, precipitation of metal sulfide minerals in the rising plume makes the measurement of AVS/CRS more appropriate for this system.

3.2.3 S^0 Extraction Method

Sample aliquots of 30-50 mL were filtered through a 0.2 µm Millipore GTTP filter and the filtrate was extracted shipboard in 5 mL of toluene for 1.5 hours. The extraction was performed by adding the filtered sample water and toluene to glass separatory funnels, which were shaken every half hour. For samples with pH > 4, 15 µL concentrated HCl were added and the sample was shaken prior to the extraction in order to release any sulfide as H_2S. The toluene layer was saved and stored in a glass test tube at -10˚C for later analysis. Filters were also stored in glass test tubes and frozen for later extraction and analysis onshore. Elemental sulfur was quantified on a HPLC C-18 column using 98 % methanol 2 % water as the eluent (Yücel et al., 2010), and the eluent was sparged with helium gas during the analysis. The pump speed was set to 1 mL/minute, the detector set at 264 nm, and the retention time for elemental sulfur was approximately eight minutes. Standard curves encompassed the concentrations observed in samples and were made using commercially available orthorhombic S_8 dissolved in toluene. The detection limit for this method is 0.1 µM.

A study by Janssen et al. (1999) indicates that microbially produced S^0 is not quantitatively extracted in organic solvents; however their study did not test extraction in toluene. Sulfur mass balance tests conducted in our laboratory using the Chesapeake Bay isolate demonstrate that we can account for over 85 % of sulfur formed from added sulfide utilizing our extraction method. Some of the missing sulfide is likely still in bacterial cells as S^0 or other oxidized intermediates. This gives us confidence that we are recovering S^0 nearly quantitatively.

Previous studies in porewaters and laboratory solutions have measured elemental sulfur using the voltammetric technique employed for sulfide measurements in our study (Rozan et al., 2000; Boyd and Druschel 2013). In those studies an additional peak attributed to elemental sulfur was measureable. Although we detected S^0 as S_8 in discrete samples using HPLC, we did not observe a signal associated with elemental sulfur using voltammetry in either the Chesapeake Bay or at the MAR. We attribute this difference to the sampling difference between discrete sampling and in situ measurements. Both of these field systems are undergoing dynamic mixing processes and voltammetry measures a very small sample volume relative to discrete samples. We note that one voltammetric scan is complete in < 2 seconds and is a snapshot measurement at a 100 μm diameter electrode relative to the discrete titanium (700 mL), or Niskin samplers (10 L), which provide an average sample in time and space.

3.2.4 Anoxygenic Phototrophic Sulfide Oxidizing Bacteria

A strain of phototrophic sulfide oxidizing bacteria was enriched from the Chesapeake Bay in 2011 from samples taken at, and directly below, the suboxic zone. Enrichments were started by injecting 1 mL of Chesapeake Bay water into 20 mL septum vials containing anoxic media with bicarbonate as the carbon source at a concentration of 17.9 mM, and a sulfide concentration of 2.5 mM (Widdel et al., 1983). The vials were incubated under ambient conditions bench top, and once growth was observed, cultures were enriched through subsequent dilutions in media.

Once enriched, laboratory cultures of the Chesapeake Bay strain were grown from a starter culture at 25˚C for 48 hours under 20 μEi m^{-2} s^{-1} light flux from full spectrum incandescent bulbs in order to maintain fresh culture stock.

3.2.5 Imaging

Scanning electron microscopy (SEM) was conducted on a Hitachi S-4700 located in the Delaware Biotechnical Institute in Newark, DE using Inca analysis software. For MAR samples, filters were prepared for SEM imaging by filtration through a 0.2 μm Nuclepore filter. The filters were dried under a stream of argon gas, then were attached to aluminum stubs with carbon paint and stored in petri dishes. Prior to analysis on the SEM, both the filters and stubs were carbon coated.

Images of bacteria and elemental sulfur particles were taken using a cryo attachment to the SEM. Sample aliquots of 0.5 mL were taken from growing cultures and from sulfide oxidation experiments, vacuum filtered through a 0.2 μm GTTP filter, and washed in HEPES buffer (1 M, pH 7.4). These filters were dried and mounted on an aluminum stub before being frozen in liquid nitrogen. Once frozen, the samples were kept in a vacuum and were coated in a gold-palladium coating. The temperature was maintained at -120 ˚C using liquid nitrogen throughout the analysis.

For both sets of samples, micrographs were taken using the Ultra-High resolution mode at 3 kV and 25 μA. Analysis with an energy dispersive x-ray spectrometer (EDS) and elemental mapping of sulfur were done under Analysis mode, at 15 kV and 25 μA.

3.2.6 Magnesium Measurements

Magnesium concentrations are used as a proxy for the degree to which the hot vent fluid has mixed with seawater. During sampling, a separate temperature sensor provided by the ROV Jason II is placed next to the sampling nozzle of the Major Sampler, but movement of the plume due to physical forcing, and visual impairment as a result of particulates mean that the measurement is not precise. Mg values provide a more accurate description of the mixing process because end-member vent water magnesium concentrations are 0 (see section 3.4 for further discussion).

Magnesium was measured in MAR samples using a Thermo Electron Corporation Finnigan Element XR Inductively Coupled Plasma Mass Spectrometer (ICP-MS) at low resolution. Prior to analysis, samples that had been acidified in nitric acid and frozen shipboard were diluted 100 times in a solution of 5.2 nM iridium in 2 % Ultrex® trace metal clean nitric acid. Preparation of dilutions and analysis with the mass spectrophotometer were conducted in a class 1000 clean room. Dilutions were made with 18megohm water (Barnstead) and Ultrex® nitric acid.

3.3 Results and Discussion

3.3.1 Chesapeake Bay

3.3.1.1 Characteristics of S^0 in the Chesapeake Bay

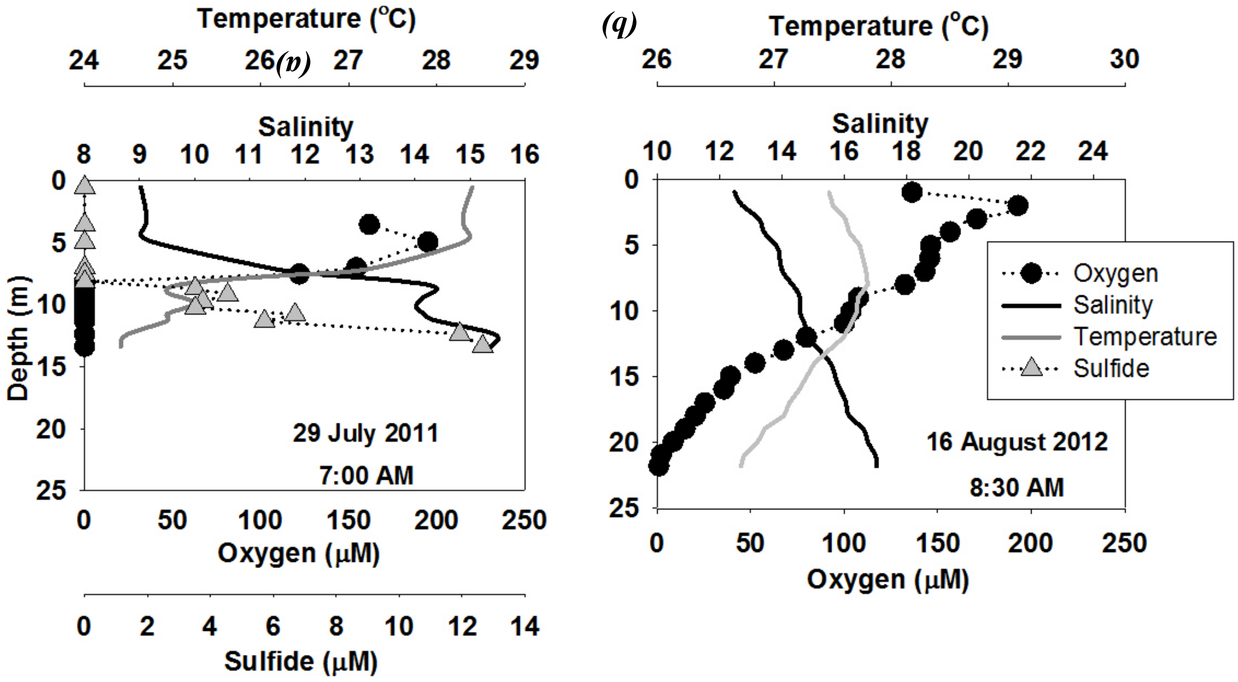

Figure 3.1 Profile of temperature and salinity measured with the ship CTD, and of oxygen and sulfide measured using *in situ* voltammetry for *(a)* 2011 and *(b)* 2012. In 2011 a sharp thermocline and halocline are present between 5 and 8 meters, corresponding to the chemocline. In 2012 the water column was more homogenous, and no clear physical or chemical interface was present.

2011. In 2011, the study site was clearly stratified with a strong thermocline and coincident chemocline. The top layer remained oxic, to about 8 meters depth and sulfide increased steadily with depth (Figure 3.1a). Although the *in situ* profile system was not utilized for the deepest waters (up to 25 m depth) measurements from discrete bottle samples confirmed the presence of sulfide up to 90 µM at those depths.

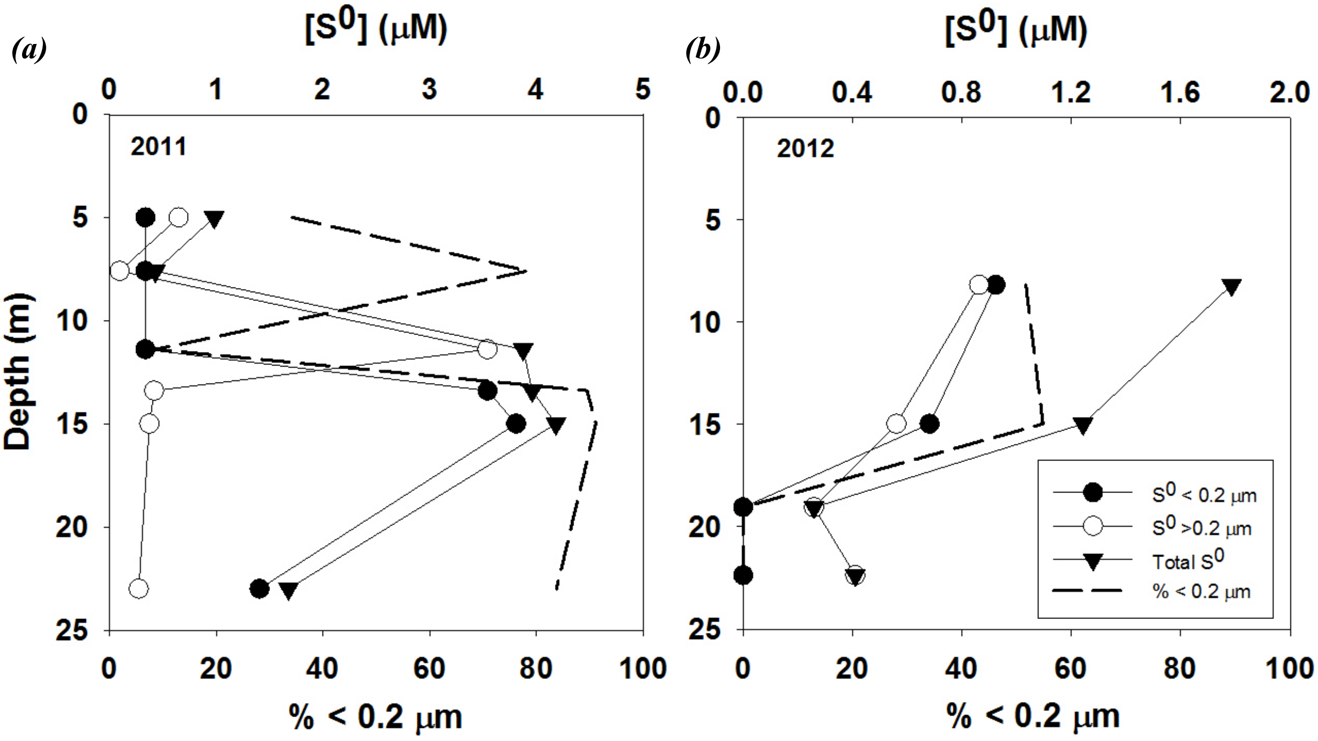

Figure 3.2 Water column concentrations and distributions of elemental sulfur in *(a)* 2011 and *(b)* 2012. In 2011 elemental sulfur concentrations peaked directly below the suboxic zone at 8 m. In 2012 elemental sulfur was present despite no detectable sulfide being present in the water column.

Figure 3.2a shows a representative profile of elemental sulfur, with a peak in concentration directly below the oxic/anoxic interface. For all samples taken in 2011, elemental sulfur concentrations ranged from below the detection limit of 0.1 μM to about 6 μM. Particulate elemental sulfur peaked at the base of the suboxic zone, followed by a peak in nanoparticulate elemental sulfur. On average, nanoparticulate elemental sulfur is 60% of the total sulfur pool, but at its maximum concentration nanoparticulate elemental sulfur constituted up to 90 % of the total elemental sulfur pool. Nanoparticulate elemental sulfur remained the dominant size fraction at depth.

2012. In contrast to 2011, the water column in 2012 was more homogenously mixed and oxygen penetrated deeper into the water column, with a suboxic zone present below 22 m. No sulfide was detected in 2012 measurements (Figure 3.1b).

A representative profile of elemental sulfur distributions from 2012 is shown in Figure 3.2b. The water column of the Bay did not have clear oxic and anoxic zones, was without a sharp thermocline, (Figure 3.1b) and sulfide was not detected. Concentrations of elemental sulfur ranged from below detection to 1.7 μM. The nanoparticulate fraction composed a smaller percentage of total sulfur with an average for all samples of 20 %. Sulfide was not detected in the water column, and there are several potential sources for the observed sulfur. One possibility is that this sulfur is left over from the recent turn over of euxinia. The Maryland Department of Natural Resources reported that much of the bay was oxic in 2012, and their data show a very limited hypoxic zone in the weeks before we sampled. Additionally, the extent to which the water column was oxygenated during our sampling makes it unlikely that the site was sulfidic immediately preceding our visit. A more likely hypothesis is that the sulfur comes from the abiotic oxidation of sulfide released during organic matter decomposition, as sulfide is an important component of proteins and enzymes such as ferredoxins, cysteine, and methionine in planktonic organisms, which typically contain about 1% sulfur by weight (Jørgensen, 1982). The lower percentage of nanoparticulate sulfur could have occurred as a strong chemocline was not present in 2012, and the lack of a chemical interface and reducing zone could result in the formation of larger particles. Dynamic biological and chemical redox cycling at the chemical interface in 2011, with oxidation occurring as sulfide fluxes up and reduction of elemental sulfur as it sinks would likely result in smaller particle size.

The presence of nanoparticulate elemental sulfur at depth in the Chesapeake during 2011 is significant for several reasons. Zerovalent sulfur can act as a chemical oxidant and reductant in the anoxic zone, can complex metals such as copper and mercury (Wang and Tessier, 2009), and may be important in organic matter sulfurization (Gun et al., 2000). In addition, elemental sulfur is important biologically. Some phototrophic sulfur bacteria and chemoautotrophic bacteria utilize it as a substrate. Sulfur reduction is an important metabolism in proteobacteria such as *Desulfurella acetivorans* (Widdel and Pfennig, 1982), *Sulfurospirillum arcachonense* (Finster et al., 1998), and *Shewanella putrefaciens* (Moser and Nealson, 1996), and elemental sulfur reduction is widespread in archaea (Canfield, 2005). In some phototrophic sulfide oxidizers, such as *Chlorobaculum tepidum,* elemental sulfur is used as an electron donor in the absence of sulfide (Chan et al., 2008). At sulfide concentrations less than 1 mM, elemental sulfur disproportionation is thermodynamically favorable (Canfield, 2005) and bacteria utilizing this metabolism are known (Thamdrup et al., 1993; Finster et al., 1998). Recently, zerovalent sulfur was found to be a key intermediate in anaerobic methane oxidation coupled to sulfate reduction by archaea as deltaproteobacteria associated with the methane oxidizing archaea were found to disproportionate the S^0 (Milucka et al., 2012).

3.3.1.2 Polysulfide Equilibria

Calculations

The solubility of elemental sulfur increases in the presence of sulfide at neutral and alkaline pH due to the formation of soluble polysulfides (Giggenbach, 1973; Kamyshny et al., 2004; Kleinjan et al., 2005). Expected polysulfide concentrations were calculated for both the Chesapeake Bay and Mid-Atlantic Ridge (see section 3.4.2) using the thermodynamic values of Kamyshny et al. (2007). Concentrations of polysulfides for chain length x= 2-8 were calculated using equation 1 and summed for the total expected polysulfide concentration.

$$(1)\ [S_x^{2-}] = \frac{e^{-\Delta G/RT}\,[H_2S]}{[H^+]}$$

For equation 1, R = 0.00831 (kJ/mol·K), T is the temperature in Kelvin (K), and ΔG is the Gibb's energy of formation (kJ/mol) determined by Kamyshny et al. (2007). The individual parameters for $[H_2S]$, T and $[H^+]$ used were those measured at each field site.

Polysulfides are measureable using the voltammetric method described earlier (Luther et al., 2001), but were not detected during *in situ* profiling. Polysulfide concentrations below the chemical interface were calculated using the thermodynamic values of Kamyshny et al. (2007) assuming saturation with respect to elemental sulfur. For the deepest part of Chesapeake Bay, polysulfide concentrations are calculated to be less than one percent of the sub 0.2 μm fraction of elemental sulfur and with values not exceeding 2 nM, which is below the detection limit of the method used (0.2 μM).

3.3.1.3 Sulfide Oxidation and Formation of Elemental Sulfur

Elemental sulfur in the Chesapeake is likely formed from a combination of abiotic oxidation and biological oxidation of sulfide. Chemical oxidation of sulfide to S^0 could occur via a two electron oxidation by iron and manganese oxides (equations 2 and 3).

(2) $2\ FeOOH + HS^- + 5\ H^+ \rightarrow 2\ Fe^{2+} + S^0 + 4\ H_2O$

(3) $MnO_2 + H_2S + 2\ H^+ \rightarrow Mn^{2+} + S^0 + 2\ H_2O$

The formed S^0 reacts with sulfide to form polysulfides and as more S^0 forms from oxidation of sulfide, the polysulfide chain increases until S_9^{2-} forms, then decomposes to S_8 and HS^- (Hoffman, 1977; Luther, 1990). In addition, when metal concentrations are high, metals react with polysulfide to form MS species and S_8 (Chadwell et al., 2001). Oxidation by manganese oxides is expected to be the dominant chemical process as manganese is a stronger oxidant than Fe(III) for sulfide (Luther, 1990) and reacts with sulfide more rapidly than Fe(III) does (Yao and Millero, 1993; Yao and

Millero, 1996). Additionally, in the Chesapeake Bay, total manganese is present at higher concentrations than total iron. In 2011, Fe^{3+} was present at concentrations up to 1 μM, Fe^{2+} concentrations were up to 2.74 μM, and total iron did not exceed 3.6 μM. In the same year, manganese oxide concentrations at the chemical interface were up to 3 μM, peaking directly above the elemental sulfur maximum, and soluble manganese concentrations were up to 4 μM. In considering these concentrations, it is important to note the stoichiometry of the oxidation of sulfide by iron or manganese. Two moles ferric iron are required to convert one mole sulfide to sulfur, while only one mole of Mn^{4+} is required for the same conversion, as illustrated in equations 3 and 4. Oxidized manganese has been shown to be the major oxidant in similar systems such as the Black Sea (Konovalov et al., 2003). Due to the higher concentrations and faster kinetics than for iron, manganese oxides are likely the dominant chemical oxidant for sulfide in the Chesapeake Bay.

In addition to abiotic processes, sulfide oxidation experiments conducted in the Chesapeake Bay in 1987 (Luther et al., 1988) and in 2012 show significant differences in sulfide oxidation rates between light and (0.96 μM/min) and dark (0.030 μM/min) conditions, and upon addition of formaldehyde (0.24 μM/min), (Figure 3.3; Hanson et al., 2013) indicating a photobiological influence on sulfide oxidation. The 2012 experiments were conducted in anoxic water samples, and anaerobic conditions were maintained through the use of a glovebag purged with ultra-high purity argon gas. That light dependent sulfide oxidation was observed in two different studies indicates that it is a common component of the sulfur cycle in the Chesapeake Bay (Hanson et al., 2013) and suggests that biotic processes may dominate sulfide oxidation and subsequent elemental sulfur formation in the Chesapeake Bay.

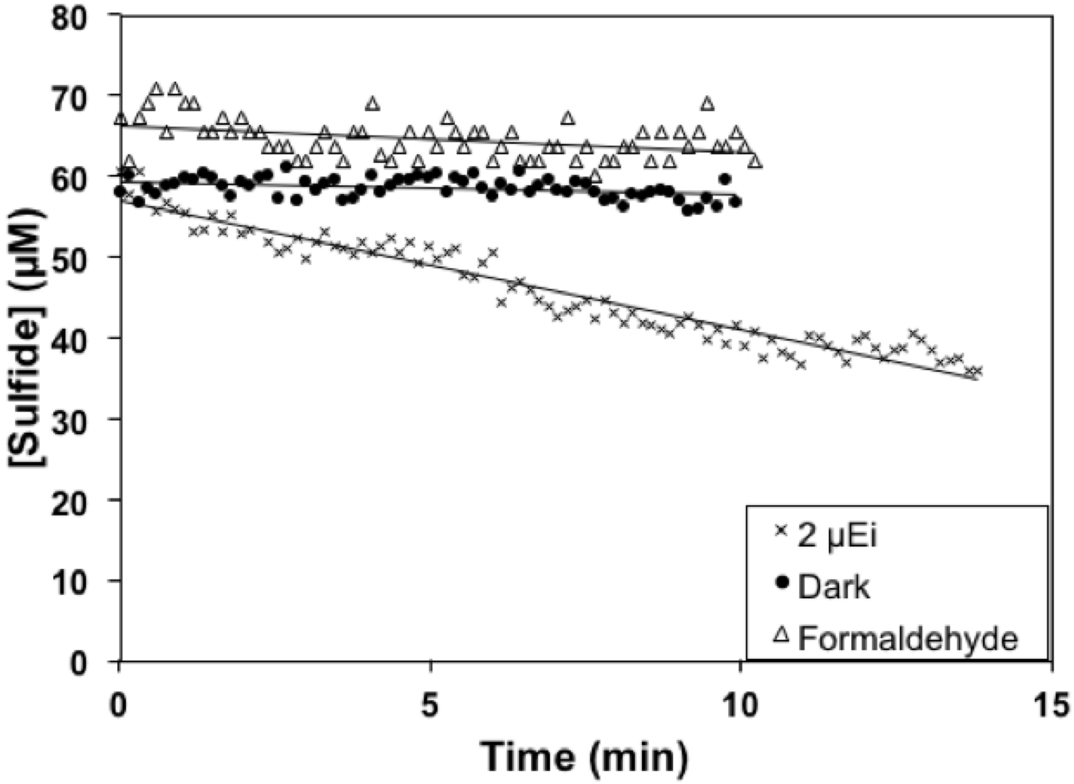

Figure 3.3 Comparison of *in situ* sulfide loss in the dark (black circles) and in the light (crosses). Small increases in light intensity (from 0-2 μEi) result in significant changes in the rate of sulfide loss.

The hypothesis that biological sulfide oxidation occurs in the Chesapeake Bay is supported by the cultures of phototrophic sulfide oxidizing bacteria enriched from the suboxic zone in 2011. The bacteria appear to be a strain of green sulfur bacteria (*Chlorobi*) that are brown in colour and are well adapted to low light environments (Hanson et al., 2013). These bacteria are shown to produce elemental sulfur as a product of sulfide oxidation. Upon completion of sulfide oxidation in experiments in which 100 μM sulfide was added to cultures in log phase growth, up to 60 μM S^0 were measured. Figure 3.4 shows SEM data of elemental sulfur produced by bacteria growing in culture on sulfide. The average size of the particles shown in the image is 50 ± 22 nm. SEM images from other portions of the filter show variations in particle sizes from 32-4700 nm, and many of the larger particles (> 1000 nm) appear to be composed of aggregated smaller particles (< 200 nm). Overall, half of the particles on the filters were smaller than 500 nm, and particles associated with bacteria were truly nanoparticulate (30-100 nm). Sulfur produced by different strains of bacteria has been shown to have different properties (Frigaard and Dahl, 2008); however as some biologically produced sulfur has shown to be resistant to aggregation (Kleinjan et al., 2003), we cannot rule out the possibility that the aggregation and growth observed on these filters may be at least partially induced by the preparatory procedure for the SEM.

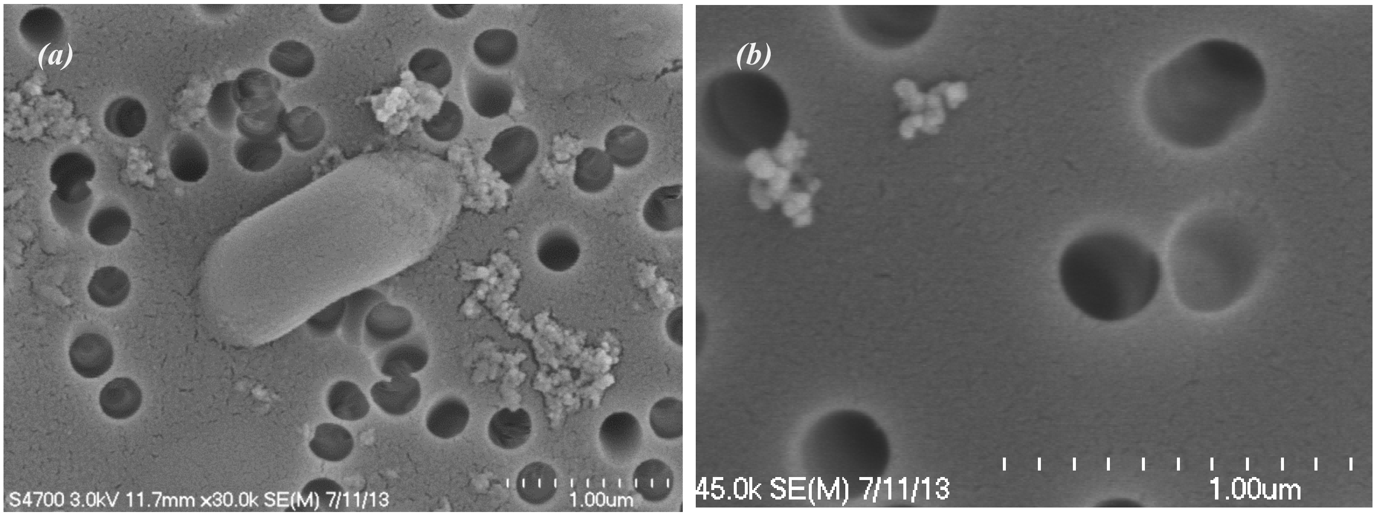

Figure 3.4 *(a)* Image of bacterium and elemental sulfur particles. The bacterium is of the strain isolated from the Chesapeake Bay and was grown in culture on sulfide for 18 hours. *(b)* Elemental sulfur nanoparticles produced by bacteria during kinetic experiments. Elemental sulfur was confirmed through EDS elemental mapping.

Due to the small size of the S_8 particles produced by Chesapeake Bay cultures, we hypothesize that the formation of nano-sulfur in the Chesapeake may be predominately biological, particularly in years when it is chemically stratified and sulfide is present in the water column. Inorganic sulfur is hydrophobic and aggregates quickly in aqueous solution; however, biologically produced elemental sulfur can have an organic coating or a hydrophilic surface, which stabilizes the nanoparticles to aggregation and growth processes (Kleinjan et al., 2003). Although the particle size of abiotically produced sulfur may initially be nanoparticulate it is expected to increase quickly in saline water (Steudel, 1996). Biologically produced sulfur may persist at small sizes due to its stability with respect to growth and aggregation. Additionally, in sulfidic solutions, biologically produced sulfur is less likely to react to form polysulfides than abiotically produced sulfur (Kleinjan et al., 2005a). The elemental sulfur observed in Chesapeake Bay could have a different reactivity with respect to forming polysulfides because at least some fraction of the elemental sulfur is produced biologically.

The relative importance of abiotic and biotic processes on the formation of elemental sulfur can differ depending upon the environment (Jorgensen et al., 1979; Li et al., 2008) and also can vary seasonally. In a stratified lake, chemical sulfide oxidation dominated in the fall and phototrophic oxidation in the spring and summer (Zerkel et al., 2012). This change is important as elemental sulfur produced by abiotic and biotic pathways differs in crystal structure, reactivity, and bioavailability (Kleinjan et al., 2003; Kleinjan et al., 2005a; Kleinjan et al., 2005b; Franz et al., 2007).

3.3.1.4 Comparison with Previously Reported Sulfur in Water Column Studies

To date only two studies have reported nanoparticulate (< 0.2 µm) elemental sulfur in environmental samples (Li et al., 2008 and Zerkle et al., 2010). Zerkle et al. (2010) measured the size distribution of elemental sulfur and found larger particles (> 0.45 µm) at the interface and smaller particles (< 0.2 µm) at depth. This distribution of elemental sulfur is similar to the data we present from the Chesapeake Bay in 2011. Li et al. (2008) observed a S^0 maximum at the chemical interface in the Cariaco Basin that was correlated to chemoautotrophic production, highlighting the potential for S^0 to be an energy source for microorganisms.

Particulate elemental sulfur concentrations and distributions have been reported in previous water column studies. Elemental sulfur concentrations up to 5 μM have been observed in the deep waters of stratified seawater lakes, with as much as 70 % passing through a 1.2 μm filter (Kamyshny et al., 2011). In a meromictic freshwater lake with sulfide levels up to 1.8 mM elemental sulfur concentrations have been found as high as 40 μM, with up to 87 % passing through a 0.2 μm filter at depth (Zerkle et al., 2010). In marine systems such as the Black Sea total elemental sulfur is present at peak concentrations of 60 to 200 nM (Luther et al., 1991; Jorgensen et al., 1991), and in the Cariaco Basin, studies have measured particulate sulfur at concentrations peaking at approximately 0.4 μM (Hastings and Emerson, 1988) and up to 1.22 μM (Li et al., 2008). In the permanently stratified sea Lake Rogoznicka, Ciglenečki et al. (1996) report up to 140 μM sulfur in the anoxic waters. In the Mariager Fjord, Zopfi et al. (2001) report zero-valent sulfur peaking at the chemocline at 17.8 μM. The highest concentrations of total elemental sulfur reported here for the Chesapeake Bay (6 μM) fall into the range that has been reported in similar environments (60 nM- 40 μM).

3.3.2 Hydrothermal Vents Along the Mid-Atlantic Ridge

3.3.2.1 Characteristics of S^0 in Buoyant Plumes

All samples were taken from within the first meter and a half of the buoyant plume. The concentration of magnesium in the samples is used as a proxy measure for the extent of mixing with ambient seawater in the rising plume. End-member vent fluid has a Mg concentration of 0 mM (Edmond et al., 1982), and end-member seawater has a Mg concentration of 53 mM. With the magnesium concentrations in the samples, it is then possible to calculate the percentage of seawater that has been entrained in the vent fluid as the plume rises. The Mg concentration and percentage of seawater mixing for each sample are given in Table 3.3.

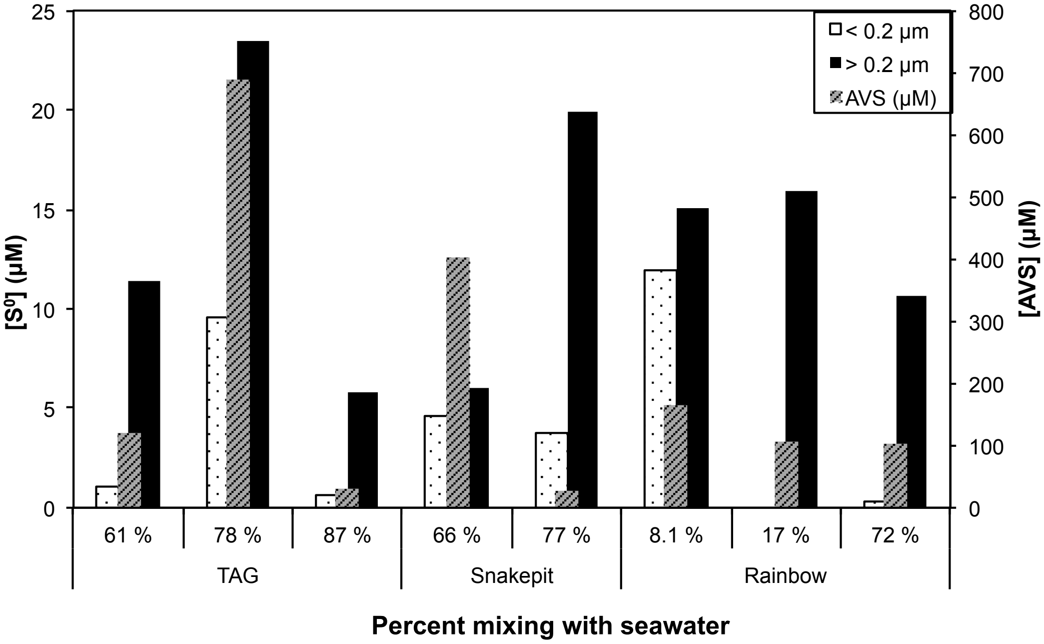

Figure 3.5 Size fractionation of elemental sulfur in the TAG, Snakepit, and Rainbow buoyant plumes as the vent water mixes with seawater. AVS concentrations are form the unfiltered portion.

Figure 3.5 shows the distribution of elemental sulfur between the particulate (> 0.2 µm) and nanoparticulate (< 0.2 µm) fractions in the buoyant plumes of the three vent sites sampled along the MAR. Nanoparticulate S_8 was present at all three vent sites and comprises a significant fraction of the total elemental sulfur pool at each of the three vent sites. The percentage of total elemental sulfur that is nanoparticulate ranges from below detection up to 44 % at Rainbow, between 15-43 % at Snakepit, and between 8-28 % at TAG.

Snakepit had the highest percentage of S^0 /unfiltered AVS at 5 %. TAG had the highest concentration of total elemental sulfur measured (33.0 µM), and Rainbow had the highest concentration of nanoparticulate elemental sulfur (12.0 µM) measured for any of the vents. The Rainbow vent site had concentrations of sulfide an order of magnitude lower, and concentrations of iron an order of magnitude higher than the other two vent sites (Table 3.1; Douville et al., 2002; Gartman et al., 2014). Due to the excess iron, oxidation of S^0, or scavenging of S^0 particles by iron oxides may be an important removal processes at this vent site.

3.3.2.2 Polysulfide Equilibria

Polysulfides were not detected at any of the sample locations in the rising plume using *in situ* voltammetry with a detection limit of 0.2 µM. Polysulfide calculations (section 3.3.1.2) for vent fluid samples under 100 ˚C give concentrations that are lower than the detection limit of the voltammetric method used (Table 3.2).

Table 3.2 Measured parameters and polysulfide concentrations calculated based on equilibrium assumptions for the rising plumes at MAR.

Vent	% mixing with seawater[a]	T (˚C)	pH	Unfiltered [AVS] (µM)	[S^0] <0.2 µm (µM)	[S^0_{Total}] (µM)	Calculated polysulfide (µM)[b]
TAG	61	247	5.53	120.2	1.03	12.5	30.7
	78	93.2	5.07	689.4	9.56	33.0	0.0849
	87	37.6	6.77	30.97	0.683	6.50	$3.65x\ 10^{-3}$
Snakepit	66	170	5.64	403.3	4.65	10.7	8.64
	77	35	6.30	27.76	3.76	23.7	$8.89x10^{-4}$
Rainbow	8.1	230	3.37	163.5	12.0	27.1	0.167
	17	80	5.43	105.5	< 0.1	15.9	0.0130
	72	31.8	7.71	101.6	0.342	11.0	0.0635

[a] Calculated based upon magnesium values (Table 3.3)
[b] Calculated using the thermodynamic values in Kamyshny et al. (2007)

The electrodes used in this study are rated only up to 100 º C, so no measurement for polysulfides was obtained for higher temperatures. Polysulfides are metastable at temperatures under 150 ˚C, but at temperatures above 150 ˚C, polysulfides degrade to form sulfite or thiosulfate (Giggenbach, 1973). Although no polysulfides were detected in the anoxic portion of the plume from which both samples were taken and voltammetric measurements were made, trace quantities of polysulfides were observed higher up in the rising plume, above the range in which discrete samples were taken. These polysulfides were detected in waters in which both oxygen and sulfide were present, demonstrating that polysulfides do occur as an intermediate of sulfide oxidation. Polysulfides could then react quickly with Fe^{2+} via equation 4 to form FeS and elemental sulfur (Luther, 1991).

(4) $Fe^{2+} + S_9^{2-} \rightarrow FeS + S_8$

This reaction is significant as polysulfides, FeS (Luther, 1991; Rickard and Luther, 1997), and elemental sulfur (Berner, 1970; Wilkin and Barnes, 1996) are all precursors to pyrite formation. The formation of pyrite at hydrothermal vents represents a mechanism for the transport of stable, reduced iron from hydrothermal vents to the greater ocean (Yücel et al., 2011; Gartman, 2014). Any additional nanoparticulate pyrite that may be formed in the rising plume would also be important as a potential transport mechanism.

3.3.2.3 Sulfide Oxidation and Formation of Elemental Sulfur

As oxygen is entrained in the plume as a result of seawater mixing, elemental sulfur production in the plume is due mainly to sulfide oxidation via an iron catalytic cycle (Ma et al., 2006). Iron is considered the primary oxidant due to thermodynamic and kinetic inhibition of the direct reaction of sulfide with oxygen (Luther et al., 2011). Neither manganese oxidation of sulfide nor a Mn catalytic cycle will occur in the plume as the chemical oxidation of aqueous Mn^{2+} does not occur below pH 9 (Stumm and Morgan, 1996; Luther, 2010), and the shipboard pH of all samples was less than 8. In the Fe catalytic cycle, oxygen entrained in the plume would oxidize the reduced iron present rapidly via the reaction represented by equation 5 (Rudnicki and

Elderfield, 1993; Yao and Millero, 1996). The oxidized iron would then be reduced by sulfide, forming elemental sulfur in the process (equation 6) (Ma et al., 2006).

(5) $4\ Fe^{2+} + O_2 + 4\ H^+ \rightarrow 4\ Fe^{3+} + 2\ H_2O$

(6) $2\ Fe^{3+} + H_2S \rightarrow 2\ Fe^{2+} + S^0 + 2\ H^+$

The rates of these abiotic processes are expected to be fast and to preclude microbial sulfide oxidation in the first meters of the buoyant plume (Winn et al., 1986). Previous measurements of the halflife of Fe^{2+} within the first 150 m of the TAG plume are approximately two minutes (Rudnicki and Elderfield, 1993). In our study oxygen was not detectable *in* situ within the first 1.5 meters of the plume, although calculations predict that oxygen should be present at concentrations of tens of micomolar based on the extent of mixing of vent fluid and seawater (Table 3.3). This indicates that entrained oxygen is consumed nearly immediately upon contact with the hydrothermal fluid, and is consistent with the kinetics of iron oxidation by oxygen (Millero et al., 1987).

We can predict the concentration of elemental sulfur that could form in the plume via the iron catalytic cycle in each of our samples (Table 3.3) using equations 5 and 6 and the known O_2 concentration of end-member seawater. We measured 270 μM oxygen in ambient deep waters with our *in situ* voltammetry system. With this value for end-member seawater, assuming end-member vent fluid to be anoxic ($[O_2] = 0$), and using the percentage of seawater mixing derived from Mg values, we can calculate the concentration of oxygen expected to have been entrained into the plume as it rises. The predicted values of elemental sulfur assume that oxygen, iron and sulfide all react quantitatively.

Table 3.3 Calculated concentrations of elemental sulfur potentially formed in the rising plume as a result of an iron catalytic cycle.

Site	**[Mg] (mM)**	**% mixing with seawater** [a]	**Predicted [O_2] (µM)**[b]	**Predicted [Fe^{3+}](µM)**[c]	**Predicted [S^0] (µM)**[c]	**Measured [S^0_{Total}] (µM)**[d]
TAG	32.1	61	161	642	321	12.5
	41.2	78	206	824	412	33.0
	45.9	87	229	917	459	6.50
Snakepit	35.2	66	175	703	352	10.7
	41.0	77	204	819	410	23.7
Rainbow	4.31	8.1	21.6	86.2	43.1	27.1
	9.12	17	45.6	182	91.2	15.9
	38.4	72	192	768	384	11.0

[a] Calculated based upon magnesium values
[b] Calculated from equation 5
[c] Calculated from equation 6
[d] Measured in this study

In all of the samples the iron catalytic cycle can account for all of the S^0 observed, and our calculations predict more total S^0 than is measured. There are several possible explanations for why there is less S^0 measured than calculated. First, the calculation assumes that all oxygen reacts with iron, and that in turn, all iron reacts with sulfide. In reality these processes are likely not quantitative as both oxygen and iron can react with other species within the plume. Hydrolysis of elemental sulfur can occur at high temperatures (Ellis and Giggenbach, 1971); however it is improbable that hydrolysis occurs in the rising plume as the hotter samples contain higher concentrations of S^0 at TAG and Rainbow than the coolest samples with highest Mg. Oxidation of elemental sulfur is also an unlikely removal processes as the reduced iron and sulfide present in the first meter of the plume will react with O_2 much more rapidly. Additionally, aggregation and precipitation from solution are not likely due to the rapid focused flow near the orifice. S^0 can react with FeS to form pyrite via equation 7 (Berner, 1970; Wilkin and Barnes, 1996). This reaction occurs under hydrothermal conditions, although slowly (Gartman and Luther, 2013), and at the *in situ* pH and sulfide concentrations, the reaction of H_2S and FeS likely dominates pyrite formation (Rickard and Luther, 1997). Both nanoparticulate and particulate pyrite have been measured in the buoyant plumes at all three vent sites (Gartman et al., 2014).

(7) $FeS + S^0 \rightarrow FeS_2$

Furthermore, the calculations are based on a single point within the plume, while the measured sulfur concentrations reflect processes occurring throughout the plume up to the point at which the sample was taken.

In addition to the iron catalytic cycle, elemental sulfur may have come from the vent itself. The hypothesis that elemental sulfur could come from the chimney wall or from inside the vent is supported by the presence of elemental sulfur particles in samples taken from within the vent orifice, shown in Figure 3.6a. Elemental sulfur particles of approximately 5 and 7 μm were found via SEM analysis of 0.2 μm filters from the TAG vent fluid (Figure 3.6a) and buoyant plume (Figure 3.6b). The 5 µm particles found in the vent fluid sample appear to be aggregates of smaller micron-sized particles, whereas the particles found higher in the rising plume are larger discrete particles.

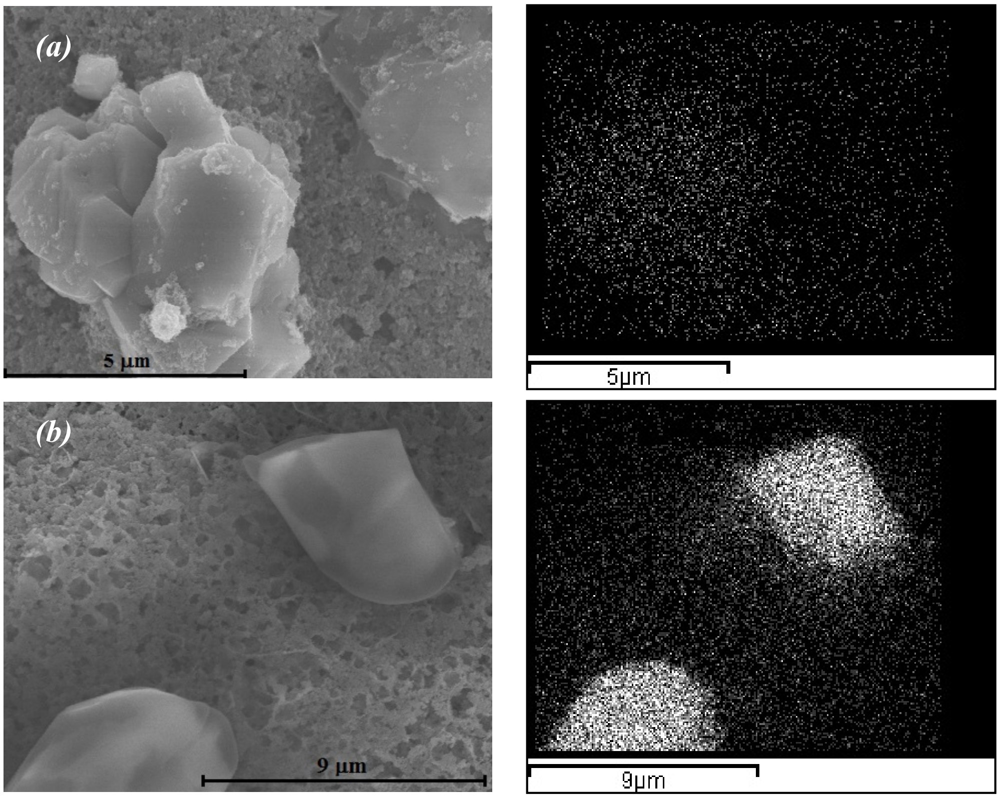

Figure 3.6 SEM images of elemental sulfur on 0.2 µm filters from *(a)* the TAG orifice and *(b)* the TAG plume with 66 % mixing with seawater. The corresponding EDS maps show the concentration of sulfur in the particles. The differences in contrast between the elemental maps are due to the duration in time of data collection.

Irrespective of the source or formation process, the presence of elemental sulfur within the plume, particularly with increasing distance from the vent orifice, is significant as it may be an important source of energy to microbes. Elemental sulfur was not detected in neutrally buoyant plume samples, which were taken approximately 400 meters above the vent orifices, and above the first few meters of the rising plume, microbial metabolism may be an important removal process for elemental sulfur. According to a model by McCollom (2000) describing energy available from minerals evolving from vents, elemental sulfur is predicted to be the largest source of energy, regardless of whether particles settle around the vent or are transported from the site. In this model, a parcel of vent fluid with an initial concentration of 7.3 mM sulfide (approximately 125 % of our maximum sulfide concentration measured; Table 3.1) would form 4 mM S^0 over its lifetime as it rises and moves from the orifice. This S^0 in turn would provide 610 calories/kg vent fluid in energy and could result in 17 mg dry weight biomass per kilogram of vent fluid, assuming 100 % efficiency in the conversion of energy to biomass. In this scenario as stated in the model, S^0 would provide 43 % of the total energy available from minerals in the plume.

3.3.2.4 Comparison with Previously Reported Sulfur in Hydrothermal Plumes

Elemental sulfur has not been extensively studied in hydrothermal vent plumes, and to the best of our knowledge, the results presented here are the first study of inorganic S^0 distribution and particle size in the first meter of buoyant hydrothermal plumes.

A model by Klevenz et al (2011) finds that elemental sulfur should not form at seawater mixing ratios less than 5 %. They show SEM micrographs of a magnesium iron silicate mineral with elemental sulfur droplets attached, and found sulfur droplets associated with talc in samples with 5 and 12 % seawater mixing. As the plume rises further and a greater proportion of seawater and oxygen are mixed in, more elemental sulfur could form from further oxidation of sulfide, and sulfur from additional sources may be entrained. For example, sulfur rich organic matter has been observed in the buoyant plume at East Pacific Rise (EPR), following an eruption (Haymon et al., 1993) and in non-buoyant plumes at EPR (Taylor and Wirsen, 1997) and Juan de Fuca (Feely et al., 1994). Feely et al. (1994) hypothesized that sulfur rich material was from bacterial detritus suspended in the water column as a result of volcanic eruptions. More recent results of sulfur rich organic matter in the non-buoyant plume at the EPR more than 1.5 years after an eruption are suggestive of either suspension of biomass located near the vents, or of water column production, such as chemosynthetic sulfide oxidation (Breier et al., 2012).

3.3.3 Comparison of the Chesapeake Bay and MAR

The Chesapeake Bay and the buoyant hydrothermal vent plumes studied along the Mid Atlantic Ridge differ in pH, temperature, trace metal content, and sulfide concentration. In the vent fluid at MAR, sulfide (measured as AVS) is up to two orders of magnitude higher than the highest concentration observed in the Chesapeake Bay (90 µM). Furthermore, sulfide oxidation occurs by different processes: in the Chesapeake Bay oxidation takes place via both the reaction of sulfide with manganese oxides and the activity of sulfide oxidizing bacteria. In contrast, sulfide oxidation in the first meter of rising hydrothermal plumes is likely strictly abiotic by iron oxides as part of an iron catalytic cycle. In addition to differences between the two systems, it is also important to note that variations exist within each system. Between 2011 and 2012 the water column of the Chesapeake changed from stratified and sulfidic to a more mixed and oxygenated system, and the fluid chemistry of the three vent sites studied along the MAR varied with respect to their sulfide and trace metal concentrations.

Despite these differences, these systems share an important similarity: in each, a dynamic sulfur cycle is present along a redox gradient. Moreover, nanoparticulate elemental sulfur comprised a significant fraction of total sulfur in each of these systems. In the Chesapeake Bay in 2011 nanoparticulate S^0 was up to 90 % of total sulfur, in 2012 it was up to 20 %, and at the MAR, it was up to 44 % of total sulfur in the first meter of the rising plumes. The presence of nanoparticulate elemental sulfur in these environments suggests that it may be a more common component of sulfidic systems than has previously been considered. This is particularly important as different oxidation processes dominate in each of these environments, demonstrating that size fractionated elemental sulfur is formed via both abiotic and biotic processes.

3.4 Conclusions

Nanoparticulate elemental sulfur is shown to be a significant component of two different sulfidic marine systems: the Chesapeake Bay and the first meter of buoyant hydrothermal vent plumes along the Mid-Atlantic Ridge.

The Chesapeake Bay varies in degree of water column stratification between 2011 and 2012. In 2011 elemental sulfur present below the suboxic zone was predominately nanoparticulate, with concentrations up to 6 μM (up to 90 % of total sulfur). In 2012 free sulfide was undetectable in the water column; however, elemental sulfur was still present, and nanoparticulate sulfur was observed up to 1.7 μM. Anoxygenic phototrophic sulfur bacteria isolated from the Chesapeake Bay are shown to produce nano-S^0 as a product of sulfide oxidation, and biological formation of elemental sulfur may be an important process in affecting its particle size and distribution in this environment. At the Mid-Atlantic Ridge, nanoparticulate sulfur concentrations up to 12 μM (up to 44 % of total sulfur) were observed in the first meter of the rising plume and nano-S^0 decreased as a fraction of the total sulfur pool as seawater mixes with the vent fluid. The dominant pathway for elemental sulfur formation in the first meter of the plume is likely abiotic sulfide oxidation via an iron catalytic cycle, in contrast to the Chesapeake Bay, which is both a chemically (by manganese oxides) and biologically controlled system with respect to sulfide oxidation.

Polysulfides were not detected for samples at either site using *in situ* methods with a 0.2 μM detection limit, and any polysulfides that formed probably converted quickly to S_8 or to FeS_2. This is corroborated at MAR by the detection of polysulfides at lower temperature, more oxic sites within the rising plume. The presence of nanoparticulate elemental sulfur in each of these environments is significant as it is more likely to be chemically reactive compared to bulk S_8, as well as being a more accessible energy source for microbes than larger particles.

REFERENCES

Berner R.A. (1970**)** Sedimentary pyrite formation. *Am. J. Sci.* **268,** 1-23.

Boyd E.S., and Druschel G.K. (2013) Involvement of Intermediate Sulfur Species in Biological Reduction of Elemental Sulfur under Acidic, Hydrothermal Conditions. *Appl. Environ. Microbiol.* **79,** 2061–2068.

Bradford M. (1976) A rapid and sensitive method for the quantitation of microgram quantities of protein utilizing the principle of protein-dye binding. *Anal. Biochem.* **72**, 248-254.

Breier J. A., Toner B. M., Fakra S. C., Marcus M. A., White S. N., Thurnherr A. M. and German C. R. (2012) Sulfur, sulfides, oxides and organic matter aggregated in submarine hydrothermal plumes at 9°50′N East Pacific Rise. *Geochim. Cosmochim. Acta* **88**, 216-236.

Canfield D. E. (2005) The sulfur cycle. In *Aquatic Microbiology*. (eds, D. E. Canfield, B. Thamdrup and E. Kristensen). Elsevier Academic Press, San Diego, CA.

Chadwell S.J., Rickard D., Luther III G.W. (2001) Electrochemical Evidence for Metal Polysulfide Complexes:Tetrasulfide ($S_4{}^{2-}$) Reactions with Mn^{2+}., Fe^{2+}, Co^{2+}, Ni^{2+}, Cu^{2+}, and Zn^{2+}. *Electroanalysis* **13**, 21-29.

Chan L. K., Morgan-Kiss R. M. and Hanson T. E. (2008) Functional Analysis of Three Sulfide:Quinone Oxidoreductase Homologs in Chlorobaculum tepidum. *J. Bacteriol.* **191**, 1026-1034.

Ciglenečki I., Kodba B. and Ćosović B. (1996). Sulfur species in Rogoznica Lake. *Mar. Chem.* **53,** 101-110.

Desbruyères D., Biscoito M., Caprais J. C., Colaço A., Comtet T., Crassous P., Fouquet Y., Khripounoff A., Le Bris N., Olu K., Riso R., Sarradin P. M., Segonzac M. and Vangriesheim A. (2001) Variations in deep-sea hydrothermal vent communities on the Mid-Atlantic Ridge near the Azores plateau. *Deep-Sea Res. Pt. I* **48**,1325-1346.

Deshpande A. S., Khomane R. B., Vaidya B. K., Joshi R. M., Harle A. S. and Kulkarni B. D. (2008). Sulfur Nanoparticles Synthesis and Characterization from H_2S Gas, Using Novel Biodegradable Iron Chelates in W/O Microemulsion. *Nanoscale Res. Lett.* **3**, 221-229.

Douville E., Charlou J. L., Oelkers E.H., Bienvenu P., Jove Colon C.F., Donval J.P., Fouquet Y., Prieur D., and Appriou P. (2002). The Rainbow vent fluids (36°14′N, MAR): the influence of ultramafic rocks and phase separation on trace metal content in Mid-Atlantic Ridge hydrothermal fluids." Chem. Geol. **184**, 37-48.

Edmond, J.M., Von Damm, K.L., McDuff, R.E., and Measures, C.I. (1982). Chemistry of hot springs on the East Pacific Rise and their effluent dispersal. *Nature* **297**, 187-9l.

Ellis A.J. and Giggenbach W. (1971). Hydrogen sulphide ionization and sulfur hydrolysis in high temperature solution. *Geochim. Cosmochim. Acta.* **35**, 247-260.

Hoffman, M. R. (1977) Kinetics and mechanism of oxidation of hydrogen sulfide by hydrogen peroixed in acidic solution. *Environ. Sci. Tech.* 11, 61-66.

Feely, R., Massoth G., Trefty J. H., Baker E., Paulson A. and Lebon G. T. (1994). Composition and sedimentation of hydrothermal plume particles from North Cleft segment, Juan de Fuca Ridge. *J. Geophys. Res.* **99**, 4985-5006.

Finster, K., Liesack W. and Thamdrup B. (1998) Elemental Sulfur and Thiosulfate Disproportionation by Desulfocapsa sulfoexigens sp. nov., a New Anaerobic Bacterium Isolated from Marine Surface Sediment. *Appl. Environ. Microb.* **64**, 119-125.

Fossing H. and Jørgensen B. B. (1989) Measurement of bacterial sulfate reduction in sediments: Evaluation of a single-step chromium reduction method. *Biogeochemistry* **8**, 205-222.

Franz B., H. Lichtenberg, Hormes J., Modrow H., Dahl C. and Prange A. (2007) Utilization of solid 'elemental' sulfur by the phototrophic purple sulfur bacterium Allochromatium vinosum: a sulfur K-edge X-ray absorption spectroscopy study. *Microbiology* **153**, 1268-1274.

Frigaard N.U. and Dahl C. (2008). Sulfur Metabolism in Phototrophic Sulfur Bacteria. *Adv. Microb. Physiol.* **54**,103-200.

Gartman A. and Luther III G.W. (2013). Comparison of pyrite (FeS2) synthesis mechanisms to reproduce natural FeS2 nanoparticles found at hydrothermal vents. *Geochim. Cosmochim. Acta.* **120**, 447-458.

Gartman A, Findlay A.J., Luther III G.W. (2014) Nanoparticulate pyrite and other nanoparticles are a widespread component of hydrothermal vent black smoker emissions. *Chem. Geol.* **366**, 32-4

Ghosh W. and Dam B. (2009) Biochemistry and molecular biology of lithotrophic sulfur oxidation by taxonomically and ecologically diverse bacteria and archaea. *FEMS Microbiol. Rev.* **33**, 999-1043.

Giggenbach W. (1973) Equilibria involving polysulfide ions in aqueous sulfide solutions up to 240 C. *Inorg. Chem.* **13**, 1724-1730.

Gun J., Goifman A., Shkrob I., Kamyshny A., Ginzburg B., Hadas O., Dor I., Modestov A. D. and Lev O. (2000) Formation of Polysulfides in an Oxygen Rich Freshwater Lake and Their Role in the Production of Volatile Sulfur Compounds in Aquatic Systems. *Environ. Sci. Tech.* **34**, 4741-4746.

Guo Y., Zhao J., Yang S., Yu K., Wang Z. and Zhang H. (2006) Preparation and characterization of monoclinic sulfur nanoparticles by water-in-oil microemulsions technique. *Powder Technol.* **162**, 83-86.

Hanson T. E., Luther III G. W., Findlay A. J., MacDonald D. J. and Hess D. (2013) Phototrophic sulfide oxidation: environmental insights and methods for kinetic analysis. *Front. Microbiol.* **4.**

Hastings D. and Emerson (1988) Sulfate reduction in the presence of low oxygen levels in the water column of the Cariaco Trench. *Limnol. Oceanogr.* **33**, 391-396.

Haymon, R. M., Fornari D. J., Damm K. L. V., Lilley M. D. and Perfi M. R. (1993) Volcanic eruption of the mid-ocean ridge along the east Pacific Rise crest at 9°45’ -52’N: direct submersible observations of seafloor phenomena associated with an eruption event in April, 1991. *Earth Planet. Sc. Lett.* **119**, 85-101.

Herszage J. and dos Santos Afonso M. (2003) Mechanism of Hydrogen Sulfide Oxidation by Manganese(IV) Oxide in Aqueous Solutions. *Langmuir* **19**, 9684-9692.

Janssen A.J.H, Lettinga G., and de Keizer A. (1999) Removal of hydrogen sulphide from wastewater and waste gases by biological conversion to elemental sulphur Colloidal and interfacial aspects of biologically produced sulphur particles. *Colloids Surf.* **151**, 389-397.

Jørgensen, B. B. (1982) Ecology of the bacteria of the sulphur cycle with special reference to anoxic-oxic interface environments. *Arch. Microbiol.* **298**, 543-561.

Jørgensen B.B., Fossing H., Wirsen C. O., Jannasch H.W. (1991) Sulfide oxidation in the anoxic Black Sea chemocline. *Deep-Sea Res.* **38**, 1083-1103.

Kamyshny, A. (2009) Solubility of cyclooctasulfur in pure water and sea water at different temperatures. *Geochim. Cosmochim. Acta* **73**, 6022-6028.

Kamyshny A., Goifman A., Gun J., Rizkov D.and Lev O. (2004) Equilibrium distribution of polysulfide ions in aqueous solutions at 25 ˚C: a new approach for the study of polysulfides' equilibria. *Environ. Sci. Tech.* **38**, 6633-6644.

Kamyshny A., Gun J., Rizkov D., Voitsekovski T., and Lev O. (2007) Equilibrium distribution of polysulfide ions in aqueous solutions at different temperatures by rapid single phase derivatization. *Environ. Sci. Tech.* **41**, 2395-2400.

Kamyshny A. and Ferdelman T. G. (2010) Dynamics of zero-valent sulfur species including polysulfides at seep sites on intertidal sand flats (Wadden Sea, North Sea). *Mar. Chem.* **121**, 17-26.

Kamyshny A., Zerkle A. L., Mansaray Z. F., Ciglenečki I., Bura-Nakić E., Farquhar J. and Ferdelman T. G. (2011) Biogeochemical sulfur cycling in the water column of a shallow stratified sea-water lake: Speciation and quadruple sulfur isotope composition. *Mar. Chem.* **127**, 144-154.

Kleinjan W. E., Keizer A. and Janssen A. J. H. (2003) Biologically Produced Sulfur. *Top. Curr. Chem.* **230**, 167-188.

Kleinjan W. E., de Keizer A. and Janssen A. J. H. (2005a) Equilibrium of the reaction between dissolved sodium sulfide and biologically produced sulfur. *Colloids Surface B* **43**, 228-237.

Kleinjan W. E., de Keizer A. and Janssen A. J. H. (2005b) Kinetics of the chemical oxidation of polysulfide anions in aqueous solution. *Water Res.* **39**, 4093-4100.

Klevenz, V., W. Bach, K. Schmidt, M. Hentscher, A. Koschinsky, S. Petersen. (2011) Geochemistry of vent fluid particles formed during initial hydrothermal fluid–seawater mixing along the Mid-Atlantic Ridge. *Geochem. Geophys. Geosyst.* **12**.

Konovalov S.K., Luther III G.W., Friederich G.E., Nuzzio, D.B., Tebo B.M.,Murray J.W., Oguz T., Glazer, B. Trouwborst R.E., Clement, B. Murray, K.J. Romanov, A.S. (2003) Lateral injection of oxygen with the Bosporus plume-fingers of oxidation potential in the Black Sea. *Limnol. Oceanogr.* **48**, 2369–2376.

Konovalov S. K., Murray J. W., Luther G. W. and Tebo B. M. (2006) Processes controlling the redox budget for the oxic/anoxic water column of the Black Sea. *Deep-Sea Res. Pt. II* **53**, 1817-1841.

Lewis, B. L., Glazer B.T., Montbriand P.J., Luther III G.W., Nuzzio D.B, Deering T., Ma S., and Theberge S. (2007) Short-term and interannual variability of redox-sensitive chemical parameters in hypoxic/anoxic bottom waters of the Chesapeake Bay. *Mar. Chem.* **105**, 296-308.

Li X., Taylor G. T., Astor Y. and Scranton M. I. (2008) Relationship of sulfur speciation to hydrographic conditions and chemoautotrophic production in the Cariaco Basin. *Mar. Chem.* **112**, 53-64.

Lichtschlag A., Kamyshny A., Ferdelman T. G. and deBeer D. (2012) Intermediate Sulfur Oxidation State Compounds in the Euxinic Surface Sediments of the Dvurechenskii Mud Volcano (Black Sea). *Geochim. Cosmochim. Acta* **105**, 130-145.

Luther III G. W. (1990) Frontier molecular orbital approach in geochemical processes. *Aquatic Chemical Kinetics*. Stumm. New York, John Wiley& Sons, Inc**:** 173-198.

Luther III G.W. (1991) Pyrite synthesis via polysulfide compounds. *Geochim. Cosmochim. Acta* **55**, 2839- 2849.

Luther G., III (2010) The Role of One- and Two-Electron Transfer Reactions in Forming Thermodynamically Unstable Intermediates as Barriers in Multi-Electron Redox Reactions. *Aquat. Geochem.* **16**, 395-420.

Luther III G. W., Church T. M., Scudlark J. R. and Cosman M. (1986) Inorganic and organic sulfur cycling in salt-marsh pore-waters. *Science* **232**, 746-749.

Luther III G.W., Church T.M., Powell D. (1991) Sulfur speciation and sulfide oxidation in the water column of the Black Sea. *Deep-Sea Res.* **38**, 1121-1137.

Luther III G. W., Rozan T. F., Taillefert M., Nuzzio D. B., Di Meo C., Shank T. M., Lutz R. A. and Cary S. C. (2001) Chemical speciation drives hydrothermal vent ecology. *Nature* **410,** 813-816.

Luther III G.W. and Rickard D.T. (2005) Metal sulfide cluster complexes and their biogeochemical importance in the environment. *J. Nanopart. Res.* **7,** 389-407.

Luther III G. W., Glazer B. T., Ma S., Trouwborst R. E., Moore T. S., Metzger E., Kraiya C., Waite T. J., Druschel G., Sundby B., Taillefert M., Nuzzio D. B., Shank T. M., Lewis B. L. and Brendel P. J. (2008) Use of voltammetric solid-state (micro)electrodes for studying biogeochemical processes: Laboratory measurements to real time measurements with an in situ electrochemical analyzer (ISEA). *Mar. Chem.* **108**, 221-235.

Luther G. W., Findlay A. J., MacDonald D. J., Owings S. M., Hanson T. E., Beinart R. A. and Girguis P. R. (2011) Thermodynamics and Kinetics of sulfide oxidation by oxygen: a look at inorganically controlled reactions and biologically mediated processes in the environment. *Front. Microbiol.* **2**.

Ma S., Noble A., Butcher D., Trouwborst R. E. and Luther III G.W. (2006) Removal of H_2S via an iron catalytic cycle and iron sulfide precipitation in the water column of dead end tributaries. *Estuar. Coast. Shelf S.* **70**, 461-472.

McCollom T. M. (2000) Geochemical constraints on primary productivity in submarine hydrothermal vent plumes. *Deep-Sea Res. Pt. I* **47**, 85-101.

Millero F.J, Sotolongo S. and Izaguirre M. (1987) The oxidation kinetics of Fe(II) in seawater. *Geochim. Cosmochim. Acta* 51,793-801.

Milucka J., Ferdelman T. G., Polerecky L., Franzke D., Wegener G., Schmid M., Lieberwirth I., Wagner M., Widdel F. and Kuypers M. M. (2012). Zero-valent sulphur is a key intermediate in marine methane oxidation. *Nature* **491**, 541-546.

Officer C. G., Biggs R. B., Taft J. L., Cronin L. E., Tyler M. A. and Boynton W. R. (1984) Chesapeake Bay anoxia: Origin, development, and significance. *Science* **23**, 22-27.

Poulton S. W. (2003) Sulfide oxidation and iron dissolution kinetics during the reaction of dissolved sulfide with ferrihydrite. *Chem. Geol.* **202**, 79-94.

Prange A., Chauvistre R., Modrow H., Hormes J., Truper H.G., Dahl C. (2002) Quantitative speciation of sulfur in bacterial sulfur globules: X-ray absorption spectroscopy reveals at least three different species of sulfur. *Microbiology* **148**, 267–276.

Pyzik A. J. and Sommer S. E. (1981) Sedimentary iron monosulfides: kinetics and mechanism of formation. *Geochim. Cosmochim. Acta* **45**, 687–698.

Rickard D. and Luther III G.W. (1997) Kinetics of pyrite formation by the H_2S oxidation of iron (II) monosulfide in aqueous solutions between 25 and 125ºC: The mechanism. *Geochim. Cosmochim. Acta* **61**,135-147.

Rozan T.F., Theberge S.M., and Luther III G.W. (2000) Quantifying elemental sulfur (S^0), bisulfide (HS^-) and polysulfides (Sx^{2-}) using a voltammetric method. *Geochim. Cosmochim. Acta* **415**, 175-184.

Rudnicki M. D. and Elderfield H. (1993) A chemical model of the buoyant and neutrally buoyant plume above the TAG vent field, 26 degrees N, Mid-Atlantic Ridge. *Geochim. Cosmochim. Acta* **57**, 2939-2957.

Schauder R. and Muller E. (1993) Polysulfide as a possible substrate for sulfur reducing bacteria. *Arch. Microbiol.* **160**, 377-382.

Sievert S. M., Kiene R. P. and Schulz-Vogt H. N. (2007) The Sulfur Cycle. *Oceanography* **20**, 117-123.

Steudel R. (1996). Mechanism for the Formation of Elemental Sulfur from AqueousSulfide in Chemical and Microbiological Desulfurization Processes. *Ind. Eng. Chem. Res.* **35**, 1417-1423.

Steudel R. (2003). Aqueous Sulfur Sols. Elemental Sulfur and Sulfur-Rich Compounds I. R. Steudel, Springer Berlin Heidelberg. **230,** 153-166.

Stumm, W. and J.J. Morgan (1996). Aquatic Chemistry, Chemical Equilibria and Rates in Natural Waters. 3rd ed. John Wiley & Sons, Inc., New York, NY, USA.

Taylor C. D. and Wirsen C. O. (1997) Microbiology and Ecology of Filamentous Sulfur Formation. *Science* **277**, 1483-1485.

Thamdrup B., Finster K., Hansen J. W. and Bak F. (1993) Bacterial Disproportionation of Elemental Sulfur Coupled to Chemical Reduction of Iron or Manganese. *Appl. Environ. Microbiol.* **59**, 101-108.

Thompson G., Humphris S.E., Schroeder B., Sulanowska M. (1988) Active vents and massive sulfides at 26°N (TAG) and 23°N (Snakepit) on the Mid-Atlantic Ridge. *Can. Mineral*. **26**, 697–711.

Troelsen H. and Jorgensen B.B. (1982) Seasonal dynamics of elemental sulfur in two coastal sediments. *Estuar. Coast. Shelf S.* **15**, 255-266.

Trouwborst R.E., Clement B. G., Tebo B. M., Glazer B. T., Luther III G.W. (2006) Soluble Mn(III) in Suboxic Zones. *Science* **313**,1955-1957.

Van Gemerden H. (1986) Production of elemental sulfur by green and purple sulfur bacteria. *Arch. Microbiol.* 146, 52-56.

Wang F. and Tessier A. (2009) Zero-Valent Sulfur and Metal Speciation in Sediment Porewaters of Freshwater Lakes. *Environ. Sci. Tech.* **43**, 7252-7257.

Widdel F. and Pfennig N. (1982) Studies on dissimilatory sulfate-reducing bacteria that decompose fatty acids II. Incomplete oxidation of propionate by Desulfobulbus propionicus gen. nov., sp. nov. *Arch. Microbiol.* **131**, 360-365.

Widdel F., Kohring G. W. and Mayer F. (1983) Studies on dissimilatory sulfate-reducing bacteria that decompose fatty acids. III. Characterization of the filamentous gliding Desulfonema limicola gen. nov., sp. nov., and Desulfonema magnum sp. nov. *Arch. Microbiol.* **134**, 286–294.

Wilkin R. T. and Barnes H.L. (1996) Pyrite formation by reactions of iron monosulfides with dissolved inorganic and organic sulfur species. *Geochim. Cosmochim. Acta* **60**, 4167-4179.

Winn C. D., Karl D.M. and Massoth G.J. (1986) Microbes in deep-sea hydrothermal plumes. *Nature* **320**, 744 – 746

Wu J. and Boyle E. A. (1998). Determination of iron in seawater by high resolution isotope dilution inductively coupled plasma mass spectrometry after $Mg(OH)_2$ coprecipitation. *Anal. Chim. Acta*. **367**, 183-191.

Yao W. and Millero F.J. (1993) The rate of sulfide oxidation by 8MnO2 in seawater. *Geochim Cosmochim Acta* **57**, 3359–3365.

Yao W. and Millero F. J.(1996) Oxidation of hydrogen sulfide by hydrous Fe(III) oxides in seawater. *Mar. Chem.* **52**, 1-16.

Yücel M., Konovalov S. K., Moore T. S., Janzen C. P. and Luther III G. W. (2010) Sulfur speciation in the upper Black Sea sediments. *Chem. Geol.* **269**, 364-375.

Zerkle A. L., Kamyshny A., Kump L. R., Farquhar J., Oduro H. and Arthur M. A. (2010) Sulfur cycling in a stratified euxinic lake with moderately high sulfate: Constraints from quadruple S isotopes. *Geochim. Cosmochim. Acta* **74**, 4953-4970.

Zopfi J., Ferdelman T. G., Jørgensen B. B., Teske A. and Thamdrup B. (2001) Influence of water column dynamics on sulfide oxidation and other major biogeochemical processes in the chemocline of Mariager Fjord (Denmark). *Mar. Chem.* **74**, 29-51.

Chapter 4

LIGHT DEPENDENT SULFIDE OXIDATION IN THE WATER COLUMN OF A STRATIFIED ESTUARY

Abstract

Sulfide oxidation is an important ecosystem process as reduced sulfur compounds negatively impact water quality, and numerous studies indicate that it is typically microbially mediated. Field studies were conducted during the summers of 2011- 2014 in the Chesapeake Bay, USA during which the redox chemistry of the stratified water column was characterized. In 2011 and 2013, phototrophic sulfide oxidizing bacteria could be cultivated from waters sampled at and below the oxic/anoxic interface, and measurements indicate that light penetration was sufficient to support populations of photosynthetic bacteria. In 2012, 2013, and 2014, light dependent sulfide light dependent sulfide uptake was observed in freshly collected water column samples. Extremely low levels of light were found to cause 2-10 fold increases over the basal uptake rate observed in dark incubations. Laboratory experiments with enrichments of phototrophic sulfide oxidizing bacteria from the Bay indicate a value for K_s of 10 μM and a V_{max} of 50 μM min^{-1} $mgprotein^{-1}$ for sulfide. Taken together, the results reported here suggest that phototrophic bacteria may make

a larger contribution to sulfide consumption in the Chesapeake Bay than has been previously considered.

4.1 Introduction

The oxidation of sulfide by oxygen is thermodynamically unfavorable for a one-electron transfer and kinetically inhibited for a two-electron transfer (Luther, 2010). Kinetic limitations on sulfide oxidation can be overcome by catalysts, either abiotic (i.e. transition metals, Yao and Millero, 1996), or biotic (i.e. sulfide:quinone oxidoreductase in various microbes, Gregersen et al. 2012). In many environments, particularly those with low oxygen levels and/or limited free transition metals, sulfide oxidation is expected to be microbially mediated (Luther et al., 2011). Primary production via biological sulfide oxidation provides an important link between the carbon and sulfur cycles (Jørgensen, 1982). Phototrophic sulfide oxidizing bacteria (PSOB) have been found in a wide array of aqueous environments in which both light and sulfide are present, including sediments (Preisler et al., 2007), hot springs (Wahlund et al., 1991), freshwater lakes (Parkin and Brock, 1981; Guerrero et al., 1985; Tonolla et al., 2003; Rimmer et al., 2008), and marine basins (Overmann, 1992). In the water column, these bacteria are typically found between 2-20 meters from the surface, and at light transmittance values from 10 % to 0.015 % of surface irradiance (Overmann, 2008). Biological rates of sulfide oxidation can be orders of magnitude faster than abiotic rates (Luther et al., 2011); thus the presence of PSOB has the potential to significantly impact the sulfur cycle and redox chemistry in the environment. The degree to which PSOB influence their environment depends upon environmental factors such as light availability, sulfide concentration, and the rates of abiotic sulfide oxidation processes (Overmann, 1997).

Investigating the presence and role of phototrophic sulfur bacteria in anoxic environments is important for understanding both modern and ancient systems. Investigating the presence and role of phototrophic sulfur bacteria in anoxic environments is important for understanding both modern and ancient systems. In modern systems, the development of sulfidic waters can cause stress or toxicity to aerobic organisms such as fish (Eghbal et al., 2004; Julian et al., 2005). Currently, the volume of low oxygen waters in oxygen minimum zones (OMZs) and coastal hypoxic zones is increasing due to a changing global climate (Deutsch et al. 2011), and many of these areas are completely anoxic for part of the year. Sulfide has been directly detected in several OMZs (Lavik et al. 2009; Schunk et al. 2013); and evidence for the cryptic cycling of sulfur, with simultaneous sulfate reduction and sulfide oxidation has also been observed (Canfield et al., 2010), even when sulfide was not directly detected. As these areas expand, the depth of anoxic water is expected to shoal, moving toward the photic zone (Stramma et al. 2010) and thus creating potential new niches for PSOB, which could play an important role in mitigating sulfide fluxes. In the ancient oceans, PSOB were likely important biogeochemical mediators during the transition of ocean chemistry from anoxic with periodic widespread sulfidic conditions to fully oxic (Hanson et al., 2013 and references therein). Environments that currently experience periodic anoxia and euxinia provide an analogue to the ancient oceans in which to study the effects of changing redox conditions on the chemistry and microbiology of a system, lending insight into the biogeochemical evolution of modern oceans. Thus, further understanding of the environmental niches occupied by PSOB, and their impact on sulfide oxidation has widespread implications.

4.1.1 Study Site

The Chesapeake Bay is a partially stratified estuary extending from the mouth of the Susquehanna River to the Atlantic Ocean (Hagy et al., 2004). Water transport is a two-layer gravitational circulation where saline water flows up-estuary and fresh water flows down (Pritchard, 1952). Salinity and temperature gradients, coupled with an influx of nutrients and subsequent biological productivity and decomposition, lead to the development of suboxic to anoxic deep-water in the summer. A suboxic zone between the oxic surface and anoxic deep layers in which neither oxygen nor sulfide is detectable may form at the interface created by density stratification. This interface is a place of dynamic chemical and biological activity and elemental cycling. In addition to annual and inter-annual variation in oxygen concentrations, shorter-term variations occur due to tidal forcing and wind-induced mixing of the water column (Lewis et al., 2007), which result in changes in the depth and extent of the interface. The seasonal development of anoxic and sulfidic waters in the Chesapeake Bay has been correlated with shifts in the bacterial community structure (Crump et al., 2007); and functional gene surveys indicate that the lower water column microbial community switches to anaerobic respiration during anoxia, potentially exacerbating the production of sulfide.

It is not clear; however, whether there are significant microbial contributions to sulfide oxidation in this system.

In this study, we present field results that indicate PSOB are a consistent, recurring, and active component of the Chesapeake Bay sulfur cycle. In addition, laboratory experiments with enrichments of PSOB obtained from the Chesapeake Bay allowed determination of kinetic parameters with respect to light and sulfide concentration. These parameters allow a preliminary investigation into the potential contribution of PSOB to sulfide oxidation in the Chesapeake Bay given observed sulfide and light profiles in this system.

4.2 Methodology

4.2.1 Sample Collection

Field studies took place at Station 858 (38º58.8’ N; 76º22’ E) in the upper Chesapeake Bay south of the Bay Bridge. This site is a hole off of the main channel in the mesohaline portion of the Bay that is approximately 25 meters deep and is one of the first sites to stratify in the spring (Lewis et al., 2007). Fieldwork was conducted from 27-30 July 2011, 17-19 August 2012, 9-13 August 2013, and 18-22 August 2014 aboard the University of Delaware’s research vessel the R/V *Hugh R. Sharp*. In 2012 and 2013 all samples were obtained from Niskin bottles on the ship’s CTD rosette and were collected in cleaned Nalgene bottles on the ship. In 2011 and 2014, samples were taken from either Niskin bottles or from water pumped to the surface by a Rule

Industries 1000 gallons per hour pump. Care was taken while sampling to avoid aeration of the samples by flushing the sample bottle three times and capping with no headspace. Sample processing was rapid (< 10 minutes) in order to preserve redox speciation in the samples.

4.2.2 Analytical Methods

4.2.2.1 Oxygen and Sulfide

Measurements of oxygen and sulfide concentrations in the water column were made using *in situ* voltammetry. The voltammetric system used a 100 μm gold-amalgam working electrode, a Ag/AgCl reference electrode, and a platinum counter electrode. In 2011 this system was interfaced to a DLK-SUB-II electrochemical analyser attached to a metal cage that was suspended over the side of the ship. In 2012 -2014 a laboratory DLK 100A potentiostat was used as water was pumped with a pump profiler and measured shipboard using a flow-through cell (MacDonald et al., 2014), which has been demonstrated to preserve *in situ* speciation (Glazer et al., 2006). Voltage was scanned from -0.1 V to -1.8 V at a scan rate of 2000 mV/second. Using this method the detection limit for oxygen is 3 μM and for sulfide and polysulfide is 0.2 μM.

4.2.2.2 Iron

Iron was determined spectrophotometrically using the ferrozine method of Stookey (1970). An Ocean Optics UV-Vis spectrophotometer was used on board the ship and analyses were conducted after sample collection and processing. Samples for iron analysis were subsampled from the Nalgene bottle and 100 mL were filtered via a 0.2 μm prefabricated Puradisc filter into a separate Nalgene bottle containing 90 μL of 12 M trace metal grade hydrochloric acid. The acid-fixed samples were allowed to sit for at least four hours prior to analysis, and all samples were taken in triplicate. Ferrous iron was determined in acid-treated samples by adding 3 mL of a 1:1 mixture of 0.01 M ferrozine and 6 M ammonium acetate buffer. After a waiting period of half an hour the absorbance at 562 nm was read. The samples were conserved and 250 μL of hydroxylamine were added to react for half an hour to reduce Fe^{3+} to Fe^{2+} in order to measure total iron. The difference between the values for total iron and Fe^{2+} in each sample gives Fe^{3+}.

4.2.3 Enrichment Methods

4.2.3.1 Bacterial Enrichments in the Field

Samples for photosynthetic sulfide oxidizing bacteria were taken within and below the suboxic zone. One mL of sample water was injected into a 20 mL septum vial containing anoxic SL-10 media specialized for PSOB containing 17.9 mM HCO_3^- as the carbon source and 2.5 mM H_2S as the sole electron donor (Overmann and Pfennig, 1989). The vials were incubated benchtop for the duration of the cruise. Upon return to land, the vials were incubated at 20-22 ºC at 5 μEi and were sub-cultured into fresh medium when growth was visibly apparent. This produced a number of stably transferable enrichments that were all similar in appearance (data not shown). One of these, CB11, was selected and used for all further experiments.

4.2.3.2 Identification of Phototrophic Bacteria in CB11

Whole cell absorption spectra for CB11 and pure cultures of related strains were collected on samples taken from actively growing cultures by syringe and transfer to a plastic cuvette. Spectra were recorded on a DU730 spectrophotometer within one minute of removal from the culture. Data for absorbance at 1 nm intervals between 400 and 1100 nm were transferred to Microsoft Excel for plotting.

For phylogenetic analysis, cells were collected by centrifugation from 1 ml of enrichment culture by centrifugation at 16,400 x g for 2 minutes. Cells were resuspended in lysis buffer containing 1 % (v/v) Triton X-100, 20 mM Tris-HCl, and 0.1 mM EDTA at pH 8.0. Cells were lysed by heating to 95 ^{o}C for 5 minutes. Debris was removed by centrifugation at 16,400 x g for 2 min and 2 ml of the supernatant was used in a PCR reaction with primers 27f (5’- GAGTTTGATYHTGGCTCAG-3’) and 1492r (5’- GGTTACCTTGTTACGACTT-3’). After treating the reaction with ExoSAP-IT according to manufacturer instructions, PCR products were inserted into pCR2.1-TOPO and clones recovered by electroporation into *Escherichia coli* strain EC100D and plating on LB agar with kanamycin (50 □g ml^{-1}). Positive clones were identified by colony PCR with primers M13r (5’- AACAGCTATGACCATG-3’) and T7P (5’- TAATACGACTCACTATAGGG-3’). PCR products of the appropriate size were sent for Sanger sequencing using the same primers after ExoSAP-IT treatment at the University of Delaware Sequencing and Genotyping Center. Vector sequence was removed and sequences from three clones were assembled into a contig using CLC Workbench v.7. The resulting sequence was aligned to 73 *Chlorobi* 16S rRNA sequences and those of *Ignavibacterium album* JCM 16511 and *Meloribacter roseum* P3M as outgroups by MUSCLE in MEGA6 (Tamura et al., 2013). The alignment was trimmed to remove excess sequence at each and a phylogenetic tree created by maximum likelihood analysis of aligned representative *Chlorobi* and outgroup sequences using the Kimura 2-parameter model allowing for both invariant sites and a gamma distribution of 5 categories for variable rate sites.

Automated ribosomal intergenic spacer analysis (ARISA, Cardinale et al., 2004) was used to determine if the CB11 enrichment contained significant amounts of other bacteria and to compare CB11 with other enrichments obtained from Chesapeake Bay samples. Lysate of culture samples was prepared and used for PCR as above, but the PCR reaction contained primers ITSF (5’-GTCGTAACAAGGTAGCCGTA-3’) and ITSReub (5’- GCCAAGGCATCCACC-3’), where ITSReub was labeled with the NED fluorophore. PCR products were mixed with a size standard (LIZ-1000) and then analyzed on 3130XL Genetic Analyzer in the University of Delaware Sequencing and Genotyping Center. The resulting electropherograms were analyzed using the freely available PeakStudio software package (http://fodorlab.uncc.edu/software/peakstudio) to calculate the sizes of fragments and peak areas. *Chlorobaculum tepidum* TLS, *Chlorobium luteolum* DSM 273, *Chlorobium limicola* DSM 245 and *Prosthecochloris aestuarii* DSM 271 were analyzed as controls and all produced ARISA peaks that matched those predicted from their complete genome sequences (data not shown). These analyses were conducted by Dr. Thomas E. Hanson.

4.2.3.3 Preparation of Enrichments for Laboratory Experiments

Laboratory enrichments of the Chesapeake Bay strain were initiated by transferring 5 mL of enriched culture into a 100 mL septum vial, which was pressurized to 10 psi with ultra-high purity argon gas and incubated in the dark for 45 minutes. The bacteria were then grown in a water bath set at 25˚C for forty-eight hours under 20 µEi full spectrum light. At the end of the growth period cells were washed three times with HEPES buffer (0.1 M, pH 7.4) to remove salts. Once washed, the cells were stored in anoxic HEPES buffer (3 mL) in a sealed 20 mL septum vial and were used in experiments the same day. Anoxic conditions were maintained while transferring the cells by using a glove bag purged with ultra-high purity argon.

4.2.3.4 Protein Measurement

Protein measurements were made using the Bradford Assay (Bradford, 1974). Briefly, a 0.5 mL aliquot of the culture is subsampled and centrifuged at 16 xg for one minute. Half of the supernatant was drawn off and then the remainder was spun down. The rest of the supernatant was decanted and the pellet was re-suspended in 1 mL cold methanol for 10 minutes, after which it was centrifuged again at 16 xg for five minutes. The methanol was decanted, and used to measure bacteriochlorophyll e at

660 nm, and the pellet was dried in air. To measure protein, pellets were suspended in equal parts NaOH (0.25 M) and HCl (0.25 M). The re-suspended samples were diluted and buffered in 15 mM potassium phosphate before the addition of the Bradford reagent. UV-Vis measurements were made at 595 nm.

4.2.3.5 Analytical Methods for Sulfide Loss Experiments

In situ voltammetry with solid-state gold amalgam electrodes was used to measure sulfide concentrations throughout the experiments (Luther et al., 2011; Hanson et al., 2013). The methods for construction and calibration of the electrodes are outlined in Luther et al. (2008). The thermostatted electrochemical cell contains ports for Argon gas delivery, a 100 µm gold-amalgam working electrode, a Ag/AgCl reference electrode and a platinum counter electrode. It was controlled using an Analytical Instrument Systems (AIS) DLK-60 potentiostat. Voltammetric scans of solutions were run from -0.1 to -1.8 V with two conditioning steps: one at -0.9 V for five seconds, which prevents sulfide from plating on to the electrode surface (equation 1), and one at -0.1 V for two seconds (equation 2).

(1) $HS^- + Hg \rightarrow HgS + 2e^-$

(2) $HgS + H^+ + 2e^- \rightarrow HS^- + Hg$

Shipboard kinetic experiments

In 2012, 2013, and 2014, kinetic experiments modeled after those of Luther et al. (1988) were conducted shipboard using anoxic bottom water. Water samples were used unfiltered, or after being filtered through either a 0.2 μm or a 0.05 μm Nuclepore filter. Experiments were set up in a glove bag purged with ultra-high purity argon gas, and the water sample was put in a glass electrochemical cell sealed with no headspace. In 2012, because no sulfide was detectable in the water column, 30 μM sulfide was added to anoxic bottom water. In 2013 and 2014 the bottom waters were sulfidic, and kinetic experiments monitored the loss of the initial sulfide present in the sample. During these experiments, sulfide loss in the electrochemical cell was monitored by solid-state voltammetry as detailed above. Light intensity was controlled using a desk lamp with a full spectrum bulb attached to a variac, which allowed for fine-tuning, and was monitored using a LI-COR Biosciences LI-1400 data logger light meter. Fifty μM (3-(3,4-dichlorophenyl)-1,1-dimethylurea (DCMU) were added to the sample water prior to experiments in order to inhibit oxygenic photosynthesis. Abiotic control experiments were also conducted by fixing the samples with 1.6 % formaldehyde prior to monitoring sulfide loss.

Laboratory kinetic experiments

Experiments were conducted to measure the effect of biomass, sulfide concentration, and light intensity on the sulfide oxidation activity of enrichments of CB11. All experiments were run in anoxic HEPES buffer (0.1 M, pH 7.4), with a cap of argon gas to maintain anoxic conditions during the experiments. Experiments were run at 25 ˚C in a thermostatted electrochemical cell. Light intensity was monitored and manipulated as noted above. Dark conditions were maintained by shrouding the electrochemical cell.

Cells were harvested for experiments during log phase growth as determined by a three-day growth curve. Experiments conducted with varying biomass were run under 5 μEi light intensity with 30 μM sulfide to determine the effect of biomass on the sulfide oxidation rate. For all further experiments, between 19 to 90 μg protein was used in each experiment in order to remain within the linear range of a plot of protein-normalized rate vs. biomass. Thus, normalizing the experimental rates to protein removes the effect of biomass on the sulfide loss rate. Sulfide concentration experiments were conducted under 5 μEi light at 5, 15, 50, 75, and 100 μM sulfide. Dark rates were obtained for each sulfide concentration and were subtracted from the experimental rate in order to separate photosynthetic activity from uptake by the cells. Experiments varying light intensity from 0 μEi to 15 μEi were run with 75 μM sulfide. Abiotic controls were conducted for each set of experimental conditions, and those rates were subtracted from the biotic experiments.

4.3 Results

4.3.1 Field results

4.3.1.1 Physical and Chemical Stratification of the Water Column

Inter-annual variation in water column chemistry and the location of the oxic/anoxic interface was evident during the four summers during which this study took place. Figure 4.1a, b, c, and d show profiles of the density, PAR, oxygen and sulfide in the water column at the study site during the summers of 2011, 2012, 2013, and 2014 respectively. In 2011 (Figure 4.1a) the water column was strongly stratified with a clear pycnocline. The depth of the oxic/anoxic interface varied between 7-10 m, and sulfide concentrations were up to 100 µM at depth. PAR profiles overlapped with sulfide. In 2012 (Figure 4.1b), due to low spring rainfall and mixing from summer storms, the water column was much more homogenous. Oxygen was present throughout the water column, with only the very deepest waters being suboxic or anoxic, well below light penetration. Free sulfide was not detected in the water column, although trace quantities of FeS were detected voltammetrically in deep water samples. In 2013 (Figure 4.1c), the water column was physically and chemically stratified, and the oxic/anoxic interface was present at about 15 meters depth. Sulfide was measured at concentrations up to 40 µM and did not overlap with detectable PAR. In 2014 (Figure 4.1d), there was a significant suboxic zone extending between depths of 10 and 13 meters and sulfide was up to 70 µM in the deep waters. PAR overlapped with the suboxic zone, but not with the sulfidic layer.

A

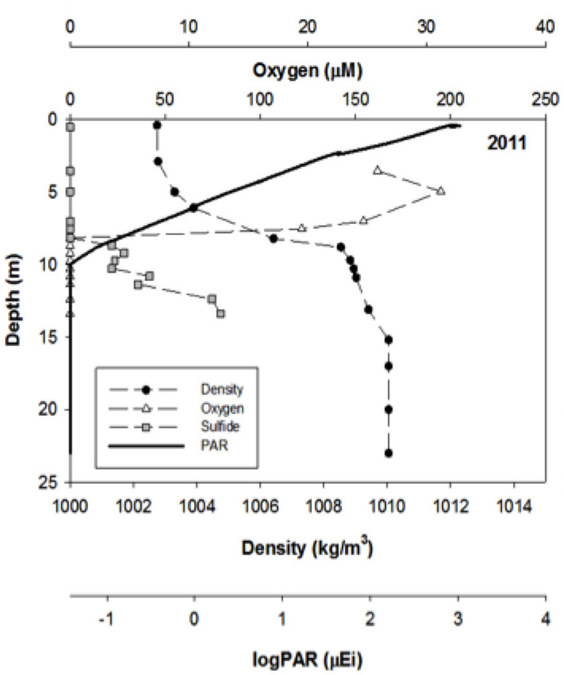
Sulfide (µM)
0
10
20
30
40
Oxygen (µM)
0
50
100
150
200
250
2011
Depth (m)
0
5
10
15
20
25
Density
Oxygen
Sulfide
PAR
1000
1002
1004
1006
1008
1010
1012
1014
Density (kg/m^3)
-1
0
1
2
3
4
logPAR (µEi)

C

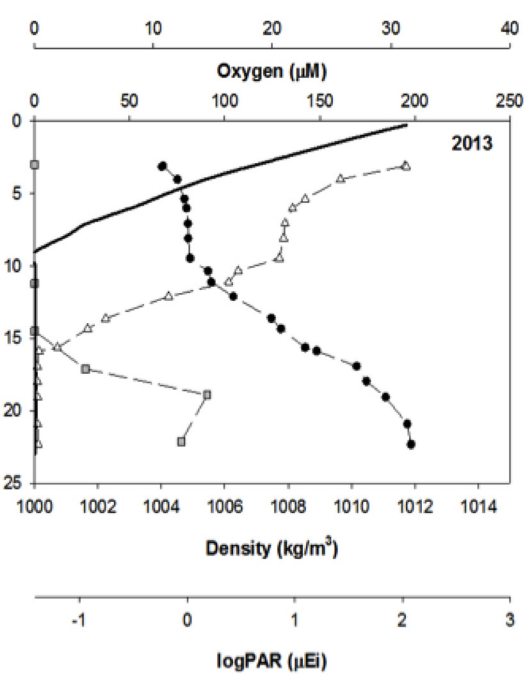
Sulfide (µM)
0
10
20
30
40
Oxygen (µM)
0
50
100
150
200
250
2013
0
5
10
15
20
25
1000
1002
1004
1006
1008
1010
1012
1014
Density (kg/m^3)
-1
0
1
2
3
logPAR (µEi)

B

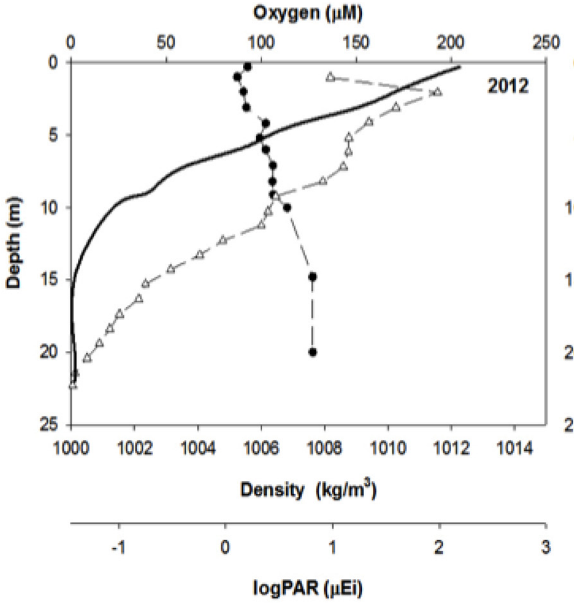
Oxygen (µM)
0
50
100
150
200
250
2012
Depth (m)
0
5
10
15
20
25
1000
1002
1004
1006
1008
1010
1012
1014
Density (kg/m^3)
-1
0
1
2
3
logPAR (µEi)

D

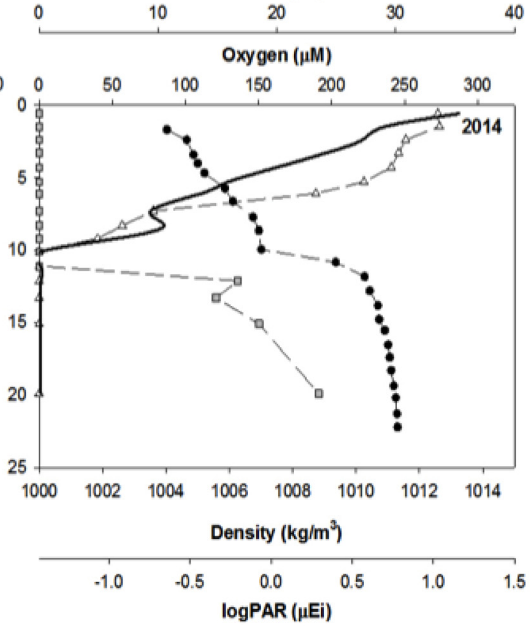
Sulfide (µM)
0
10
20
30
40
Oxygen (µM)
0
50
100
150
200
250
300
2014
0
5
10
15
20
25
1000
1002
1004
1006
1008
1010
1012
1014
Density (kg/m^3)
-1.0
-0.5
0.0
0.5
1.0
1.5
logPAR (µEi)

Figure 4.1 Physical and chemical characteristics of the Chesapeake Bay water column over four subsequent summers. (a) In 2011 the water column was strongly stratified, with a clear pycnocline. Oxygen concentration was below detection at approximately 8 m depth, after which sulfide increased at depth. (b) In 2012 the water column was not strongly stratified, and oxygen was present in the deep waters, with only the last few meters above the sediments becoming suboxic. Sulfide was not detected; however trace amounts of FeS were observed directly above the sediment/water interface. (c) In 2013 the water column was stratified. Oxygen was depleted at depths around 13 m and sulfide was observed at depth. (d) In 2014 the water column was also stratified, and oxygen was below detection at 9.5 m. Sulfide was present at 12 m.

4.3.1.2 Sulfide Oxidizing Bacteria Cultures.

Phototrophic sulfide oxidizing bacteria were successfully enriched in cultures from the Chesapeake in 2011 and 2013, both years in which physical and chemical gradients were established and sulfide was present in the water column. In each of these years, the bacteria were found at and directly beneath the oxic/anoxic interface (Table 4.1).

Table 4.1 Location and characteristics of successful phototrophic sulfide oxidizing bacteria enrichments from the Chesapeake Bay.

								ARISA peak	
Year	**Date**	**Time**	**Depth (m)**	**[H_2S] (µM)**	**PAR (µEi)**	**pH**	**T (ºC)**	**bp**	**area %**
2011	28-Jul	7:20	11.4	<0.2	0.039	7.1	24.9	578	94
			13.5	10.4	0.038	7.03	24.4	578	100
	30-Jul	8:30	6.88	<0.2	0.271	7.1	26.8	578	95
			11.3	45.8	0.038	7.05	24.3	581	56
								578	40
2013	9-Aug	7:00	18.9	14.5	<0.034	7.36	25.3	578	98
		13:30	14.9	9.4	0.038	7.39	25.2	578	98
	11-Aug	7:30	13.3	<0.2	0.038	7.36	25.3	578	99
			18.1	21.8	<0.034	7.35	25.3	578	97
	12-Aug	7:40	13.1	<0.2	0.038	7.44	25.4	578	98
			17.1	13.25	<0.034	7.42	25.3	578	98

Intact cell absorption spectra of one of the successful enrichments, CB11, showed features suggesting that this enrichment is dominated by *Chlorobi* (Figure 4.2). The peaks at 469 and 720 nm are likely from antenna bacteriochlorophylls in the chlorosome and the small feature at 810 nm is likely from the baseplate bacteriochlorophyll. Extraction of the pigments into methanol produced a strong absorbance at 665 nm characteristic of bacteriochlorophyll e (Gloe et al., 1975). The spectrum of the enrichment is qualitatively similar to that of other *Chlorobi* that contain Bchl e (Manske et al, 2005, and references therein). Results were similar for all other positive enrichments (data not shown).

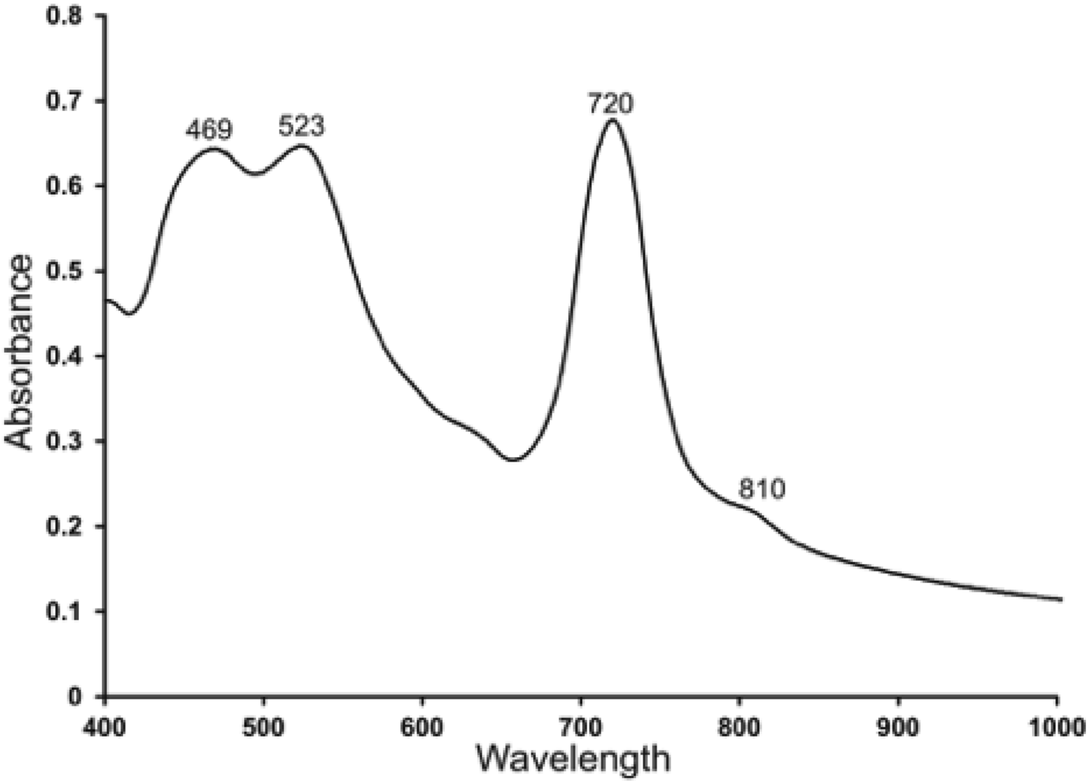

Figure 4.2 Intact cell absorption spectrum of enrichment CB11. The wavelengths of relevant features are noted.

Sequencing of three independently cloned 16S rRNA PCR products from enrichment CB11 produced identical results. Phylogenetic analysis of the sequence shows that the strain dominant in CB11 is most closely affiliated with *Prosthecochloris vibrioformis* (Figure 4.3). Enrichment CB11 was analyzed by ARISA and found to contain one major peak of 578 bp in size that accounted for 94% of the total peak area detected in the sample. This same peak was the dominant ARISA peak observed in most other positive enrichments analyzed (Table 4.1). In the one enrichment where it was not dominant, it was the other major peak detected. The 581 bp ARISA peak dominating that enrichment likely arose from another member of the *Chlorobi* as determined by sequencing of 16S rRNA clones (data not shown). These data were provided by Dr. Thomas E. Hanson.

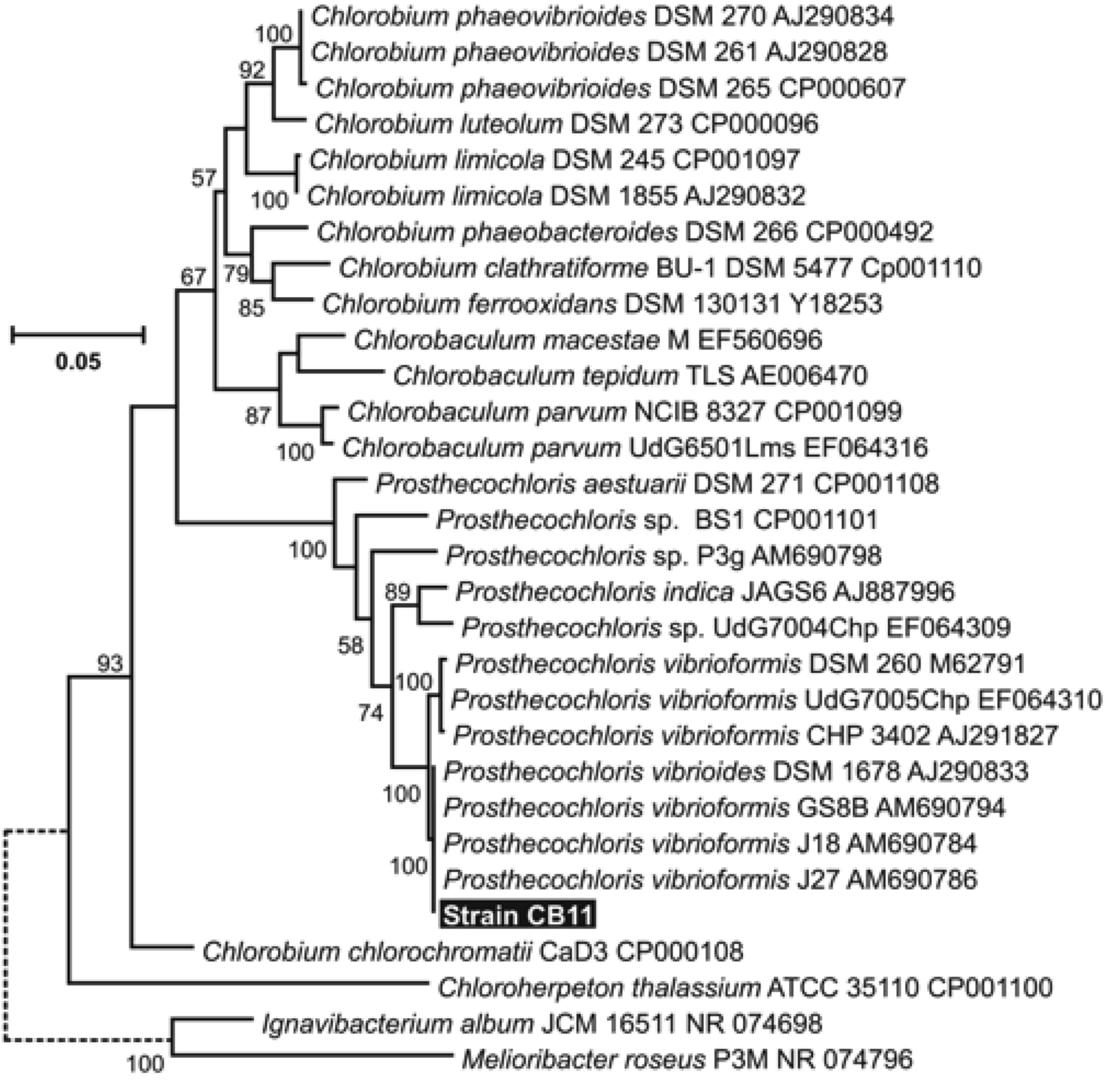

Figure 4.3 Maximum likelihood phylogenetic tree of the *Chlorobiaceae* based on a 1,238 bp alignment of 16S rRNA sequences including the sequence derived from enrichment CB11. Sequences collected from databases are identified by organism names as proposed by Imhoff and Thiel (2010), followed by strain designations, and accession numbers. Numbers at the nodes indicate the percent support observed from 1,000 bootstrap replicates. Only those values >50% are shown. The dashed branches were shortened horizontally. For all other branches, the scale bar indicates 0.05 substitutions per site.

4.3.1.3 Light Dependent Sulfide Oxidation in Field Samples

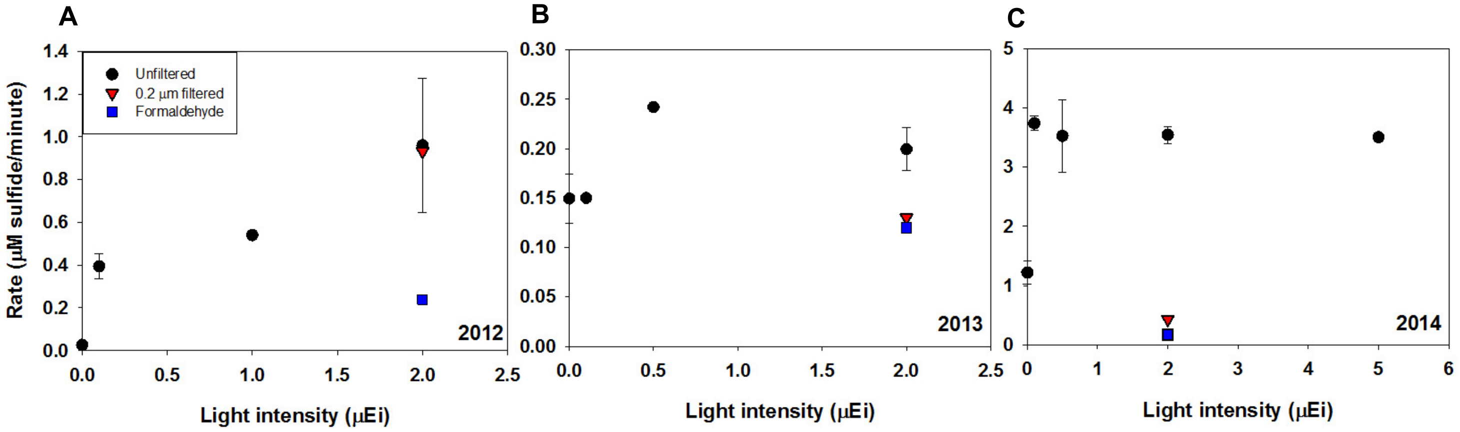

Figure 4.4 Experiments conducted shipboard demonstrating light dependent sulfide oxidation in anoxic Chesapeake Bay water samples in (a) 2012, (b) 2013, and (c) 2014.

In 2012, free sulfide was not detectable in the water column; however, light dependent sulfide loss was observed upon the addition of sulfide to bottom water samples, as demonstrated by Figure 4.4a. This sulfide loss activity was size dependent: filtration through a 0.2 µm filter had no significant effect on the rate of sulfide loss compared to experiments with unfiltered waters; however filtration through a 0.05 µm filter effectively stopped sulfide loss. Treatment of the anoxic water sample with formaldehyde also significantly decreased the sulfide loss rate when compared to untreated water (from 0.96 to 0.34 µM/minute).

In 2013 and 2014, sulfide was present in the water column, and experiments monitored the loss of the naturally occurring sulfide. In 2013, samples were taken from sulfidic waters directly below the oxic/anoxic interface at depths ranging from 14-19 meters. Figure 4.4b shows the effect of increasing light intensity on the rate of sulfide loss (10-20 μM initial sulfide) in 2013. Both the addition of formaldehyde (to a final concentration of 1.6 %) and filtration through a 0.2 μm filter resulted in a decrease in the rate of sulfide loss to approximately equal that of the dark rate.

Water samples for the 2014 experiments were collected below the interface, at approximately 15 m depth, and sulfide concentrations were 50-60 μM. In 2014, rates of sulfide loss were an order of magnitude higher than in 2013 (Figure 4.4c). Sulfide loss in the dark was a third of that in the light; however there were no significant differences between rates at varying light intensities (0.1-5 μEi) as observed in previous years (Figure 4.4a and 4.4b). This difference could be because the redox interface was higher in the water than in 2013, and thus was exposed to higher light intensities. Given these favorable conditions, the community of phototrophic sulfide oxidizing bacteria would be active and primed for sulfide oxidation. Also unique to this year was the observation of polysulfides in kinetic experiments conducted in the light, indicated by a doublet peak at -0.7 V in the voltammetric scan (Rozan et al., 2000; Luther et al., 2001). A representative scan is depicted in Figure 4.5. Polysulfides are produced during the metabolism of some green and purple PSOB (Prange et al., 2007) and are the first product of sulfide oxidation by the enzyme sulfide:quinone oxidoreductase (Griesbeck et al., 2002), and so their presence supports sulfide oxidation activity by PSOB. The dark rate (1.22 μM/min) in 2014 is an order of magnitude higher than the formaldehyde-treated rate (0.17 μM/min), suggesting that sulfide loss in the dark is due to biological uptake. Sulfide is readily transported through the cell membrane (Riahi and Rowley, 2014), and uptake of sulfide in the dark is observed in laboratory cultures of PSOB as well, and will be discussed further.

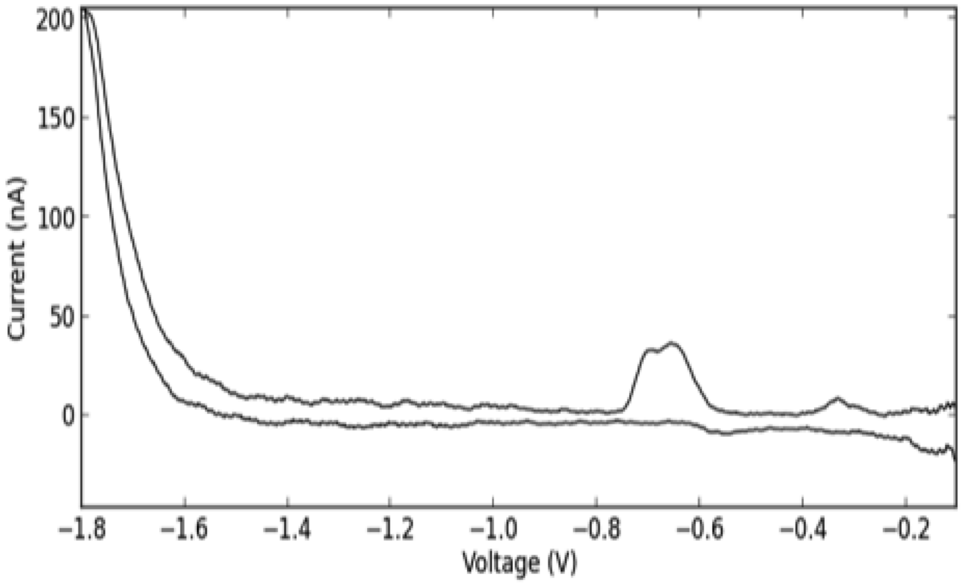

Figure 4.5: Voltammetric scan demonstrating the presence of polysulfides (doublet at -0.7 V).

The data shown in Figure 4.4 strongly indicate sulfide loss due to PSOB activity. First, addition of formaldehyde significantly inhibited sulfide loss, indicating a biological rather than a chemical process, and the abiotic rate from formaldehyde treated samples was comparable over all three years. Second, addition of DCMU as an inhibitor of photosystem II did not affect the sulfide loss rate, demonstrating that O_2 production by cyanobacteria was not the cause of sulfide loss. Finally, the effect of low-intensity light variations on the sulfide loss rate and the successful enrichment of phototrophic sulfide oxidizing bacteria in both 2011 and 2013 indicate that the observed anoxic, light dependent sulfide loss in anoxic Chesapeake Bay waters is due to the activity of phototrophic sulfur bacteria, and not chemotrophic sulfide oxidizing bacteria.

One prior study in the Chesapeake Bay has shown rapid sulfide loss (with a half-life for sulfide of approximately 15 minutes) in water samples exposed to light, which did not appear to be due to oxidation by oxygen or trace metals as this sulfide loss was not observed in the dark or in water samples that had been fixed with formaldehyde (Luther et al., 1988), a finding similar to the results presented above. The reproducibility in light dependent sulfide loss in four separate years (1987, 2012, 2013, and 2014) is highly significant as it suggests that it is a common component of the Chesapeake Bay sulfur cycle despite interannual redox variation.

4.3.2 Kinetics of Sulfide Oxidation in Enrichment CB11

For the following discussion, sulfide loss refers to the sum of two specific processes that will be differentiated when possible. Sulfide uptake indicates the portion of sulfide loss that consists of any sulfide taken into the cells that cannot definitively have been known to have been oxidized. (e.g., sulfide loss observed in the dark). Sulfide oxidation indicates the portion of sulfide loss that is known to have resulted in oxidation (through measurement of oxidation products). CB11 has been shown to produce nanoparticulate sulfur as a product of sulfide oxidation (Chapter 3).

In order to investigate the effects of changing light intensity, sulfide concentration, and biomass on the sulfide oxidation rate of phototrophic sulfur bacteria, kinetic experiments were conducted in the laboratory using CB11 enrichments grown under laboratory conditions as detailed in previously. The doubling time for the bacteria was determined to be 10 hours, and all experiments were completed at time intervals of less than one hour, well below the doubling time.

4.3.2.1 Determination of Kinetic Parameters with Varying Sulfide Concentration

Figure 4.6a shows the relationship between sulfide concentration and the rate of sulfide oxidation at saturating light intensity. The first five points, encompassing sulfide concentrations ranging from 5-75 μM, were modeled in Figure 4.6b using the Michaelis-Menten model for enzyme kinetics (equation 3) to estimate the maximum rate of sulfide oxidation, V_{max}, and the half saturation constant, K_s (a measure of the affinity of the enzyme). S is the substrate concentration, which in this case is sulfide.

$$(3)\ v = \frac{V_{max} \cdot [S]}{[S] + K_s}$$

The data can be algebraically transformed via equation 4 to create a linear Lineweaver-Burke double reciprocal plot (not shown) in order to obtain a more accurate estimate for V_{max} and K_s.

$$(4)\ \frac{1}{v_0} = \frac{K_s}{V_{max} \cdot [S]} + \frac{1}{v_{max}}$$

Although the rate data follow Michaelis-Menten kinetics at low sulfide concentrations, this description of the kinetics is not accurate for the entire data set. At higher sulfide concentrations (> 75 μM) the rate data display characteristics of substrate inhibition and were modeled using the substrate inhibition model (equation 5, Figure 4.6d) proposed by Luong et al. (1986).

$$(5)\ v = \frac{V_{max} \cdot [S]}{[S] + K_s} \times \left(1 - \frac{S}{S_{max}}\right)^n$$

This model includes a term for S_{max}, the threshold substrate concentration, above which activity is completely inhibited. The exponent, n, is a fitting term that describes the shape of the inhibition. In modeling the data in Figure 4.6, n was set to equal 1, describing a linear decrease in the rate of sulfide loss after 50 μM. The kinetic parameters derived from each of these models: Michaelis-Menten, Lineweaver-Burke, and the substrate inhibition model are summarized in Table 4.2.

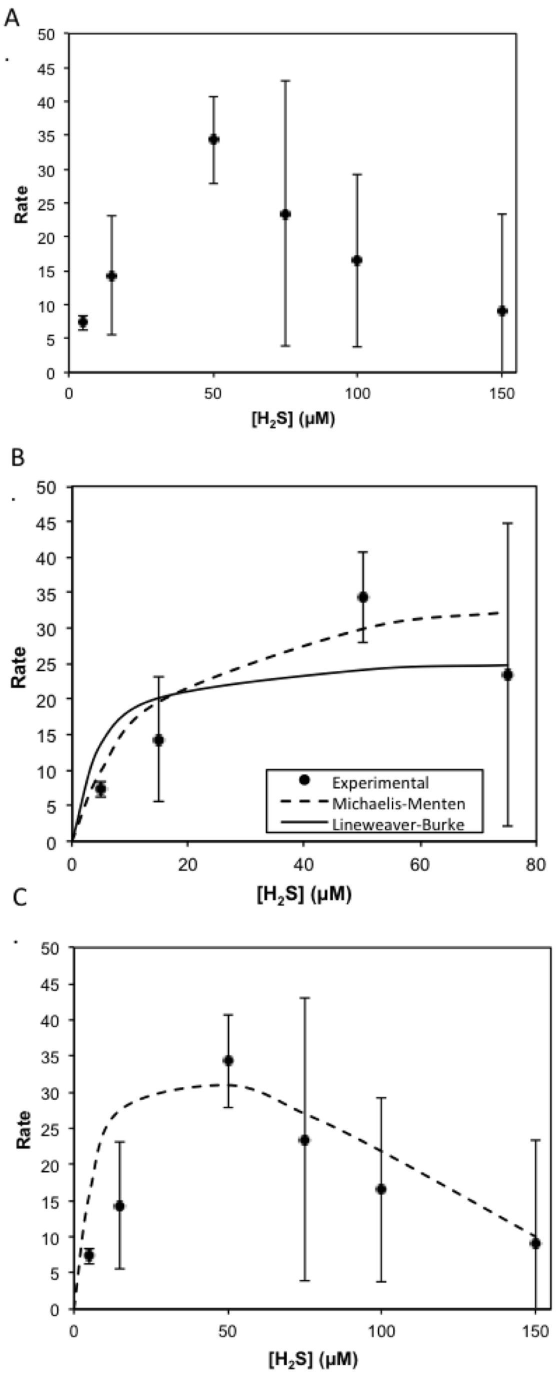

Figure 4.6 (a) The effect of sulfide concentration on rate of sulfide loss at saturating light intensities (b) Comparison of model fit to the first part of the dataset shown in (a) for parameters determined by Michaelis-Menten and Lineweaver – Burke (c) Substrate inhibition model of the entire curve. Rate is in μM sulfide/minute/mg protein. Rate has units of μMmin^{-1}mg protein^{-1}.

Table 4.2 Comparison of kinetic parameters derived from enzyme activity models.

Model	**V_{max} (μM/min/mg protein)**	**K_s (μM)**	**S_{max} (μM)**
Michaelis-Menten	39 ± 2.9	14 ± 3.6	--
Lineweaver-Burke	26	4.5	--
Substrate inhibition model[a]	51 ± 4.6	11 ± 4.4	190 ± 18

[a] Equation 5, from Luong et al. (1986)

These values for both V_{max} and K_s fit within the sulfide range CB11 would experience in the Chesapeake Bay (≤ 100 μM) and are comparable to the kinetic parameters determined for *Chlorobi* and other green sulfur bacteria (van Gemerden and Mas, 1995). Given that the substrate inhibition model is the only model used to fit the entire data set, the maximum rate and half saturation constant derived from that model are the best description of the kinetic parameters of CB11.

Although substrate inhibition is the most likely reason for the trend observed in Figure 4.6a, two other explanations may also explain the high variability in the data. First, the experiments were conduced using enrichments, not isolated cultures. The presence of other organisms in the experiments could obscure the effects of sulfide concentration on the sulfide oxidation rate. Parkin and Brock (1980) demonstrate differences in response to sulfide concentration between laboratory cultures and natural populations of sulfide oxidizing bacteria based on the rate of sulfide supply to the bacteria. If the local rate of sulfide supply or production is fast, such as when sulfide-oxidizing bacteria live in conjunction with sulfate reducing bacteria, the concentration of sulfide is not important. Secondly, as an organism living in an environment that is highly variable with respect to sulfide concentration, the bacteria studied here may be capable of utilizing a wide range of sulfide concentrations, particularly because light is the predominant factor limiting photosynthetic sulfide oxidation at the depths from which the bacteria were found.

4.3.2.2 Determination of Kinetic Dependence on Light Intensity

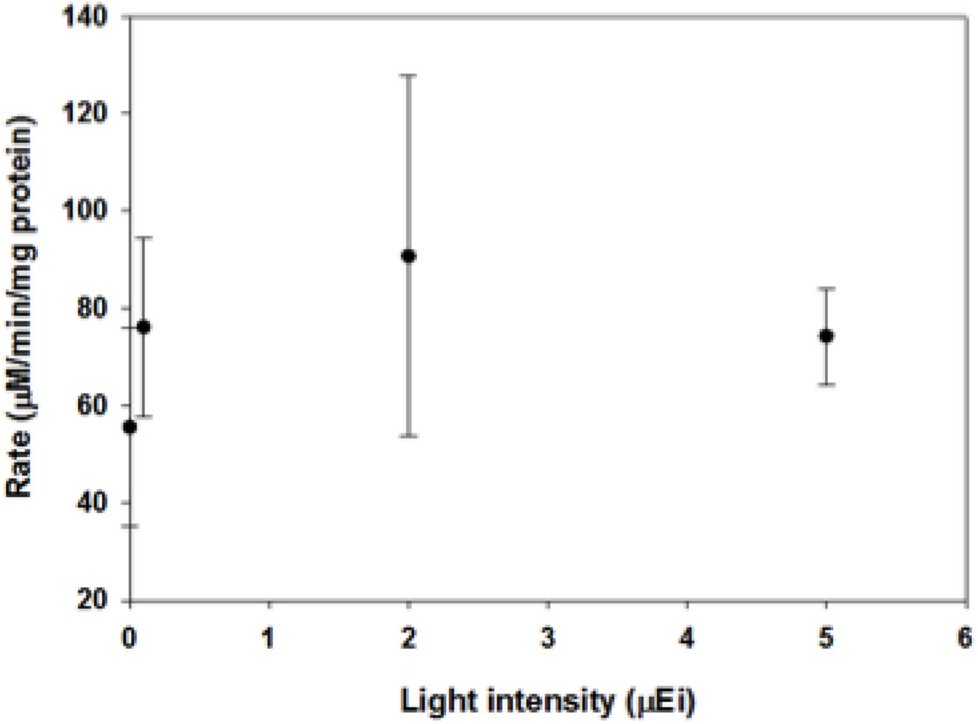

Figure 4.7 Effect of light intensity on the sulfide oxidation rate of laboratory grown enrichments. A rate of sulfide uptake is observed in the dark, and saturation of the rate occurs at low light intensity.

Figure 4.7 shows the effect of light intensity on the sulfide oxidation rate of laboratory grown CB11 enrichments. Small increases in light intensity result in significant changes in the sulfide oxidation rate over the dark uptake rate, similar to the results observed in field experiments (Figure 4.4a, b, c). Saturation of the rate is also evident after 2 μEi, indicating that photoinhibition occurs at very low light intensities.

An important component of Figure 4.7 is that a significant rate of sulfide loss is observed in the dark (57 μM min^{-1} mg protein^{-1}). Photosynthetic sulfide oxidation cannot occur under dark conditions, as light is required for the oxidation of the quinone pool (Shahak and Hauska, 2008); however uptake of sulfide for later oxidation may occur, as is done with stored elemental sulfur (Overmann, 1997). This dark rate is observed in other phototrophic sulfide oxidizing bacteria such as *Chlorobaculum tepidum* and RSC1, a red colored green sulfur bacterium isolated from a Bahamian sinkhole (Findlay, MacDonald, Hanson, and Luther, unpublished data). Dark uptake is significant as it suggests that sulfide may be stored inside the cell for future oxidation, and that uptake and oxidation of sulfide are independent processes.

The results of experiments with varying light intensity and those with varying sulfide concentrations suggest the optimum conditions with respect to the maximum sulfide oxidation rate for these bacteria are approximately 50 μM sulfide and 2 μEi light intensity. A direct comparison between the field and lab results is not possible because the biomass in laboratory experiments is likely much higher and more concentrated than the biomass *in situ* and in the kinetic experiments conducted in the field. However, sulfide loss rates over different light intensities in both the field and lab are within the same order of magnitude and show similar responses to small changes in light intensity. This has wide environmental implications as small changes in the depth of the chemical interface (and thus in the light reaching it) could greatly impact the sulfide oxidation capacity of the Chesapeake Bay and similar systems where these organisms are present.

4.4 Discussion

The results presented above strongly indicate that *Chlorobi* are a consistent component of the Chesapeake Bay ecosystem, despite variable redox conditions, and that they can oxidize sulfide at rates significantly higher than abiotic rates. The significance of these findings will be explored further in the following discussion.

4.4.1 Effect of Redox Conditions on PSOB in the Chesapeake Bay

The difference in the effects of filtration on the sulfide loss rate between 2012 and 2013-2014 can be explained by potential effects of the water chemistry on the physiology of sulfide oxidizing bacteria. In 2012, sulfide was not detected in the water column, although low concentrations of FeS and H_2S may have been diffusing from the sediments. In this case, the bacteria would be in low sulfide environments well below the photic zone, experiencing occasional exposure to oxygen. Under these conditions, any phototrophic sulfide oxidizing bacteria present would likely be small, and could pass through a 0.2 μm filter. Light intensity has been found to affect the cell size of phototrophic sulfide oxidizers (Manske et al., 2005), and cells growing in low substrate conditions also have a smaller cell volume (Baker et al., 1983; Lebaron and Joux, 1994). In 2013 and 2014, when sulfide was present and the anoxic interface was higher in the water column and closer to the photic zone, phototrophic sulfur bacteria would have been larger, and caught on the 0.2 µm filter. Bacteria grown in laboratory enrichment cultures from the Chesapeake Bay are approximately 1-5 µm; however naturally occurring bacteria are known to have smaller cell size than those grown in culture (Lebaron and Joux, 1994), and pico-bacteria less than 1 µm have been found in the Chesapeake previously (Malone et al., 1991; Chen et al., 2006).

4.4.2 Viability of PSOB at *in situ* Light Levels.

The light dependent sulfide loss observed in the Chesapeake Bay samples suggests that the bacteria present are active, or have the potential to be active given sufficient light and sulfide. The variability in the physical stratification of the water column (Figure 4.1a-d) means that the location of the redox interface changed with respect to the photic zone between years. Traditionally, the photic zone is delineated by light intensities > 1% of surface intensity. Using this definition, the base of the photic zone was located at 3.5 m in 2011, at 6 m in 2012, at 4 m in 2013, and at 9 m in 2014. However, as demonstrated above (Figure 4.4a-c) PSOB are capable of significant sulfide oxidation activity at light intensities as low as 0.0067 % surface intensity (0.1 µEi). The detection limit of the PAR sensor used was 0.034 µEi, which is higher than light intensities at which phototrophic activity has been observed, and so the depth at which PAR fell below the detection limit can be used to extend the photic zone. In 2011 this depth was 10 m, in 2012 it was 14 m, in 2013 it was 9 m and in 2014 it was 11 m. In 2011, the chemical interface was typically located between 7-10 m, and so fell within this extended photic zone. In contrast, in 2012 the suboxic zone was at 20 m, and so was below the photic zone. In 2013 the interface was situated between 13-15 m and so was below the extended photic zone, although a shoaling of the interface throughout the cruise brought it to the base of this extended photic zone. In 2014 the interface was situated between 9-12 m depth, and so was located on the edge of the extended photic zone.

A study by Manske et al. (2005) found cultures of PSOB to be photosynthetically active at light intensities down to 0.015 μEi, and field studies have established that short term variation in the light intensity at the interface can lead to photosynthetic growth, a build-up of green sulfur bacteria, and maintenance of the population (Rimmer et al., 2008; Marschall et al., 2010). The location of the interface in the Chesapeake Bay is known to vary tidally (Lewis et al., 2007) and so this process could be a factor in maintaining PSOB populations. Additionally, field studies in the Black Sea have found that although most cells in the green sulfur bacteria population are photosynthetically inactive, and do not grow; the cells are capable of maintaining their viability at light intensities as low as 0.0014 μEi, (Marschall et al., 2010). Furthermore, a study by Zerkle et al. (2010) found S^0 produced by phototrophic bacteria at the chemical interface of a stratified lake during the autumn months, when the interface is below the photic zone. Our results, along with these studies, suggest that for low-light adapted phototrophs the photic zone may extend further than has been traditionally thought.

4.4.3 Potential Contribution of PSOB to Primary Production

Parkin and Brock (1980b) demonstrate a correlation between the contribution of photosynthetic sulfur bacteria to total primary production and the fraction of surface light to which they are exposed. At the oxic-anoxic interface of the Chesapeake Bay in 2011, the maximum light intensity was 0.4 % of surface irradiance. According to the relationship outlined by Parkin and Brock (1980a) phototrophic sulfur bacteria could have contributed up to 5 % of total primary production. In 2013, when the interface was located lower in the water column, and the maximum light intensity was < 0.01% of surface, sulfur bacteria could have accounted for up to 0.1 % of primary production. In 2014, the maximum light intensity at the redox interface was 0.7 % of surface irradiance and PSOB could have contributed up to 10 % of total primary production.

4.4.4 Potential Impact of PSOB on Sulfide Oxidation in the Chesapeake Bay

Based upon the evidence presented above, phototrophic sulfide oxidation is an important component of the sulfur cycle in the Chesapeake Bay during periods in which the water column is stratified; however, abiotic sulfide oxidation is also expected to occur. Oxidized iron and manganese are the two dominant oxidants for sulfide at the chemical interface (equations 6 and 7).

(6) $2\ FeOOH + H_2S + 4\ H^+ \rightarrow 2\ Fe^{2+} + S^0 + 4\ H_2O$

(7) $MnO_2 + H_2S + 2\ H^+ \rightarrow Mn^{2+} + S^0 + 2\ H_2O$

In order to compare the fraction of biotic to abiotic sulfide oxidation in the Chesapeake, the rates of each process were calculated using parameters from the suboxic zone from 2013 and 2014. These two years were selected as they are the two years in which light dependent sulfide loss experiments were conducted with field samples and sulfide was detected in the water column. Given the following rate laws, and the concentrations of reactants as measured in the field, the potential *in situ* rates of sulfide oxidation via iron oxides, manganese oxides, and phototrophic bacteria may be estimated, and are compared in Table 4.3.

Using the rate constant derived by Yao and Millero (1996) and measured concentrations of iron and sulfide, we can determine the rate of sulfide oxidation by iron(III). The highest concentration of iron measured at the chemical interface for both 2013 and 2014 was 1.5 μM (2013). Equation 8 shows the rate law for sulfide oxidation by hydrous iron oxides as defined by Yao and Millero (1996) is

$$(8)\quad \frac{-d[H_2S]_T}{dt} = k\,[H_2S]_T\,[Fe(OH)_3]$$

where k at 25 ˚C is 148 $M^{-1}min^{-1}$.

Equation 9 shows the rate law for sulfide oxidation by manganese(IV) oxides as derived by Yao and Millero (1993). The value for k in seawater at 25 ˚C is 436 $M^{-1}minute^{-1}$. The highest concentration of MnO_2 at the chemical interface (2013) was 6 μM in 2013 and 2 μM in 2014.

$$(9)\quad \frac{-d[H_2S]_T}{dt} = k\,[H_2S]_T\,[MnO_2]$$

The rate constant and *in situ* rate of sulfide loss due to phototrophic sulfide oxidizing bacteria were derived using data from the laboratory experiments discussed aboveThe rate of sulfide metabolism for phototrophic bacteria is assumed to be dependent on both light and sulfide concentration (Guerrero et al., 1985), and the reaction can thus be described by equation 10.

$$(10)\quad \text{rate} = k\,[H_2S]^a[\text{light}]$$

where $[H_2S]$ is in M and light is in μEi. The rate order for sulfide was calculated by the method of initial rates using laboratory experiments with enrichments that isolated the effects of sulfide on sulfide oxidation rates in bacterial enrichments (Figure 4.5a). The order of reaction (a) for sulfide was determined to be 1 from this experimental data. Light is a continuous flux during these measurements and does not become depleted; thus PSOB activity can be described by a pseudo-first order rate expression that is dependent solely upon the sulfide concentration at a specific light intensity. The rate equation then becomes

$$(11)\quad \text{rate} = k\,[H_2S]$$

in which the value of k will change with the light intensity. In addition to light, this value for k is dependent upon other environmental conditions, and in particular, on the biomass of PSOB at the interface. Using the rates from Figure 4.4b and 4.4c and the sulfide concentration measured during those experiments (15 μM in 2013 and 50 μM in 2014), a value for k may be derived at a specific light intensity (in this case 0.1 μEi) for 2013 and 2014. The expected biotic rate of sulfide oxidation at the chemical interface is predicted based upon eq. 11, with the value for k and the sulfide concentration measured at the interface.

Table 4.3 Comparison of sulfide oxidation rates for 2013 and 2014.

Pathway for sulfide oxidation	**[H_2S] (μM)**	**[] oxidant**	**k**	**Rate**
2013				
Iron oxides	4	1.5 μM[a]	148 $M^{-1}min^{-1}$	0.89 nM/min
Manganese oxide	4	6 μM[b]	436 $M^{-1}min^{-1}$	11 nM/min
Phototrophic sulfide bacteria	4	0.1 μEi[c]	0.10 min^{-1}	400 nM/min
2014				
Iron oxides	10	1.5 μM[a]	148 $M^{-1}min^{-1}$	2.2 nM/min
Manganese oxide	10	2 μM[b]	436 $M^{-1}min^{-1}$	8.72 nM/min
Phototrophic sulfide bacteria	10	0.1 μEi[c]	0.075 min^{-1}	750 nM/min

[a] Maximum measured concentration of Fe^{3+} at the interface

[b] Maximum measured concentration of manganese oxide at the interface

[c] Lowest light intensity for which measurements of H_2S loss rates were made (Figure. 4.4) and is representative of light intensities measured at the interface in 2011.

4.4.5 Estimate of PSOB Biomass in the Chesapeake Bay

Using the rates obtained for laboratory cultures, and *in situ* measurements of both light intensity and sulfide we are able to estimate the biomass present at the redox interface in 2013 and 2014. Figure 4.8 depicts the relationship between biomass (mg protein) and rate of sulfide oxidation (µM/minute) for laboratory enrichments of the Chesapeake Bay strain.

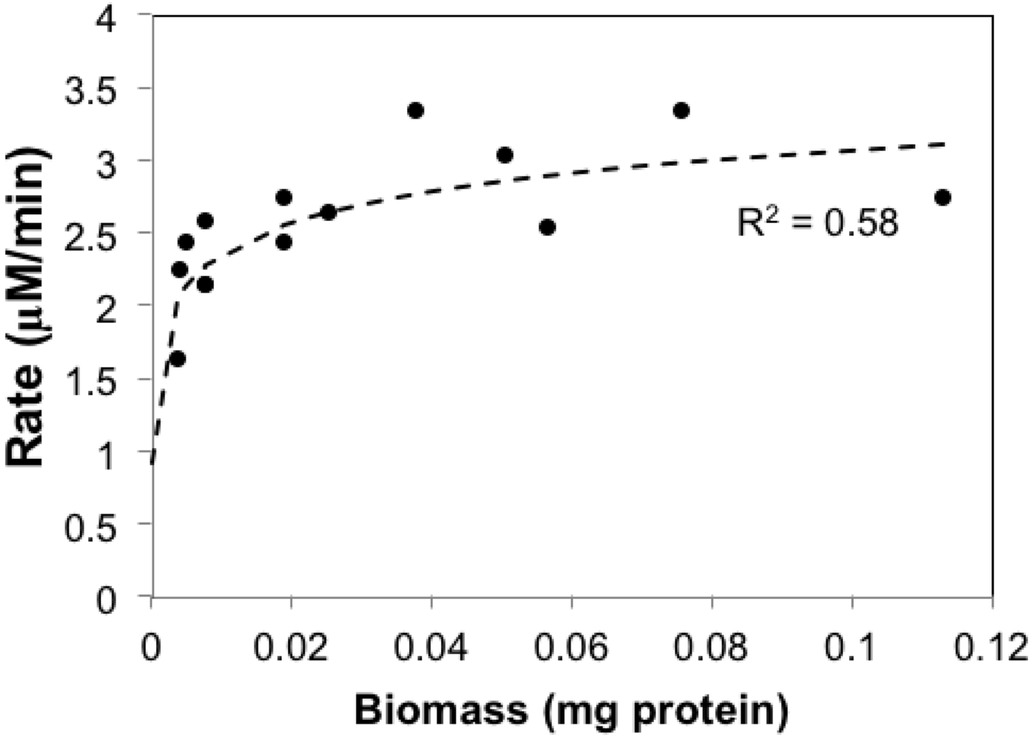

Figure 4.8 Relationship between biomass and the rate of sulfide oxidation for the laboratory grown CB11 enrichment of phototrophic sulfur bacteria from the Chesapeake Bay.

In order to use the relationship in Figure 4.8 to determine biomass from the rates measured *in situ* in the Chesapeake, we use a rate constant calculated for 5 µEi, derived from the experimental data as above to correlate the *in situ* rate with the rate measurements obtained under laboratory conditions (30 µM sulfide, and 5 µEi light intensity). With this rate, we then use the relationship between rate and biomass to calculate that the biomass of phototrophic sulfide oxidizers in the Chesapeake Bay is 11 μg protein L^{-1} in 2013 and 20 μg protein/L in 2014. Protein was calibrated with bacteriochlorophyll e in order to make a direct comparison with the literature values reported as BChl reviewed in Van Gemerden and Mas (1995). It should be noted that under low light conditions, phototrophic sulfur bacteria may increase the efficiency of photosynthesis by increasing their pigment content (Broch-Due et al., 1978), and so BChl is not a direct measure of cell abundance. The ratio of BChl e to protein for CB11was determined to be 2.25, and from this we estimate that concentration of bacteriochlorophyll e in the Chesapeake Bay to be 24 μg/L in 2013 and 46 μg/L in 2014. In other stratified environments, the density of phototrophic sulfide oxidizing bacteria can vary from 0.94 μg/L to 28 mg/L bacteriochlorophyll e. Higher concentrations are observed in permanently stratified lakes and in microbial mats, while lower concentrations are found in light-limited pelagic environments such as the Black Sea. Our estimate for the Chesapeake Bay falls in the lower portion of this range, consistent with the low light conditions in the water column. Another way of estimating the population size is to use published values of cellular protein content in marine bacteria (6-33 x 10^{-14} g $cell^{-1}$, Zubkov et al., 1999). This leads to *Chlorobi* populations of ~1 x 10^{8} cells L^{-1} in 2013 or 2 x 10^{8} cells L^{-1} in 2014. Given a mean bacterial population size of 4 x 10^{9} cells L^{-1} for the summertime Chesapeake Bay (calculated from data in Kan et al., 2006), the observed sulfide consumption rates could be explained if CB11 type *Chlorobi* account for 3-5% of the total bacterial community.

Based upon these calculations, if the populations of PSOB present in 2013 and 2014 were exposed to 0.1 μEi light (the lowest light intensity at which measurements of light-dependent sulfide oxidation were made), they could account for up to 97 % of the total sulfide oxidation in the Bay during the day in 2013, and 96 % during the day in 2014, indicating that sulfide oxidation at the oxic-anoxic interface would be dominated by biological oxidation via PSOB. The capacity of these bacteria for sulfide oxidation will be affected by changes in the interface depth and corresponding changes in light intensity, as demonstrated by the increase in the sulfide oxidation rate between 2013 and 2014, which is likely due to an increase in the PSOB population. Although the interface typically received less than 0.1 μEi light in 2013, its location in the water column was variable. This means that the sulfide oxidation capacity of the system could change on time scales of hours, as tides affect the depth of the interface (24); days, with diel light cycles; and months, as oxygen is depleted, and sulfide accumulates in the bottom waters (May – August).

4.4.6 Phototrophic Sulfide Oxidation in Other Systems

The rates derived from the kinetic experiments conducted shipboard are significant as they are one of the first reports of phototrophic sulfide loss rates in natural samples. Mandernack and Tebo (1999) measured an *in situ* sulfide loss of 240 µM/day at the oxic/anoxic interface of the Framvaren Fjord (Norway); however noticed no difference between sulfide loss in the dark versus in the light. Both azide and DCMU inhibited sulfide removal 70 and 80% respectively. Guerrero et al. (1985) measured specific rates of CO_2 uptake and H_2S oxidation throughout the microbial plate in two stratified lakes, demonstrating sulfide limitation in the upper, and light limitation in the lower, portions of the bacterial layer. Similar experiments conducted in the Black Sea measured sulfide loss rates of 1.5-3.6 µM/day, but failed to demonstrate light dependent sulfide loss (Jørgensen et al., 1991), and experiments done by Luther et al. (1991) also supported anaerobic chemical, not biological, sulfide oxidation at the Black Sea suboxic zone. Glaeser and Overmann (2003) measured photosynthetic CO_2 assimilation in consortia of phototrophic sulfur bacteria at low light intensities (0.4-1.1 µEi) in a holomictic lake, and Marschall et al. (2010) observed light dependent incorporation of bicarbonate at low light intensities (0.149 and 0.055 µEi) in Black Sea samples in which bacterial cells had been concentrated. The activity of the bacteria became light saturated at 1 µEi, a finding similar to the results we present in this study from the Chesapeake Bay (Figure 4.4a, b, c). Based on calculated doubling times of GSB populations, Manske et al. (2005) attribute less than 0.01 % of anaerobic sulfide oxidation in the Black Sea to phototrophic sulfide oxidation. In contrast, we find here that small populations of PSOB could account for nearly all (96 – 97 %) of the observed anaerobic sulfide oxidation in the Chesapeake Bay.

It is well established that phototrophic sulfur bacteria are found in most environments in which sulfidic waters or sediments are located within the photic zone (Guerrero et al., 1985; van Gemerden and Mas, 1995; Overmann, 2008). More recently, viable phototrophic sulfide oxidizing bacteria have been found in extremely low light environments in the Black Sea (Overmann et al., 1992; Manske et al., 2005; Marschall et al., 2010), a hydrothermal vent at the East Pacific Rise (Beatty et al., 2005) and a stratified lake: Lake Kinnaret (Rimmer et al, 2008). The consistent presence of PSOB in the light-limited water column of the Chesapeake Bay and observation of light-dependent sulfide loss in field samples adds to the growing evidence that phototrophic sulfide oxidizing bacteria may be a significant component of environments previously considered to be light-limited.

4.5 Conclusions

Phototrophic sulfide oxidizing bacteria were found at and below the redox interface in the Chesapeake Bay in 2011 and 2013 at light intensities ranging from below the detection limit up to 0.271 μEi. Sulfide oxidation experiments conducted shipboard in 2012, 2013, and 2014 demonstrated light dependent sulfide loss similar to a previous finding from the Chesapeake (Luther et al., 1988). The rates obtained in these experiments are comparable with sulfide oxidation rates obtained in laboratory experiments for enrichments of phototrophic sulfide oxidizers from the Chesapeake Bay. Sulfide oxidation activity of these bacteria was characterised by significant increases in the sulfide loss rate with small variations in light intensities (0.1-5 μEi) and photoinhibition at < 5 μEi**.**

The potential contribution of phototrophic sulfide oxidizers to sulfide oxidation was estimated to be up to 97 % in 2013 and 96% in 2014 during the day, indicating that these bacteria play a dominant role in mediating sulfide oxidation in the Chesapeake Bay sulfur cycle. Furthermore, these bacteria provide a mechanism for sulfide oxidation in anoxic waters. Using the rates of light dependent sulfide loss obtained in the field, and the relationship between rate and biomass obtained in laboratory experiments we calculate the concentration of phototrophic sulfide oxidizers in the Chesapeake to be 24 μg BCl e/L in 2013 and 46 μg/L in 2014. These results are significant for several reasons. First, we provide the first approximations of sulfide oxidation activity by PSOB in field samples and provide kinetic parameters under environmentally relevant light intensities and sulfide concentrations in the laboratory. Second, we demonstrate that phototrophic sulfide oxidizing bacteria are an integral component in the Chesapeake Bay sulfur cycle, and that their biological activity has important implications for sulfide removal in this system. Finally, the presence of PSOB below the photic zone and the observation of low-light dependent sulfide loss in both the lab and field indicate that PSOB could contribute to sulfide oxidation in environments previously considered to be light-limited.

REFERENCES

Baker R.M., Singleton F.L., Hood M.A. (1983) Effects of nutrient deprivation on Vibrio cholera. *Appl Environ Microbiol*. **46**, 930–940. Correction in: *Appl Environ Microbiol* 1984 May, **47**, 1193.

Beatty J.T. (2005). An obligately photosynthetic bacterial anaerobe from a deep-sea hydrothermal vent. *Proc Nat Acad Sci* **102**, 9306-9310.

Bergstein T., Henis Y., Cavari B.Z. (1979) Investigations on the photosynthetic sulfur bacterium Chlorobium phaeobacteroides causing seasonal blooms in Lake Kinneret. *Can J Microbiol* **25**, 999–1007.

Bradford M. (1976). A rapid and sensitive method for the quantitation of microgram quantities of protein utilizing the principle of protein-dye binding. *Anal Biochem* **72**, 248-254.

Broch-Due M, Ormerod J.G, Fjerdingen B.S. (1978) Effect of light intensity on vesicle formation in *Chlorobium*. *Arch Microbiol* **116**, 269-274.

Canfield D.E., Stewart F.J., Thamdrup B., De Brabandere L., Dalsgaard T., Delong E.F., Revsbech N.P., Ulloa O. (2010) A Cryptic Sulfur Cycle in Oxygen-Minimum–Zone Waters off the Chilean Coast. *Science* **330**, 1375 – 1378.

Cardinale M., Brusetti L., Quatrini P., Borin S., Puglia A.M., Rizzi A., Zanardini E., Sorlini C., Corselli C., and Daffonchio D. (2004) Comparison of different primer sets for use in automated ribosomal intergenic spacer analysis of complex bacterial communities. *Appl Environ Microbiol.* **70**, 6147-6156

Chen F., Wang K., Kan J., Suzuki M.T., Wommack E.K. (2006). Diverse and Unique Picocyanobacteria in Chesapeake Bay, Revealed by 16S-23S rRNA Internal Transcribed Spacer Sequences. *Appl Environ Microbiol* **72**, 2239-2243.

Cohen Y., Krumbein W.E., Shilo M. (1977) Solar Lake (Sinai): Distribution of photosynthetic microorganisms and primary production. *Limnol Oceanogr*. **22**, 609-620.

Crump B.C., Peranteau C., Beckingham B., Cornwell J.C. (2007) Respiratory succession and community succession of bacterioplankton in seasonally anoxic estuarine waters. *App Environ Microbiol* **73**, 6802-6810.

De Levie R. (2004) Advanced Excel for scientific data analysis, Oxford University Press: New York.

Deutsch C., Brix H., Ito T., Frenzel H., Thompson L. (2011) Climate-forced variability of ocean hypoxia. *Science*. **333**, 336-339.

Eghbal M.A., Pennefather P.S., O'Brien P.J. (2004) H_2S cytotoxicity mechanism involves reactive oxygen species formation and mitochondrial depolarisation. *Toxicology* **203**, 69–76.

Findlay A.J, Gartman A, MacDonald D., Hanson T.E., Shaw T., Luther III G.W. (2014) Distribution and size fractionation of elemental sulfur in aqueous environments: The Chesapeake Bay and Mid-Atlantic Ridge. *Geochim Cosmochim Acta* **142**: 334-348.

Glaeser J., Overmann J. (2003) Characterization and in situ carbon metabolism of phototrophic consortia. *Appl Environ Microbiol* **69**, 3739-3750.

Glazer B.T., Luther III G.W., Konavalov S.K., Friederich G.E., Nuzzio D.B., Trouborst R.E., Tebo B.M., Clement B., Murray K., Romanov A.S. (2006) Documenting the suboxic zone of the Black Sea via high-resolution real-time redox profiling. *Deep-Sea Res* **53**, 1740-1755.

Gloe A., Pfennig N., Brockmann Jr. H., Trowitzsch W. (1975) A new bacteriochlorophyll from brown-colored chlorobiaceae. *Arch Microbiol* **102**,103-109.

Gregersen L.H., Bryant D.A., Frigaard N. (2011) Mechanisms and evolution of oxidative sulfur metabolism in green sulfur bacteria. *Front Microbiol* **2**, 116.

Griesbeck C., Hauska G., Schütz M. (2002) Biological sulfide oxidation: Sulfide-Quinone Reductase (SQR), the primary reaction. *In* Pandalai SG (ed): Recent Research Developments in Microbiology, Vol. 4, 179-203. Research Signpost, Trivadrum, India.

Guerrero R., Montesinos E., Pedros-Alio C., Esteve I., Mas J., van Gemerden H., Hofman P.A.G., Bakker J.F. (1985) Phototrophic Sulfur Bacteria in Two Spanish Lakes: Vertical Distribution and Limiting Factors. *Limnol Oceanogr*. **30**, 919-931.

Hagy J.D., Boynton W.R., Keefe C.W., Wood K.V. (2004) Hypoxia in Chesapeake Bay, 1950-2001: Long-Term Change in Relation to Nutrient Loading and River Flow. *Estuaries* **27**, 634-658.

Hanson T.E., Luther III G.W., Findlay A.J., MacDonald D.J., Hess D. (2013) Phototrophic sulfide oxidation: environmental insights and methods for kinetic analysis. *Front Microbiol* **4,** 382**.**

Imhoff J.F. and Thiel V. (2010) Phylogeny and taxonomy of Chlorobiaceae. *Photosynth Res.* **104**, 123-36.

Jørgensen B.B., Fossing H., Wirsen C.O., Jannasch H.W. (1991) Sulfide oxidation in the anoxic Black Sea chemocline*. Deep Sea Res* **38**, 1083-1103.

Jørgensen B.B. (1982) Ecology of the bacteria of the sulphur cycle with special reference to anoxic-oxic interface environments. *Arch Microbiol* **298**, 543-561.

Julian D., April K.L., Patel S., Stein J.R., and Wohlgemuth S.E. **(**2005) Mitochondrial depolarization following hydrogen sulfide exposure in erythrocytes from a sulfide-tolerant marine invertebrate. *J Exp Biol* **208**, 4109–4122.

Kan J., Crump B.C., and Wang K., Chen F. (2006) Bacterioplankton community in Chesapeake Bay: Predictable or random assemblages. *Limnol Oceanogr* **51**, 2157-2169.

Lebaron P., and Joux F. (1994) Flow cytometric analysis of the cellular DNA content of Salmonella typhimurium and Alteromonas haloplanktis during starvation and recovery in seawater. *Appl Environ Microbiol* **60,** 4345–4350.

Lavik G., Stührmann T., Brüchert V., Van der Plas A., Mohrholz V., Lam P., Mussmann M., Fuchs B.M., Amann R., Lass U., Kuypers M.M. (2009) Detoxification of sulphidic African shelf waters by blooming chemolithotrophs. *Nature.* **457**, 581-584.

Lewis B.L., Glazer B.T., Montbriand P.J., Luther III G.W., Nuzzio D.B., Deering T., Ma S., Theberge S. (2007) Short-term and interannual variability of redox-sensitive chemical parameters in hypoxic/anoxic bottom waters of the Chesapeake Bay. *Mar Chem* **105**, 296-308.

Luong J.H.T. (1986) Generalization of monod kinetics for analysis of growth data with substrate inhibition. *Biotech Bioeng* **29**, 242-248.

Luther III G.W., Ferdelman T., Tsamakis E. (1988) Evidence suggesting anaerobic oxidation of the bisulfide ion in Chesapeake Bay. *Estuaries* **11**, 281-285.

Luther III G.W., Findlay A.J., MacDonald D.J., Owings S.M., Hanson T.E., Beinart R.A., Girguis P.R. (2011) Thermodynamics and Kinetics of sulfide oxidation by oxygen: a look at inorganically controlled reactions and biologically mediated processes in the environment. *Front Microbiol* **2**, 62.

Luther III G.W., Church T.M., Powell D. (1991) Sulfur speciation and sulfide oxidation in the water column of the Black Sea. *Deep-Sea Res.* **38**, 1121-1137.

Luther III G.W., Glazer B.T., Ma S., Trouwborst R.E., Moore T.S., Metzger E., Kraiya C., Waite T.J., Druschel G., Sundby B., Taillefert M., Nuzzio D.B., Shank T.M., Lewis B.L., and Brendel P.J. (2008) Use of voltammetric solid-state (micro)electrodes for studying biogeochemical processes: Laboratory measurements to real time measurements with an in situ electrochemical analyzer (ISEA). *Mar Chem* **108**, 221-235.

Luther III G.W. (2010) The Role of One- and Two-Electron Transfer Reactions in Forming Thermodynamically Unstable Intermediates as Barriers in Multi-Electron Redox Reactions. *Aquat Geochem* **16**, 395-420.

Luther III G.W., Glazer B.T., Hohmann L., Popp J.I., Taillefert M., Rozan T.F., Brendel P.J., Theberge S.M., Nuzzio D.B. (2001) Sulfur speciation monitored in situ with solid state gold amalgam voltammetric microelectrodes: polysulfides as a special case in sediments, microbial mats and hydrothermal vent waters. *J Env Monit* **3**, 61-66.

MacDonald D.J., Findlay A.J., Hredzak-Showalter P., Krepski S.T., McAllister S.M., Cone S., Scott J., Bennett S., Chan C.S., Emerson D., Luther III G.W. (2014) Using *in situ* voltammetry as a tool to search for iron oxidizing bacteria: from fresh water wetlands to hydrothermal vent sites. *Environ Sci Process Impact* **6**, 2117-2126.

Malone T.C., Ducklow H.W., Peele E.R., and Pike S.E. (1991) Picoplankton carbon flux in Chesapeake Bay. *Mar Ecol Progr Ser* **78**, 11-22.

Mandernack K.W. and Tebo B.M. (1999) In situ sulfide removal and CO2 fixation rates at deep-sea hydrothermal vents and the oxic/anoxic interface in Framvaren Fjord, Norway. *Mar Chem* **66**, 201-213.

Manske A.K., Glaeser J., Kuypers M.M., and Overmann J. (2005) Physiology and phylogeny of green sulfur bacteria forming a monospecific phototrophic assemblage at a depth of 100 meters in the Black Sea. *Appl Environ Microbiol* **71**, 8049-8060.

Marschall E., Jogler M., Hessge U., and Overmann J. (2010) Large-scale distribution and activity patterns of an extremely low-light-adapted population of green sulfur bacteria in the Black Sea. *Environ Microbiol* **12**, 1348-1362.

Overmann J., Cypionka H., and Pfennig N. (1992) An extremely low-light-adapted phototrophic sulfur bacterium from the Black Sea. *Limnol Oceanogr*. **37**, 150-155.

Overmann J. and Pfennig N. (1989) *Pelodictyon phaeoclathratiforme* sp. nov., a new brown-colored member of the *Chlorobiaceae* forming net-like colonies. *Arch Microbiol* **152**, 401–406

Overmann J. (2008) Ecology of Phototrophic Sulfur Bacteria. *In* Hell R, Dahl C, Knaff DB, Leustek T (ed), Sulfur Metabolism in Phototrophic Organisms, 1st ed, vol 27. Springer, Dordrecht, The Netherlands.

Overmann, J. (1997) Mahoney Lake: A case study of the ecological significance of Phototrophic sulfur bacteria. *In* Jones G (ed), Advances in Microbial Ecology, 1st ed, vol 15. Plenum Press, NY.

Parkin T.B. and Brock T.D. (1980a) Photosynthetic bacterial production in lakes: The effects of light intensity. *Limnol Oceanogr* **25**, 711-718.

Parkin T.B. and Brock T.D. (1980b) The effects of light quality on the growth of phototrophic bacteria in lakes. *Arch Microbiol* **125**, 19-27.

Parkin T.B. and Brock T.D. (1981) The role of phototrophic bacteri in the sulfur cycle of a meromictic lake. *Limnol Oceanogr*. **26**, 880-890.

Prange A., Chauvistre R., Modrow H., Hormes J., Truper H.G., and Dahl C. (2002) Quantitative speciation of sulfur in bacterial sulfur globules: X-ray absorption spectroscopy reveals at least three different species of sulfur. *Microbiology* **148**: 267–276.

Preisler A., de Beer D., Lichtschlag A., Lavik G., Boetius A., and Jørgensen B.B. (2007) Biological and chemical sulfide oxidation in a Beggiatoa inhabited marine sediment. *ISME Jour.* **1**, 341-353.

Pritchard D.W. (1952) Salinity distribution and circulation in the Chesapeake Bay estuarine system. *J Mar Res* **11**, 106-123.

Riahi S. amd Rowley C.N. (2014) Why can hydrogen sulfide permeate cell membranes? *J Amer Chem Soc* **136**, 15111-15113.

Rimmer A., Ostrovsky I., and Yacobi Y.Z. (2008) Light availability for *Chlorobium phaebacteroides* development in Lake Kinneret. *J Plankton Res* **30**, 765-776.

Rozan T.F., Theberge S.M., and Luther III G.W. (2000) Quantifying elemental sulfur (S^0), bisulfide (HS^-) and polysulfides (Sx^{2-}) using a voltammetric method. *Geochim Cosmochim Acta* **415**:175-184.

Schunck H., Lavik G., Desai D.K., Großkopf T., Kalvelage T., Löscher C.R., Paulmier A., Contreras S., Siegel H., Holtappels M., Rosenstiel P., Schilhabel M.B., Graco M., Schmitz R.A., Kuypers M.M., Laroche J. (2013) Giant hydrogen sulfide plume in the oxygen minimum zone off Peru supports chemolithoautotrophy. *PLoS One* **8**, 68661.

Shahak Y. and Hauska G. (2008) Sulfide Oxidation from cyanobacteria to humans: Sulfide-Quinon Oxioreductase (SQR) p. 319-335. *In* Hell R, Dahl C, Knaff DB, Leustek T (ed), Sulfur Metabolism in Phototrophic Organisms, 1st ed, vol 27. Springer Dordrecht, The Netherlands.

Stookey L.L. (1970) Ferrozine---a new spectrophotometric reagent for iron. *Anal Chem* **42**, 779-781.

Stramma .L, Schmidtko S., Levin L.A., Johnson G.C. (2010) Ocean oxygen minima expansions and their biological impacts. *Deep-Sea Res I.* **57**, 587-595.

Tamura K., Stecher G., Peterson D., Filipski A., and Kumar S. (2013) MEGA6: Molecular Evolutionary Genetics Analysis Version 6.0. *Mol Biol Evol.* **30**, 2725-2729.

Tonolla M., Peduzzi S., Hahn D., Peduzzi R. (2003) Spatio-temporal distribution of phototrophic sulfur bacteria in the chemocline of meromictic Lake Cadagno (Switzerland). *Microb Ecol* **43,** 89-98.

VanGemerden H., Mas J. (1995) Ecology of Phototrophic Sulfur Bacteria, p 49-85. *In* Blankenship RE, Madigan MT, Bauer CE (ed), Anoxygenic Photosynthetic Bacteria. 1st ed, vol 2. Springer, Dordrecht, The Netherlands.

Wahlund T.M., Woese C.R., Castenholz R.W., Madigan M.T. (1991) A thermophilic green sulfur bacterium from New Zealand hot springs, Chlorobium tepidum sp.nov. *Arch Microbiol* **156,** 81-90.

Yao W., Millero F.J. (1993) The rate of sulfide oxidation by δMnO_2 in seawater. Geochim Cosmochim Acta **57**, 3359–3365.

Yao W., Millero F.J. (1996) Oxidation of hydrogen sulfide by hydrous Fe(III) oxides in seawater. Mar Chem **52**,1-16.

Zerkle A.L., Kamyshny A., Kump L.R., Farquhar J., Oduro H., Arthur M.A. (2010) Sulfur cycling in a stratified euxinic lake with moderately high sulfate: Constraints from quadruple S isotopes. *Geochim Cosmochim Acta* **74**, 4953-4970.

Zubkov M.V., Fuchs B.M., Eilers H., Burkill P.H., Amann R. (1999) Determination of total protein content of bacterial cells by SYPRO staining and flow cytometry. *Appl Environ Microbiol.* **65**,3251-7.

Chapter 5

INVESTIGATION OF THE EFFECT OF REDOX VARIABILITY ON SULFIDE OXIDATION AT THE OXIC/ANOXIC INTERFACE OF A STRATIFIED ESTUARY USING A NUMERICAL MODEL

Abstract

The decomposition of organic matter via sulfate reduction leads to the accumulation of sulfide in the sediments and bottom waters of many stratified systems. This sulfide is then oxidized via an array of biotic and abiotic reactions. A one dimensional diffusion-reaction model was developed and applied to four years of physical and chemical data from the stratified water column of the Chesapeake Bay in order to investigate sulfide oxidation in the Bay. These datasets and model simulations highlight both short-term and interannual variation in the physical structure and the distribution of key redox species (O_2, H_2S, S^0, Fe^{2+}, Mn^{2+}, FeOOH, MnO_2) throughout the water column. The model evaluates links between oxygen, sulfur, iron, and manganese cycling, and includes the novel consideration of the activity of phototrophic sulfide oxidizing bacteria, which are known to be a common component of the Bay. Model simulations demonstrate that phototrophic sulfide oxidation can account for over half of total sulfide oxidation, depending upon the depth of the oxic/suboxic/anoxic interface. The results of this study quantify the variable role that phototrophic sulfide oxidizing bacteria play in sulfide oxidation in the Chesapeake

Bay as the location of the oxic/anoxic interface within the water column, the incident light intensity, and the flux of sulfide to the interface vary.

5.1 Introduction

Redox cycling in many systems is driven by the microbial decomposition of organic matter via a series of electron acceptors ($O_2 > NO_3^- > MnO_2 > FeOOH > SO_4^{2-}$) (Froelich et al. 1979). The preferential use of oxygen results in the formation of three distinct zones: (1) the oxic, in which organic matter oxidation is carried out by oxygen, (2) the suboxic ($[O_2] < 3$ μM; $[H_2S] < 0.2$ μM), in which organic matter is oxidized primarily by nitrate, manganese oxides, and iron oxides, and (3) the anoxic, where sulfate reduction dominates. This succession of redox zones is ubiquitous in sediments, and is observed in the water column of density-stratified systems where oxygen consumption by decomposition exceeds reaeration, leading to the depletion of oxygen at depth (Diaz, 2001). Sulfide accumulates in these anoxic deep waters as a result of sulfate reduction.

Less than 20 % of the sulfide produced by microbial sulfate reduction is removed via sedimentary burial as pyrite (Jørgensen, 1982), meaning that the majority of sulfide is eventually reoxidized. The eight-electron oxidation of sulfide to sulfate occurs in multiple steps via a suite of chemical and biological processes, forming a wide array of intermediates (e.g. S_x^{2-}, S^0, $S_2O_3^{2-}$). Sulfide oxidation has widespread environmental significance; for example, sulfide is toxic to aerobic organisms, causing problems such as fish kills (Luther et al., 2004). Additionally, intermediate species such as elemental sulfur and polysulfides play a role in geochemical reactions like pyrite formation (Luther, 1991), and both sulfide and its oxidation intermediates are widely used in microbial metabolisms (Frigaard and Dahl, 2008, and references therein). Furthermore, the cycling of sulfur is closely connected to other elemental cycles, including those of manganese, iron, carbon, and phosphorus (Jørgensen and Nelson, 2004).

Due to the complexity of the sulfur cycle, the wide variety of potential oxidants for sulfide, and unknown turnover rates for intermediate species, measurement of products and reactants gives limited information about the specific processes that govern the observed distribution of sulfur compounds and other redox species. One tool by which the importance, impact, and rates of some of these processes may be assessed is the development of numerical models. Redox models have been developed and applied to a variety of sedimentary environments (Di Toro and Fitzpatrick, 1993; Wang and Capellan, 1996; Boudreau et al., 1998; Hunter et al., 1998; Di Toro, 2000), and more recently, progress has been made in the application of such models to the water column, most notably to that of the Black Sea (Yakushev and Nerentin, 1997; Oguz et al., 2001; Konavolov et al., 2006; Yakushev et al., 2007). There remain, however, important processes that have not yet been quantified or added to models.

One of these processes is sulfide oxidation by phototrophic bacteria. Biological sulfide oxidation can occur at rates that are orders of magnitude higher than abiotic chemical oxidation (Luther et al., 2011), and phototrophic sulfide oxidizing bacteria

(PSOB) are commonly found at the oxic/anoxic interface of stratified fresh and marine water columns (Guerrero et al., 1985; Overman, 1992; Tonolla et al., 2003; Manske et al., 2005; Rimmer et al., 2008; Marschall et al, 2010). Despite their prevalence and expected impact, sulfide oxidation by PSOB has not been explicitly included in redox models or sulfide budgets to date due to a lack of kinetic information and uncertainty about how to parameterize their activity (Oguz et al., 2001). Yakushev et al. (2007) attributed measurements of dark CO_2 fixation to phototrophic sulfide oxidation in a model of the Black Sea suboxic zone. They calculated that it accounted for approximately 30 % of total sulfide oxidation; however, this is not an accurate representation of phototrophic sulfide oxidation because PSOB cannot conduct photosynthesis in the dark.

In Chapter 4, the kinetics of sulfide oxidation under environmentally relevant light intensities and sulfide concentrations by a strain of *Chlorobiaceae* (CB11) enriched from the stratified water column of the Chesapeake Bay were described. In the study presented here, these data will be used to include sulfide oxidation by PSOB in the development of a one-dimensional model of the redox chemistry of the water column of a seasonally stratified estuary, the Chesapeake Bay. This model is applied to data collected over a four-year study in order to investigate sulfide oxidation in the Chesapeake Bay, with particular focus on the dynamics of phototrophic sulfide oxidation.

5.2 Methodology

5.2.1 Field Sampling

Study Site. Physical and chemical characteristics were measured in the stratified water column of a shallow hole just south of the Chesapeake Bay Bridge (38°58.8′ N; 76°22′ E) in the mesohaline portion of the Chesapeake Bay during four sequential summers (27-30 July 2011, 17-19 August 2012, 9-13 August 2013, and 18-22 August 2014) on the R/V *Hugh R. Sharp*. The hole is approximately 25 m deep, 4 km long, and 0.8 km wide, bordered on the west by the main shipping channel and on the east by Kent Island (Lewis et al., 2007). In the summer, the water column stratifies, with an oxic surface layer and anoxic bottom waters that are often sulfidic. Unlike permanently stratified anoxic marine systems, such as the Black Sea that have a predictable water column structure that has developed over years (Murray et al., 1995), the physical and chemical stratification of the Bay varies with short-term processes such as tides (Lewis et al., 2007), wind speed, and wind direction (Scully, 2010); and with longer-term seasonal and interannual shifts in nutrient input, production, and rainfall (Hagy et al., 2004). Furthermore, the suboxic zone between the oxic surface and anoxic deep waters in the Chesapeake Bay is transient. During the flood and ebb tides, the top and bottom waters move with respect to each other, creating a shear interface between the oxic and anoxic layers, which decreases the extent of the suboxic zone (Lewis et al., 2007).

Sample Collection. Samples were collected in Nalgene bottles either from Niskin bottles on the shipboard CTD or from Nalgene tubing attached to a plastic water pump. Sample collection and processing were rapid (< 10 minutes) in order to minimize redox changes in the samples. Salinity, temperature, and oxygen data were collected from the ship's CTD sensor and used to plan sampling depths. PAR measurements were made using an *in situ* FIRe sensor (MacDonald et al., submitted), and chlorophyll was determined from the ship's fluorometer. Chlorophyll concentrations were obtained by converting the voltage from the fluorometer on the ship's CTD using the relationship outlined by Lorenzen (1966).

5.2.2 *In situ* Water Column Chemistry

Profiles of oxygen and sulfide in the water column were made using *in situ* voltammetry (Luther et al., 2008). The electrode system consists of a 100 μm gold amalgam working electrode, a Ag/AgCl reference electrode, and a platinum counter electrode. In 2011, this system was interfaced to a DLK-SUB-II electrochemical analyzer attached to a metal cage that was suspended over the side of the ship. In 2012 -2014, a DLK 100 potentiostat was used and measurements were made shipboard using a flow-through cell, which has been confirmed to preserve *in situ* speciation (Glazer et al, 2006; MacDonald et al., 2014). Voltage was applied from -0.1 V to -1.8 V at a scan rate of 2000 mV/second. Using this method the detection limit is 3 μM for oxygen and 0.2 μM for sulfide and polysulfide.

5.2.3 Analytical Techniques

5.2.3.1 Iron

Iron was determined spectrophotometrically using the ferrozine method of Stookey (1970). Analyses were conducted after sample collection and processing. 90 mL of sample water were either poured unfiltered or were filtered via a 0.2 µm prefabricated Puradisc filter into a separate Nalgene bottle containing 90 µL of 12 M trace metal grade hydrochloric acid. The acid-fixed samples were allowed to sit for at least four hours prior to analysis, and all analyses were conducted in triplicate. Ferrous iron was determined by adding 3 mL of a 1:1 mixture of 0.01 M ferrozine and 6 M ammonium acetate buffer. After a waiting period of half an hour the absorbance at 562 nm was read. In order to measure total iron, 250 µL hydroxylamine were added to reduce Fe^{3+} to Fe^{2+}. The difference between the values for total iron and Fe^{2+} gives Fe^{3+}.

5.2.3.2 Elemental Sulfur

Samples for elemental sulfur were taken by filtering 30 mL of sample water through a 0.2 µm GTTP Millipore filter. The filtrate was extracted on the ship in 5 mL toluene for 1.5 hours. Prior to extraction, 15 µL concentrated HCl were added to the filtrate in order to eliminate sulfide as H_2S gas. Filters were frozen and extracted in toluene overnight upon return to shore. Elemental sulfur was quantified on an HPLC using 98% methanol 2 % water as the eluent (Möckle, 1984; Yücel et al., 2010), which was sparged with helium gas during the analysis. The pump speed was set to 1 mL/minute, the detector set at 264 nm, and the peak for elemental sulfur from S_8 was observed after approximately eight minutes.

5.3 Model Design

5.3.1 Description of Model

A one-dimensional diffusion-reaction model that consists of a series of partial differential equations was developed to quantify interactions between oxygen, sulfur, iron, and manganese in the water column of the Chesapeake Bay. A complete list of the chemical species included in the model is provided in Table 5.1.

Table 5.1 Chemical species considered by the model

Species	Symbol	State
Oxygen	O_2	Dissolved
Sulfide	H_2S*	Dissolved
Elemental sulfur	S^0	Solid
Manganese(II)	Mn^{2+}	Dissolved
Manganese(IV) oxides	MnO_2	Solid
Iron(II)	Fe^{2+}	Dissolved
Iron(III) oxides	FeOOH	Solid

* For notation purposes, H_2S refers to $\Sigma H_2S + HS^-$

Figure 5.1 depicts the conceptual framework of the model. As the model is designed to approximate the structure of the water column at steady state, lateral transport is ignored and only vertical transport of chemical species is considered. The source of oxygen in the model is rearation at the atmosphere-water interface. Sulfide diffuses into the water column from the sediments, which are the primary location of sulfate reduction (Roden and Tuttle, 1993). This sulfide is oxidized chemically by oxygen, iron oxides, or manganese oxides; and biologically by phototrophic sulfide oxidizing bacteria. Reduced iron and manganese also diffuse from the sediments, then are cycled within the water column. Manganese is microbially oxidized by oxygen to form manganese(IV) oxides, which are chemically reduced by sulfide. Iron is oxidized by oxygen to form iron oxides, which are reduced by sulfide. Although microaerophilic iron-oxidizing bacteria have been enriched from the suboxic zone and likely mediate iron oxidation at low O_2 concentrations when abiotic oxidation is slow (MacDonald et al., 2014), they are not explicitly considered in this model due to a lack of information about their kinetics.

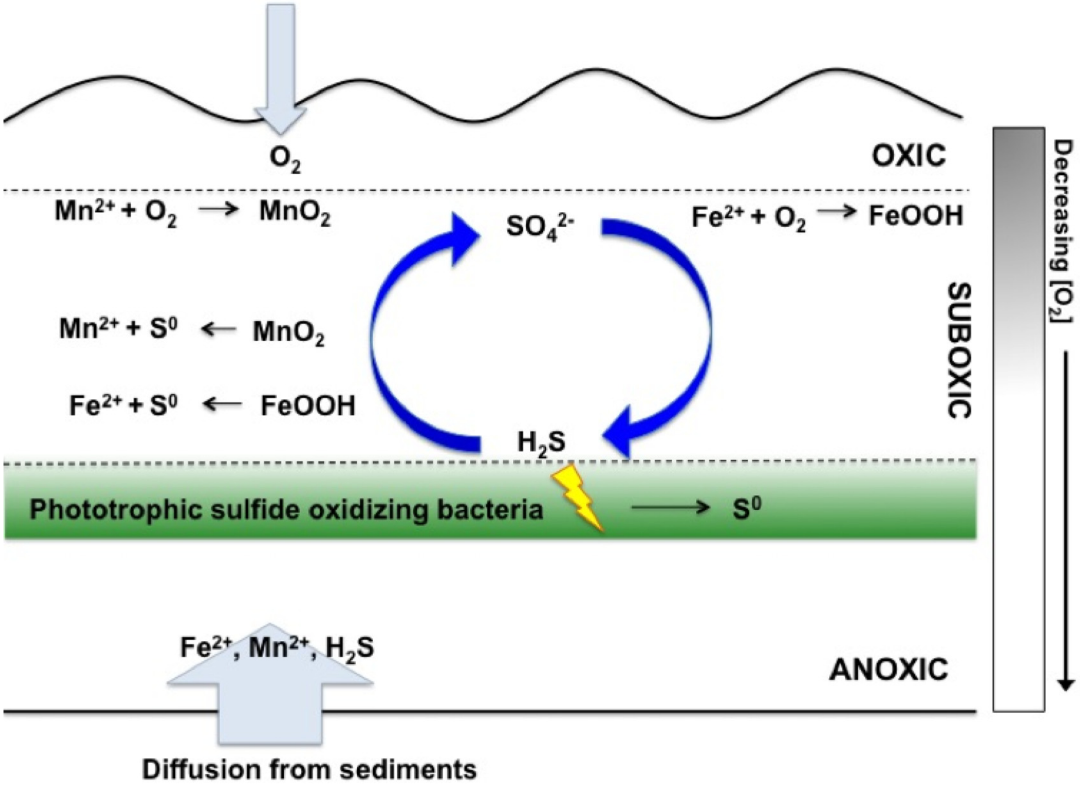

Figure 5.1 Conceptual model of redox cycling in the water column of the Chesapeake.

5.3.2 Reactions

5.3.2.1 Redox Reactions

The following reactions were used to describe the processes depicted in Figure 5.1. The stoichiometric equations and model representation of the reactions described below, as well as the values of kinetic parameters with references are summarized in Table 5.2 at the end of this section.

Oxygen oxidizes organic matter, the kinetics of which are described by Michaelis-Menten kinetics (Bourdreau, 1992, equation 1 in Table 5.2).

$$(1)\ \frac{d[O_2]}{dt} = -k_1 r_{oc} C_{org} \frac{[O_2]}{K_{O2}+[O_2]}$$

C_{org} is the organic carbon concentration, which was calculated from chlorophyll assuming a ratio of 50 mg C per mg of Chl (Chapra, 1997). k_1 is the rate constant for organic matter decomposition, r_{oc} is the ratio of oxygen consumed per unit carbon, which is 1 $\mu MO_2\ \mu MC^{-1}$, assuming a Redfield ratio, and K_{O2} is the half saturation constant for oxygen.

All other redox reactions (equations 2-6 in Table 5.2) are treated as second order and represented by the form rate = -k[oxidant][reductant]. Oxygen abiotically oxidizes sulfide and Fe^{2+} via equations 3 and 4. For notation purposes, Fe^{3+} is assumed to be present as iron oxide particles and nanoparticles, and is represented in the model as FeOOH (Table 5.1). Although Fe^{2+} oxidation by oxygen is dependent upon pH, and is second order with respect to hydroxide concentration (Millero, 1987), the pH in the Chesapeake is relatively constant with depth (7.5 ± 0.5), and so equation 4 is treated as second order overall (Table 5.2).

Sulfide reduces FeOOH to Fe^{2+} and is oxidized to S^0 via equation 5. Oxygen also oxidizes Mn^{2+} to MnO_2 (equation 6). At the pH of the Bay all manganese oxidation is microbially mediated (Tebo, 1991). Manganese oxidation rates were measured in the field and are approximately an order of magnitude faster than those measured in the Black Sea (B. Tebo, personal communication). MnO_2 is reduced by sulfide, which is oxidized to S^0 (equation 7).

Elemental sulfur disproportionation is included via equation 8. Sulfur disproportionation is energetically favourable at sulfide concentrations < 1 mM and is microbially mediated (Canfield et al., 2005).

5.3.2.2 Oxygenic Photosynthesis and Respiration

Photosynthesis and respiration are determined through the relationship correlating these processes to chlorophyll concentrations as outlined by Chapra (1997) (equations 9 and 10).

$$(9)\quad P = r_{0a}\ G_{max}\ \theta^{T-20}\ \phi_L(I)[Chla])$$

where r_{oa} is the oxygen generated in μM mg $Chla^{-1}$, G_{max} is the growth rate, $\theta = 1.066$, ϕ_L describes attenuation due to light intensity, T is temperature (26 °C), and Chla is the concentration of chlorophyll a in mg L^{-1}. Respiration is calculated via equation 10

$$(10)\quad R = r_{0a}\ k_{ra}\ \theta^{T-20}\ [Chla]$$

where k_{ra} is the respiration rate and all other parameters are as above.

5.3.2.3 Anaerobic Phototrophic Sulfide Oxidation

Chapter 4 demonstrated that phototrophic sulfide oxidizing bacteria are a significant and common component of the sulfur cycle in the Chesapeake Bay. Even during periods where the redox interface lies beneath the photic zone, PSOB are likely still present, and could become active when the light intensity is sufficient (e.g. Jørgensen, 1987).

Autotrophic phototsynthetic sulfide oxidation occurs via equation 8, forming elemental sulfur as an obligate intermediate (Chan et al., 2008; Chapter 3). The rate of sulfide oxidation by phototrophic bacteria is dependent on both light intensity and sulfide concentration (Guerrero et al., 1985). In order to parameterize PSOB activity, the model of phytoplankton growth described in Chapra (1997), based on the formulation presented by Di Toro et al. (1971) and used by Cerco et al. (1993) for the current Chesapeake Bay eutrophication models (equation 11) was adapted using the kinetic data determined in Chapter 4.

$$(11)\quad K_g(T,N,L) = k_g(T)\phi_N(N)\phi_L(L)$$

k_g is the growth rate, which is a function of T (temperature), N (nutrient concentration), and L (light intensity). $k_g(T)$ is the dependence of the growth rate upon temperature, $\phi(N)$ is the attenuation due to limiting nutrient or substrate concentrations, and $\phi(L)$ describes the attenuation due to diminishing light intensity. As the temperature of the Chesapeake Bay has a narrow range between years (24-27 ^{o}C) and is consistent with the experimental conditions used for the determination of kinetic parameters, $k_g(T)$ is ignored. $\phi(N)$ is calculated by equation 12

$$(12)\quad \phi_N(N) = \frac{[N]}{K_sN+[N]}$$

where [N] represents the sulfide concentration ([H_2S]) and KsN is the half saturation constant (K_s), which has a value of 14 ± 3.6 μM.

Sulfide oxidation by the PSOB enriched from the Chesapeake Bay becomes saturated at very low light intensities. Thus, ϕ(L) is calculated using the equation proposed by Steele (1965) that describes attenuation of growth after a saturating light intensity (equation 13).

$$(13) \quad \phi_L(L) = \frac{I(z)}{I_{sat}}\, e^{\left(-\frac{I(z)}{I_{sat}}+1\right)}$$

Where I(z) is light intensity and I_{sat} is the optimum light intensity for growth as determined experimentally and has a value of 2.8 ± 0.52 μEi.

The activity of phototrophic sulfide oxidizing bacteria may then be described by the overall equation (equation 14)

$$(14) \quad \frac{d[H_2S]}{dt} = -k_8\, \frac{[H_2S]}{K_SN + [H_2S]}\, \frac{I(z)}{I_{sat}}\, e^{\left(-\frac{I(z)}{I_{sat}}+1\right)}$$

The light profile for equation 14 is calculated via equation 15

$$(15) \quad I(z) = I_i\, e^{(-k_{ext}\, z)}$$

where I_i is the incident light at the surface, k_{ext} is the extinction coefficient as calculated for each year by MacDonald et al., (in preparation), and z is depth

Table 5.2 Parameterization of biogeochemical processes considered by the model. Kinetic parameters were adapted from literature values (Fuji et al., 2002; Millero, 1991; Poulton et al., 2004; Tebo, 1991; Lewis and Landing, 1991; Oguz et al., 2001; Konavolov et al., 2006; Yakushev et al., 2007). Parameters for phototrophic sulfide oxidation were taken from Chapter 4.

Description	Reaction	Model representation	Symbol	Kinetic parameters		
Redox reactions:						
(1) *organic matter remineralisation*	$CH_2O + O_2 \rightarrow CO_2 + H_2O$	$k_1 r_{oc} C_{org} \frac{[O_2]}{K_{O2} + [O_2]}$	R1	k_1	0.1	d^{-1}
				r_{oc}	1	$\mu MO_2\ \mu MC^{-1}$
				K_{O2}	3	μM
(2) *sulfide oxidation by oxygen*	$HS^- + ½\ O_2 + H^+ \rightarrow S^0 + H_2O$	$k_2[H_2S][O_2]$	R2	k_2	0.05	$\mu M^{-1}d^{-1}$
(3) *iron oxidation by oxygen*	$4\ Fe^{2+} + O_2 + 3\ H_2O \rightarrow 4\ FeOOH + 2\ H^+$	$k_3[Fe^{2+}][O_2]$	R3	k_3	0.1	$\mu M^{-1}d^{-1}$
(4) *sulfide oxidation by iron*	$2\ FeOOH + HS^- + 5\ H^+ \rightarrow 2\ Fe^{2+} + S^0 + 4\ H_2O$	$k_4[FeOOH][H_2S]$	R4	k_4	0.2	$\mu M^{-1}d^{-1}$
(5) *manganese(II) oxidation by oxygen*	$Mn^{2+} + O_2 + H_2O \rightarrow MnO_2 + 4H^+$	$k_5[Mn^{2+}][O_2]$	R5	k_5	0.5	$\mu M^{-1}d^{-1}$
(6) *sulfide oxidation by manganese(IV)*	$2\ MnO_2 + 2\ HS- + 6\ H^+ \rightarrow 2Mn^{2+} + 2\ S^0 + 4\ H_2O$	$k_6[MnO_2][H_2S]$	R6	k_6	1	$\mu M^{-1}d^{-1}$
Biological processs:						
(7) *S^0 disproportionation*	$2\ S^0 + 4\ H_2O \rightarrow H_2S + SO_4^{2-} + 6\ H^+$	$k_7[S^0]$	R7	k_7	0.01	d^{-1}
(8) *phototrophic sulfide oxidation*	$H_2S + light \rightarrow S^0$	$k_8 \frac{[H_2S]}{K_sN + [H_2S]} \frac{I(z)}{I_{sat}} e^{(-\frac{I(z)}{I_{sat}}+1)}$	R8	k_8	1	$\mu M^{-1}d^{-1}$
				K_sN	14	μM
				I_{sat}	2.8	μEi
(9) *Photosynthesis*		$r_{0a}\ G_{max}\ \theta^{T-20}\ \phi_L(I)[Chla])$	P			
(10) *Respiration*		$r_{0a}\ k_{ra}\ \theta^{T-20}\ [Chla]$	R			
light attenuation		$I(z) = I_i\ e^{(-k_{ext}\ z)}$	light	k_{ext}		

5.3.3 Mass Balance Equations

The distribution of the modeled species (O_2, H_2S, S^0, Fe^{2+}, FeOOH, Mn^{2+}, and MnO_2) was calculated via the following set of partial differential equations (Table 5.3), in which D is the vertical diffusion coefficient, W is the settling rate, t is time, and z is depth. The first term on the right-hand side of the equation indicates vertical diffusion, followed by settling for solid species (S^0, MnO_2, FeOOH), and the kinetic data for the biological and chemical redox reactions are described above and detailed in Table 5.2.

Table 5.3 Model equations. The equations are solved using finite differences. Parameter definitions are found in the above paragraph and Table 5.2.

Mass Balance equations

$$(16)\quad \frac{\partial[O_2]}{\partial t} = \frac{\partial}{\partial z}\left(D\frac{\partial[O_2]}{\partial z}\right) + P - R - R1 - \frac{1}{2}R2 - \frac{1}{2}R3 - \frac{1}{4}R5$$

$$(17)\quad \frac{\partial[H_2S]}{\partial t} = \frac{\partial}{\partial z}\left(D\frac{\partial[H_2S]}{\partial z}\right) - R2 - R4 - R6 + \frac{1}{2}R7$$

$$(18)\quad \frac{\partial[S^0]}{\partial t} = \frac{\partial}{\partial z}\left(D\frac{\partial[S^0]}{\partial z}\right) - W\frac{\partial[S^0]}{\partial z} + R2 + R4 + R6 - R7 + R8$$

$$(19)\quad \frac{\partial[Fe^{2+}]}{\partial t} = \frac{\partial}{\partial z}\left(D\frac{\partial[Fe^{2+}]}{\partial z}\right) - R5 + R6$$

$$(20)\quad \frac{\partial[FeOOH]}{\partial t} = \frac{\partial}{\partial z}\left(D\frac{\partial[FeOOH]}{\partial z}\right) - W\frac{\partial[FeOOH]}{\partial z} + R5 - R6$$

$$(21)\quad \frac{\partial[Mn^{2+}]}{\partial t} = \frac{\partial}{\partial z}\left(D\frac{\partial[Mn^{2+}]}{\partial z}\right) - R3 + R4$$

$$(22)\quad \frac{\partial[MnO_2]}{\partial t} = \frac{\partial}{\partial z}\left(D\frac{\partial[MnO_2]}{\partial z}\right) - W\frac{\partial[[MnO_2]}{\partial z} + R3 - R4$$

5.3.4 Numerical Method

Equations 16-22 were solved using the method of finite differences (as in Oguz et al., 2001). Vertical integration was conducted for a 25 m water column discretized into 50 sections, giving a grid spacing of 0.5 m. Diffusion was solved using centered differences, the settling term was calculated using backward differences, and integration over time was calculated using forward differences. A time step of 0.01 days was used for the solution, and the model was allowed to reach steady state with an integration time of 1000 days. The equations are solved using a programming script written in Python.

An O_2 flux was set as the surface boundary condition assuming reaeration by equation 23.

$$(23) \quad \frac{d[O_2]}{dt} = k_{la} \ ([O_{2sat}] - [O_{2i}]) \ / \ H$$

O_{2sat} is the saturated oxygen concentration (260 µM at 25 °C, S = 15 ppt), O_{2i} is the oxygen concentration for the first layer of the model, and k_{la} is the rearation constant calculated via equation 24 (Thomann and Fitzpatrick, 1982).

$$(24) \quad k_{la} = \left(3.93 \ \frac{\sqrt{U_0}}{H^{3/4}} + \frac{0.728 \ U_w{}^{0.5} - 0.317 U_w - 0.0372 \ U_w{}^2}{H}\right) H$$

U_o is the average tidal velocity (set as 0.178 m s^{-1} after Xiong and Berger (2010)), U_w is the wind speed 10 meters above the surface (set at 5 m s^{-1} after Scully (2010)), and H is average depth (25 m). Using these parameters, a k_a of 1.3 m d^{-1} was calculated.

For the bottom boundary condition, concentrations of Fe^{2+}, H_2S, and Mn^{2+} were set based upon linear extrapolation from the measured bottom water concentrations, assuming that the sediments are the predominant source of reduced species. The imposition of these boundary conditions at the sediment-water interfaces allows the model to be decoupled from the sediments for simplicity. The initial concentration for all species in the water column was set to zero, and zero-flux conditions were set for the first grid spacing at the surface and bottom boundaries.

5.4 Results and Discussion

The structure of the results section will be as follows. The physical and chemical characteristics of the water column will be described first for each of the four years of sampling. Some of these data have been presented previously (Chapter 3; Chapter 4) and are summarized briefly here as a means to provide context for the presentation and discussion of the modeling results that will follow.

5.4.1 Physical and chemical variability of the water column

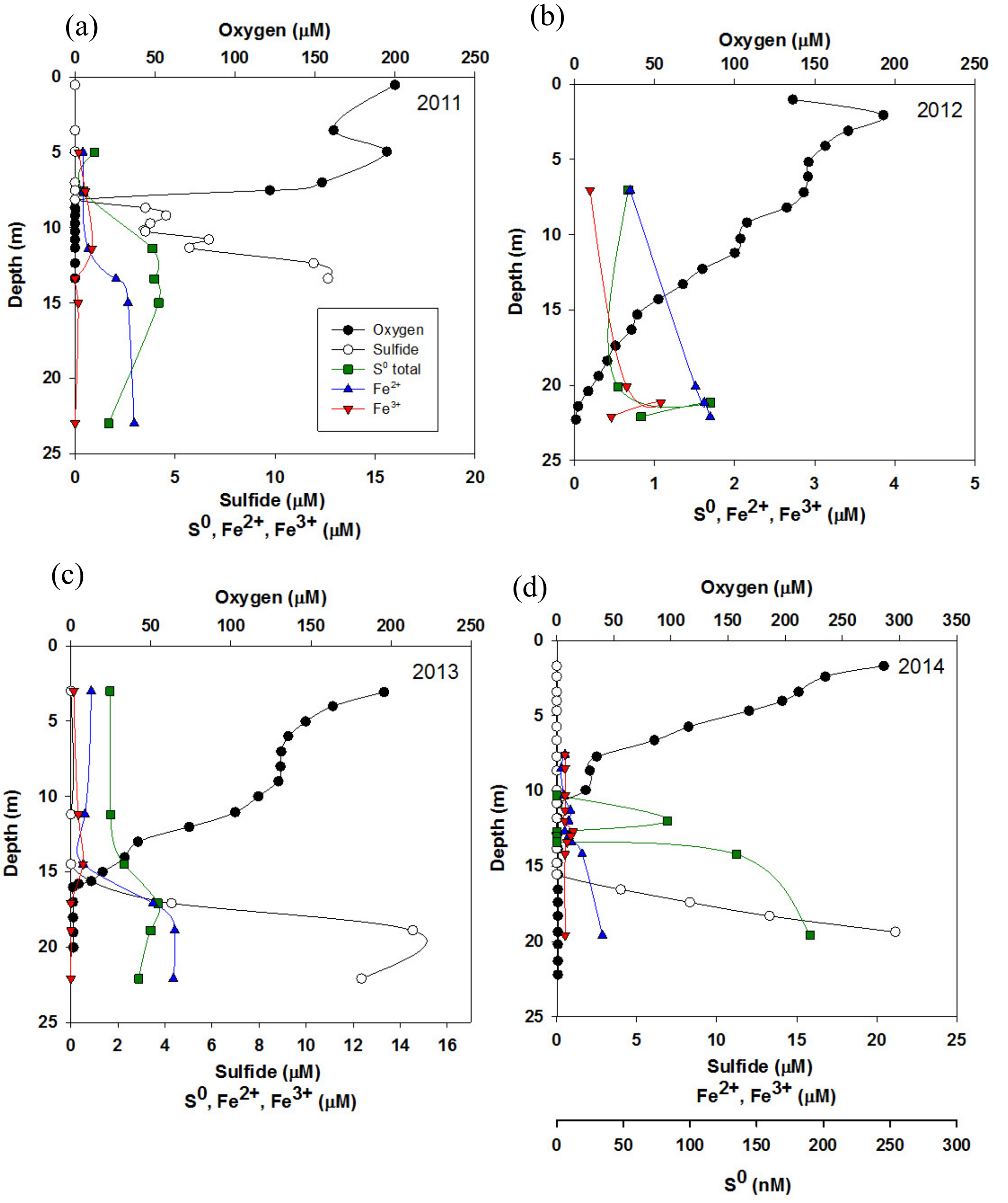

Figure 5.2 Representative profiles of key redox species (O_2, H_2S, total S^0, unfiltered Fe^{2+}, and unfiltered Fe^{3+}) and density for (a) 2011, (b) 2012, (c) 2013, and (d) 2014.

5.4.1.1 2011

Figure 5.2a depicts the redox structure of the water column in 2011. Due to high spring rainfall and warm temperatures, the water column was stratified with temperature and salinity gradients resulting in a pycnocline starting between 4-5 meters depth. Oxygen was depleted (< 3 μM) between 5-7 meters depth. Sulfide was present < 1 meter after the disappearance of oxygen, and often the oxygen and sulfide profiles overlapped. Sulfide concentrations increased with depth up to 100 μM. Elemental sulfur concentrations were up to 6 μM with peak concentrations at the chemical interface, and up to 90 % of elemental sulfur was < 0.2 μm at depth (Chapter 3). Unfiltered Fe^{3+} dominated in the oxygenated surface water, peaking in the suboxic zone at concentrations up to 1 μM, and maximum concentrations of Fe^{3+} coincided with those of S^0. In the deep water, unfiltered Fe^{2+} increased to concentrations up to 3.5 μM.

5.4.1.2 2012

In 2012, due to a dry spring, a pycnocline was not present, and as a result the water column was chemically more homogeneous than in 2011 (Figure 5.2b). Oxygen penetrated into the deep waters (≥ 22 m) and free sulfide was not detected in the water column. Trace amounts of FeS were measured in samples taken from suboxic waters above the sediment-water interface, so some sulfide may have been diffusing from the sediments. Despite the lack of detectable free sulfide, elemental sulfur was observed in the water column at concentrations up to 1.7 μM, comparable to those observed in the oxic part of the water column in 2011 (Chapter 3). S^0 was mainly in the > 0.2 µm fraction. Unfiltered Fe^{3+} concentrations were up to 1.5 µM at the top of the suboxic zone (22 m). Unfiltered Fe^{2+} concentrations up to 2 µM were located in the suboxic zone above the sediment-water interface.

5.4.1.3 2013

Figure 5.2c shows the redox structure of the water column in 2013. A pycnocline was present in the water column, although located deeper than in 2011. The redox conditions changed throughout the four days of the study as the depth of oxygen penetration decreased from 16-17 m to 13 m on the final day. Along with the decrease in oxygen penetration depth, sulfide concentrations in the bottom waters increased from 15 µM up to 40 µM over the four days of sampling and sulfide was detected higher in the water column. Throughout the cruise, maximum concentrations of S^0 (≤ 8 µM) were located at the base of the suboxic zone. A shift in elemental sulfur particle size occurred from the beginning to the end of the cruise, with elemental sulfur in the < 0.2 µm size fraction dominating in the beginning and in the > 0.2 µm size fraction dominating by the end of the cruise. Unfiltered Fe^{3+} concentrations were up to 0.65 µM, with peak concentrations at the top of the suboxic zone, directly above peak S^0 concentrations. Unfiltered Fe^{2+} concentrations increased up to approximately 5 µM with depth.

5.4.1.4 2014

A pycnocline was present between 10 – 12 meters depth in 2014 (Figure 5.2d). Oxygen was depleted by 8-10 m, and a large suboxic zone up to 3.5 m thick was present. Sulfide was detected between 12 – 13 m, and increased with depth to concentrations up to 75 μM. Despite the high sulfide concentrations, elemental sulfur was not as prevalent in 2014 as in previous years. S^0 was detected in only 4 of 26 samples at concentrations up to 0.19 μM, an order of magnitude lower than concentrations observed in previous years. Figure 5.2d shows the only water column profile obtained of elemental sulfur. Elemental sulfur in the > 0.2 μm fraction was present at 12 meters, and in the < 0.2 μm fraction at 14.2 and 19.6 m, and was not detected in the samples taken at 12.7 m, 13.0 m, and 13.4 m. In addition to this profile, one other measurement of 0.04 μM S^0 (< 0.2 μm) was made in the deep waters (22.2 m) in a separate profile. Polysulfides were detected *in situ* in 2014 at 15 m depth, 1-2 meters below the appearance of sulfide. It is thus possible that the elemental sulfur measured in the deep waters was from S^0 in polysulfides, which would degrade upon acidification of the samples (Kamyshny et al., 2004). Polysulfides are indicative of microbial sulfide oxidation as they were also observed in incubation experiments that year (Chapter 4) and are a known product of microbial sulfur metabolism (Frigaard and Dahl, 2008). Iron concentrations in 2014 were comparable to those measured in 2011 and 2013 with unfiltered Fe^{3+} concentrations up to 1 μM at the interface, and unfiltered Fe^{2+} up to 4 μM at depth.

5.4.2 Modeling Results

5.4.2.1 Model Calibration

The model developed in section 5.3 was applied to the datasets outlined above (section 4.1) in order to further explore the dynamics of redox cycling in the Bay. Prior to this application, the model was used to predict the salinity profiles from each year in order to ensure that the calculations for diffusion and the density structure of the water column were correct. Salinity profiles were used as a proxy for density because the halocline is the predominate factor controlling the density structure in the Bay. The diffusion coefficient was varied with depth, and surface and bottom boundary salinity concentrations were set and allowed to diffuse throughout the water column to steady state. The resulting modeled profiles correctly predict the observed salinity profiles, and it is over this physical structure that the model simulations for each year's dataset were run. Figure 5.3 compares the modeled salinity profile to the salinity profile obtained from the CTD for each year of the study (2011-2014), and gives the diffusion coefficient used at each depth (minimum values are on the order of 10^{-5} cm^2s^{-1}). Salinity profiles from both the beginning and end of the 2013 cruise are shown in order to model the shift in redox conditions described in section 5.4.1.3. The profiles shown in Figure 5.3 are important because this physical structure of the water column is what drives the chemical stratification and the distribution of biogeochemical processes.

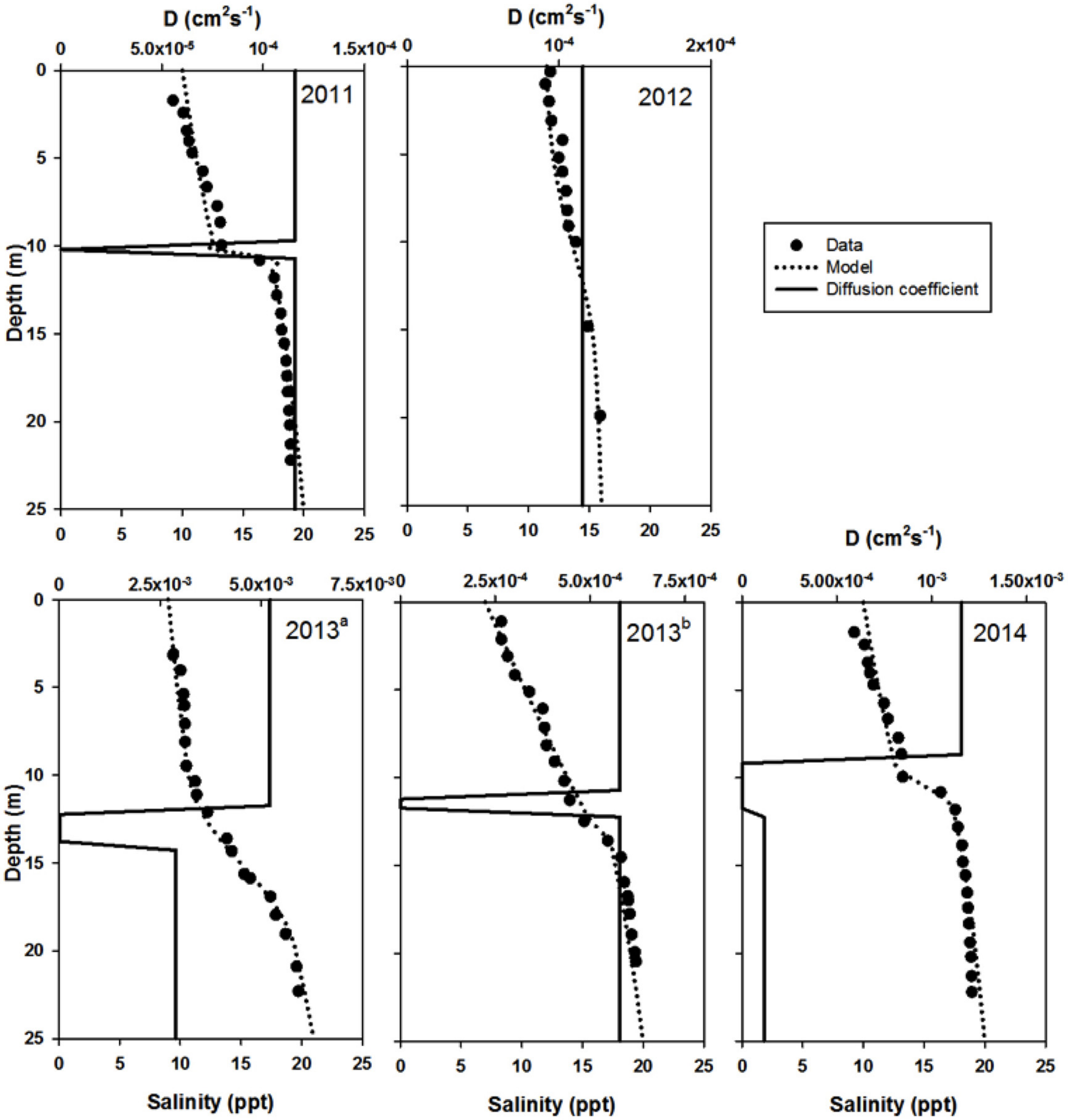

Figure 5.3 Calibration to salinity (2011-2014). Minimum values for D are on the order of 10^{-5} cm^2s^{-1}

5.4.2.2 Application to Chesapeake Bay Dataset

Table 5.4 provides a summary of the parameters used for each model simulation. Representative datasets from 2011, 2012, and 2014 were used for the calibration and compared to model output. Due to the shift in redox conditions observed over the four days of the 2013 cruise, profiles from the first (2013[a]) and final (2013[b]) days were modeled separately for that year in order to allow investigation into the effect of this shift on sulfide oxidation and the activity of PSOB. For all model simulations, boundary concentrations of H_2S, Fe^{2+}, and Mn^{2+} were changed based on linear extrapolation of the observed profiles, and the extinction coefficient for light (equation 16) was calculated from PAR profiles for each year (MacDonald et al, in prep). The incident light intensity (I_i) was held constant for all years and was determined from an average of measured light intensities at high noon. All kinetic parameters outlined in Table 5.2 were held constant.

Table 5.4 Parameters used for each model simulation. The concentration of H_2S, Fe^{2+}, and Mn^{2+} corresponds to the bottom boundary condition for those species.

	[H_2S] (µM)	**[Fe^{2+}] (µM)**	**[Mn^{2+}] (µM)**	**k_{ext} (m^{-1})**	**W (md^{-1})**	**I_i (µEi)**
2011	80	4	10	1.01	2	1500
2012	1	3	5	0.93	2	1500
2013[a]	30	6	17	1.05	2	1500
2013[b]	45	5	10	1.05	2	1500
2014	80	5.5	10	1.17	2	1500

[a] Beginning of the cruise (data from 10 August 2013)
[b] End of the cruise (data from 13 August 2013)

The results of the model simulations outlined above are shown in Figures 5.4 – 5.8 for all species in Table 5.1 during each year. In the following section, first the accuracy of the modeled profile fit to each redox species will be assessed for each simulation. This will be followed by a discussion of (1) quantification of sulfide oxidation processes for each model simulation, including the impact of PSOB, (2) investigation into the dynamics of phototrophic sulfide oxidation, and (3) the distribution of sulfide oxidation processes in the water column of the Chesapeake Bay. The Mn^{2+} data in Figures 5.4 – 5.8 were generously provided by Andrew Madison, Shannon Owings, and Veronique Oldham; and MnO_2 data were provided by Drs. Bradley Tebo and Matthew Jones.

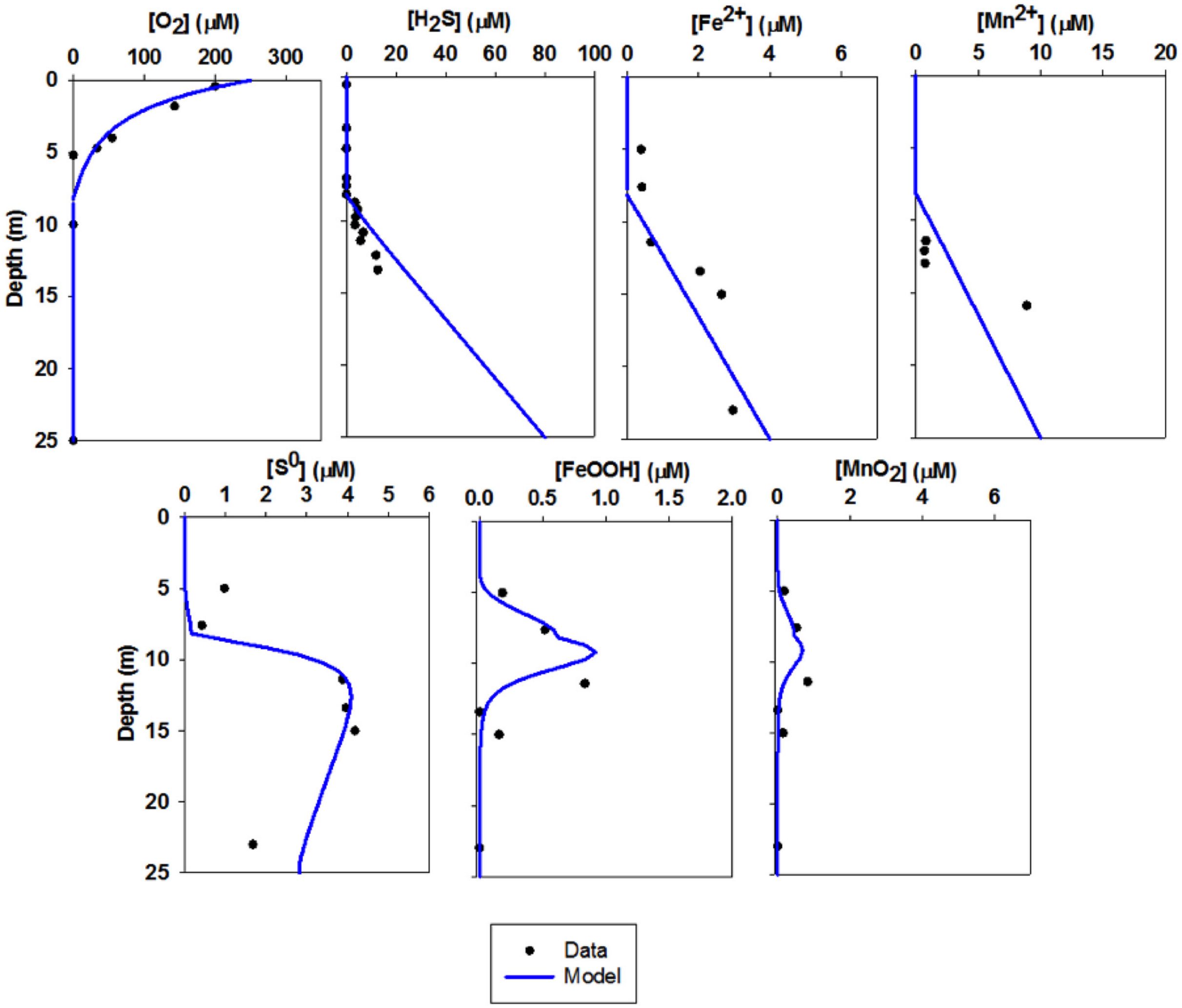

Figure 5.4 Comparison of modeled and measured values in 2011.

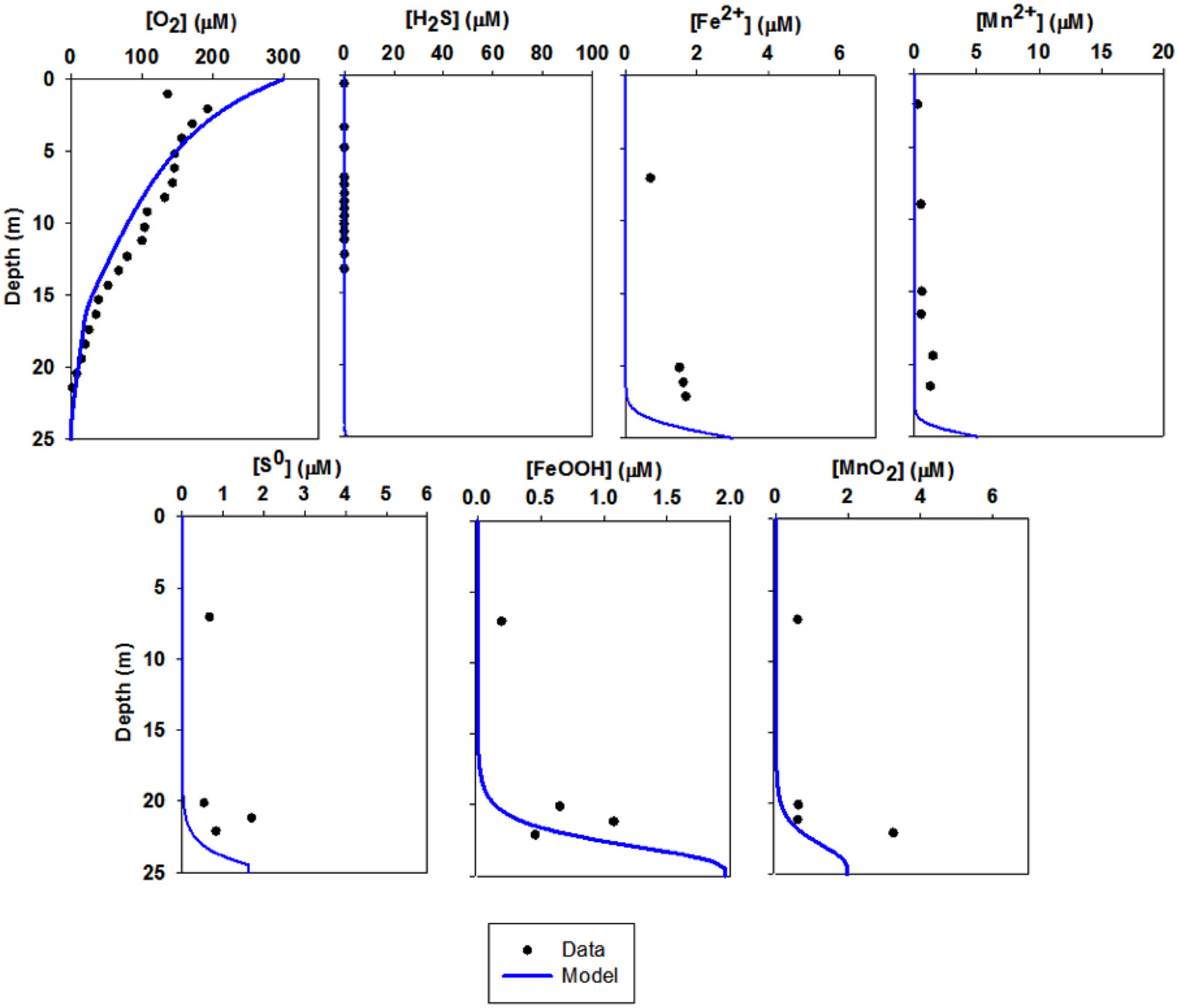

Figure 5.5 Comparison of modeled and measured values for 2012.

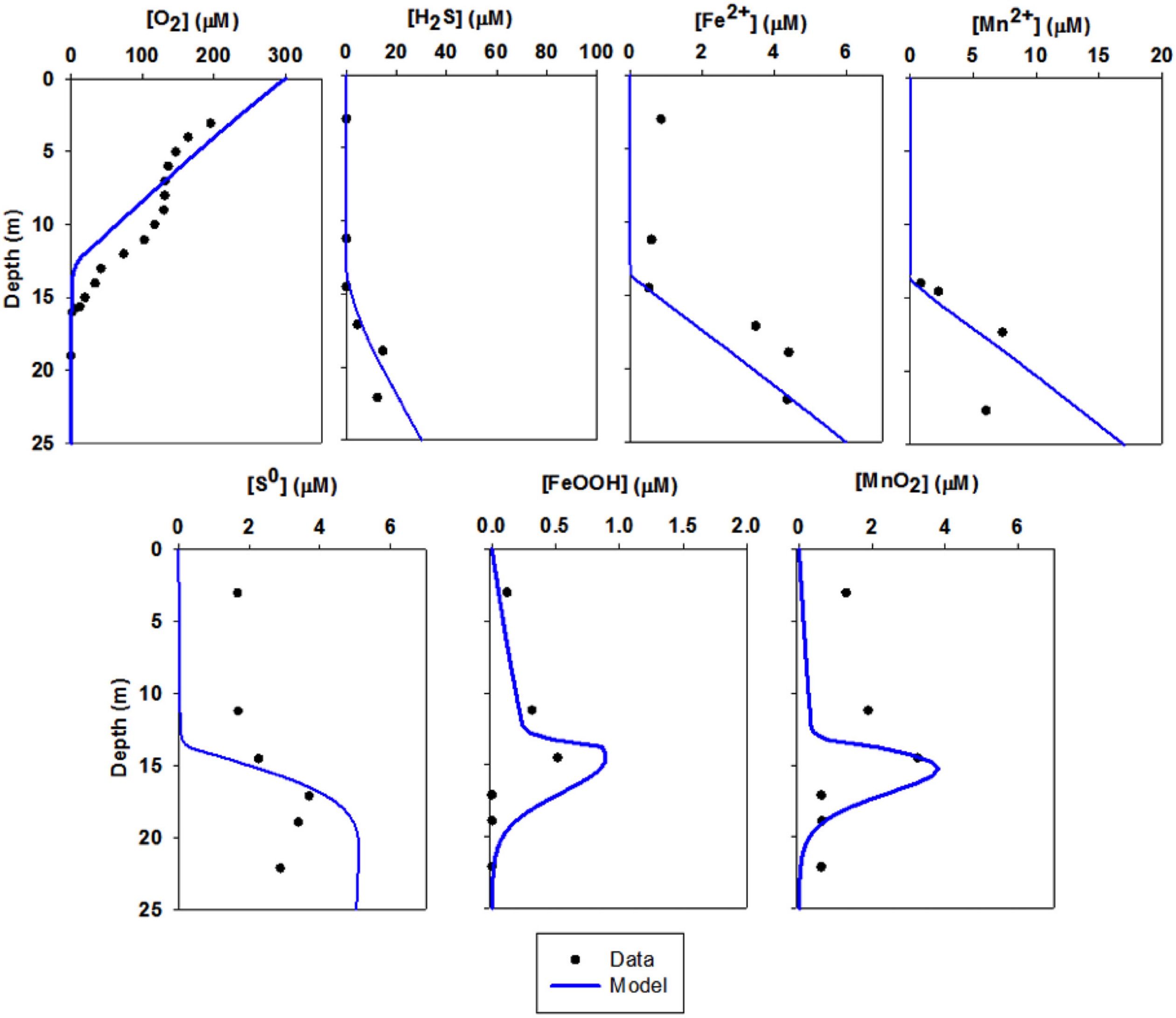

Figure 5.6 Comparison of modeled and measured values for the first day of the 2013 cruise.

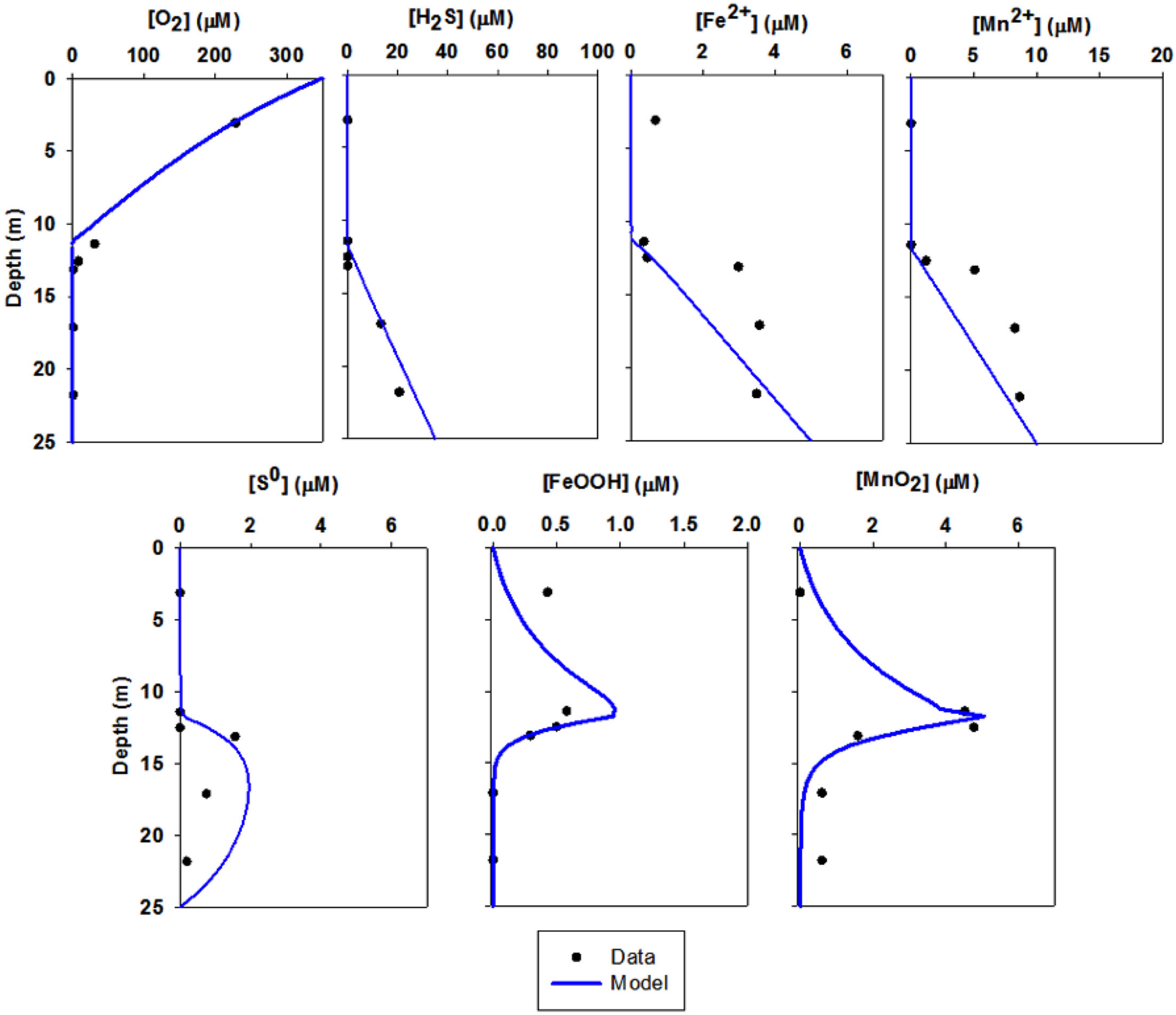

Figure 6.7 Comparison of modeled and measured values during the end of the 2013 cruise.

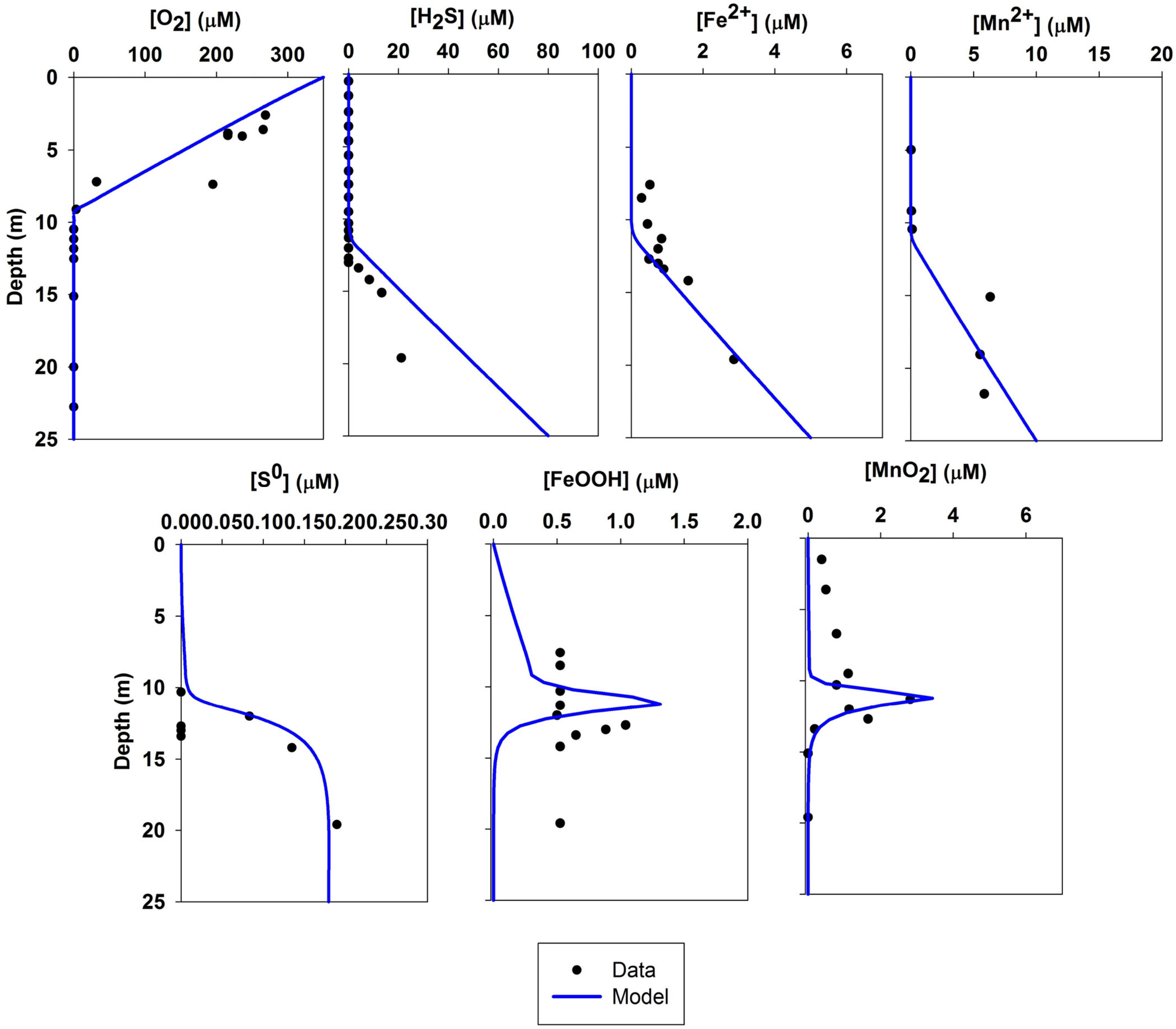

Figure 5.8 Comparison of modeled and measured values in 2014. Please note the change in scale for S^0 from Figures 5.4 – 5.7. S^0 concentrations were approximately an order of magnitude lower in 2014 than in the previous years.

5.4.2.2.1 Oxygen

The model does a good job predicting the depth of oxygen penetration for each of the four years, although it underestimates oxygen penetration in 2013[a] by one meter. Correct oxygen profiles were critical for the distribution of other species. In all simulations, the majority (> 90 %) of oxygen consumption in the oxic layer is by organic matter decomposition (Table 5.5), consistent with prior descriptions of Chesapeake Bay anoxia (Taft et al., 1980).

Table 5.5 Depth-integrated consumption of oxygen for the entire water column

	2011	**2012**	**2013[a]**	**2013[b]**	**2014**
O_2 reactions			% of total		
decomposition	99.7	96	93	99	99.7
respiration	0.28	0.24	0.16	0.26	0.25
sulfide	0.01	0	0.29	0.03	0.02
iron	0.01	1.5	0.86	0.08	0.00
manganese	0.04	2.2	5.5	0.18	0.01

[a] For the beginning of the cruise (data from 10 August 2013)
[b] For the end of the cruise (data from 13 August 2013)

It should be noted that although the modeled oxygen profiles fit the data well, the model provides an oversimplified view because it predominately considers the dynamics of biological processes. In reality, physical as well as biological processes are important in regulating oxygen concentrations in the Chesapeake Bay. During ebb and flood tides, the top and bottom layers of the estuary are moving with respect to each other, creating turbulence at the boundary and mixing oxygen into the anoxic layer. Advection of oxygen at depth is important in the Chesapeake, contributing approximately 50 % of the total O_2 input (Kemp, 1980). This is similar to the Black Sea, where horizontal inflow at depth of oxygen from the Bosporus Plume is essential for the oxygen balance (Konavolov and Murray, 2001). Finally, both wind speed and direction strongly influence the oxygenation of the water column and the depth of the oxic/anoxic interface (Scully, 2010).

O_2 consumption in the suboxic zone. Figure 5.9 depicts the impact of equations 1, 3, 4, 6 and 10 on oxygen depletion in suboxic waters ($[O_2] < 3$ μM). In this part of the water column, Mn^{2+} oxidation is a significant cause of oxygen depletion, accounting for 29 % of suboxic O_2 consumption in 2011, dominating suboxic O_2 consumption in 2012 (58 %) and 2013 (74 % and 54%), and accounting for nearly a quarter (23 %) of suboxic O_2 loss in 2014. This result is consistent with the results of modeling experiments of the Black Sea suboxic zone that found manganese oxidation vital in order to recreate the proper extent of the suboxic layer (Oguz et al., 2001). Oxidation of iron accounts for up to 40 % of oxygen consumption. Sulfide oxidation represents less than 10 % of suboxic oxygen depletion in all simulations. Thus, sulfide does not directly represent a major sink for oxygen, consistent with the kinetics of sulfide oxidation by oxygen (Luther et al., 2011).

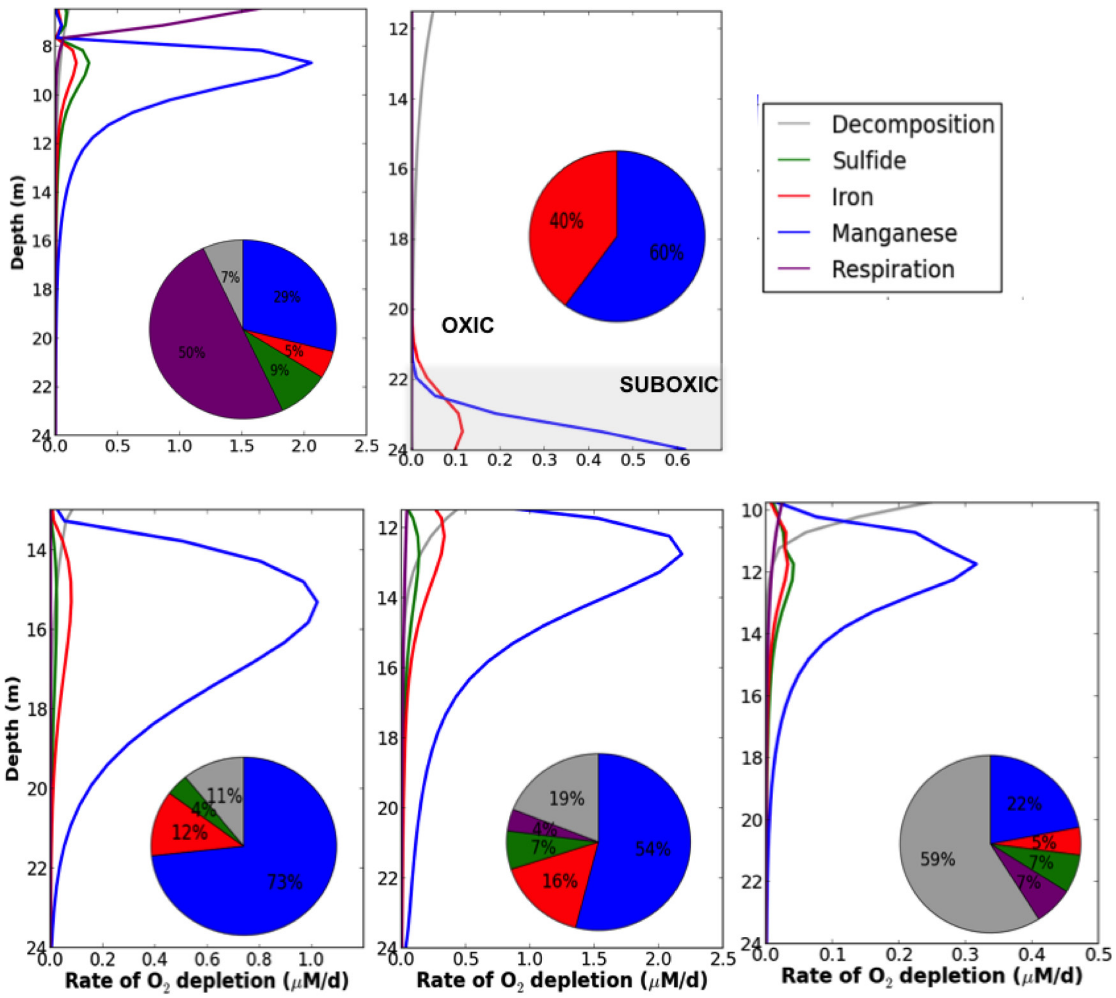

Figure 5.9 O_2 consumption in suboxic waters ($[O_2] < 3$ μM) (a) 2011, (b) 2012, (c) 2013^a, (d) 2013^b, and (e) 2014. Please note that for (b) 2012, the shaded area designates the suboxic zone $[O_2] < 3$ μM and the pie chart represents oxygen consumption processes in that zone.

5.4.2.2.2 Iron and Manganese

Fe^{2+} and Mn^{2+}. The model does a good job predicting the observed Fe^{2+} and Mn^{2+}profiles from the 2011 (Figure 5.4), 2013 (Figures 5.6 and 5.7), and the 2014 (Figure 5.8) datasets. In 2012, the model struggles to reproduce the Fe^{2+} and Mn^{2+} profiles, underestimating concentrations in the oxic portion of the water column (Figure 5.5). Furthermore, the model does not predict the low concentrations of reduced iron in the oxic zone that are observed in the 2011 or 2013[a] profiles. The presence of Fe^{2+} in the oxic layer could be due to (1) turbulent mixing between the top and bottom layers during tidal flow, (2) surface deposition of reduced iron, or (3) microbial activity. None of these processes is explicitly considered in the model, and so it cannot precisely predict the observed profiles.

FeOOH and MnO_2. In 2011, the modeled peak concentrations of both iron and manganese oxides were located one meter shallower than the observed peaks. For iron, this could be due to the activity of iron oxidizing bacteria in the suboxic zone, which would produce iron oxides at depths below peak abiotic production. For manganese, this could be due to the presence of significant quantities of Mn^{3+} in the water column of the Bay (Oldham et al., 2015), as the inclusion of Mn^{3+} in redox models has been demonstrated to be important in the accurate reproduction of manganese and iron profiles (Madison, 2012). In 2012, the modeled iron and manganese oxide peaks are again offset; however, in this case the model predicts peak concentrations occurring at depths 1 – 2 meters lower than those observed (Figure 5.5). There are two potential explanations for the offset in the modeled MnO_2 and

FeOOH profiles in the 2012 dataset. First, as mentioned previously, the model does not accurately predict the Fe^{2+} and Mn^{2+} profiles in 2012, which would result in a shift in the depth at which oxidation would occur. Second, it is likely that mixing along the sediment/water interface occurs due to tidal movement that could re-suspend settling particles, a process not included in the model. The model simulations for 2013^a and 2013^b (Figure 5.6 and 5.7), accurately predict the location of both the iron and manganese oxide peaks. In the model simulation for 2014, the modeled MnO_2 peak corresponds to the observed peak concentrations, although the model does not reproduce the MnO_2 concentrations in the oxic zone (Figure 5.8). This MnO_2 could be from a source not considered by the model, such as manganese released and oxidized during phytoplankton lysis (Madison, 2012) or from riverine input. The iron oxide peak in 2014 is again more shallow than the observed, similar to the 2011 simulation.

5.4.2.2.3 Sulfide and Elemental Sulfur

Sulfide. As demonstrated in Figure 5.4, the model fits the observed profile of sulfide well in 2011. In 2012, sulfide was not detected in the water column; however in suboxic bottom waters, the presence of S^0 and the detection of trace quantities of FeS in the suboxic waters above the sediment-water interface suggested that low concentrations of sulfide were likely fluxing from the sediments and oxidized rapidly, so a boundary condition of 1 μM sulfide was set for the 2012 simulation. The model correctly predicts the sulfide profiles for both datasets from 2013 (Figures 5.6 and 5.7). The modeled sulfide profile is slightly overestimated for 2014 (Figure 5.8).

Elemental sulfur. The model fit to the profiles of elemental sulfur in Figures 5.4 – 5.8 is quite good. In 2011 (Figure 5.4) the model accurately predicts the location of peak elemental sulfur concentrations. In 2012 (Figure 5.5), the model estimates the depth of peak sulfur concentrations two meters deeper than the observed peak. There are several possible explanations for this. First, the modeled profiles of oxidized iron and manganese are also deeper than the observed profiles, as previously mentioned. Both manganese and iron oxides oxidize sulfide; thus this would contribute to the offset in the sulfur profile. Second, observed elemental sulfur could be forming from a process not considered by the model, such as the oxidation of FeS. In 2013 (Figure 5.6 and 5.7) and 2014 (Figure 5.8), the model provides a good approximation of the elemental sulfur profile. The model does not predict the observed concentrations of elemental sulfur in the oxic zone in 2011, 2012, or 2013[a], probably because this S^0 likely forms from sulfide released during organic matter decomposition, which is then oxidized (Chapter 3); a processes that is not included in the model.

Effect of PSOB on S^0 profiles. The effect of PSOB on the profiles of sulfide and elemental sulfur was investigated by running the model simulation from 2011 with the parameter for sulfide oxidation by PSOB (R8) removed from the calculation in equation 19. The results of these calculations are shown in Figure 5.10 compared with the results of the original simulation that included PSOB. In the model simulation without sulfide oxidation by PSOB, the elemental sulfur peak occurs three meters shallower than and at concentrations approximately half those produced by the model simulation with PSOB. Sulfide diffuses two meters higher into the water column, indicating that anaerobic phototrophic sulfide oxidation may play a role in controlling the upward flux of sulfide to the oxic layer.

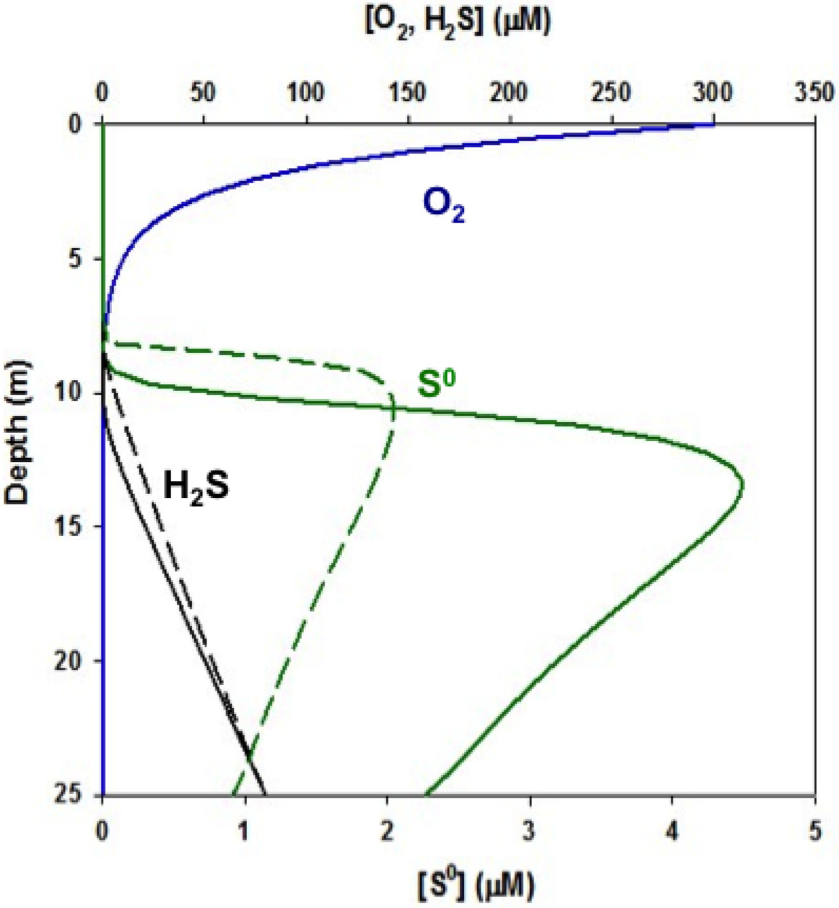

Figure 5.10 Comparison of model simulation with PSOB (solid lines) and model simulation run without PSOB (dashed lines).

Overall, the model is able to approximate profiles of key redox species from five datasets representing years with different physical and chemical conditions. In particular, the model accurately reproduces the observed profiles of elemental sulfur in the anoxic portion of the water column, indicating that sulfide oxidation, including that by PSOB is correctly calculated, and that the model can be used to investigate their impact on sulfide oxidation for each dataset.

5.4.2.3 Interannual Variation in Sulfide Oxidation Processes

The impacts of each sulfide oxidation process for the model simulations shown in Figures 5.4 – 5.8 are given in Table 5.5. In 2011, sulfide oxidation by phototrophic sulfide oxidizing bacteria was the dominant process (53 %), followed by abiotic oxidation by manganese oxides (37 %). In 2012, phototrophic sulfide oxidation did not occur because light was completely attenuated in the anoxic water above the sediments, and sulfide was oxidized primarily by manganese (87 %) and iron (12 %) oxides. In 2013, manganese was the dominant oxidant for sulfide both in the beginning (90 %) and end (59 %) of the cruise. PSOB did not contribute to sulfide oxidation in the beginning of the cruise as the interface was located too deep to receive sufficient light. However, as a result of the three-meter shoaling of the oxic/anoxic interface (from 16 m to 13 m depth, Figures 5.6 and 5.7) PSOB comprised 3 % of sulfide oxidation in the simulation of the end of the cruise, emphasizing the highly dynamic nature of both the redox structure of the water column and sulfide oxidation processes. In 2014, manganese oxides (51 %) were the dominant sulfide oxidation process, followed by oxygen (30 %) and PSOB accounted for 13 % of sulfide oxidation.

Table 5.6 The depth-integrated rate of sulfide oxidation and percentage of total consumption of sulfide by each process considered by the model.

	2011		**2012**		**2013**[a]		**2013**[b]		**2014**	
	μMd^{-1}	**% of total**	**μMd^{-1}**	**% of total**	**μMd^{-1}**	**% of total**	**μMd^{-1}**	**% of total**	**μMd^{-1}**	**% of total**
Sulfide oxidation by										
oxygen	1.0	6.1	1.4×10^{-3}	0.4	0.22	2.6	1.6	5.1	1.3	31
iron	0.61	3.7	4.6×10^{-2}	12	0.64	7.5	10	33	0.25	6.2
manganese	6.1	37	0.32	87	7.7	90	18	59	2.1	51
PSOB	8.8	53	0	0	0	0	0.85	2.8	0.52	13
Total	16.5		0.37		8.6		31		4.1	

[a] For the beginning of the cruise (data from 10 August 2013)
[b] For the end of the cruise (data from 13 August 2013)

The results summarized in Tables 5.5 and 5.6 indicate that the majority of oxygen and sulfide consumption does not occur via the direct oxidation of sulfide by oxygen. Although present in lower concentrations than oxygen, iron and manganese play an important role in facilitating sulfide oxidation in the Bay, and connect redox cycling between the oxic and anoxic layers of the water column through a catalytic cycle. In this cycle, reduced iron and manganese are oxidized by oxygen (equations 3 and 5), and in turn oxidize sulfide to regenerate the reduced metals (equations 4 and 6). In this manner oxidizing potential is transferred from the oxic layer to the suboxic and anoxic layer, and this process has been demonstrated to control the flux of sulfide in other stratified inland bay systems (Ma et al., 2006). In the Chesapeake Bay, Fe^{2+}

oxidation is likely both abiotic and biotic, as microaerophilic iron oxidizing bacteria have been enriched from the suboxic zone in the Chesapeake Bay (MacDonald et al., 2014). These bacteria would increase the rate of iron oxidation in the suboxic zone, where O_2 concentrations are low and the abiotic oxidation rate is slow, further fueling the catalytic cycle described above. Manganese oxidation by oxygen is completely biotic, and microbial manganese oxidation is crucial for the *in situ* generation of MnO_2, as abiotic manganese oxidation does not occur below pH 9 (Stumm and Morgan, 1996). Thus, iron and manganese oxidizing organisms provide a critical link between oxygen consumption and sulfide oxidation in the Bay.

Another important aspect of Table 5.6 is that the rates of sulfide oxidation per day calculated by the model vary between the years and are consistent with the observed concentrations of elemental sulfur. Concentration maxima of elemental sulfur correspond to the balance of production and consumption rates, and not to the concentration of sulfide (Zopfi et al., 2004). The highest concentrations of S^0 were observed in 2011 ($[S^0] \leq 6$ μM; $H_2S \leq 100$ μM) and 2013 ($[S^0] \leq 8$ μM; $H_2S \leq 35$ μM). Although it is unknown what the consumption rate for sulfur was in this system for any of the years, the sulfide oxidation rates calculated for the 2011 and 2013^b simulations were higher than in the other years. In contrast, the sulfide oxidation rate calculated by the model for 2014 was lower than in 2011 and 2013, corresponding to lower observed sulfur concentrations (Figure 5.2d). As the kinetic parameters did not change between years (Table 5.2), variation in these rates is due to differences in the density structure of the water column between years (Figure 5.3) that affect diffusion of oxidants and reductants across the pycnocline. Diffusion across this interface will be slower across a sharper pycnocline as observed in 2014 than across a more gradual pycnocline, as in 2013 (Figure 5.2 and Figure 5.3).

In addition to changes in the production rate, another explanation for the low concentrations of elemental sulfur in 2014 may be high consumption rates. For example, sulfur-reducing bacteria may live within a bloom of PSOB (Overmann, 1997). Other microbes also utilize elemental sulfur, such as the facultative anaerobe *S. putrifaciens,* which is capable of extremely fast sulfur metabolism and comprises up to 80% of total culturable bacteria in similar stratified environments (Moser and Nealson, 1996). Sampling in 2014 occurred later in the summer than in previous years, when the water column had been sulfidic for a longer period of time. A shift in microbial community composition has been documented throughout the seasonal oxic-anoxic-oxic transition (Crump et al., 2007), and so microbial populations metabolizing sulfide oxidation intermediates such as S_8 may be more important later in the stratification period, when they have had time to respond to changing water column chemistry. The model cannot currently be used to investigate these processes due to a lack of information about processes and rates of S_8 consumption; however this would be a good addition to the model as more information becomes available.

5.4.3 Model Experiments Exploring the Dynamics of PSOB

In order to further investigate the dynamics of phototrophic sulfide oxidation in the Chesapeake Bay, several modeling experiments were conducted in which key parameters governing kinetics and light intensity were changed. All of these experiments used the model parameters from the 2011 simulation (Figure 5.3a, Table 5.4) because the contribution of phototrophic sulfide oxidation was the highest in that year (Table 5.5). These experiments are discussed below, and the results are presented in Table 5.7, and Figures 5.11 – 5.12.

5.4.3.1 Uncertainty in Kinetic Parameters for Phototrophic Sulfide Oxidation

A sensitivity analysis was conducted in order to determine the effect of uncertainty in the kinetic parameters for PSOB on the model output. The value of the half saturation constant (K_s in equation 15) is 14 ± 3.6 μM, and the saturating light intensity (I_{sat} in equation 14) is 2.8 ± 0.52 μEi. Model simulations using the parameters from the 2011 dataset (Table 5.4; Table 5.7) were run with K_s and I_{sat} ± one standard deviation. A low estimate of phototrophic sulfide oxidation was obtained using a saturating light intensity of 2.28 μEi and a K_s of 17.6 μM (K_s is a measure of the affinity of the enzyme for the substrate and a higher K_s indicates lower affinity). In this scenario, PSOB account for 46 % of sulfide oxidation at a rate of 6.9 μMd^{-1}. Similarly, using a saturating light intensity of 3.32 μEi and a K_s of 10.4 μM, a high estimate was obtained in which PSOB account for 63 % of sulfide oxidation at a rate of 13 μMd^{-1}. These results are compared with the original simulation in Table 5.7. The near doubling in the sulfide oxidation rate between the minimum and maximum rate estimates demonstrates the importance of constraining these parameters with experimental data.

5.4.3.2 Sensitivity of Phototrophic Sulfide Oxidation to Changes in Light

The effect of variation in the light intensity on phototrophic sulfide oxidation was investigated in three specific ways. First, using the parameters for the 2011 model simulation, the depth of the pycnocline was deepened. This allowed oxygen to penetrate deeper into the water column in order to explore how changes in the depth of the oxic/anoxic interface (as well as light intensity reaching the sulfidic zone) would affect the activity of PSOB. The results are summarized in Table 5.7. Shifting the interface one meter deeper in the water column caused a 25 % reduction in the original rate of sulfide oxidation by PSOB. Deepening the interface by two meters resulted in a 40 % reduction in sulfide oxidation by PSOB. This experiment imitates the consequences of the short-term changes in in the depth of the oxic/anoxic interface such as those observed over four days during the 2013 cruise, as well those expected over hours, with wind or tidal variation (Lewis et al., 2007).

Table 5.7 Summary of model experiments varying kinetic parameters for PSOB and the depth of the pycnocline.

Experiment	$[H_2S]$ (μM)	k_{ext}	I_i (μEi)	Pycnocline depth	Isat (μEi)	Ks (μM)	H_2S oxidation rate (μMd^{-1})
Original simulation (2011)	80	1.01	1500	10 m	2.8	14	8.8
Sensitivity analysis - high estimate	80	1.01	1500	10 m	3.32	10.4	13
Sensitivity analysis -low estimate	80	1.01	1500	10 m	2.28	17.6	6.9
Interface - 1 m deeper	80	1.01	1500	11 m	2.8	14	6.6
Interface - 2 m deeper	80	1.01	1500	12 m	2.8	14	5.28

Two other experiments were conducted in order to further investigate the effect of changes in the light profile on PSOB. As phototrophic sulfide oxidation depends upon both light and sulfide, model simulations were run in which sulfide was held constant (20 μM) throughout the water column in order to isolate the effect of the small variation in the light profiles from each year (k_{ext} in Table 5.3) on sulfide oxidation. Figure 5.11a shows the calculated light profiles for each of the four years in units of logPAR. Slight variation of the light profiles resulted in changes up to a meter in the depth of maximum phototrophic sulfide oxidation (Figure 5.11b), reflecting the sensitivity of phototrophic sulfide oxidation to small variations in light intensity that was observed experimentally in Chapter 4.

.

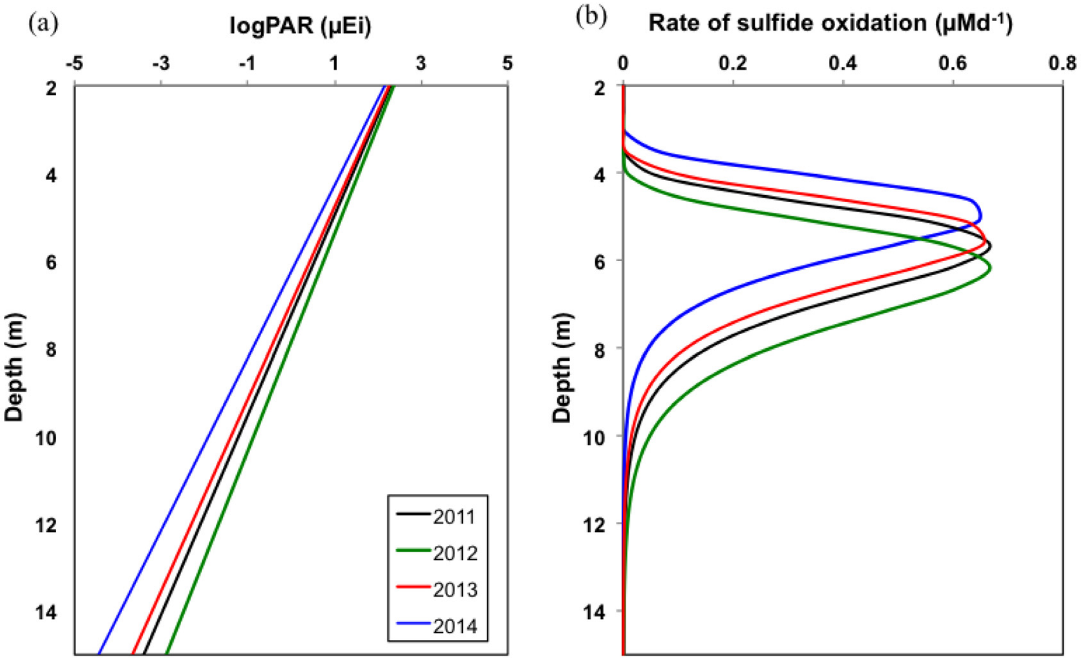

Figure 5.11 Effect of (a) small variations in the light profiles from each year due to changes in the extinction coefficient on (b) the peak location in the water column of phototrophic sulfide oxidation when sulfide is held constant throughout the water column. Please note the depth scale is truncated in order to show detail.

Finally, the incident surface light (I_i in equation 15) was varied from 0 – 2000 μEi in order to assess the effect of diel light variation on PSOB. All other parameters were used from the 2011 model simulation. The results of the experiment, shown in Figure 5.12, display a linear dependence of phototrophic sulfide oxidation upon surface light intensity because the light intensity at the interface only reaches a maximum of 0.2 μEi at 2000 μEi surface light intensity, well below the saturating light intensity for PSOB in the Chesapeake Bay. Figure 5.12 indicates that the sulfide oxidation rate at the oxic/anoxic interface will change significantly throughout the day due to fluctuations in phototrophic sulfide oxidation activity.

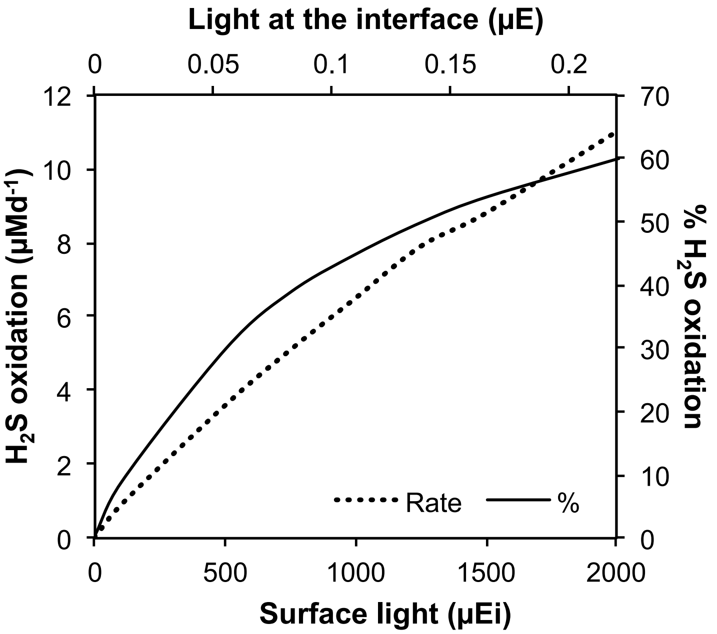

Figure 5.12 Effect of changing the surface light intensity on phototrophic sulfide oxidation at the interface.

The results of the experiments detailed above (Table 5.7, Figure 5.11 – 5.12) highlight the effect that changes in light due to diel cycles and short-term tidal or wind-driven variations in the depth of the suboxic zone will have on sulfide oxidation in the water column due to the impact on PSOB. Furthermore, these results demonstrate that PSOB will play the most significant role in years in which oxygen is depleted quickly, and the oxic/suboxic/anoxic interface is shallow. These conditions occur in years in which a large area of the water column is suboxic to anoxic and the health of the Bay is particularly poor (Boesch et al., 1991; MD DNR reports 2011-2014), so the activity of PSOB has implications for the consideration of oxygen and sulfide dynamics for management strategies in these years.

5.4.4 Effect of Water Column Redox Variability on the Distribution of Sulfide Oxidation Processes

The preceding discussion highlights the effect of the interannual and short-term variability in the physical and chemical characteristics of the water column in the Chesapeake Bay on sulfide oxidation processes during four separate years. Thus far, the results have been presented chronologically in order to investigate important differences between years; however the redox scenarios exemplified by the datasets in Figure 5.2 - 5.8 also depict the progression from a more oxic to a more sulfidic water column as the degree of stratification increases. Figure 5.13 shows the distribution of sulfide oxidation processes for each model simulation arranged by the shallowing of the oxic/anoxic interface. The depth at which the light intensity is 0.1 µEi is indicated as it is the lowest light intensity at which measurements of phototrophic sulfide oxidation have been made in field and lab experiments from the Chesapeake Bay (Chapter 4). In this arrangement, 2012 represents an extreme example in which the water column is mostly oxic and the oxic/anoxic interface is deep, whereas 2011 represents the opposite extreme in which the water column is primarily sulfidic and the interface is shallow. PSOB are controlled by the opposing gradients of light and sulfide, and Figure 5.13 illustrates the response of PSOB to a progression of increased stratification, with the interface moving toward the photic zone. As the oxic/anoxic interface shoals and receives more light, the contribution of sulfide oxidizing bacteria to total sulfide oxidation increases (Figure 5.13, Table 5.6). Furthermore, the progression in Figure 5.13 not only emphasizes the degree of physical and chemical variability experienced by the Bay between years, but also mirrors the transition that will happen as stratification sets up and degrades each year.

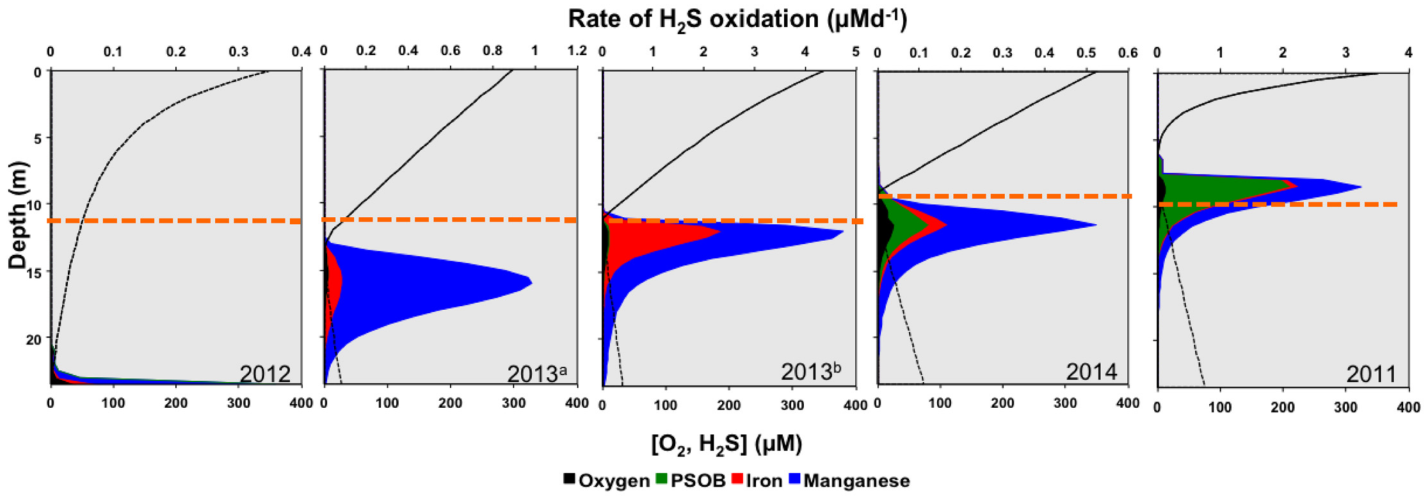

Figure 5.13 Distribution and rate of sulfide oxidation processes and oxygen as the interface moves up in the water column. The orange dashed line signifies the depth at which light intensity is 0.1 μEi. Note that different processes dominate sulfide oxidation at different depths (see text for further discussion).

Another important feature of Figure 5.13 is that it demonstrates that although a specific sulfide oxidation process might dominate overall (Table 5.5), different processes are important at different depths. For example, in 2011, although phototrophic sulfide oxidation is the dominant process, manganese oxides dominate sulfide oxidation deeper in the water column, where the rate of phototrophic sulfide oxidation decreases due to light limitation. In 2012 and 2013^{a} manganese oxides dominate sulfide oxidation at all depths; however, in 2013^{b}, iron oxides dominate sulfide oxidation around 10 m, then oxidized manganese quickly takes over. In 2014, although phototrophic sulfide oxidation accounts for only 13 % of sulfide oxidation overall, it dominates at the surface of the sulfide oxidizing layer, followed by manganese oxides at depth (solid phases form, then settle into the anoxic zone). This zonation of sulfide oxidation processes is significant because it could act as a net, with each successive zone oxidizing the sulfide that is beyond the oxidation capacity of the zone below it. This also demonstrated the important of considering multiple sulfide oxidation pathways, because although they are interconnected, each of these processes will react differently to changes in the physics and chemistry of the water column.

A final consideration is that the transition depicted in Figure 5.13 has implications not only for the Chesapeake Bay and similar systems, but may also be applied conceptually to the chemical evolution of ancient to modern oceans. Approximately 1800 million years ago, the oxygenation of the atmosphere and subsequent increases in continental weathering led to increased seawater sulfate concentrations (Poulton et al., 2004). The higher sulfate concentrations resulted in increased sulfate reduction and sulfide production, and ocean chemistry transitioned from anoxic and iron rich to anoxic and sulfur rich. Between 1800 and 700 million years ago, oxygenic photosynthesis became more prevalent and the surface layer of the ocean became oxic, resulting in a chemically stratified ocean with an oxic surface and anoxic, sulfidic deep layer (Canfield, 1998). The depth of the oxic/anoxic interface would have retreated deeper into the water column as more oxygen dissolved into the surface layer. The Chesapeake Bay can be considered an analogue of the ancient ocean during the later period of this transition (Hanson et al., 2013), and Figure 5.13 illustrates the potential changes in the distribution and relative importance of biological phototrophic and chemical sulfide oxidation as ocean chemistry progressed towards the fully oxic oceans of the modern day.

5.5 Conclusions

The redox chemistry of the stratified Chesapeake Bay water column was characterized in the field during four summers from 2011 - 2014. A one-dimensional diffusion-reaction redox model was developed and applied to these data in order to investigate the processes responsible for the distribution of key redox species (O_2, ΣH_2S, S^0, Fe^{2+}, Mn^{2+}, FeOOH, MnO_2) and the oxidation of sulfide. Chemical pathways for sulfide oxidation by oxygen, iron oxides, and manganese oxides were considered. The model also incorporates the oxidation of sulfide to elemental sulfur by PSOB, which was parameterized by adapting models of phytoplankton growth to phototrophic sulfide oxidation using the results of kinetic studies detailed in Chapter 4.

The model is able to accurately reproduce profiles of the previously mentioned redox species from five datasets representative of different physical and chemical conditions in the Chesapeake Bay.

The calculated contribution of PSOB to sulfide oxidation was found to be variable between model simulations. In 2011, PSOB accounted for 53% of sulfide oxidation. In 2012, PSOB did not contribute to sulfide oxidation, as the anoxic waters were only present at the sediment/water interface, well below the photic zone. In 2013, the oxic/anoxic interface was located deep in the water column; however, a shoaling of the interface observed over four days led to an increase in the contribution of phototrophic sulfide oxidation from 0 to 2.8 %. In 2014, the oxic/anoxic interface was higher in the water column and PSOB accounted for 13 % of sulfide oxidation. Further modeling experiments that changed the location of the pycnocline within the water column led to significant changes in the sulfide oxidation rate by PSOB (25 % decrease for a one meter deepening of the interface and a 40 % decrease for a two meter deepening). Variation in the light profile between 2011 – 2014 resulted in fluctuations of up to a meter in the ideal depth of phototrophic sulfide oxidation. Investigation of the distribution of sulfide oxidation processes revealed that different processes dominated at different depths, creating zones of sulfide oxidation that could act as a net for sulfide flux to the oxic layer.

These results are the first inclusion of PSOB activity into redox models, and quantitatively illustrate the important, but highly variable effect that PSOB have on redox conditions in the environment. Furthermore, the datasets and model simulations for each year provide examples for the evolution of the Chesapeake Bay water column from more oxic to more sulfidic. Taken in reverse, this progression provides insights into potential changes in sulfide oxidation that occurred during the transition in ocean chemistry from the anoxic/sulfidic ancient oceans to the oxic modern oceans.

REFERENCES

Boesch D.F., Brinsfield R.B, and Magnien R.E. (1991) Chesapeake Bay eutrophication: scientific understanding, ecosystem restoration, and challenges for agriculture. *J Environ Qual.* **30**, 303-320.

Boudreau B.P., Mucci A., Sundby B., Luther II G.W., and Silverberg N. (1998) Comparative diagenesis at three sites on the Canadian continental margin. *J Mar Res* **56**, 1259-1284.

Canfield D.E., Habicht K.S., Thamdrup B. (2000) The Archean sulfur cycle and the early history of atmospheric oxygen. *Science* **288**, 658–661.

Canfield D.E., Thamdrup B., Kristensen E. (2005) Aquatic Microbiology, In Southward AJ, Tyler PA, Young CM, Fuiman LA (ed). Advances in Marine Biology, 48, Elsevier Acad Press, Amsterdam – Tokio, 640.

Cerco C.F. and Cole T. (1993) Three-dimensional eutrophication model of Chesapeake Bay. *J Environ Engin.* **119**, 1006 – 1025.

Chan L.K., Morgan-Kiss R., Hanson T.E. (2008). Sulfur oxidation in *Chlorobium tepidum*: genetic and proteomic analyses. In Microbial sulfur metabolism ed Christiane Dahl, Cornelius Friedrich Springer press Heidelberg, Germany.

Chapra S. (1997) Surface water-quality modeling. Waveland Press, Inc. Long Grove IL, USA.

Chesapeake Bay Foundation – State of the Bay 2014 Saving a National Treasure - Chesapeake Bay Foundation. (n.d.). Retrieved January 19, 2015, from http://www.cbf.org

Crump B. C., Peranteau C., Beckingham B. and Cornwell J.C. (2007) Respiratory succession and community succession of bacterioplankton in seasonally anoxic estuarine waters. Appl Environ Microbiol. **73**, 6802-6810.

De Levie, R. (2004) *Advanced Excel for scientific data analysis*; Oxford University Press: New York.

Diaz R.J. (2001). Overview of Hypoxia around the World. *J Environ Qual*. **30**, 275–281.

Di Toro D.M., O'Connor D.I., and Thomann R.V. (1971) A Dynamic model of the phytoplankton populations in the Sacramento – San Joaquin Delta. *Advance Chem.* **106**, 131 – 180.

Di Toro D.M. and Fitzpatrick J.J. (1993) Chesapeake Bay sediment flux model. U.S. Army Corps of Engineers, Waterways Experiment Station, Tech. Report EL-93-2.

Di Toro D.M. (2000) Sediment Flux Modeling. John Wiley and Sons, NY, NY, USA.

Findlay A.J., Gartman A., MacDonald D., Hanson T.E., Shaw T., Luther III G.W. (2014) Distribution and size fractionation of elemental sulfur in aqueous environments: The Chesapeake Bay and Mid-Atlantic Ridge. *Geochim Cosmochim Acta* **142**, 334-348.

Frigaard N.U. and Dahl C. (2008). Sulfur Metabolism in Phototrophic Sulfur Bacteria. *Adv Microb Physiol.* **54**,103-200.

Froelich, P., Klinkhammer, G. & Bender, M. (1979) Early oxidation of organic matterin pelagic sediments of the eastern equatorial Atlantic: suboxic diagenesis. *Geochim Cosmochim Acta* **43**, 1075-1090.

Glazer B.T., Luther, G.W III., Konavlov S.K., Friederich G.E., Nuzzio D.B., Trouwborst R.E., Tebo B.M., Clement B., Murray K., Romanov A.S. (2006) Documenting the suboxic zone of the Black Sea via high-resolution real-time redox profiling. Deep Sea Res. **53**,1740-1755.

Guerrero, R., E. Montesinos, C. Pedros-Alio, I. Esteve, J. Mas, H. van Gemerden, P.A. G. Hofman and J. F. Bakker (1985) Phototrophic Sulfur Bacteria in Two Spanish Lakes: Vertical Distribution and Limiting Factors. *Limnol Oceanogr.* **30**, 919-931.

Gun J., Goifman A., Shkrob I., Kamyshny A., Ginzburg B., Hadas O., Dor I., Modestov A. D. and Lev O. (2000) Formation of Polysulfides in an Oxygen Rich Freshwater Lake and Their Role in the Production of Volatile Sulfur Compounds in Aquatic Systems. *Environ Sci Tech.* **34**, 4741-4746.

Hagy J.D., Boynton W.R., Keefe C.W., Wood K.V. (2004) Hypoxia in Chesapeake Bay, 1950-2001: Long-Term Change in Relation to Nutrient Loading and River Flow. *Estuaries* **27**, 634-658.

Hanson T.E., Luther III G.W., Findlay A.J., MacDonald D.J. and Hess D. (2013) Phototrophic sulfide oxidation: environmental insights and methods for kinetic analysis. *Front. Microbiol.* **4.**

Hunter K.S., Wang Y., Van Capellen P. (1998) Kinetic modeling of microbially-driven redox chemistry of subsurface environments: coupling transport, microbial metabolism and geochemistry. *J Hydrol.* **209**, 53-80.

Jonas R.B. and Tuttle J.H. (1990). Bacterioplankton and Organic Carbon Dynamics in the Lower Mesohaline Chesapeake Bay. *Appl Environ Microbiol.* **56**, 747-757.

Jørgensen, B.B. (1982) Ecology of the bacteria of the sulphur cycle with special reference to anoxic-oxic interface environments. *Arch Microbiol.* **298**, 543-561.

Jørgensen B.B., Cohen Y., Revsbech N.P. (1988) Photosynthetic Potential and Light-Dependent Oxygen Consumption in a Benthic Cyanobacterial Mat. *Appl Environ Microbiol.* **54**, 176-182.

Jørgensen B.B. and Nelson D.C. (2004). Sulfide oxidation in marine sediments: Geochemistry meets microbiology. In Sulfur Biogeochemistry ed Amend JP, Edwards KJ, and Lyons TW. The Geological Society of America, Boulder, CO.

Kamyshny A., Goifman A., Gun J., Rizkov D., and Lev O. (2004) Equilibrium distribution of polysulfide ions in aqueous solutions at 25 ˚C: a new approach for the study of polysulfides' equilibria. *Environ Sci Tech.* **38**, 6633-6644.

Kemp W.M. and Boynton W.R. (1980). Influence of biological and physical processes on dissolved oxygen dynamics in an estuarine system: implications for measurement of community metabolism. *Estuarine and Coastal Marine Science*. **11**, 407-431.

Konovalov S.K., Murray J.W. (2001) Variations in the chemistry of the Black sea on a time scale of decades (1960–1995). *J Mar Syst*. **31**, 217–243.

Konovalov S.K., Murray J.W, Luther III G.W., Tebo B.M. (2006). Processes controlling the redox budget for the oxic/anoxic water column of the Black Sea. *Deep-Sea Res. II* **53**, 1817–1841

Lewis B. L., Glazer B.T., Montbriand P.J., Luther III G.W., Nuzzio D.B, Deering T., Ma S., and Theberge S. (2007) Short-term and interannual variability of redox-sensitive chemical parameters in hypoxic/anoxic bottom waters of the Chesapeake Bay. *Mar Chem.* **105**, 296-308.

Lorenzen C.J. (1966) A method for the continuous measurement of in vivo chlorophyll concentration. *Deep Sea Res.* **13**, 223-227.

Luther III G. W., Glazer B. T., Ma S., Trouwborst R. E., Moore T. S., Metzger E., Kraiya C., Waite T. J., Druschel G., Sundby B., Taillefert M., Nuzzio D. B., Shank T. M., Lewis B. L. and Brendel P. J. (2008) Use of voltammetric solid-state (micro)electrodes for studying biogeochemical processes: Laboratory measurements to real time measurements with an in situ electrochemical analyzer (ISEA). *Mar. Chem.* **108**, 221-235.

Luther G. W., Findlay A. J., MacDonald D. J., Owings S. M., Hanson T. E., Beinart R. A. and Girguis P. R. (2011) Thermodynamics and Kinetics of sulfide oxidation by oxygen: a look at inorganically controlled reactions and biologically mediated processes in the environment. *Front. Microbiol.* **2**.

Luther III G.W. (1991) Pyrite synthesis via polysulfide compounds. *Geochim. Cosmochim. Acta* **55**, 2839- 2849.

Ma S., Noble A., Butcher D., Trouwborst R. E. and Luther III G.W. (2006) Removal of H_2S via an iron catalytic cycle and iron sulfide precipitation in the water column of dead end tributaries. *Estuar. Coast Shelf S.* **70**, 461-472.

MacDonald, D.J., Findlay, A.J., Hredzak-Showalter P., Krepski S.T., McAllister S.M., Cone S., Scott J., Bennett S., Chan C.S., Emerson D., Luther G.W. III (2014) Using *in situ* voltammetry as a tool to search for iron oxidizing bacteria: from fresh water wetlands to hydrothermal vent sites. *Environ Sci Process impacts.* doi:10.1039/C4EM00073K

Madison (2012). *Biogeochemical cycling of soluble manganese(III) in marine porewaters.* University of Delaware dissertation.

Manske A. K., Glaeser J., Kuypers M. M., and Overmann J. (2005) Physiology and phylogeny of green sulfur bacteria forming a monospecific phototrophic assemblage at a depth of 100 meters in the Black Sea. *Appl Environ Microbiol*. **71**, 8049-8060.

Marschall E., Jogler M., Hessge U., and Overmann J. (2010) Large-scale distribution and activity patterns of an extremely low-light-adapted population of green sulfur bacteria in the Black Sea*.* *Environ Microbiol*. **12**, 1348-1362.

Maryland Department of Natural Resources Resource Assessment Service. (2011-2014). Retrieved January 19, 2015, from http://mddnr.chesapeakebay.net/eyesonthebay/.cfm

Millero F.J, Sotolongo S. and Izaguirre M. (1987) The oxidation kinetics of Fe(II) in seawater. *Geochim. Cosmochim. Acta* **51**,793-801.

Möckel, H.J. (1984) Retention of sulphur and sulphur organics in reversed-phase liquid chromatography. *Journal of Chromatography* **317**, 589-614.

Moser D.P. and Nealson K.H. (1996) Growth of the facultative anaerobe Shewanella putrefaciens by elemental sulfur reduction. *Appl Environ Microbiol* **62**, 2100–2105.

Murray J.W., L.A. Codispoti and G.E. Friederich. (1995) Oxidation-reduction environments: the suboxic zone in the Black Sea. In: Huang C.P., O'Melia C.R., Morgan J.J. (Eds) Aquatic Chemistry: Interfacial and Interspecies Processes. ACS Advances in Chemistry Series. No. 224. pp. 157-176.

Oguz T., J.W. Murray and A. Callahan (2001) Modeling redox cycling across the suboxic-anoxic interface zone in the Black Sea. *Deep Sea Res*. **48**, 761-787.

Oldham V.E., Owings S.M., Jones M., Tebo B.M., and Luther III G.W. (2015) Evidence for the presence of strong Mn(III)-binding ligands in the water column of the Chesapeake Bay. *Mar Chem.* Doi 10.1016/j.marchem.2015.02.008.

Overmann J., Cypionka H., and Pfennig N. (1992) An extremely low-light-adapted green sulfur bacterium from the Black Sea. *Limnol Oceanogr.* **37,** 150-155.

Overmann J. (1997). Mahoney Lake: A case study of the ecological significance of Phototrophic sulfur bacteria. Advances in Miccrobial Ecology, Volume 15 ed G. Jones Plenum Press, NY.

Poulton S.W., Fralick P. W., and Canfield D.E. (2004) The transition to a sulphidic ocean approximately 1.84 billion years ago. *Nature* **431**, 173-177.

Rimmer A., Ostrovsky I., Yacobi Y.Z. (2008) Light availability for Chlorobium phaeobacteroides development in Lake Kinneret. *J Plankton Res.* **30**, 765-776.

Roden E.E. and Tuttle J.H. (1993). Inorganic sulfur cycling in mid and lower Chesapeake Bay sediments. *Mar Ecol Prog Ser.* **93**, 101-118.

Scully M.E. (2010) Wind Modulation of Dissolved Oxygen in Chesapeake Bay. Estuaries and Coasts **33**, 1164–1175.

Steele J.H. (1965) Notes on some theoretical problems in production ecology. In Primary Production in Aquatic Environments, C.R. Goldman ed., University of California Press, Berkely, CA.

Stookey, L. L. (1970). Ferrozine---a new spectrophotometric reagent for iron. *Anal Chemi* **42**, 779-781.

Stumm, W. and J.J. Morgan (1996). Aquatic Chemistry, Chemical Equilibria and Rates in Natural Waters. 3rd ed. John Wiley & Sons, Inc., New York, NY, USA.

Taft J.L., Taylor W.R., Hartwig, E. O., Loftus R. (1980) Seasonal oxygen depletion in Chesapeake Bay. *Estuaries* **3**, 242.

Tebo B.M. (1991) Manganese (II) oxidation in the suboxic zone of the Black Sea.Deep Sea Res A, **38,** S883–S905.

Tonolla M., Peduzzi S., Hahn D., and Peduzzi R. (2003) Spatio-temporal distribution of phototrophic sulfur bacteria in the chemocline of meromictic Lake Cadagno (Switzerland). *Microb Ecol.* **43**, 89-98.

Tuttle, J. H., R. B. Jonas, and T. C. Malone. (1987). Origin, development and significance of Chesapeake Bay anoxia. In S. K. Majumdar, L. W. Hall, and H. M. Austin (eds.), Contaminant Problems and management of living Chesapeake Bay resources, pp. 442—472. Pennsylvania Academy of Sciences Press, Easton, Pennsylvania.

Van Cappellen P. and Wang Y. (1996) Cycling of iron and manganese in surfacesediments: a general theory for the coupled transport and reaction of carbon,oxygen, nitrogen, sulfur, iron, and manganese. *Amer Jour Sci*. **296**, 197–243.

Xiong Y., and Berger C.R. (2010) Chesapeake Bay tidal characteristics. *J Water Res Protect*. **2,** 619-628.

Yakushe E.V. and Neretin L.N. (1997) One dimensional modeling of nitrogen and sulfur cycles in the aphotic zone of the Black and Arabian Seas. *Global Biogeochem Cycles* **11**, 401-414.

Yakushev E.V., Pollehne F., Jost G., Kuznetsov I., Schneider, B. & Umlauf, L.(2007) Analysis of the water column oxic/anoxic interface in the Black andBaltic seas with a numerical model. *Mar Chem* **107**, 388-410.

Yao W, Millero F.J. (1993). The rate of sulfide oxidation by δMnO_2 in seawater. Geochim Cosmochim Acta 57: 3359–3365

Yao, W. and Millero F. J. (1996) Oxidation of hydrogen sulfide by hydrous Fe(III) oxides in seawater. *Mar Chem.* **52**, 1-16.

Yücel M., Konovalov S.K., Moore T.S., Janzen C.P. and Luther III G.W. (2010) Sulfur speciation in the upper Black Sea sediments. *Chem Geol.* **269**, 364-375.

Zopfi J., Ferdelman T.G., and Fossing H. (2004) Distribution and fate of sulfur intermediates – sulfide tetrathionite, thiosulfate, and elemental sulfur – in marine sediments. In Sulfur Biogeochemistry ed Amend JP, Edwards KJ, and Lyons TW.The Geological Society of America, Boulder, CO.

Chapter 6

CONCLUDING REMARKS AND FUTURE DIRECTIONS

The chemical cycle of sulfur in the environment is complex and often is linked with both trace metal chemistry and microbial processes. The oxidation of sulfide has importance implications for modern environments, where sulfide plays a variable role either as a toxin, as a ligand for reduced metals, or for fuel for microbial metabolism; as well as for deepening understanding of how ancient oceans functioned. The work presented in this dissertation has focused on the formation of metal sulfide particles and nanoparticles, initial oxidation of sulfide to form elemental sulfur and the size fractionation of elemental sulfur in the environment. The work described in the above chapters represents one of the first studies to integrate chemical, biological, and modeling approaches in order to understand the relative importance of different sulfide oxidation processes and size fractions of zero-valent sulfur and metal sulfides in the environment. Below, the major findings of this study are highlighted and questions that remain for future study are posed.

6.1 Metal and Sulfur Dynamics in Buoyant Vent Plumes

Chapter 2 presented a study of sulfur and metal sulfide particle dynamics in the early stages of buoyant hydrothermal vent plumes (< 1.5 meters from the orifice), and highlighted the importance of variations in vent fluid composition in controlling the partitioning of metals into sulfides and other particles in the initial mixingzone. Specifically, differences in metal associations in the Rainbow plume suggest the formation of different precipitates than at TAG or Snakepit due to the low sulfide and high iron concentrations in the Rainbow vent fluid. Nitric acid-extractable metals were found in the < 0.2 μm fraction at all three vent sites, indicating their incorporation into nanoparticulate pyrite. This is significant because it means that trace metals in addition to iron will be stabilized in these nanoparticles, and could be dispersed to the larger oceans.

There are still many unanswered questions concerning the chemistry of metals in vent plumes and their distribution to the oceans. It is only recently that metal sulfide nanoparticles have begun to be studied in vent fluid (Yücel et al., 2011) and buoyant plumes (Gartman et al., 2014; this work); however new results from GEOTRACES work indicate that high dissolved iron concentrations in the deep oceans are associated with the TAG hydrothermal plume (Sedwick et al., 2014). Thus, further investigations of size-fractionated particles in the vent fluid, the rising plume, and the neutrally buoyant plume are needed in order to determine the impact of hydrothermal venting on marine trace metal budgets.

Another major question that remains from this study is the role of metal-containing nanoparticles other than sulfides. Specifically, results from Chapter 2 strongly suggest the formation of iron silicates through reverse weathering in the buoyant plume. This would have further implications for estimating the transport of iron from vent plumes, as silicate particles would behave differently from sulfide or oxide particles. Moreover, the observation of reverse weathering in hydrothermal plumes would be novel and highly significant.

6.2 Nanoparticulate Elemental Sulfur

In Chapter 3, size-fractionated elemental sulfur was documented in both the water column of the Chesapeake Bay and in buoyant hydrothermal vent plumes along the Mid-Atlantic Ridge. In particular, nanoparticulate (< 0.2 μm) elemental sulfur was found to be a significant constituent of both environments. In the Chesapeake Bay, the oxidation of sulfide to elemental sulfur is both chemical and biological; and manganese oxides represent an important abiotic pathway for sulfide oxidation. Furthermore, a novel strain of phototrophic sulfide oxidizing bacteria was found in the sub and anoxic waters of the Chesapeake Bay, and demonstrated to produce nanoparticulate elemental sulfur as a product of sulfide oxidation. In the first meter of buoyant plumes, sulfide oxidation is expected to be abiotic due to the high temperatures and flow rate. Here, an iron catalytic cycle in which Fe^{2+} is oxidized by oxygen to Fe^{3+}, which then oxidizes sulfide to S^0, regenerating Fe^{2+}, can account for all elemental sulfur observed in this portion of the plume. The presence of nanoparticulate (< 0.2 μm) elemental sulfur in both systems is significant as they represent two distinct environments governed by different sulfide oxidation processes. This indicates that nanoparticulate S^0 is formed by both abiotic and biotic sulfide oxidation.

The presence of nanoparticulate elemental sulfur raises interesting questions regarding the speciation and reactivity of zero-valent sulfur in the environment. Nanoparticles may behave differently than their bulk mineral counterparts due to changes in structure, high surface area to volume ratio, and small size (Hochella et al., 2008). Nanoparticulate S^0 thus may have different reactivity than bulk S_8, which would affect its role in geochemical reactions such as pyrite formation, or in microbial processes such as reduction, oxidation, or disproportionation. The observation of nanoparticulate sulfur in both the Chesapeake Bay and bouyant vent plumes indicates that it forms via both abiotic and biotic processes; however it is unknown whether there is a difference between the speciation of sulfur found in the vent plumes and that in the Chesapeake Bay, as in addition to any size-related changes, biologically produced S^0 is also known have different characteristics than bulk S_8.

6.3 Light Dependent Sulfide Oxidation

Sulfide oxidation in the Chesapeake Bay was investigated in more detail in Chapter 4. Specifically, this part of the study aimed to answer questions raised by work done by Luther et al. (1988), which demonstrated light-dependent sulfide oxidation in bottom water samples from the Chesapeake Bay. This sulfide oxidation activity appeared to be biological as it was halted upon treatment of samples with formaldehyde; however, it remained unclear what process was responsible for the observed activity.

In order to elucidate sulfide oxidation processes, a series of kinetic experiments was conducted using water samples from the anoxic/sulfidic portion of the water column. In these experiments, small increases in very low light intensities resulted in significant changes in the rate of sulfide loss. Treatment of samples with DCMU to inhibit oxygenic photosynthesis did not affect sulfide loss; however treatment with formaldehyde caused significant reduction in sulfide loss. These experiments strongly suggested that PSOB were responsible for the observed light-dependent sulfide oxidation.

Additional experiments were conducted in the laboratory using the enrichment cultures of PSOB (CB11) presented in Chapter 3. These experiments quantified the effects of biomass, sulfide concentration, and light intensity on the specific rate of sulfide oxidation by these bacteria. The kinetic parameters (V_{max} and K_m) that were determined are in good agreement with those of other strains of green sulfide oxidizing bacteria. Photo-inhibition of sulfide oxidation occurred at very low light intensities (approximately 3 μEi). Calculations based on both sets of experiments estimated that *Chlorobi* need only comprise 3 – 5 % of the overall microbial community in the water column in order to account for all light-dependent sulfide loss.

There are several noteworthy aspects of the study that deserve further attention. Light dependent sulfide oxidation was observed in four separate years, over several decades (1987, 2012, 2013, and 2014), indicating that it and PSOB are a common component of the Chesapeake Bay system in years with very different redox conditions. This leads to the question of whether the community of sulfide oxidizing bacteria changes significantly between years or throughout the onset or degradation of stratification. For example, a complete shift in the microbial community from phototrophic to chemotrophic after mixing of the lake was recently observed in Lake Rogoznica (Pjevac et al., 2015). A similar shift in the phototrophic community from purple sulfur bacteria to green sulfur bacteria was documented in Lake Cadango due to disturbances in the chemocline (Decristophoris et al., 2009). Additionally, the presence of other sulfur-metabolizing bacteria in the water column, would aid understanding of the cycling of other sulfur species such as nanoparticulate elemental sulfur.

Furthermore, the dark uptake of sulfide observed in laboratory experiments has interesting implications. It is unknown whether the cells are actively taking up and storing sulfide or if it is a passive process, as sulfide diffuses readily into the cell (Riahi, 2014). In either case, this may be important ecologically, as it would allow the bacteria to acquire sulfide in deeper waters, then to move up in the water column to higher light intensities in order to oxidize this sulfide. This would be particularly important in systems with a large suboxic zone separating the sulfidic layer from the photic zone (e.g. the Chesapeake Bay in 2014).

6.4 Redox Model of the Chesapeake Bay

In Chapter 5, a one dimensional diffusion-reaction model of the Chesapeake Bay water column was developed. The purpose of this model was to assess the effect of observed variability in stratification and redox conditions on sulfide oxidation by

PSOB. The activity of PSOB was included using an algae growth model adapted with the kinetic parameters determined experimentally in Chapter 4. Model simulations of five datasets taken from four separate years of field sampling provided examples of different physical and chemical conditions in the water column. These simulations demonstrated that the contribution of PSOB to sulfide oxidation was strongly dependent upon the location of the oxic/anoxic interface in the water column, which affects the intensity of light reaching it.

The redox model developed in this chapter provides a foundation for further modeling studies, and there are several important additions that may be made to the model in order to create a more accurate and versatile representation of the Chesapeake Bay water column. Due to the quantity of chemical and biological data collected during the four-year study, the role of other chemical reactions, such as between Fe and MnO_2, and the inclusion of Mn^{3+} cycling, or microbial processes, such as iron oxidation or manganese oxidation, could be added and explored.

6.5 The Role of Nanoparticles, Trace Metals, and Microorganisms in Sulfur Cycling

This dissertation investigated key aspects of sulfur cycling along redox gradients by integrating chemical, biological, and numerical approaches. In particular, this work has highlighted the important role of nanoparticles (both metal sulfides and elemental sulfur) and different sulfide oxidation processes in two very distinct marine environments. Although they have variable physical, chemical, and biological characteristics, the Chesapeake Bay and buoyant vent plumes are similar in that each contains a redox interface along which sulfur is dynamically cycled and in which nanoparticles are a significant component. These findings illustrate the importance of considering two aspects of environmental studies that are only beginning to be explored: (1) the composition of the operationally-defined "dissolved" fraction, and (2) the role of fundamental reaction steps in overall biogeochemical processes (Luther, 2010). Further research in both of these areas will enhance our understanding of complex and dynamic marine environments past and present; and will provide insight for potential future changes.

REFERENCES

Decristophoris P.M.A., Peduzzi S., Ruggeri-Bernardi N., Hahn D., Tonolla M. (2009) Fine scale analysis of shifts in bacterial community structure in the chemocline of Lake Cadagno, Switzerland. *J Limnol*. **68,** 16-24.

Gartman A., Findlay A.J., Luther III G.W. (2014) Nanoparticulate pyrite and other nanoparticles are a widespread component of hydrothermal vent black smoker emissions. *Chem. Geol.* **366**, 32-4.

Hochella, M. F., S. K. Lower, Maurice P. A., Lee Penn R., Sahai N, Sparks D. L., Twining B.S. (2008). Nanominerals, Mineral Nanoparticles, and Earth Systems. *Science* **319**, 1631-1635.

Luther, G., Ferdelman T., Tsamakis E. (1988). Evidence suggesting anaerobic oxidation of the bisulfide ion in Chesapeake Bay. *Estuaries* **11**, 281-285.

Luther, G., III (2010). The Role of One- and Two-Electron Transfer Reactions in Forming Thermodynamically Unstable Intermediates as Barriers in Multi-Electron Redox Reactions. *Aquat Geochem.* **16**, 395-420.

Pjevac P, Kolević M, Berg JS, Bura-Nakić E, Ciglenečki I, Amann R, Orlić S. (2015) Community shift from phototrophic to chemotrophic sulfide oxidation following anoxic holomixis in a stratified seawater lake. *Appl Environ Microbiol*. doi:10.1128/AEM.02435-14.

Riahi S., Rowley C.N. (2014) Why can hydrogen sulfide permeate cell membranes? *J Amer Chem Soc* **136**, 15111-15113.

Yücel, M., Gartman A., Chan, C.S., Luther G.W., III. (2011). Hydrothermal vents as a kinetically stable source of iron-sulphide-bearing nanoparticles to the ocean. *Nature Geosci* **4**, 367-371.

Appendix A

SULFIDE OXIDATION KINETICS IN RSC1

A.1 Methods

A.1.1 Culturing Procedure

Cultures of RSC1 were started by transferring 5 mL of a densely grown starter culture into a 100 mL septum vial containing anoxic media (get media comp), which was pressurized to 10 psi with ultrahigh purity argon gas and incubated in the dark for forty-five minutes. The vial was then place in a water bath set at 27˚C and cells were grown for forty hours under 20 μEi light provided by 60 W full-spectrum bulbs. At the end of the growth period cells were washed with HEPES buffer (0.1M, pH 7.4) and centrifuged three times for 10 minutes at 6000 rpm. Once washed, the cells were stored in anoxic HEPES buffer in order to be used in experiments. Anoxic conditions were maintained throughout the washing and transfer steps through the use of a glovebag purged with argon gas. Biomass measurements were done using the Bradford protein assay (Bradford 1976). In order to prepare the sample for the protein assay, 1 mL cells were centrifuged at 16 xg for one minute. At this time half of the supernatant was decanted and the cells were spun again for another minute. The remainder of the supernatant was decanted, and the pellet was re-suspended in 1 mL methanol and incubated in the refrigerator for ten minutes before being centrifuged for five minutes. The methanol was decanted and the pellet was frozen for up to two weeks. To make the protein measurement the pellets were thawed and resuspended in half a milliliter NaOH (0.25M) for 10 min, after which 0.5 mL HCl (0.25M) was added to neutralize the suspension. This solution was diluted and 200 µL diluted sample were added to 600 µL KPO_4^{2-} buffer and 200 µL dye. After 30 minutes the absorbance at 594nm was read and converted to protein.

A.1.2 Experimental Procedure

A.1.2.1 Analytical Methods

Solid state voltammetry using a 100 µm gold amalgam working electrode, a Ag/AgCl reference electrode, and a platinum counter electrode (Brendel and Luther 1995) was applied to monitor sulfide loss in experiments. Experiments were set up in a capped thermo-statted electrochemical cell with ports for the electrodes and for purging with argon gas to remove oxygen from the buffer. The electrodes were connected to a DLK 60 potentiostat (Analytical Instrument Systems, (AIS) Inc.) run by AIS software. Voltammetric scans are run every nine seconds at 2V/second from -0.1 V to -1.8 V with a two step conditioning process and stirring of the solution in between. Voltage is held at 0.9 V for five seconds to remove any sulfide from the electrode surface, and at -0.1 V for two seconds. Sulfide reacts via equation 1, giving a peak at -0.7 V under these experimental conditions.

(1) $HgS + H^+ + 2e^- \rightarrow HS^- + Hg$

The current is converted to concentration using standard additions of sulfide.

Stock solutions of HEPES and sulfide are made from salts dissolved in deoxygenated deionized water. Na_2S salts are washed and dried in order to remove the oxidized layer prior to use in making sulfide solutions.

A.1.2.2 Experimental Methods

A forty-eight hour growth curve (Figure A.1) was done in order to ensure that cells are harvested during log phase growth. Cells were cultured following the procedure outlined above, and subsamples of the culture were taken for protein measurements throughout the experiment.

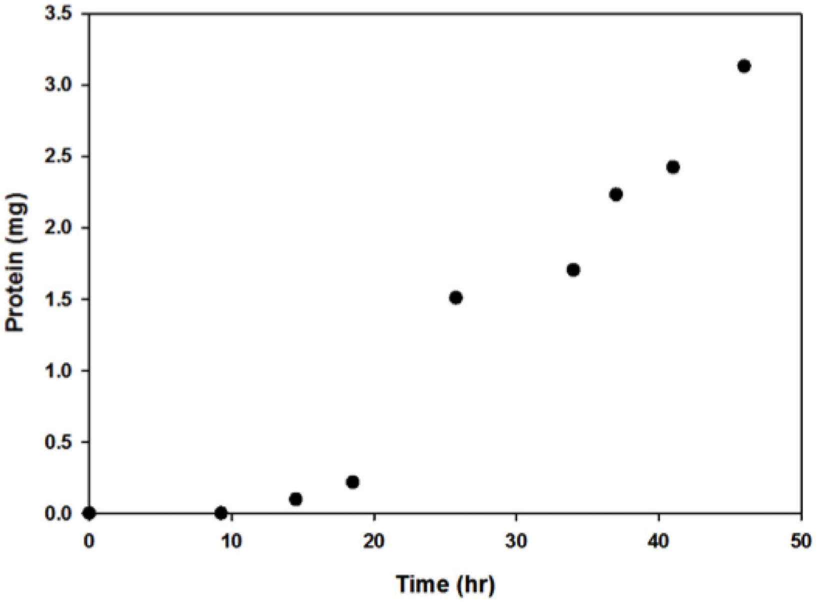

Figure A.1 Growth curve for RSC1

Kinetic experiments were conducted at 26 ˚C in 20 mL HEPES buffer (0.1M, pH 7.4) that were added to the electrochemical cell and purged of oxygen for four minutes. After the solution was anoxic, the appropriate quantity of cells was added, and sulfide was spiked in. Experiments were run over the course of an hour with sulfide loss tracked by the electrochemical method outlined above. Light intensity was monitored using a LI-COR Biosciences LI-1400 light meter and was provided by a desk lamp equipped with a 60 W full spectrum bulb. Light was manipulated by attaching the lamp to a variac.

Biomass, sulfide concentration, and light intensity were individually manipulated, and all experiments were conducted in triplicate. Experiments conducted varying biomass were run at under 5µEi light intensity and with 30µM sulfide. Sulfide concentration experiments were also conducted under 5 µEi light. Sulfide concentrations used were 5, 15, 25, 50, and 75 µM. For these experiments, 0.5 mL cells was used to remain between 0.025 and 0.07 mg protein in each experiment, which is within the linear range of a plot of protein normalized rate vs. biomass (Figure A.2).

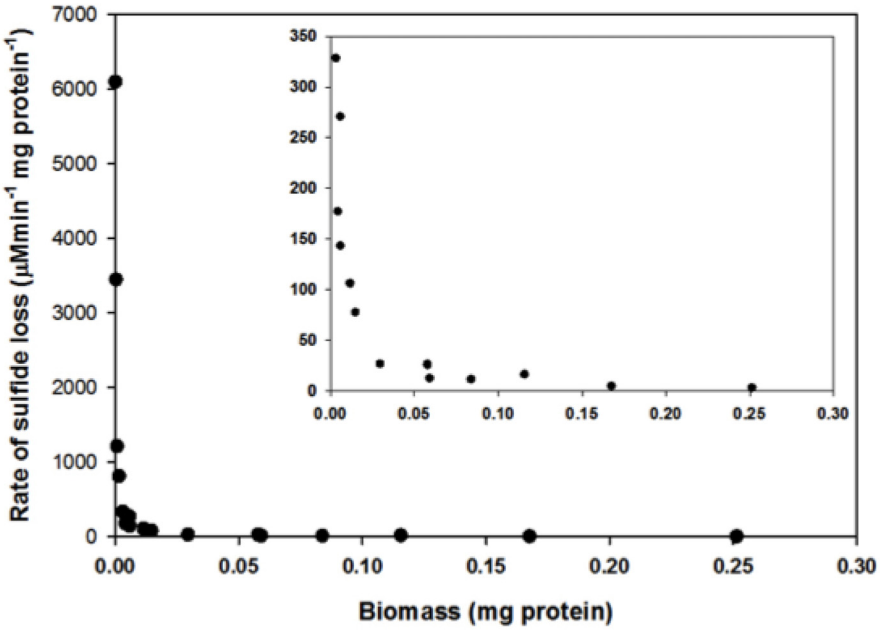

Figure A.2 The effect of biomass on the rate of sulfide loss.

Dark rates were also obtained for varying sulfide concentrations (5, 15, 25, 50, 75 µM) and were subtracted from the overall rates obtained for each sulfide concentrations. 0.5mL of cells was used in each experiment, retaining the protein between 0.025 and 0.058 mg in the experiment. For these experiments, lab lights were turned off, the electrochemical cell was covered in aluminum foil, and a box was placed over the setup. The light meter confirmed that no light penetrated this set up. Experiments were done varying light intensity from dark (0 µEi) to 15 µEi. These experiments were run using 0.5 mL of cells (0.031-0.55 mg protein) and 75 µM sulfide. Lights in the lab were turned off, a cardboard box was placed around the electrochemical setup and light source to ensure that light intensity did not fluxuate while the experiments were progressing.

A.2 Results

Figure A.3a shows the rate variation over a range of sulfide concentrations. These kinetics were found to fit the Michaelis-Menten model, with a v_{max} of 44.7 μM/minute/mg protein and a half saturation constant (k_m) of 39.2 μM. In order to obtain a more accurate estimate of the kinetic parameters, the data were then plotted on a Lineweaver-Burke plot (Figure A.3b). Using this method, a v_{max} of 50 μM/minute/mg protein and a k_m of 26.3 μM were obtained, which are similar in magnitude to the parameters determined from the Michaelis-Menten plot.

The effect of light intensity on the sulfide oxidation rate is shown in Figure A.4. Similar to the data for the Chesapeake Bay strain, small increases in light intensity lead to significant changes in the sulfide oxidation rate. There is also a dark rate of 19.9 μM/minute/mg protein, and the rate appears to become saturated after 2 μEi Furthermore, the dependence on light is demonstrated again in a plot of rate versus protein in the experiment (Figure A.2) which shows an exponential decrease in protein normalized rate with increasing biomass. The decrease in the specific rate with increasing biomass is likely due to the subsequent increase in light attenuation within the electrochemical cell in which the experiments are conducted.

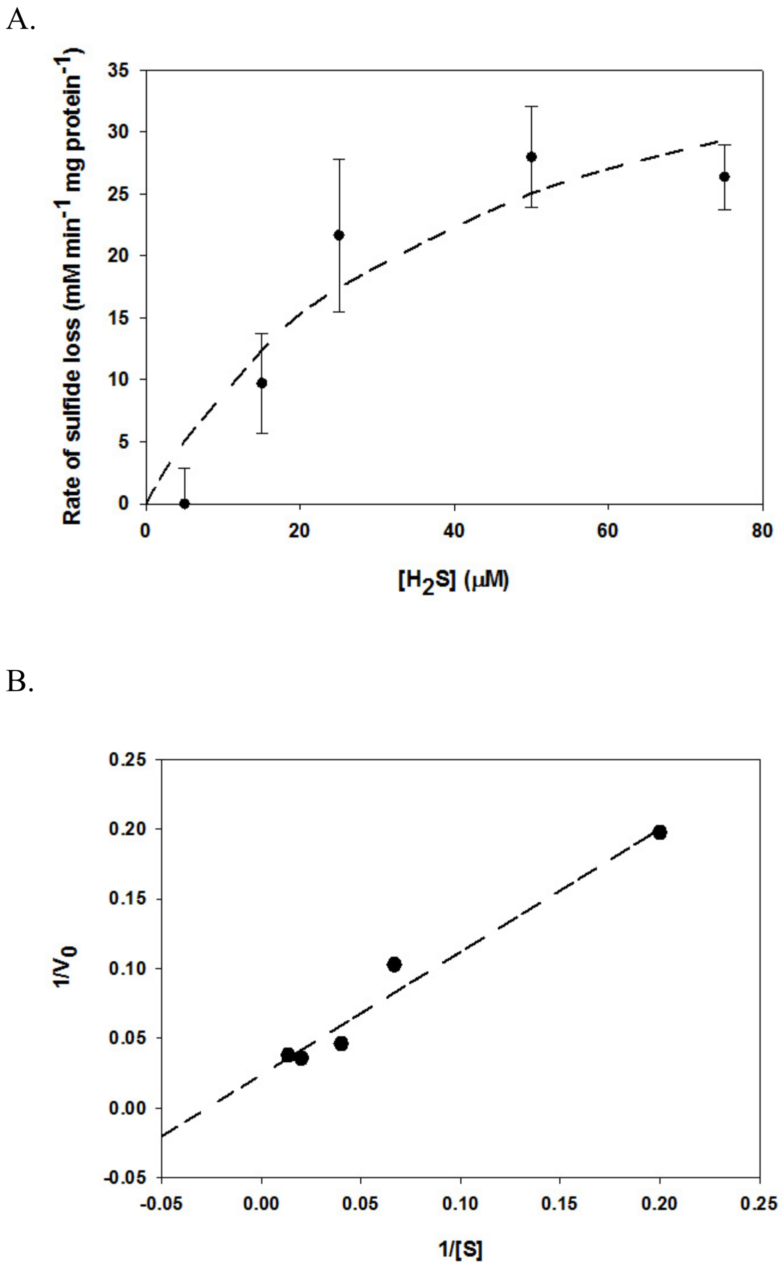

Figure A.3 (a) Michaelis-Menten plot of sulfide oxidation kinetics in RSC1. (b) Lineweaver-Burke transformation of the data in (a).

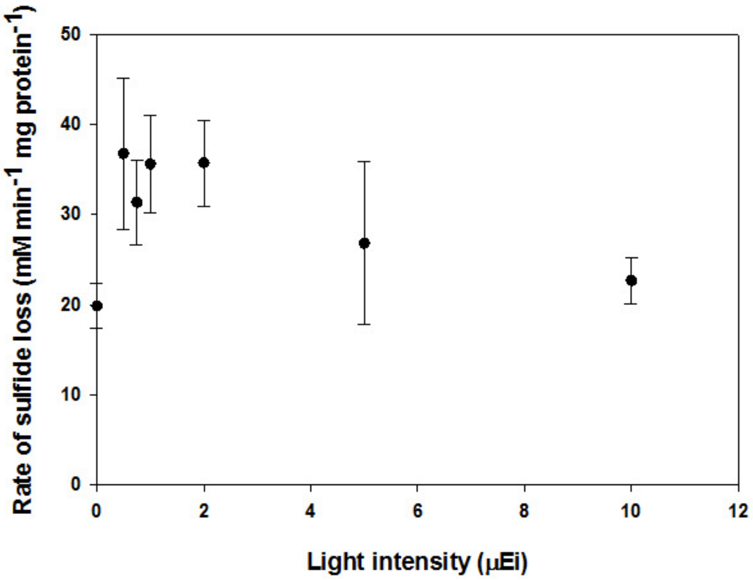

Figure A.4 Effect of light intensity on sulfide oxidation kinetics in RSC1.

A.3 Comparison to Other GSB

The maximum rate for RSC1 is approximately the same as that ascertained for the Chesapeake Bay strain using the substrate inhibition model (Chapter 4, Table 4.3). Similar values for v_{max} indicate that the enzyme systems in use have a similar turnover rate (Berg et al., 2002). The k_m values for RSC1 are higher than those of the Chesapeake Bay strain, indicating weaker enzyme-substrate binding for RSC1.

REFERENCES

Bradford M. (1976) A rapid and sensitive method for the quantitation of microgram quantities of protein utilizing the principle of protein-dye binding. *Anal Biochem.***72**, 248-254.

Brendel P. J. and Luther III G. W. (1995) Development of a Gold Amalgam Voltammetric Microelectrode for the Determination of Dissolved Fe, Mn, O_2, and S(-II) in Porewaters of Marine and Freshwater Sediments. *Environ Sci Technol.* **29**, 751-761.

Berg J.M., J.L. Tymoczko and L.Stryer (2002). The Michaelis-Menten Model Accounts for the Kinetic Properties of Many Enzymes. Biochemistry. 5th edition. New York: W H Freeman;. Section 8.4, Available from: http://www.ncbi.nlm.nih.gov/books/NBK22430/

Appendix B

COMPUTER CODE FOR CHESAPEAKE BAY MODEL

```
import numpy as np
from scipy.integrate import odeint
import matplotlib.pyplot as plt
import csv

print 'running model simulation for 2011'

nspecies = 7
nrxns = 8

#Initial conditions (uM)
O2sat =  input(Please enter the saturated O2 concentration: ')
H2Sit = input(Please enter an initial H2S concentration: ')
Fe2it = input(Please enter an initial Fe2 concentration: ')
Mn2it = input(Please enter an initial Mn2 concentration: ')

#Parameters for P & R
Ii = 1500 #uEi
T = 25 #deg C

#Parameters for PSOB
Isat = 3 #5 uEi
Ks = 14 #10 uM

kO2 = 3
kL = 1.4

#Solution parameters
N = 50  # number of points to discretize
L = 25.0 # total depth (m)
Z = np.linspace(0, L, N) # depth position
h = L / (N - 1)
```

```
        tfinal = 10000.0 #days
        Ntsteps = 1000000
        dt=tfinal/(Ntsteps-1)

        t = np.linspace(0.0, tfinal, Ntsteps)

        #Kinietic parameters (uM-1 d-1)
        k1 = 0.1
        k2 = 0.05
        k3 = 0.1
        k4 = 0.2
        k5 = 0.5
        k6 = 1
        k7 = 0.01

        k_ext =  input(Please enter the extinction coeficient for light: ')
        W =  input(Please enter a sinking rate: ') #sinking, m d-1

        #Make an array for D (m2 d-1)
        D=np.zeros(50)
        D[0:] =
        D[:50] =

        alpha = D[0] *dt / h**2
        if alpha > 0.25:
           raise Exception, 'Does not satisfy requirements for numerical stability.
Change dt or D'
        print dt

        C_zt=[] #container for timesteps
        C = np.zeros((nspecies, 50))
        C_zt +=[C]

        #Make an array for light, photosynthesis and respiration
        I = np.zeros(50)
        Chl = np.zeros(50)
        Corg = np.zeros(50)
        for d in range(len(Z)):
           I[d]=Ii * np.exp(-k_ext * Z[d])
           Chl[d] =  #Chl in mg/L
        light = I
        Corg = Chl * 4200 #C in uM
```

```
    #plt.plot(Corg, -Z)
    #plt.show()

    for j in range(1, Ntsteps):
       N = np.zeros(C.shape)

       N[0,0] =  kL * (O2sat - N[0,1])
       N[1,-1] = H2Sit
       N[3,-1] = Fe2it
       N[5, -1] = Mn2it

       P = 10.25 * Chl[1:-1]
       R = 1.025 * Chl[1:-1]
       R1 = k1 * Corg[1:-1] * (C[0,1:-1] / (kO2 + C[0,1:-1]))
       R2 = k2 * C[0,1:-1] * C[1,1:-1]
       R3 = k3 * C[0,1:-1] * C[3,1:-1]
       R4 = k4 * C[1,1:-1] * C[4,1:-1]
       R5 = k5 * C[0,1:-1] * C[5,1:-1]
       R6 = k6 * C[1,1:-1] * C[6,1:-1]
       R7 = k8 * C[2,1:-1]
       R8 = C[1,1:-1] / (Ks + C[1,1:-1]) * ((light[1:-1] / Isat) * np.exp(-light[1:-1] /
Isat + 1 ))


       N[0,1:-1] = (D[1:-1] *dt / h**2 * C[0,2:] + (1 - 2 * D[1:-1] *dt / h**2) *
C[0,1:-1] + D[1:-1] *dt / h**2 * C[0,0:-2]) + ((P - R - R1 - 0.5 * R2 - 0.5 * R3 - 0.25 *
R5) *dt) #O2
       N[1,1:-1] = (D[1:-1] *dt / h**2 * C[1,2:] + (1 - 2 * D[1:-1] *dt / h**2) *
C[1,1:-1] + D[1:-1] *dt / h**2 * C[1,0:-2]) + ((- R2 - R4 - R6 + 0.5 * R7 - R8) *dt)
#H2S
       N[2,1:-1] = (D[1:-1] *dt / h**2 * C[2,2:] + (1 - 2 * D[1:-1] *dt / h**2) *
C[2,1:-1] + D[1:-1] *dt / h**2 * C[2,0:-2]) + ((R2 + R4 + R6 - R7 + R8) * dt) - (W *
(C[2,1:-1]- C[2,0:-2]) * dt)#S0
       N[3,1:-1] = (D[1:-1] *dt / h**2 * C[3,2:] + (1 - 2 * D[1:-1] *dt / h**2) *
C[3,1:-1] + D[1:-1] *dt / h**2 * C[3,0:-2]) + ((- R3 + R4) *dt) #Fe2
       N[4,1:-1] = (D[1:-1] *dt / h**2 * C[4,2:] + (1 - 2 * D[1:-1] *dt / h**2) *
C[4,1:-1] + D[1:-1] *dt / h**2 * C[4,0:-2]) + ((R3 - R4) * dt) - (W * (C[4,1:-1] -
C[4,0:-2]) * dt)#Fe3
       N[5,1:-1] = (D[1:-1] *dt / h**2 * C[5,2:] + (1 - 2 * D[1:-1] *dt / h**2) *
C[5,1:-1] + D[1:-1] *dt / h**2 * C[5,0:-2]) + ((- R5 + R6) * dt) #Mn2
       N[6,1:-1] = (D[1:-1] *dt / h**2 * C[6,2:] + (1 - 2 * D[1:-1] *dt / h**2) *
C[6,1:-1] + D[1:-1] *dt / h**2 * C[6,0:-2]) + ((R5 - R6) * dt) - (W * (C[6,1:-1] -
C[6,0:-2]) * dt)#MnO2
```

```
        #Zero flux boundary for solids
        N[0,-1] = N[0,-2]
        N[2,-1] = N[2,-2]
        N[4,-1] = N[4,-2]
        N[6,-1] = N[6,-2]

        oxygen = N[0,:]
        sulfide = N[1,:]
        sulfur = N[2,:]
        iron2 = N[3,:]
        iron3 = N[4,:]
        manganese2 = N[5,:]
        manganese4 = N[6,:]

        C[:] = N
        C_zt += [N]

    #Export solution
    arraylen=len(Z)
    datasave1 = np.zeros([arraylen, nspecies+2])
    file = open('/Users/User/Desktop/diffrxn_soln 2011.csv','w')
    csvfile=csv.writer(file)
    for ds in range(0,arraylen):
        datasave1[ds,0] = Z[ds]
        datasave1[ds,1] = D[ds]
        datasave1[ds,2] = oxygen[ds]
        datasave1[ds,3] = sulfide[ds]
        datasave1[ds,4] = sulfur[ds]
        datasave1[ds,5] = iron2[ds]
        datasave1[ds,6] = iron3[ds]
        datasave1[ds,7] = manganese2[ds]
        datasave1[ds,8] = manganese4[ds]

    csvfile.writerow(["Depth", "D", "Oxygen", "Sulfide", "Sulfur", "Iron(II)",
"Iron(III)", "Manganese(II)", "Manganese(IV)"])
    for dsrow in datasave1:
        csvfile.writerow(np.around(dsrow,decimals=20))
    file.close()
    print "results written to file"

    #Export reactions
    arraylen2=(len(Z)-2)
```

```
    datasave2 = np.zeros([arraylen2, nrxns+3])
    file = open('/Users/User/Desktop/rxnrates 2011.csv','w')
    csvfile=csv.writer(file)
    for ds in range(0,arraylen2):
        datasave2[ds,0] = Z[ds]
        datasave2[ds,1] = R1[ds]
        datasave2[ds,2] = R2[ds]
        datasave2[ds,3] = R3[ds]
        datasave2[ds,4] = R4[ds]
        datasave2[ds,5] = R5[ds]
        datasave2[ds,6] = R6[ds]
        datasave2[ds,7] = R7[ds]
        datasave2[ds,8] = R8[ds]
        datasave2[ds,9] = P[ds]
        datasave2[ds,10] = R[ds]
    csvfile.writerow(["Depth", "R1", "R2", "R3", "R4", "R5", "R6", "R7", "R8", "P", "R"])
    for dsrow in datasave2:
        csvfile.writerow(np.around(dsrow,decimals=20))
    file.close()
    print "reaction rates written to file"
    print "Model run complete"
```

Appendix C

PERMISSIONS

ELSEVIER LICENSE
TERMS AND CONDITIONS

Apr 03, 2015

This is a License Agreement between Alyssa Findlay ("You") and Elsevier ("Elsevier") provided by Copyright Clearance Center ("CCC"). The license consists of your order details, the terms and conditions provided by Elsevier, and the payment terms and conditions.
All payments must be made in full to CCC. For payment instructions, please see information listed at the bottom of this form.

Supplier

Elsevier Limited
The Boulevard,Langford Lane
Kidlington,Oxford,OX5 1GB,UK

Registered Company Number

1982084

Customer name

Alyssa Findlay

Customer address

700 Pilottown Road

LEWES, DE 19958

License number

3601441251459

License date

Apr 03, 2015

Licensed content publisher

Elsevier

Licensed content publication

Geochimica et Cosmochimica Acta

Licensed content title

Distribution and size fractionation of elemental sulfur in aqueous environments: The Chesapeake Bay and Mid-Atlantic Ridge

Licensed content author

None

Licensed content date

1 October 2014

Licensed content volume number

142

Licensed content issue number

n/a

Number of pages

15

Start Page

334

End Page

348

Type of Use

reuse in a thesis/dissertation

Portion

full article

Format

electronic

Are you the author of this Elsevier article?

Yes

Will you be translating?

No

Title of your thesis/dissertation

Sulfide oxidation and (nano)particle formation along redox gradients in the marine environment

Expected completion date

May 2015

Estimated size (number of pages)

280

Elsevier VAT number

GB 494 6272 12

Permissions price

0.00 USD

VAT/Local Sales Tax

0.00 **USD / 0.00** GBP

Total

0.00 USD

Terms and Conditions

INTRODUCTION

1. The publisher for this copyrighted material is Elsevier. By clicking "accept" in connection with completing this licensing transaction, you agree that the following terms and conditions apply to this transaction (along with the Billing and Payment terms and conditions established by Copyright Clearance Center, Inc. ("CCC"), at the time that you opened your Rightslink account and that are **available at** any time at http://myaccount.copyright.com).

GENERAL TERMS

2. Elsevier hereby grants you permission to reproduce the aforementioned material subject to the terms and conditions indicated.

3. Acknowledgement: If any part of the material to be used (for example, figures) has appeared in our publication with credit or acknowledgement to another source, permission must also be sought from that source. If such permission is not obtained then that material may not be included in your publication/copies. Suitable acknowledgement to the source must be made, either as a footnote or in a reference list at the end of your publication, as follows:

"Reprinted from Publication title, Vol /edition number, Author(s), Title of article / title of chapter, Pages No., Copyright (Year), with permission from Elsevier [OR APPLICABLE SOCIETY COPYRIGHT OWNER]." Also Lancet special credit - "Reprinted from The Lancet, Vol. number, Author(s), Title of article, Pages No., Copyright (Year), with permission from Elsevier."

4. Reproduction of this material is confined to the purpose and/or media for which permission is hereby given.

5. Altering/Modifying Material: Not Permitted. However figures and illustrations may be altered/adapted minimally to serve your work. Any other abbreviations, additions, deletions and/or any other alterations shall be made only with prior written authorization of Elsevier Ltd. (Please contact Elsevier at permissions@elsevier.com)

6. If the permission fee for the requested use of our material is waived in this instance, please be advised that your future requests for Elsevier materials may attract a fee.

7. Reservation of Rights: Publisher reserves all rights not specifically granted in the combination of (i) the license details provided by you and accepted in the course of this licensing transaction, (ii) these terms and conditions and (iii) CCC's Billing and Payment terms and conditions.

8. License Contingent Upon Payment: While you may exercise the rights licensed immediately upon issuance of the license at the end of the licensing process for the transaction, provided that you have disclosed complete and accurate details of your proposed use, no license is finally effective unless and until full payment is received from you (either by publisher or by CCC) as provided in CCC's Billing and Payment terms and conditions. If full payment is not received on a timely basis, then any license preliminarily granted shall be deemed automatically revoked and shall be void as if never granted. Further, in the event that you breach any of these terms and conditions or any of CCC's Billing and Payment terms and conditions, the license is automatically revoked and shall be void as if never granted. Use of materials as described in a revoked license, as well as any use of the materials beyond the scope of an unrevoked license, may constitute copyright infringement and publisher reserves the right to take any and all action to protect its copyright in the materials.

9. Warranties: Publisher makes no representations or warranties with respect to the licensed material.

10. Indemnity: You hereby indemnify and agree to hold harmless publisher and CCC, and their respective officers, directors, employees and agents, from and against any

and all claims arising out of your use of the licensed material other than as specifically authorized pursuant to this license.

11. No Transfer of License: This license is personal to you and may not be sublicensed, assigned, or transferred by you to any other person without publisher's written permission.

12. No Amendment Except in Writing: This license may not be amended except in a writing signed by both parties (or, in the case of publisher, by CCC on publisher's behalf).

13. Objection to Contrary Terms: Publisher hereby objects to any terms contained in any purchase order, acknowledgment, check endorsement or other writing prepared by you, which terms are inconsistent with these terms and conditions or CCC's Billing and Payment terms and conditions. These terms and conditions, together with CCC's Billing and Payment terms and conditions (which are incorporated herein), comprise the entire agreement between you and publisher (and CCC) concerning this licensing transaction. In the event of any conflict between your obligations established by these terms and conditions and those established by CCC's Billing and Payment terms and conditions, these terms and conditions shall control.

14. Revocation: Elsevier or Copyright Clearance Center may deny the permissions described in this License at their sole discretion, for any reason or no reason, with a full refund payable to you. Notice of such denial will be made using the contact information provided by you. Failure to receive such notice will not alter or invalidate the denial. In no event will Elsevier or Copyright Clearance Center be responsible or liable for any costs, expenses or damage incurred by you as a result of a denial of your permission request, other than a refund of the amount(s) paid by y**ou to Elsevier** and/or Copyright Clearance Center for denied permissions.

LIMITED LICENSE

T**he following** terms and conditions apply only to specific license **types:**

15. Translation: This permission is granted for non-exclusive world English rights only unless your license was granted for translation rights. If you licensed translation rights you may only translate this content into the languages you requested. A professional translator must perform all translations and reproduce the content word for word preserving the integrity of the article. If this license is to re-use 1 or 2 figures the**n permission is granted for non-exclusiv**e world rights in all languages.

16. Posting licensed content on any Website: The following terms and conditions apply as follows: Licensing material from an Elsevier journal: All content posted to

the web site must maintain the copyright information line on the bottom of each image; A hyper-text must be included to the Homepage of the journal from which you are licensing at http://www.sciencedirect.com/science/journal/xxxxx or the Elsevier homepage for books at http://www.elsevier.com; Central Storage: This license does not include permission for a scanned version of the material to be stored in a central repository such as that provided by Heron/XanEdu.

Licensing material from an Elsevier book: A hyper-text link must be included to the Elsevier homepage at http://www.elsevier.com . All content posted to the web si**te must maintain the copyright information lin**e on the bottom of each image.

Posting licensed content on Electronic reserve: In addition to the above the following clauses are applicable: The web site must be password-protected and made available only to bona fide students registered on a relevant course. This permission is granted **for 1 year only. You** may obtain a new license for future website posting.

17. For **journal au**thors: the following clauses are applicable in addition to the above:

Preprints:

A preprint is an author's own write-up of research results and analysis, it has not been peer-reviewed, nor has it had any other value added to it by a publisher (such as formatting, copyright, technical enhancement etc.).

Authors can share their preprints anywhere at any time. Preprints should not be added to or enhanced in any way in order to appear more like, or to substitute for, the final versions of articles however authors can update their preprints on arXiv or RePEc with their Accepted Author Manuscript (see below).

If accepted for publication, we encourage authors to link from the preprint to their formal publication via its DOI. Millions of researchers have access to the formal publications on ScienceDirect, and so links will help users to find, access, cite and use the best available version. Please note that Cell Press, The Lancet and some society-owned have different pre**print policies. Information** on these policies is available on the journal homepage.

Accepted Author Manuscripts: An accepted author manuscript is the manuscript of an article that has been accepted for publication and which typically includes author-incorporated changes suggested during submission, peer review and editor-author communications.

Authors can share their accepted author manuscript:

- immediately

via their non-commercial person homepage or blog

by updating a preprint in arXiv or RePEc with the accepted manuscript

via their research institute or institutional repository for internal institutional uses or as part of an invitation-only research collaboration work-group

directly by providing copies to their students or to research collaborators for their personal use

for private scholarly sharing as part of an invitation-only work group on commercial sites with which Elsevier has an agreement

- after the embargo period

via non-commercial hosting platforms such as their institutional repository

via commercial sites with which Elsevier has an agreement

In all cases accepted manuscripts should:

- link to the formal publication via its DOI

- bear a CC-BY-NC-ND license - this is easy to do

- if aggregated with other manuscripts, for example in a repository or other site, be shared in alignment with our hosting policy not be added to or enhanced in any way to appear more like, or to substitute for, the published journal article.

Published journal article (JPA): A published journal article (PJA) is the definitive final record of published research that appears or will appear in the journal and embodies all value-adding publishing activities including peer r**eview co-ordination, copy-editin**g, formatting, (if relevant) pagination and online enrichment.

Policies for sharing publishing journal articles differ for subscription and gold open access articles:

Subscription Articles: If you are an author, please share a link to your article rather than the full-text. Millions of researchers have access to the formal publications on

ScienceDirect, and so links will help your users to fin**d, access, cite, and u**se the best available version.

Theses and dissertations which contain embedded PJAs as part of the formal submission can be posted publicly by the awarding institution with DOI links back to the formal publications on ScienceDirect.

If you are affiliated with a library that subscribes to ScienceDirect you have additional private sharing rights for others' research accessed under that agreement. This includes use for classroom teaching and internal training at the institution (including use in course packs and courseware programs), and inclusion of the article for grant funding purposes.

Gold Open Access Articles: May be shared according to the author-selected end-user license and should contain a CrossMark logo, the end user license, and a DOI link to the formal publication on ScienceDirect.

Please refer to **Elsevier's posting policy** for further information.

18. For book authors the following clauses are applicable in addition to the above: Authors are permitted to place a brief summary of their work online only. You are not allowed to download and post the published electronic v**ersion of your cha**pter, nor may you scan the printed edition to create an electr**o**nic version. Posting to a repository: Authors are permitted to post a summary of their chapter only in their institution's repository.

19. Thesis/Dissertation: If your license is for use in a thesis/dissertation your thesis may be submi**tted to your institution** in either print or electronic form. Should your thesis be published commercially, please reapply for **permission. These r**equirements include permission for the Library and Archives of Canada to supply single copies, on demand, of the complete thesis and include permission for Proquest/UMI to supply single copies, on demand, of the complete thesis. Should your thesis be published commercially, please reapply for permission. Theses and dissertations which contain embedded PJAs as part of the formal submission can be posted publicly by the awarding institution with DOI links back to the formal publications on ScienceDirect.

Elsevier Open Access Terms and Conditions

You can publish open access with Elsevier in hundreds of open access journals or in nearly 2000 established subscription journals that support open access publishing. Permitted t**hird party re-use of these open access ar**ticles is defined by the author's choice of Creative Commons user license. See our open access license policy for more information.

Terms & Conditions applicable to all Open Access articles published with Elsevier:

Any reuse of the article must not represent the author as endorsing the adaptation of the article nor should the article be modified in **such a way as to damage the author's honour or reputation. If any changes have be**en made, such changes must be clearly indicated.

The author(s) must be appropriately credited and we ask that you include the end user license and a DOI link to the formal publication on ScienceDirect.

If any part of the material to be used (for example, figures) has appeared in our publication with credit or acknowledgement to another source it is the responsibility of the user to ensure their reuse complies with the terms and conditions determined by the rights holder.

Additional Terms & Conditions applicable to each Creative Commons user license:

CC BY: The CC-BY license allows users to copy, to create extracts, abstracts and new works from the Article, to alter and revise the A**rticle and to make commercial use of the Article (including reuse and/or resale of the** Article by commercial entities), provided the user gives appropriate credit (with a link to the formal publication through the relevant DOI), provides a link to the license, indicates if changes were made and the licensor is not represented as endorsing the use made of the work. The full details of the license are available at http://creativecommons.org/licenses/by/4.0.

CC BY NC SA: The CC BY-NC-SA license allows users to copy, to create extracts, abstracts and new works from the Article, to alter and revise the Article, provided this is not done for commercial purposes, and that **the user gi**ves appropriate credit (with a link to the formal publication through the relevant DOI), provides a link to the license, indicates if changes were made and the licensor is not represented as endorsing the use made of the work. Further, any new works must be made available on the same conditions. The full details of the license are available at http://creativecommons.org/licenses/by-nc-sa/4.0.

CC BY NC ND: The CC BY-NC-ND license allows users to copy and distribute the Article, provided this is not done for commercial purposes and further does not permit distribution of the Article if it is changed or **edited in an**y way, and provided the user gives appropriate credit (with a link to the formal publication through the relevant DOI), provides a link to the license, and that the licensor is not represented as endorsing the use made of the work. The full details of the license are available at